Kinesin-1
Cargo recognition and activation

Sanger, Anneri

Awarding institution:
King's College London

Kinesin-1 : Cargo recognition and activation

Anneri Sanger

2016

A thesis submitted to King's College London for the degree of Doctor of Philosophy

Randall Division of Cell and Molecular Biophysics,
King's College London,
Guy's Campus,
London,
SE1 1UL

ACKNOWLEDGEMENTS

First and foremost, praise and thanks go to my saviour Jesus Christ for the many blessings given to me. My sincere gratitude goes to my supervisors, Dr. Mark Dodding and Dr. Roberto Steiner for their support, guidance and encouragement throughout the course of my PhD, without which completion of this work would not have been possible. I would also like to thank everyone in the Randall Cell Motility group, past and present, who have always been available for advice and support over the last few years. Assistance from other members of staff at King's College London has been invaluable, in particular Dr. Stefano Pernigo for his work on the crystal structure. I would also like to give a special thanks to my husband, Charles and my parents for their love, support and prayers throughout my PhD.

ABSTRACT

The hetrotetrameric microtubule motor protein, kinesin-1 plays a central role in the intracellular transport of protein, ribonuclear protein, vesicles and organelles on microtubules. Kinesin-1 is composed of two heavy (KHC) and two light chains (KLC). In the absence of cargo, kinesin-1 exists in an autoinhibited state where the C-terminal tail of a single heavy chain binds to the N-terminal motor domain. KLCs contribute to the maintenance of this regulated state although the mechanism is unknown. Kinesin-1 is activated upon cargo binding. Cargo have been shown to bind to the tetratricopeptide repeat (TPR) domain of KLC and the C-terminal tail of KHC. KLCs recognise a short peptide sequence present in many cargo that is characterised by a tryptophan flanked by acidic residues (W-acidic). The aim of this thesis was to further investigate these cargo recognition mechanisms with the goal of providing a framework for understanding the general principles of kinesin-1 cargo recognition and cargo dependent activation. This was pursued by attempting a detailed molecular dissection of the mechanism of recognition of lysosomal cargo adaptor SKIP which carries a pair of W-acidic motifs. In this thesis the crystal structure of the TPR domain of KLC2 in complex with a tryptophan-acidic motif derived from SKIP is presented and the key residues responsible for the interaction are identified. Further studies revealed a direct interaction between SKIP and a specific site on the C-terminal tail of KHC. Mapping of the KHC binding site on SKIP revealed both shared and distinct determinants for the KHC and KLC interaction, and binding to either may be mutually exclusive. Mutational separation of the KHC and KLC binding enabled the investigation of this novel KHC-cargo interaction in SKIP mediated cargo transport. Based on these findings a model is proposed to explain how SKIP may activate kinesin-1 to promote anterograde lysosome transport.

CONTENTS

TABLE OF FIGURES

TABLE OF TABLES

ABBREVIATIONS

ADP	Adenosine diphospate
AP-MS	Affinity purification mass spectrometry
APS	Ammonium persulphate
ATP	Adenosine triphospate
BDNF	Brain-derived neurotrophic factor
CRMP-2	Collapsin response mediator protein-2
CSTN-1	Calsyntenin-1
CC1/2	Coiled-coil 1/2
Cit	Citruline
CMT	Charcot-Marie-Tooth
DIC	Dynein intermediate chains
DLIC	Dynein intermediate light chains
EB-1	End binding protein-1
ERK	Extracellular signal-regulated kinase
FEZ-1	Fasciculation and elongation protein zeta 1
FHA	Forkhead associated
γ–TuRC	γ-tubulin ring complex
GAP	GTPase-Activating Proteins
GCPs	γ-tubulin complex components
GDP	Guanosine diphosphate
GFP	Green fluorescent protein
GEF	Guanine nucleotide exchange factors
GRIF-1	GABAA receptor interacting factor-1
GTP	Guanosine triphosphate
HA	Hemagglutinin
HAP-1	Huntingtin associated protein-1
HSP	Hereditary Spastic Paraplegia
HSV1	Herpes simplex virus
ID	Intrinsically Disordered
IPTG	Isopropyl β-D-1-thiogalactopyranoside
JIP	JNK-interacting protein
KHC	Kinesin heavy chain
KIM	KLC-interacting motif
KLC	Kinesin light chain
LC	Dynein light chains

LZ	leucine zipper
LIS1	Lissencephaly 1
MAP	Mitogen-activated protein
MAPK	Mitogen-activated protein kinases
mRNA	Messenger Ribonucleic acid
MTOC	Microtubule organising centre
NudE	Nuclear distribution protein E
NudEL	NudE-like
PBS	Phosphate-buffered saline
PCM	Pericentriolar material
PFA	Paraformaldehyde
PH	Plekstrin Homology
PVDF	Polyvinylidene difluoride
RanBP	Ran binding protein
RUN	RPIP8, UNC-14, and NESCA
RZZ	Rod–ZW10–Zwilch
SCV	Salmonella-containing vacuole
SEC	Size exclusion chromatography
SKIP	SifA and kinesin-interacting protein
SNAP	Synaptosome associated protein
TAMRA	carboxytetramethylrhodamine
TEMED	Tetramethylethylenediamine
TPR	Tetratricopeptide repeat
TRAK -1/2	Trafficking kinesin protein -1/2
TWEEN	Polyoxyethylenesorbitan monolaurate

CHAPTER 1 . INTRODUCTION

1.1 Cytoskeletal motors

The cytoskeleton is composed of microtubules, actin filaments and intermediate filaments that interact to form a complex network which maintains cell shape, is involved in many cellular processes such as cell motility, endocytosis and cytokinesis and allows for the dynamic control over the spatial distribution of subcellular components.

There are three classes of cytoskeletal motors; myosin, dynein and kinesins. All cytoskeletal motors contain a motor domain (also called the head) that has one or more adenosine triphosphate (ATP) binding sites as well as a binding site for the actin filament or microtubule tract. Cytoskeletal motors utilise energy released from ATP hydrolysis to drive conformational changes which results in the production of force for movement. Myosin interacts with actin filaments, and dynein and kinesins interact with microtubules. Figure 1.1 shows a schematic of representative examples of these motor proteins.

A subset of cytoskeletal motors actively transport intracellular cargo along cytoskeletal filaments to their appropriate destination. Unlike diffusion, this transport is independent of concentration and is also highly specific as it allows the transport of specific cargo to specific destinations. Transport by motors also allows for the directed movement and control of the positioning of larger subcellular components that would otherwise only travel very short distances by diffusion. How motor proteins are regulated and are able to transport cargo at the correct time to the correct location is an important biological question. Transported cargoes include proteins required for large macromolecular structures such as cilia and centrosomes, proteins involved in signaling, membrane bound organelles (e.g. nucleus, mitochondria), mRNAs, and cytoskeletal filaments (Vale, 2003).

The cytoskeleton is a dynamic structure and remodeling of the cytoskeleton is required for cell migration as well as meiosis and mitosis. Motors are also involved in regulating cytoskeletal dynamics. For example kinesin-8, kinesin-13 and kinesin-14 family proteins function to destabilise microtubules (Gupta et al., 2006, Mayr et al., 2007, Varga et al., 2006, Endow et al., 1994, Desai et al., 1999, Hunter et al., 2003).

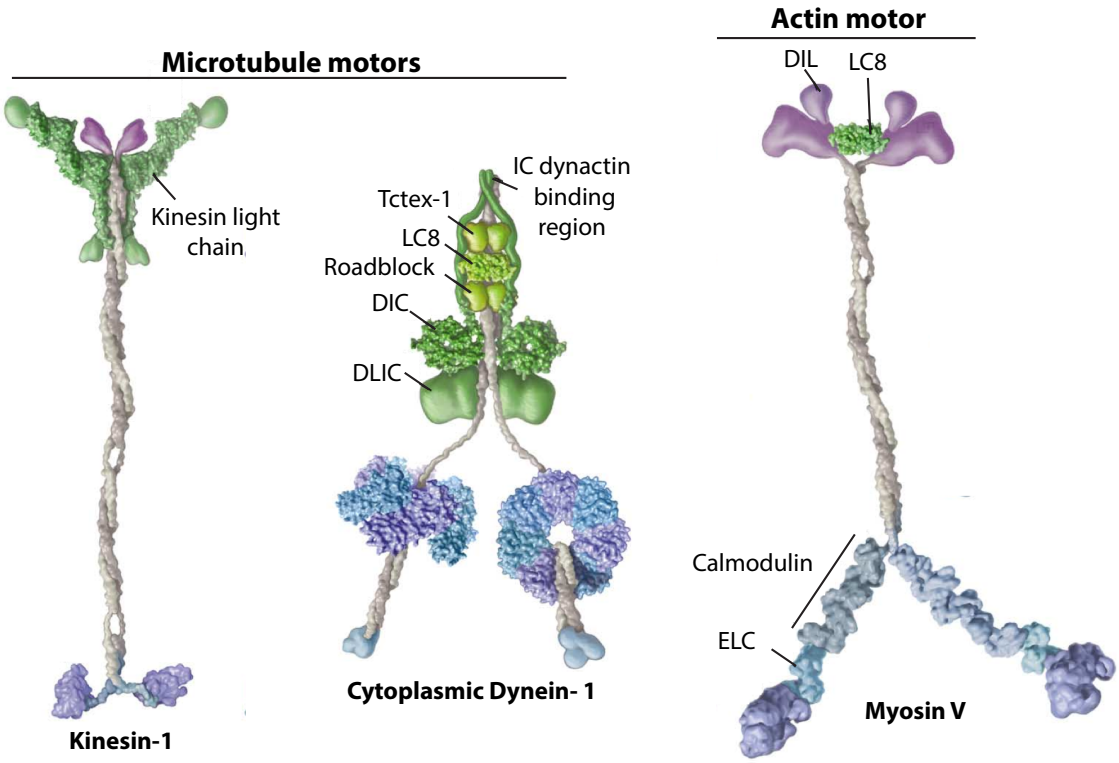

Figure 1.1. Examples of motor proteins from three major superfamilies: kinesin-1, cytoplasmic dynein and myosin-V.
Kinesin-1; dark purple: motor domains; purple: heavy chain cargo attachment site; green: kinesin light chains. Cytoplasmic dynein-1; blue: microtubule binding domains, dark purple and blue ring: six AAA+ domains, green: associated protein subunits (DLIC: Light intermediate chains, DIC: Intermediate chains, Tctex-1: Tctex-1/rp3 light chains, roadblock: roadblock light chains, LC8: LC8 light chains) Myosin V; dark purple: motor domain; blue an grey: extended α helical neck region (ELC: essential light chain and calmodulin binding region) Purple: DIL (conserved ~100 residue C-terminal domain); green: LC8 light chains. Adapted from (Vale, 2003).

1.2 Myosin

The myosin superfamily consists of at least 35 classes (Odronitz and Kollmar, 2007). With the exception of class VI myosins (Wells et al., 1999), all of the myosin classes studied thus far have been shown to move to the barbed end of actin filaments (Sweeney and Houdusse, 2010, Wells et al., 1999). Myosins move on actin filaments and are involved in a wide range of functions in cells such as cell adhesion, cell motility, movement of mRNA, movement of pigment granules, cytokinesis, endocytosis and exocytosis (Hammer and Sellers, 2012).

The best characterised member of the myosin superfamily is muscle myosin II that forms part of the sarcomere with actin filaments and is required to generate force for muscle contraction. Most myosin heavy chains are composed of three domains; an N terminal motor domain that is responsible for ATP hydrolysis as well as actin binding, an extended α helical neck region containing one or more IQ motifs that bind light chains (calmodulin or other members of the E-F hand family of proteins) and a C-terminal tail which vary dependent on myosin class and is involved in cargo binding or dimerisation of heavy chains (Krendel and Mooseker, 2005). Movement is driven by ATPase activity of the motor domain, which hydrolyses ATP to ADP.Pi, which is subsequently released and exchanged for ATP (Rief et al., 2000). Upon ATP hydrolysis the myosin 'lever arm' undergoes a conformational change and bends the myosin head to a position further along the actin filament. Binding of the myosin head to the actin filament stimulates the release of Pi, which triggers a second conformational change and movement along the filament (power stroke).

Class V myosins are important in organelle transport (shown in Figure 1.1). Myosin V carries intracellular cargo processively along actin tracks in a hand-over-hand manner alternating the positions of the leading and trailing heads, resembling the action of kinesin-1 along microtubules (Warshaw et al., 2005). The step size was shown to be 36nm using optical trapping nanometry (Mehta et al., 1999). Electron microscopic images further showed myosin V molecules associated with actin with the two heads spaced 36 nm apart (Walker et al., 2000). The walking of myosin V along actin tracks were also visualised by high-speed atomic force microscopy (Kodera et al., 2010). Although the motor domains of myosin V and kinesin-1 share no sequence homology and have distinct motile (Svoboda et al., 1993, Walker et al., 2000) and enzymatic

properties (Bagshaw and Trentham, 1974, Hackney, 1988), structurally the catalytic domains are very similar (Kull et al., 1996).

1.3 Dyneins

The dynein family of motor proteins can be divided into two groups; axonemal and cytoplasmic. Cytoplasmic dyneins are important in cargo transport whereas axonemal dyneins function in driving the bending of cilia and flagella (Gibbons, 1981, DiBella and King, 2001). Dynein 1B and dynein 2 are involved in intraflagellar transport, moving cargo along the axoneme to the cell body, whereas dynein-1 is the only dynein responsible for minus-end directed transport of diverse cargos on microtubules in the cytoplasm (Schroer et al., 1989). Examples of cargo include organelles such as endosomes (Driskell et al., 2007), lysosomes (Jordens et al., 2001), and mitochondria (Pilling et al., 2006), components of the centrosome (Young et al., 2000), transcription factors (Harrell et al., 2004), cytoskeletal filaments (Shah et al., 2000) and mRNA-containing ribonucleoprotein complexes (Wilkie and Davis, 2001).

Cytoplasmic dynein-1 is a homodimer consisting of two dynein heavy chains (DHC) each containing a C-terminal motor domain composed of six AAA+ (ATPases associated with diverse activities) modules (Neuwald et al., 1999) referred to as AAA1-AAA6. AAA1 is the main site of ATP hydrolysis for force generation (Kon et al., 2004) and AAA2–AAA4 bind nucleotides and appear to be required for regulation (Cho et al., 2008). The C-terminal region of the heavy chain spans between AAA6 and the stalk base. The N-terminal, lever-like linker swings by approximately 17nm during the ATPase cycle between AAA2 and the stalk base allowing for the forward movement of the motor (Roberts et al., 2009). Dynein intermediate chains (DIC) dynein intermediate light chains (DLIC) and dimers of three light chains (LC); the Tctex1 light chains, the Roadblock light chains; and the LC8 light chains binds to DHC (Pfister et al., 2006). This is shown in Figure 1.1.

Within cells cytoplasmic dynein interacts with several regulatory proteins that regulate its function and localisation. Adaptors include dynactin, lissencephaly 1 (LIS1), nuclear distribution protein E (NudE) and NudE-like (NudEL), Bicaudal D, Rod–ZW10–Zwilch (RZZ) and Spindly (Kardon and Vale, 2009). Dynactin is the best characterised of the adaptors and is a large multi-subunit protein complex consisting of the following subunits: p150Glued, p62,

dynamintin (p50), Arp11, Arp1, β- actin, CapZ α/β, p24, p27 and p25 (Schroer, 2004). Dynactin has a large range of functions including mitotic spindle assembly and organelle transport (Schroer, 2004). Dynactin was first identified as an activator of dynein mediated vesicle transport (Gill et al., 1991). More recently dynactin has been shown to enhance the initial recruitment of dynein onto microtubules and promotes processivity through functioning as a tether to microtubules and decreasing the detachment rate of dynein from microtubules (Ayloo et al., 2014, King and Schroer, 2000).

Dynein mostly moves in 8nm steps although variable step sizes 8 - 32 nm have been observed (Mallik et al., 2004, Toba et al., 2006) as well as lateral and backward stepping (Reck-Peterson et al., 2006).

1.4 Kinesin Superfamily

The kinesin superfamily can be divided into 14 sub families (Lawrence et al., 2004). Kinesins 1-3 generally function in cargo transport along microtubules and Kinesin 4-14 are thought to function predominantly in meiosis and mitosis (Verhey and Hammond, 2009). All kinesins contain a motor domain with an adenosine triphosphate (ATP) binding site that is coupled to a site that allows binding to microtubules. The location of the motor domain gives an indication of the direction of transport. In general kinesins with an amino-terminal motor domain undergo motility to the plus end of microtubules, which tend to be located in the cell periphery, whereas kinesins with a carboxy-terminal motor (Kinesin-14 family) undergo minus end-directed motility. When the motor domain is located in the center of the kinesin molecule (Kinesin-13 family), the kinesin functions to destabilize microtubules at their plus and minus ends (Hirokawa et al., 2009). There are however a few exceptions for example Kinesin-8 and Kinesin-14 families can both walk along and destabilize microtubules (Gupta et al., 2006, Mayr et al., 2007, Varga et al., 2006). Some kinesins for example kinesin-5 also undergo diffusion along the microtubule surface in an ATP-independent manner, which may allow the motor to stay microtubule associated for longer (Kwok et al., 2006). Kinesin-5 also functions as a microtubule polymerase (Chen and Hancock, 2015).

1.5 Microtubules

Microtubules are polymers of alpha and beta tubulin heterodimers that assemble to form protofilaments. The hollow cylindrical microtubule usually consists of 13 protofiliments (Evans et al., 1985). Microtubules are intrinsically polar, with the end that exposes β-tubulin (plus end) growing more rapidly than the end that exposes α-tubulin (minus end). Typically, microtubule arrays are radial with the minus end anchored at the microtubule organising centre (MTOC) and the plus end pointing to the cell periphery. Mitotic cells however have two radial arrays giving rise to the bipolar mitotic spindle.

The centrosome is the main MTOC in animal cells. The centrosome is made up of a central pair of centrioles surrounded by pericentriolar material (PCM). The main cellular nucleator of microtubules is the γ-tubulin ring complex (γ-TuRC) that localises to the MTOC and is composed of γ-tubulin and the γ-tubulin complex components (GCPs) 2, 3, 4, 5 and 6. (Moritz et al., 1995, Teixido-Travesa et al., 2012, Zheng et al., 1995). The PCM contains proteins such as pericentrin and ninein that are involved in the nucleation as well as anchoring of microtubules (Azimzadeh and Bornens, 2007, Teixido-Travesa et al., 2012). Nucleation can also be associated with other sites such as the Golgi complex (Luders and Stearns, 2007, Miller et al., 2009, Rivero et al., 2009). Linear, non-centrosomal microtubule arrays are typical of polarized, non-migratory cells such as epithelial cells, terminally differentiated neuronal cells and skeletal muscle fibres (myotubes) (Bartolini and Gundersen, 2006).

GTP bound αβ-tubulin forms a stabilizing cap to the GDP lattice and allows for microtubule growth. As a new αβ-tubulin dimer is added to the protofilament the previous tubulin bound GTP is hydrolysed (David-Pfeuty et al., 1977). Loss of the stabilizing cap through GTP hydrolysis leads to rapid depolymerisation, which is characterized by peeling of protofilaments (Carlier et al., 1984, Mitchison and Kirschner, 1984) (Figure 1.2). This is also called “catastrophe”. “Rescue” refers to the transition from shrinking to growing. Microtubules can rapidly switch between phases of growth and shrinkage. This switching of microtubules between cycles of growth and shrinkage is known as dynamic instability. Rapid turnover of microtubules is essential for the remodeling of the cytoskeleton that occurs during mitosis and cell migration. Although the amount of available tubulin is one of the key factors that determine the rate of microtubule growth and shrinkage, the dynamic properties of

microtubules are not solely explained through local tubulin concentration, many different regulatory proteins control the dynamics of microtubules. Microtubule-associated proteins (MAPs) may function as stabilising proteins. For example end binding protein-1 (EB1) is a plus-end tracking protein (+TIPs) that stabilise the tubular conformation of microtubules through binding to the GTP cap (Maurer et al., 2012). Other proteins, such as kinesin-13 and kinesin-8, function to destabilise microtubules. Kinesin-13 promotes catastrophe through promoting the bending of protofilaments into an outward curved conformation (Moores et al., 2002, Newton et al., 2004). Kinesin-8 also promotes microtubule disassembly through depolymerisation at the plus end. Kinesin-8 also depolymerise longer microtubules faster than shorter ones (Varga et al., 2006).

Microtubules undergo post translational modifications, which include tyrosination, acetylation, glutamylation glycalation, detyrosination, deacetylation, deglutamylation and deglycalation (Garnham and Roll-Mecak, 2012). As well as regulating dynamics, post-translational modification can affect processivity, (Wang and Sheetz, 2000, Reed et al., 2006) recruitment (Hammond et al., 2010, Reed et al., 2006) and subcellular targeting (Ikegami et al., 2007) of kinesin and dynein motors.

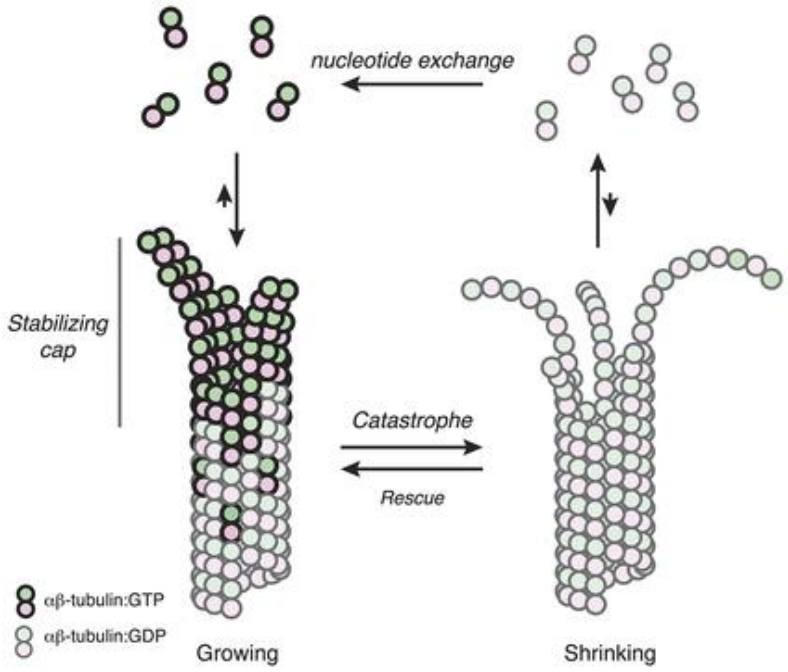

Figure 1.2. Schematic of the cycle of microtubule polymerisation.
The hollow cylindrical microtubule usually consists of 13 protofiliments. Microtubules are intrinsically polar, with the plus end growing more rapidly than the minus end. GTP bound αβ-tubulin forms a stabilizing cap to the GDP lattice and allows for microtubule growth. As a new αβ-tubulin dimer is added to the protofilament the previous tubulin bound GTP is hydrolysed. Loss of the stabilizing cap through GTP hydrolysis leads to rapid depolymerisation, which is characterized by peeling of protofilaments The switch from microtubule growth to shrinkage is referred to as “catastrophe” and the switch from shrinkage to growth is referred to as “rescue” (Brouhard and Rice, 2014).

1.6 Kinesin-1

Kinesin-1 (also known as conventional kinesin), was the first kinesin family motor to be discovered. It was first isolated from squid giant axons by virtue of its capacity to bind to microtubules in an ATP dependent manner (Vale et al., 1985a) and was shown to exist predominantly as a heterotetramer of two heavy chains (KHC) and two light chains (KLC) (Hirokawa et al., 1989, Kuznetsov et al., 1988). Kinesin-1 plays a key role in the intracellular transport of proteins, nucleic acids and membrane bound organelles such as mitochondria and lysosomes along microtubules (Hirokawa et al., 2009).

1.6.1 Kinesin heavy chains

There are three mammalian genes that encode the kinesin-1 heavy chains; Kif5A, Kif5B and Kif5C. Kif5A and Kif5C are expressed in predominantly neuronal cells whereas Kif5B is ubiquitously expressed (Kanai et al., 2000, Xia et al., 1998). The kinesin heavy chains form a homodimer (DeBoer et al., 2008) consisting of two globular heads that are the sites of ATP hydrolysis and microtubule binding and functions as the motor domain, a region known as the neck links these to an extended alpha-helical coiled coil domain (stalk) and a C-terminal tail region (Figure 1.3). The neck plays a crucial role in the mechanism of kinesin-1 movement on microtubules (discussed in 1.6.6). The C-terminal domain is important for cargo binding and interaction with the light chains. The KLC binding site has been mapped to residues 771-813 on Kif5B. Within this heavy chain region are four highly conserved heptad repeats that interact with the heptad repeat at the N-terminus of KLC (Diefenbach et al., 1998). The extreme C-terminus of KHC contains a highly conserved autoinhibitory region that contributes to regulation of the motor.

The C-terminal tail of KHC has been shown to also contain an ATP-independent microtubule binding site (Hackney and Stock, 2000, Navone et al., 1992, Yonekura et al., 2006). This binding site has been mapped to residues 892-914 (Kif5B) with the interaction being mediated by largely complementary electrostatic interactions between the tail and microtubules (Seeger and Rice, 2010). The function of this second microtubule binding site is not fully understood. There has been a variety of suggestions, for example Seeger and Rice suggests that if cargo binds to one tail peptide the free KHC tail could tether to or diffuse along microtubules and keep kinesin-1 in close contact,

enhancing the processivity of the motor. Dietrich et al., 2008 suggest that the function may be to pause the motor in an inactive autoinhibited state on microtubules and propose that the reason why inactive kinesin is not found to be microtubule bound may be due to regulatory proteins masking the tail-microtubule interaction preventing kinesin-1 from binding to microtubules. The binding sites of several cargo also span this ATP-independent microtubule binding region. Thus, the C-terminal tail of KHC is likely crucial in coordinating cargo binding and kinesin-1 activity.

The majority of KHC exists in complex with KLC, however a proportion of KHC in mammalian cells has been reported to exist without KLC (DeLuca et al., 2001). Roughly 50% of KHC in CV-1 cells were shown to exist without KLC and approximately 14% of KHC in mouse brain extracts lacks KLC (Sun et al., 2011, Gyoeva et al., 2004). KLC could also not be detected within photoreceptors (Mavlyutov et al., 2002). This KLC free component may have specific cargo transport functions. KLC independent transport has been demonstrated in the transport of mitochondria where KLC antagonises the binding of the cargo adaptor Milton to the heavy chain. Binding of KLC and Milton appear to be mutually exclusive (Glater et al., 2006, Cai et al., 2005). Cytoplasmic streaming and mRNA localisation to the posterior pole of the *Drosophila* oocyte is also KLC independent (Palacios and St Johnston, 2002).

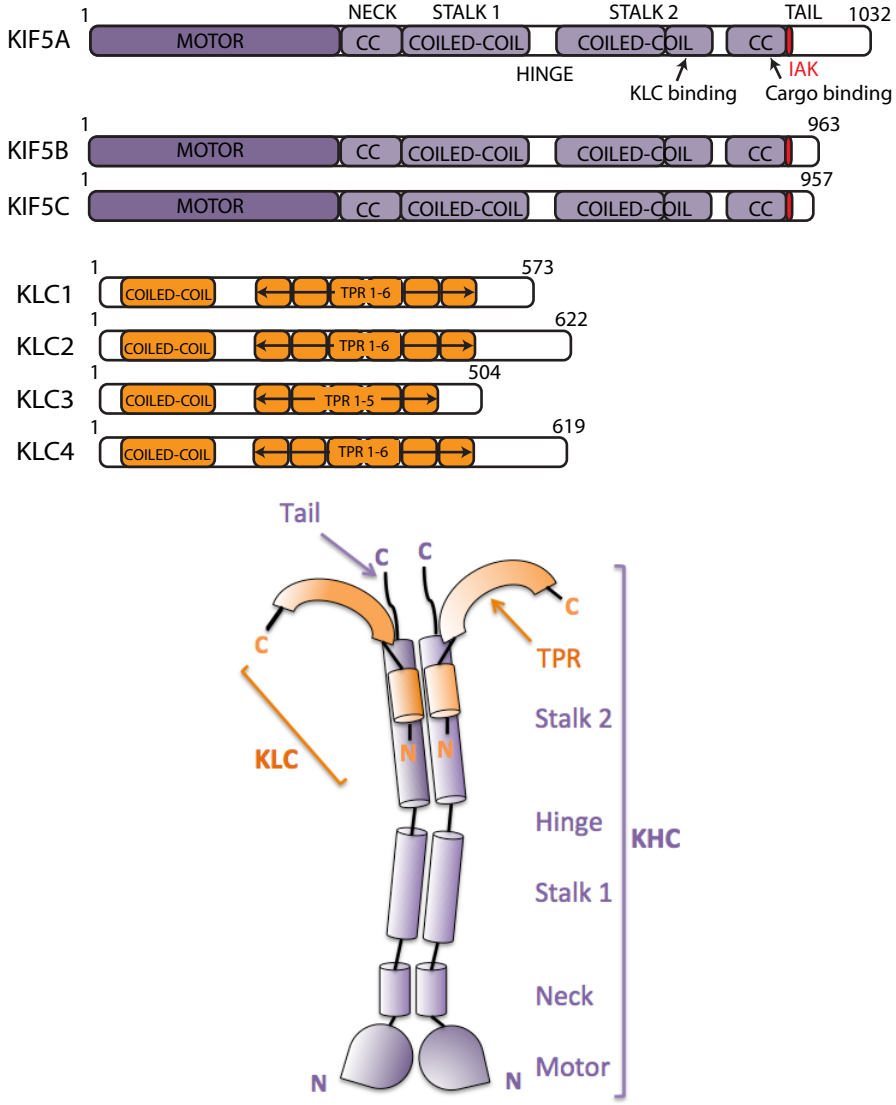

Figure 1.3. Schematic of Kinesin-1.
Top: The three kinesin heavy chains (KHC) are shown in purple Kif5A, Kif5B and Kif5C with the motor domain and coiled coil (CC) region highlighted as well as the autoinhibitory IAK sequence. The four kinesin light chains (KLC) are shown in orange with the coiled-coil heptad repeat region as well as the TPR domain highlighted. Bottom: Schematic of kinesin-1 showing the make-up of the kinesin-1 tetramer. Kinesin-1 consists of two heavy chains and two light chains. The heptad repeat region of KHC interacts with the heptad repeat at the N-terminus of KLC. The motor domain, neck, hinge, coiled coil stalk regions (1 and 2) as well as the C-terminal tail of KHC highlighted as well as the tetratricopeptide repeat (TPR) domain of KLC.

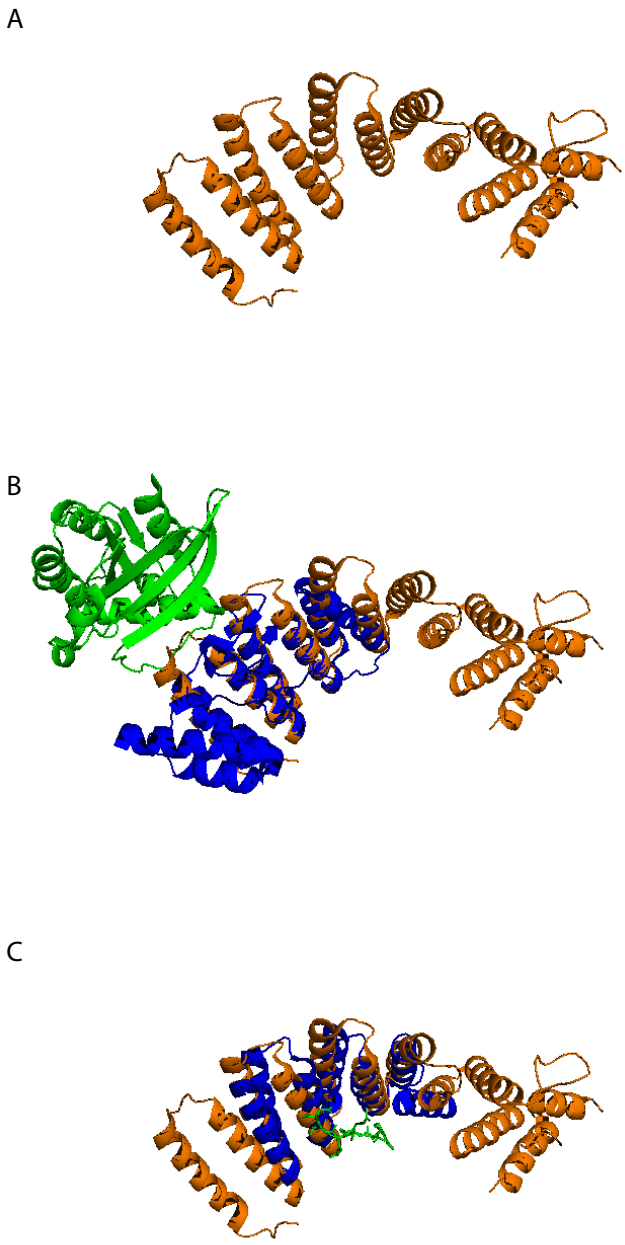

Figure 1.4 Structural alignment of KLC1-TPR domain with TPR domains of HOP1 and p67phox showing multiple modes of cargo binding.
(A) KLC1-TPR domain (PDB: 3CEQ) (orange) (B) KLC1-TPR domain (orange) is aligned with the p67phox TPR domain (blue) in complex with Rac1 (Yellow) (PDB:1E96) using PyMOL align function illustrating the similar interface on the outer surface of KLC1 to p67phox. (C) KLC1-TPR domain (orange) is aligned with the HOP1 TPR domain (blue) in complex with Hsc70 peptide (green) (PDB:1ELW) using PyMOL align function illustrating the similar interface of KLC1 with HOP1 on the inner groove.

1.6.2 Kinesin Light Chains

The kinesin-1 light chains are encoded by 4 genes in mammalian cells (KLC1, KLC2, KLC3 and KLC4) which, like the heavy chains have distinct tissue expression profiles. KLC1 is expressed mainly in neuronal cells, KLC2 is expressed ubiquitously and KLC3 is expressed within spermatids. (Rahman et al., 1998, Junco et al., 2001) KLC4 has not yet been characterized, although all four types are expressed in HeLa (Maliga et al., 2013).

Initially, immunoprecipitation analysis suggested that KLC (KLC1 or KLC2) forms homodimers (Gyoeva et al., 2004) that associate with KHC (Kif5A, Kif5B or Kif5C) homodimers, but do not show a clear specificity for a particular heavy chain (DeBoer et al., 2008). Maliga et al., 2013 however demonstrated by combining BAC transgenomics with the sensitivity of affinity purification mass spectrometry (AP-MS) that KLCs can form asymmetric motor complexes in HeLa cells with mixed light chains, suggesting that there may be a large array of kinesin-1 forms possible in mammalian cells. The variability in the light chain may enhance functional diversity and allow multiple types of cargo to be transported. Within the KLC binding region of KHC are heptad repeats that interact with the heptad repeat containing N-terminus of KLC. Since all of the KLCs interact within this same region, if two of the same KLCs were to bind, other regulatory factors would be necessary to ensure specific recognition and binding of two of the same KLCs. One possibility of how this may occur is if kinesin-1 is assembled cotranslationally, homodimerising before binding to KHC.

Kinesin light chains (KLC) can be divided into three domains; a well conserved N-terminal region that contains a coiled-coil (heptad repeat) and binds to KHC (Diefenbach et al., 1998), a conserved tetratricopeptide repeat (TPR) domain and a variable C-terminal domain that both play a role in cargo binding. Cargo can interact directly with the KLC TPR domain to mediate transport. Alternative splicing within the C-terminal domain of KLC1 results in the expression of various KLC isoforms (McCart et al., 2003). The KLC isoforms have been shown to have differential association with the Golgi apparatus, mitochondria and rough endoplasmic reticulum. The C-terminal region of KLC was therefore suggested to play a role in targeting kinesin-1 to different cellular structures (Gyoeva et al., 2000, Khodjakov et al., 1998, Wozniak and Allan, 2006).

1.6.3 TPR domains

A TPR domain consists of a tandem array of TPR motifs (two anti-parallel α-helices composed of 34 amino acids residues) typically forming a structure with an amphipathic groove that can bind target peptides and proteins. TPR domains have been identified that consist of between 3–16 TPR motifs (D'Andrea and Regan, 2003). KLC is composed of 5 or 6 illustrated in Figure 1.3.

Proteins have been shown to bind to various regions of TPR domains. The C-terminal residues of the Hsp90 chaperone have been shown to bind in an extended conformation to the concave groove of the protein phosphatase 5 (Ppp5) TPR domain (Cliff et al., 2006), as well as the TPR2A domain of HOP1 (Scheufler et al., 2000). The C-terminal residues of the Hsp70 chaperone also binds in an extended conformation to the concave groove of the HOP1 TPR1 domain. In all three cases a ‘‘carboxylate clamp’’ in the inner groove of the TPR domain is utilised to interact with the C-terminal residues of Hsp90 and Hsp70 respectively. The peroxisomal targeting signal-1 was also shown to bind in an extended conformation to the TPR domains of human PEX5 (Gatto et al., 2000). The loop regions that connect the helices in a TPR bundle have also been shown to mediate the association with cargo proteins. For example the structure of the TPR domain of p67phox in complex with Rac.GTP revealed that Rac.GTP is recognized through the loops connecting the TPR repeats (Lapouge et al., 2000). The structural alignment of KLC1 TPR domain with p67phox as well as HOP1 illustrates a similar interface on the outer surface to p67phox a well as a similar interface on the inner groove to HOP1, suggesting that recognition of cargo by the KLC TPR domain is therefore likely to be highly varied (Figure 1.4).

1.6.4 Cargo binding by kinesin-1

1.6.4.1 KHC: Cargo interaction

Kinesin-1 transports a large array of proteins, membrane-bound organelles such as vesicles, mitochondria, lysosomes and the nucleus. Many proteins that interact with kinesin-1 function as adaptors to other proteins and organelles. The binding sites for several cargo have been mapped to the C-terminal tail of KHC. Ong et al. showed through yeast two-hybrid assays that the C-terminus of the endoplasmic reticulum membrane protein, Kinectin interacted directly with

the C-terminal tail of KHC (residues 836-890 of Kif5A and residues 833-900 of Kif5B). Kinectin is an anchor for kinesin-dependent organelle motility *in vivo* (Ong et al., 2000). Another KHC binding partner has been reported to be Myosin Va. In a yeast two-hybrid assay Kif5B residues 763-856 were shown to interact with Myosin Va (Huang et al., 1999).

The tail domains of Kif5B and Kif5C, but not Kif5A, were shown to interact directly *in vivo* with Ran-binding protein 2 (RanBP2) (Cai et al., 2001). A connecting segment between the Ran GTPase binding domains, RBD2 and RBD3, termed JX2 in RanBP2 were shown to be responsible for the interaction with KHC. The molecular determinants of this specific interaction were further assessed by Cho et al. They showed that RanBP2 specifically interacts with Kif5C (827-936) and equivalent Kif5B region but does not interact with Kif5A. Through making M912S mutation unique to Kif5C (and equivalent on Kif5B) binding was lost. M912 was therefore identified as the residue that determines which Kif5 RanBP2 is able to bind to (Cho et al., 2007).

Through yeast two-hybrid assays, the N-terminus of the SNARE proteins synaptosome associated protein 23 and 25 (SNAP23 and SNAP25) were also shown to interact directly with the C-terminal tail of Kif5B (residues 814-907). The heptad repeat region of SNAP23 and SNAP25 (residues 45-84 SNAP 25 numbering) is likely to be the minimal binding region (Diefenbach et al., 2002a). Diefenbach et al. also showed using the same method, the interaction of Kif5B (residues 867-894) with the C-terminal RNA binding domain of HSV-1 tegument protein US11. The KHC:US11 interaction is suggested to have a major role in the anterograde transport of unenvoloped HSV nucleocapsids (Diefenbach et al., 2002b).

Through yeast two-hybrid as well as immunoprecipitation assays, γ-aminobutyric acid, type A (GABAA) receptor interacting factor-1 (GRIF-1) (residues 124-283) were shown to interact with Kif5C (Brickley et al., 2005). Smith et al further showed through immunoprecipitation as well as yeast two-hybrid studies that GRIF-1 interacts with the C-terminal region of Kif5C (residues 827-957). Through confocal imaging strategies GRIF-1 was shown to bind to Kif5C as well as the tetrameric kinesin-1 (Smith et al., 2006). Both TRAK1 (also called OIP106/MILTON1) and TRAK2 (also called GRIF-1/OIP98 or Milt2) were shown to co-immunoprecipitate with Kif5C. The interactions were also verified through Förster resonance energy transfer (FRET) studies

(Brickley et al., 2011). Randall et al. further refined the binding region and showed that TRAK2 binding to Kif5A is dependent on multiple binding regions. TRAK2 has been shown to bind to Kif5A residues (942-961), (877-885) and (861-877) (Randall et al., 2013). TRAK2 is also shown to bind to the Kif5A equivalent region on Kif5C. TRAK1 however retained the ability to co-immunoprecipitate Kif5A in the absence of the cargo binding domains identified for TRAK2. The stalk and tail regions of Kif5A, Kif5B and Kif5C were also shown to interact directly with the alpha-amino-3-hydroxy-5-methyl-4-isoxazolepropionate (AMPA) receptor subunit-GluR2-interacting protein GRIP-1 (Setou et al., 2002). Dystrobrevin is another example of a scaffold protein that was shown to bind to the C-terminal tail of Kif5A through pull-down and co-immunoprecipitation experiments (Macioce et al., 2003, Ceccarini et al., 2005).

Kv3.1 N-terminal T1 tetramers, but not monomers, directly bind to Kif5 tail residues (Kif5A 863-932, Kif5B 865-934 also termed the T70 region) (Xu et al., 2010). The Kv3.1 T1 binding site was further mapped to residues 875-919 (Kif5B) (Barry et al., 2013). Barry et al. also shows basic amino acid residues at positions 892-894 (RKR) to be essential for the interaction. No binding is however observed when the binding site is further truncated at either end to 870–896, 875–896 or 892–912, or through truncation and removal of the RKR sequence (865–891, 865–886, 913–934, 897–934, and 902–934).

The AnkG-binding site in the Kif5 motor is the T70 region, the exact same binding site for the Kv3.1 T1 domain. Mutation of residues 892-894; RKR to DDD did not pull down AnkG MB (the N-terminal membrane-binding domain of AnkG that contains 24 ankyrin repeats) domain. Smaller fragments of Kif5B also did not bind, suggesting a large region consisting of multiple binding sites is required for AnkG binding as for the Kv3.1 T1 domain (Barry et al., 2014).

Through yeast two-hybrid analysis UNC-76 was shown to bind to residues 850–975 of *Drosophila* KHC tail domain (Gindhart et al., 2003). FEZ1, the mammalian homologue of UNC-76, was also shown to bind to the C-terminal tail of KHC residues 750-955. Deletion of the inhibitory region and surrounding residues results in loss of binding to residues 750-910. Mutation of residues 908-917 or 947-955 to alanine abolished binding (Blasius et al., 2007).

A direct interaction between the C-terminal tail of KHC and JIP3 was shown in vitro through a GST pulldown of GST tagged Kif5C residues 807–956 and His tagged JIP3 (Sun et al., 2011). Thus, research over many years has

highlighted the importance of the C-terminal region of KHC in recruitment of many different cargoes. The molecular basis of this recognition appears to be highly complex. Despite much progress, notably very few common principles have emerged.

1.6.4.2 KLC: Cargo interaction

JIP proteins

The first demonstration of a direct interaction between conventional kinesin-1 light chain and a cargo was through yeast two-hybrid screening of a mouse brain cDNA library using the KLC1 TPR domain as bait. Three scaffolding proteins for the JNK signaling pathway were found to interact with the TPR domain of KLC1: the c-jun NH2-terminal kinase (JNK)–interacting proteins (JIPs) JIP-1, JIP-2, and JIP-3. Through immunoprecipitation assays the identical C-terminal sequences in JIP1 and JIP2 (PTEDIYLE) were shown to be essential for binding to KLC TPR domain. Co-immunoprecipitation experiments also showed the coprecipitation of JIP-1 with cytoplasmic as well as transmembrane signaling molecules; dual leucine zipper kinase (DLK) and the Reelin receptor, ApoER2 respectively. This suggested that through the binding of JIP-1 to kinesin-1, other cargo might also be transported as part of a multiprotein complex by kinesin-1 (Verhey et al., 2001). KLC TPR motifs bind to internal residues in JIP3 (Sunday Driver). Bowman et al. showed a direct interaction between the NH2-terminal half of JIP-3 and KLC1/2 TPR domain through yeast two-hybrid as well as GST pulldown assays (Bowman et al., 2000). In agreement with this, yeast two-hybrid screening of a mouse brain cDNA library using the KLC TPR domain as bait also only contained the amino terminal portion of JIP3 (Verhey et al., 2001). Kelkar et al. showed that the interaction between KLC1 TPR domain and JIP3/JIP4 is mediated by the leucine zipper domains of JIP3/JIP4 (Kelkar et al., 2005).

Like JIP1-4, the leucine zipper-containing scaffolding protein, JLP also associates with JNK as well as KLC. The second leucine zipper (LZII) of JLP was shown to be responsible for this interaction. This was shown through the use of LZII of JLP as bait in yeast two-hybrid screening of a mouse brain cDNA library. Nguyen et al. further identifies a “leucine zipper-like” domain in KLC and shows that mutation of KLC1 residues L280, L287, V294 and L301 to alanine results in loss of binding to JLP (Nguyen et al., 2005). However, this region is

unlikely to function as a leucine zipper as the residues mutated form part of the TPR domain of KLC as shown by the structure published by Zhu et al. (Zhu et al., 2012). All of the residues that were mutated are also not accessible to bind to JLP simultaneously. The structure would therefore not allow leucine zipper dimerization to occur between JLP LZII and KLC. It is more likely that one or more of the residues mutated are sequence specific elements required for binding via an alternative mechanism.

Other light chain cargo

Several other cargo that interact with the TPR domain of KLC were also identified. Saturable binding of β-amyloid precursor protein (APP) to KLC was shown with a stoichiometry of 2 APP per KLC. The apparent Kd was found to be approximately 18±4 nM for KLC1 and 16±3 nM for KLC2. The binding was also shown to be direct through GST-pulldown assays of KLC1 (GST-TPR) and purified APP-GFP (Kamal et al, 2000). Using predicted C-terminal alpha-helical subdomain of human wild-type torsinA as bait in a yeast two-hybrid assay KLC TPR was identified as a binding partner. The interaction between TorsinA and KLC1 was confirmed by GST pulldown assays and co-immunoprecipitation (Kamm et al., 2004). The C-terminal region of collapsin response mediator protein-2 (CRMP-2) (residues 440-572) was also shown to directly bind to the TPR domain of KLC through use of recombinant protein (Kimura et al., 2005). CRMP-2 is important for axon differentiation and is enriched at the distal part of growing axons in primary hippocampal neurons. The highly conserved integral membrane protein, Kidins220/ARMS was also shown to be a binding partner of KLC through yeast two-hybrid screen and confirmed though GST pulldown and co-immunoprecipitation assays. A relatively short sequence (NSQDSSIEISKLTDKVQAEYRDAYREYIAQMSQLEGGTGS) was further shown to be sufficient for the interaction between Kidins220/ARMS and KLC1, termed KLC-interacting motif (KIM). This sequence does not bear any similarities with other proteins shown to interact with KLC (Bracale et al., 2007). The interaction with Kidins220/ARMS is mediated by KLC1 residues 83–296. This region includes part of the heptad repeat region as well as a section of the TPR domain including TPR motif 1 and 2. The neuronal protein, Huntingtin-associated protein-1 (HAP-1) is another protein that has been shown to be involved in neuronal transport interacts directly with KLC2 via its C-terminus.

This was shown through yeast two-hybrid assay, GST pulldown, and co-immunoprecipitation (McGuire et al., 2006).

Thus, in a manner comparable to KHC, KLC also appears to interact with a wide range of intracellular cargoes. Again, whether there are common underlying molecular mechanisms had not been determined.

Recognition of tryptophan based motifs by KLC

There are a number of examples in eukaryotic cells where transport and trafficking machinery recognise particular peptide motifs within cargo proteins. For example, the clathrin adaptors recognise YxxΦ and acidic-dileucine motifs typically found in the cytoplasmic domains of transmembrane proteins that allow for their recruitment into vesicles. Similarly, importins can recognise mono- or bi-partite basic motifs that target proteins for nuclear import. Given this, it is perhaps surprising that motif recognition and common molecular determinants have not yet emerged as a common principle in motor-cargo recognition.

Over recent years studies have begun to suggest that a short peptide sequence characterized by a tryptophan flanked by acidic residues (tryptophan-acidic motif) is responsible for the binding of several cargo proteins to kinesin-1 (Figure 1.5). The neuronal transmembrane protein, calsyntenin-1 (CSTN-1, also referred to as alcadein) was shown to interact with the TPR domain of KLC1. GST pulldown assays demonstrated that two highly conserved tryptophan-aspartic acid containing segments (KENEMDWDDS and ATRQLEWDDS) in the cytoplasmic domain of calsyntenin-1 mediate binding to the KLC1 TPR domain. Point mutations of the tryptophan to alanine significantly reduced binding to KLC1 (Konecna et al., 2006, Araki et al., 2007). Yeast two-hybrid screen from a mouse adult brain cDNA library using caman ataxia protein, caytaxin as bait identified KLC1 to be a binding partner of caytaxin. Residues 115-120 of caytaxin (ELEWED) were shown through GST pulldown assays to be responsible for the binding to the TPR domain of KLC1 (Aoyama et al., 2009). The endosomal trafficking protein Gadkin was also shown to contain a similar motif (DLEWEDEE). Mutation of the highly conserved tryptophan results in loss of binding between KLC2 and Gadkin (Schmidt et al., 2009). More recently, similar motifs were identified in the lysosomal kinesin-1 adaptor SKIP (discussed in detail in 1.9).

Moreover, closely related motifs in Vaccinia virus transmembrane protein, A36 were found to mediate the interaction with KLC1 and KLC2 to promote the transport of poxvirus vaccinia virus from its golgi localised site of assembly to the cell periphery where it is released. In experiments where the cytoplasmic domain of A36 was removed and replaced with tryptophan acidic regions of SKIP and CSTN1, KLC was recruited and transport of vaccinia virus to the cell periphery was promoted in the absence of A36 suggesting that these motifs can function outside of the context of the host protein in a modular fashion. Dodding et al. also suggest that the tryptophan motif is often bipartite and through bioinformatic analysis identified related bipartite tryptophan-based motifs in over 450 human proteins. Kinesin-1 recruitment may therefore occur through many cargo and adaptors (Dodding et al., 2011). Yeast two-hybrid analysis using the nuclear envelope protein Nesp4 (residues 129-339) as bait, identified KLC 1-4 as possible binding partners for Nesp4. Immunofluorescence assays revealed that co-expression of Nesp4 and KLC results in accumulation of KLC at the nuclear envelope. Nesp4 was also shown to co-immunoprecipitate with KLC (Roux et al., 2009). Another Kinesin-1 binding protein, BNIP-2, functions as an adaptor involved in vesicular transportation in the cytoplasm. BNIP-2 also contains a tryptophan-acidic motif, EFEWED and was shown through immunoprecipitation to interact with KLC through the conserved WED motif (Akamatsu et al., 2015).

Zhu et al. presented the first biochemical data showing that single motifs that are 10 residues in length are sufficient in binding kinesin-1. Isothermal titration calorimetry (ITC) experiments showed that a 10 residue peptide centering on the tryptophan-acidic motif of CSTN-1 interacted with KLC1 TPR domain with a Kd of 50μM. The C-terminal 10 residues of JIP-1 were also sufficient for the interaction with KLC1 TPR domain and interacted with KLC1 TPR domain with a Kd of 9.4μM (Zhu et al., 2012). Through isothermal titration calorimetry the specific interaction between KLC1 and JIP1 were attributed to residue N343 in the fourth TPR repeat. KLC2 with the corresponding residue S328 did not interact with JIP1, however mutation of this residue within KLC2 to asparagine (N) allowed binding to JIP1. For the binding of the tryptophan-acidic motif containing protein called calsyntenin-1 a different site located within the groove not involving N343 was identified (Zhu et al., 2012). It was therefore hypothesised that whilst both bind to the concave groove, JIP1 binds to an

alternative site in the groove of the TPR domain. This work also suggested that KLC1/2 TPR domains could also confer specificity.

The TPR domains from KLC1 and KLC2, share a sequence homology of 87% identity between the two forms when residues 232 to 495 of KLC1 and 217 to 480 of KLC2 are compared (Zhu et al., 2012). How the different KLC TPR domains recognise specific cargo is not fully understood. KLC1 and KLC2 share several cargo, although there are some that bind specifically to one or the other KLC TPR domain. For example HAP1(McGuire et al., 2006), CRMP-2(Kimura et al., 2005) and CSTN-1 (Araki et al., 2007) are able to bind to both KLC1 and KLC2 whereas TorsinA (Kamm et al., 2004) and JIP1 (Zhu et al., 2012) bind preferentially to KLC1.

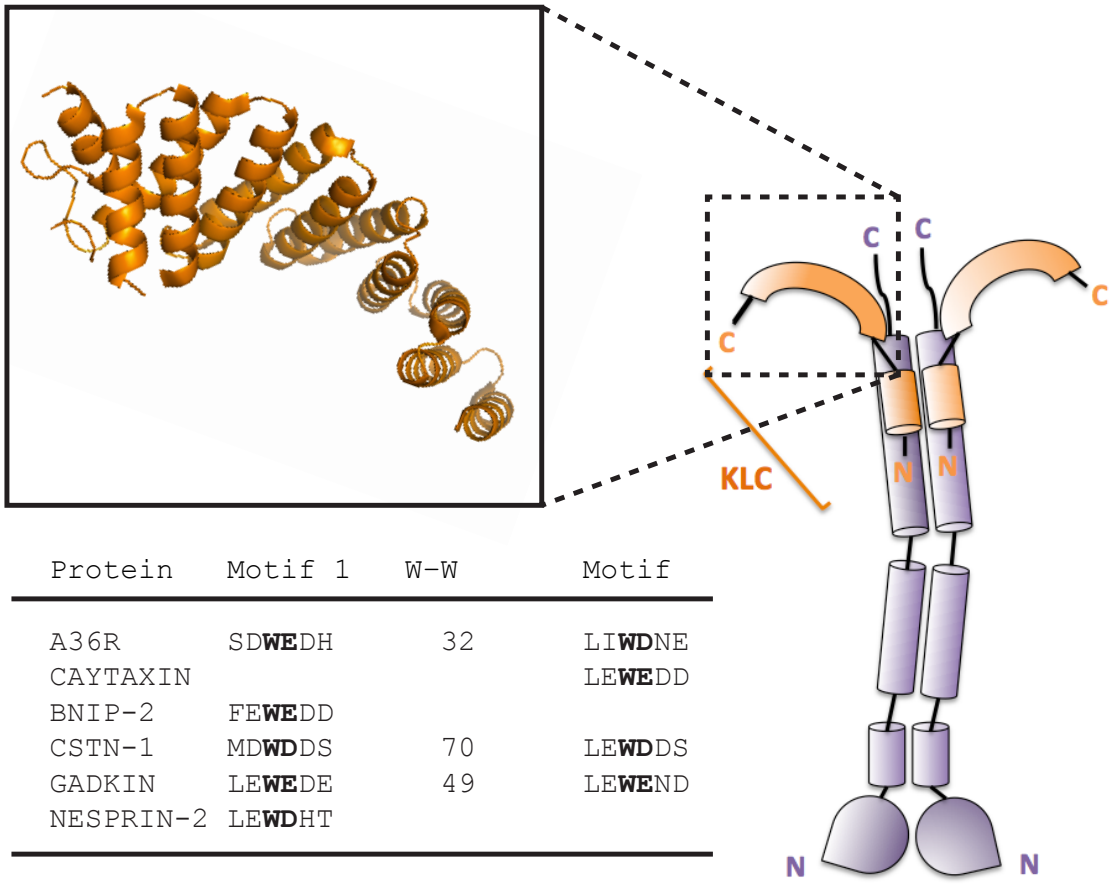

Protein	Motif 1	W–W	Motif
A36R	SD**WE**DH	32	LI**WD**NE
CAYTAXIN			LE**WE**DD
BNIP-2	FE**WE**DD		
CSTN-1	MD**WD**DS	70	LE**WD**DS
GADKIN	LE**WE**DE	49	LE**WE**ND
NESPRIN-2	LE**WD**HT		

Figure 1.5 Functional tryptophan-acidic KLC binding motifs are found in a wide range of proteins.

Kinesin Heavy Chain (KHC) is shown in purple, Kinesin Light Chain (KLC) is in orange with the tetratricopeptide repeat (TPR) domain boxed. The structure shown in the solid box is that of the KLC2 TPR domain PDB code 3CEQ (Zhu et al., 2012). The table shows the WD/E motifs in proteins previously shown to interact with KLC. W–W indicates the number of residues separating the two tryptophans if there are two motifs in the protein.

1.6.5 Regulation of cargo binding to kinesin-1

1.6.5.1 Phosphorylation of kinesin-1

How kinesin-1 distinguishes between different cargo and is able to specifically transport each cargo, as well as how loading and unloading of cargo in specific locations occurs is not fully understood. Phosphorylation of Kif5-KLC complexes by protein kinase A (PKA) has however been shown to inhibit association of the kinesin-1 motor with synaptic vesicles (Sato-Yoshitake et al., 1992). Glycogen synthase kinase 3 has also been shown to phosphorylate KLC and inhibit the association of kinesin-1 with membrane-bounded organelles as well as signaling protein, Smad2 (Morfini et al., 2002, Manser et al., 2012, Morfini et al., 2006). More recent work by Vagnoni et al. has shown that phosphorylation of ser460 in KLC1 reduces binding of calsyntenin, but does not affect the binding of HAP1A, CRMP2, JIP1 or Kidins220 and is therefore able to modulate cargo selectivity. Ser460 is a predicted mitogen-activated protein kinase (MAPK) target and an extracellular-signal regulated kinase (ERK) has been shown to phosphorylate this residue *in vitro* (Vagnoni et al., 2011). As mentioned in section 1.6.4.2 JIP1 is suggested to bind to an alternate site within the TPR domain of KLC when compared to calsyntenin-1. The binding of CRMP-2 and Kidins220/ARMS to KLC TPR domain is also not achieved through a tryptophan-acidic motif. Phosphorylation may therefore only affect tryptophan acidic motif containing cargo that is likely to bind within the same region as calsyntenin-1, and in such a way the regulation by phosphorylation of Ser460 may be less specific and affect other cargo that binds within the same region within the TPR groove.

1.6.5.2 Phosphorylation of cargo

Phosphorylation of cargo functioning as adaptors can also regulate association of other cargo with motors. For example UNC76 binds directly to Kif5, and functions as a Kif5 adaptor by associating with synaptotagmin-1. Phosphorylation of UNC76 by UNC51 (autophagy-related kinase) allows UNC76 to interact with synaptotagmin-1. Dephosphorylation results in the loss of this association (Toda et al., 2008). Phosphorylation of the tail (at ser 1029) by Ca^{2+}/calmodulin dependent protein kinase (CaMKII) has been shown to disrupt the interaction of kinesin-2 family, Kif17 with LIN10 (also known as MINT1) which in turn results in loss of binding of N-methyl-D-aspartate receptor

subunit NR2B containing vesicles through disruption of the scaffold complex LIN10-LIN2-LIN7 (Guillaud et al., 2008). This raises the question whether phosphorylation of kinesin-1 heavy chain tail could also play a role in the regulation of cargo binding.

1.6.5.3 GTPase-activating proteins and guanine nucleotide exchange factors.

GTPase-activating proteins (GAPs) and guanine nucleotide exchange factors (GEFs) may also regulate the association and dissociation of kinesins and their cargo. Guanosine triphosphate (GTP) bound Rab GTPases binds to Rab effector proteins. The Rab effector protein DENN/MADD binds preferentially to the GTP bound form of Rab3. DENN/MADD interacts with kinesin-3 family proteins, Kif1A and Kif1Bβ. Another example of a Rab effector is the kinesin-6 family protein, Kif20B, that specifically interacts with the GTP bound form of Rab6 (Echard et al., 1998). The kinesin-1 cargo SKIP has also been shown to bind specifically to the GTP-bound form of Arl8. Arl8 was shown to be responsible for attaching SKIP to lysosomes (Rosa-Ferreira and Munro, 2011).

1.6.5.4 Calcium levels

Calcium levels may also regulate cargo transport by kinesin-1. Kinesin-1 heavy chain interacts with the transmembrane protein of the outer mitochondrial membrane, Miro via the adaptor protein, Milton (Glater et al., 2006, Stowers et al., 2002, Fransson et al., 2006). EF hand motifs of Miro mediate calcium-dependent arrest of mitochondrial motility. Several models have been proposed describing how the arrest in motility occurs, but there is little consensus (Saotome et al., 2008, Wang and Schwarz, 2009, Macaskill et al., 2009).

Regulation of cargo transport by kinesin-1 is not fully understood. The examples given here have suggested possible mechanisms of regulation through phosphorylation of cargo, GTPases and calcium levels.

1.6.6 Motility of Kinesin-1

The Kinesin-1 motor takes 8nm steps in a hand-over hand stepping mechanism (Asbury et al., 2003, Kaseda et al., 2003, Svoboda et al., 1993, Yildiz et al., 2004). Each step involves the hydrolysis of a single ATP molecule (Schnitzer and Block, 1997). Kinesin-1 is highly processive and maintains an interaction

with the microtubule for several steps before dissociating from the microtubule (Block et al., 1990, Hackney, 1995, Howard et al., 1989). Figure 0.4 shows a model of the kinesin-1 hand over hand stepping mechanism.

When kinesin-1 is not bound to microtubules, ADP binds to both heads. Once one head attaches to the microtubule, it releases ADP. The head that remains detached retains the ADP molecule (Hackney, 1994). ATP then binds to the attached head, resulting in a conformational change in the neck linker (indicated by >>). Neck-linker docking is the binding of a 15 amino acid length peptide (the neck linker) to the catalytic core of the motor (Rice et al., 1999, Asenjo et al., 2006, Clancy et al., 2011, Sindelar and Downing, 2010).

The neck-linker induces internal strain between the two heads (Yildiz et al., 2008) to enable the movement of the detached head to the forward binding site. The head binds strongly to the microtubule releasing ADP. The internal strain created, prevents the binding of ATP to the forward head (red) (Hackney, 2005, Uemura and Ishiwata, 2003). Only after hydrolysis of ATP and the release of phosphate by the rear head is the internal strain released and ATP able to bind to the forward head. At this point the heads have changed positions and kinesin-1 has moved 8nm along the microtubule (Kawaguchi, 2008). This mechanism requires coordinated movement of the front and rear motor domains and has been proposed to be facilitated by a gating mechanism. Two main models have been proposed; one involves gating of the front motor with inhibited nucleotide binding to the front head (Klumpp et al., 2004, Rosenfeld et al., 2001) while the other proposes gating of the rear motor involving an accelerated ATP hydrolysis of the rear motor and so an accelerated release of the rear head (Crevel et al., 2004, Schief et al., 2004). More recent evidence has been provided that the supports the front head gating mechanism suggesting that kinesin-1 is gated by the backward orientation of its neck linker until the rear head releases from the microtubule (Dogan et al., 2015).

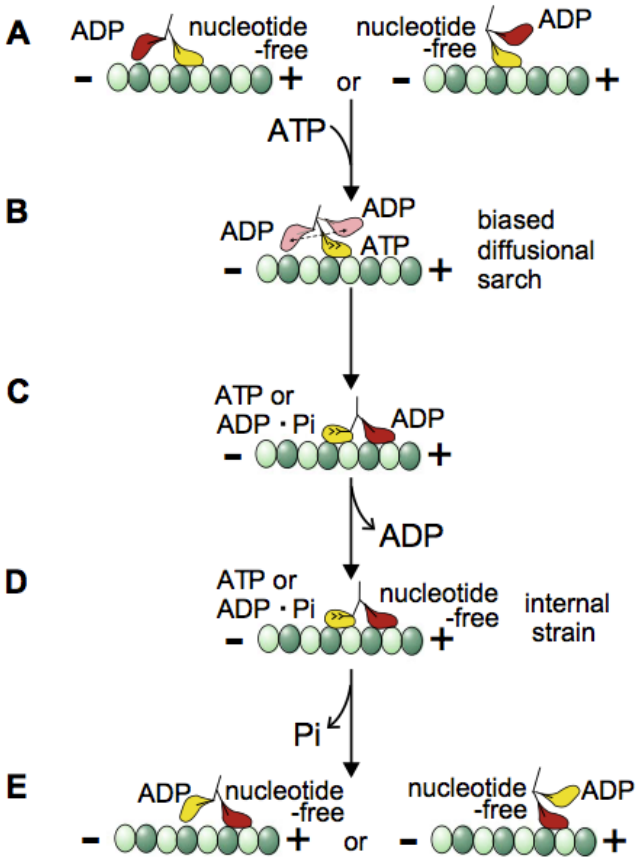

Figure 1.6. Model of the kinesin-1 stepping mechanism
When kinesin-1 is not bound to microtubules, ADP binds to both heads. (A) Once one head attaches to the microtubule, it releases ADP. The head that remains detached retains the ADP molecule. (B) ATP then binds to the attached head resulting in neck-linker docking (indicated by >>) and induces internal strain between the two heads (Yildiz et al., 2008). This enables a biased diffusional search by the detached head for the next forward binding site. (C and D) The head binds strongly to the microtubule and ADP is released. The internal strain created, prevents the binding of ATP to the forward head (red). (E) Only after hydrolysis of ATP and the release of phosphate by the rear head is the internal strain released and ATP able to bind to the forward head. At this point the heads have changed positions and kinesin-1 has moved 8nm along the microtubule. (Taken from (Kawaguchi, 2008).

1.6.7 Autoinhibition

When not transporting cargo, kinesin-1 adopts a folded conformation, where the heavy chain C-terminal tail inhibits the motor domain (Figure 1.8). The folded conformation was first observed in bovine adrenal medulla kinesin, by electron microscopy using low-angle rotary shadowing technique (Hisanaga et al., 1989). Subsequently sedimentation experiments illustrated that the sedimentation coefficient increased upon lowering the ionic strength and that the folding was an intrinsic property of kinesin heavy chains (Hackney et al., 1992, Stock et al., 1999).

The tail region of KHC that contains a highly conserved isoleucine-alanine-lysine motif (IAK) and surrounding residues (893-937) were shown to interact in a salt dependent manner with the motor region (1-365) (Stock et al., 1999). An increase in the salt concentration lowers the affinity of the interaction. Friedman and Vale showed that the full length motor moved 10 times less frequently and exhibits discontinuous movement compared to the truncated kinesin lacking the C-terminal tail (Friedman and Vale, 1999). The C-terminal tail domain of KHC also negatively regulates the ATPase activity of the motor. Low ATPase activity is observed for the native kinesin-1 tetramer compared to a truncated kinesin-1 where the tail domain is deleted. Deletion of the hinged region that is required for the folding of KHC into the autoinhibited conformation also results in increased ATPase activity (Coy et al., 1999). This regulation is abolished upon deletion of the IAK region (Hackney and Stock, 2000). Further work refined the region of the C-terminal tail required for autoinhibition and highlighted the importance of the conserved IAK motif and surrounding residues (Yonekura et al., 2006, Dietrich et al., 2008).

A major step in understanding came with the discovery that only one of the two tail peptides is necessary for binding and inhibition of ADP release from both motor domains, leading to proposition of the ‘half-site’ inhibition mechanism (Hackney et al., 2009). This was verified when the X-ray crystal structure of this tail monomer-motor dimer was recently solved and offered important insights into the mechanism of autoinhibition (Kaan et al., 2011). The location and function of the second tail peptide in this autoinhibited state is not known. The motor tail complex further revealed that in the autoinhibited conformation, movement of the motor domains are restricted due to cross-linking of the motor domains at the coiled-coil and also the tail interface (Figure

1.7). This prevents undocking of the neck linker and in turn prevents ADP release. The structure revealed that the binding site for the tail domain is on the opposite side of the motor domain to the nucleotide-binding site, ruling out previously suggested models involving the tail blocking the release of ADP and the tail peptide interacting with the Switch I region (Dietrich et al., 2008). The possibility that the tail could interact with the neck linker or coiled coiled region is also ruled out. The structure also shows the microtubule binding sites exposed, therefore ruling out steric interference with microtubule binding (Kaan et al., 2011).

Although this folding can occur in the absence of kinesin light chains, the light chains appear to be able to affect autoinhibition. However, their role is controversial. Immunofluorescence microscopy and microtubule co-sedimentation experiments demonstrated that the binding of KHC to microtubules is inhibited by co-expression of KLC, suggesting that they support the autoinhibited state (Verhey et al., 1998). ATPase activity is also further reduced in the presence of KLC (Coy et al., 1999). This enhanced inhibition has been suggested to occur by KLC pushing the KHC motor domains apart, however this explanation would appear to be incompatible with the double lockdown mechanism described above (Cai et al., 2007). Wong and Rice however suggest that KLC are activators of kinesin-1, and help to destabilise the autoinhibited state, through suppressing the tail-head and tail microtubule interactions (Wong and Rice, 2010). The Verhey group proposed a model where cargo binding to both KHC and KLC is required for the release of autoinhibition and activation of transport of Kinesin-1 (Blasius et al., 2007).

1.6.8 Autoinhibition in other kinesins

Kinesin-2, kinesin-3, kinesin-7 and kinesin-13 families have also been shown to be regulated by autoinhibition. The kinesin-2 family member, Kif17, as well as the Kinesin-7 family member, CEnPE, is found in an autoinhibited state within cells. The mechanism of autoinhibition appears to be similar to that of kinesin-1 as it involves direct interactions of the C-terminal tail with their motor domains (Imanishi et al., 2006, Espeut et al., 2008).

Autoinhibition of Cenp-E is relieved by phosphorylation of the Cenp-E tail by MPS1 and/or CDK1-cyclin B. Kif17 is activated by protein kinase C (PKC) allowing it to bind to microtubules. Kif17 has several predicted PKC

phosphorylation sites and could therefore be regulated by PKC directly. PKC could on the other hand also prevent cargo that may be required for the activation of the Kif17 motor from binding (Espenel et al., 2013).

The C-terminus of the kinesin-13 motor, MCAK has also been shown to bind to the two motor domains and regulates its activity through this conformational switch. Tubulin is suggested to trigger the dissociation of the C-terminal tail from the motor. MCAK functions as a microtubule depolymerase that regulates microtubule dynamics (Talapatra et al., 2015).

Kinesin-3 motor, Kif1A also exists endogenously as an autoinhibited dimer. The forkhead associated (FHA) and the coiled-coil 2 (CC2) domains have been shown to contribute to autoinhibition by blocking microtubule binding. Additional mechanisms, may involve the coiled coil 1 (CC1) domain. Similar to kinesin-1, activation occurs upon cargo binging (Hammond et al., 2009).

For all the kinesin motors mentioned, autoinhibition prevents unnecessary ATP hydrolysis and movement of kinesin motors on the microtubule tract as well as maintains the proper cellular localisation of the motors.

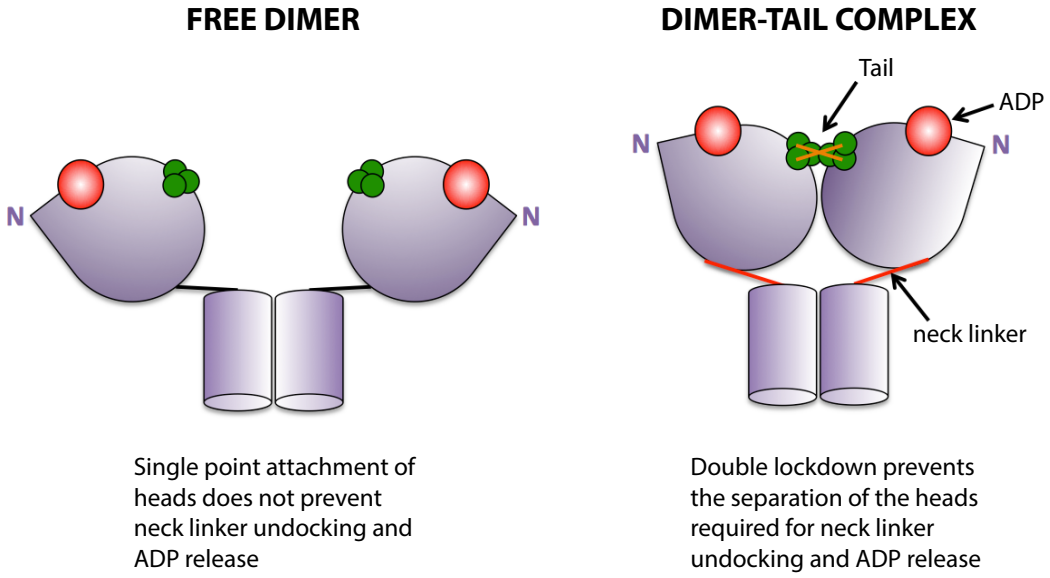

Figure 1.7. Model for double lockdown mechanism of autoinhibition
The kinesin heavy chain motor domain is represented in purple. The double lockdown mechanism prevents the separation of the motor domains that is required for neck linker (red, sticks) undocking and ADP (red, spheres) release. Ser181 residues (green spheres) are apart in the free dimer bit close together in the presence of tail (orange, sticks) binding and are on opposite sides of the tail interface (based on Kaan et al 2011).

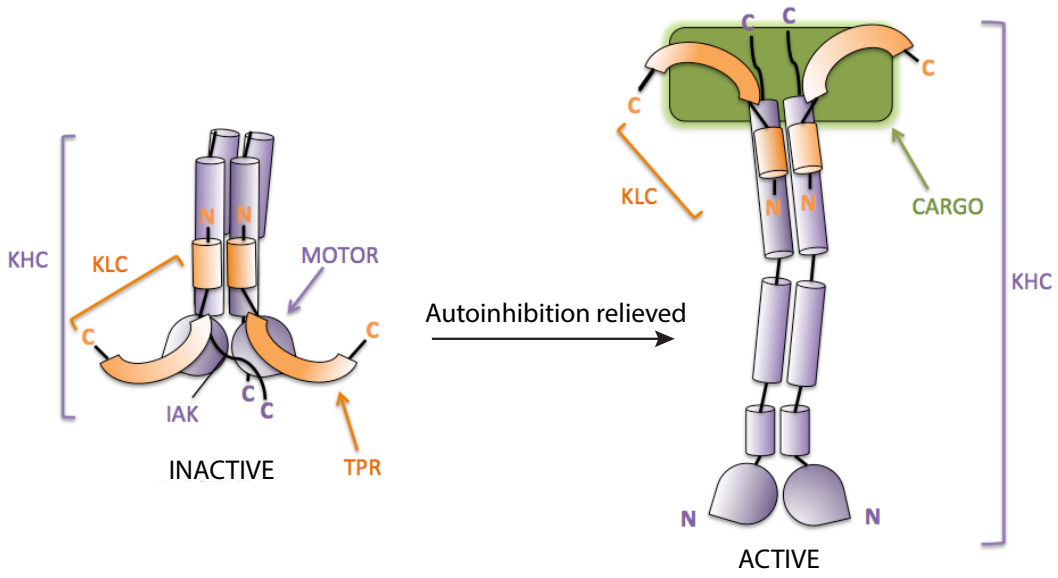

Figure 1.8. Schematic of Kinesin-1 in a folded inactive state and a cargo bound unfolded active state.
Kinesin heavy chain (purple), Kinesin light chain (orange) and Cargo (green)

1.7 Coordination and competition between motors in bi-directional transport

Live cell imaging as well as in vitro studies have shown that many cargo proteins are transported bi-directionally by kinesin-1 and dynein to the plus and minus ends of microtubules, respectively. Numerous cargos have been shown to bind to oppositely directed motors simultaneously (Soppina et al., 2009, Hendricks et al., 2010, Encalada et al., 2011). 1-2 Kinesins and 6-12 dyneins have been shown to act together to move a single organelle along the microtubule (Hendricks et al., 2012, Hendricks et al., 2010, Rai et al., 2013). Bi-directional movement of cargo has been described by several models (Gross, 2004, Muller et al., 2008, Fu and Holzbaur, 2014). Two models that describe the interactions of opposing kinesin and dynein motors to the same cargo are the tug of war model and the coordination model.

In the tug of war model the team of motors that applies the greater force determines the direction of transport and the coordination model suggests that motors are regulated so that only a single type of motor is switched on at any one time. With regard to how motors are able to coordinate the direction of movement, motors with opposite-polarity have been shown to activate one another by physical or mechanical interactions (Ally et al., 2009, Encalada et al., 2011). The physical contact may occur through the direct interaction of KLC with dynein intermediate chain or through the interaction of KLC with other dynein accessory subunits (Ligon et al., 2004, Martin et al., 1999). The mechanical activation of opposite polarity motors has been suggested to occur through plus and minus end directed motors pulling against each other (Ally et al., 2009). Motors of opposite polarity are also able to bind to the same cargo or adaptor proteins. Cargo proteins or adaptors may therefore play a role in the coordination of the direction of transport. For example, huntingtin binds directly to the intermediate chain of dynein (Caviston et al., 2007) as well as to HAP1 (huntingtin associated protein 1). HAP1 also interacts with the p150Glued subunit of dynactin (Engelender et al., 1997) as well as interacting with kinesin-1 (McGuire et al., 2006).

Phosphorylation of cargo can also alter the directionality of transport. JIP1 binds directly to KHC stalk and tail and the p150Glued subunit of dynactin. Phosphorylation of residue S421 of JIP1 by JNK is shown to enhance binding to

KHC C-terminal tail and promotes anterograde transport (Fu and Holzbaur, 2013).

Inhibition or knockout studies have however shown that inhibiting one motor results in reduced transport in both directions, which suggests co-dependence between the motors. In order to resolve this, three models were proposed in conjunction with the tug of war model by Hancock involving microtubule tethering, mechanical activation and steric disinhibition. In the microtubule tethering mechanism motors are suggested to remain weakly bound to the microtubule when inactive and bind strongly when the motor is active. Inhibition of one motor results in loss of cargo transport of the opposing motor due to a reduction in tethering, which may also lead to dissociation of the cargo. In the mechanical activation mechanism motors are activated by the opposing motor pulling on the cargo. When the opposing motor is inhibited, cargo transport does not occur due to there not being opposing forces and the motor being inactive. In the steric disinhibition mechanism, cargo bound motors remain in an autoinhibited state. Inhibition is relieved and transport commences upon the direct interaction of the opposing motor or other regulatory proteins. Inhibition of a motor in one direction results in the reduced motility of the opposing motor due to the one motor no longer being activated (Hancock, 2014).

1.8 Role in disease

Disruption of transport can occur due to mutations in the genes that encode motor proteins or cargo (that are associated either directly or indirectly with motor proteins). Defects in transport have been shown to be associated with several neurodegenerative and neurodevelopmental diseases such as Huntington's disease, Alzheimer's disease and multiple forms of Charcot–Marie–Tooth disease (CMT) (Millecamps and Julien, 2013, Hirokawa et al., 2010, De Vos et al., 2008).

Huntington's disease is caused by polyQ stretches within the huntingtin protein. The underlying mechanism that results in Huntington's disease remains unclear. Huntingtin associated protein-1, HAP1, binds KLC1, highlighting the involvement of HAP-1 in anterograde transport in neuronal cells (McGuire et al., 2006). HAP1-Kif5 complex mediates delivery of $GABA_A$ receptors to synapses and this transport is disrupted by mutant huntingtin (Twelvetrees et al., 2010). A

key role of huntingtin is to promote BDNF transport (involving HAP1 and dynactin) and over expression of mutant huntingtin disrupt the transport of BDNF (Gauthier et al., 2004). Phosphorylated huntingtin promotes kinesin-1 dependent anterograde transport and dephosphorylated huntingtin results in detachment of kinesin-1 and an increase in retrograde transport of vesicles and proteins including BDNF (Colin et al., 2008). Huntingtin also binds to directly to dynein intermediate chain and acts in a complex with dynactin and huntingtin-associated protein-1 (HAP-1) to facilitate vesicular transport in the retrograde direction (Caviston et al., 2007). Wong and Holzbaur showed that polyQ-huntingtin disrupts predominantly retrograde transport of autophagosomes (Wong and Holzbaur, 2014).

Alzheimer's disease is characterised by neurofibrillary tangles containing paired helical filaments with hyperphosphorylated microtubule associated protein tau as well as amyloid plaques that are areas of degenerating neurites surrounding a core of amyloid-β peptide. The amyloid- β peptide is derived from serial proteolysis of APP by β and γ-secretases. Axonal transport defects have been described as an early pathological feature of Alzheimer's disease (Hirokawa et al., 2010). It has been a controversial issue whether transport defects are caused by amyloid-β accumulation or arise due to it. APP was initially shown to interact directly with kinesin light chain (Kamal et al., 2000). However, Lazarov et al. give evidence that the interaction is not direct and show that endogenous APP does not co-fractionate with kinesin-1 in membrane fractions or detergent homogenates prepared from mouse brain (Lazarov et al., 2005). Satpute-Krishnan supports the first study that there is a direct interaction between APP and kinesin-1. They identify a C-terminal short peptide sequence from APP and show that it is sufficient to mediate anterograde transport of peptide-conjugated beads in the squid giant axon (Satpute-Krishnan et al., 2006). Morihara et al. identify kinesin light chain-1 splice variant E (KLC1vE) as a modifier of amyloid-β accumulation (Morihara et al., 2014). Gan et al. propose that KLC1vE triggers amyloid-β accumulation through reducing APP transport. The transport of other KLC1 cargo that regulate amyloidogenesis is also impaired by KLC1vE (Gan et al., 2015). Anterograde APP transport has also been shown to be mediated by direct binding to kinesin-1 cargo JIP-1 (Scheinfeld et al., 2002). Fu et al. also show that JIP1 interacts with p150Glued, a subunit of the retrograde dynein–dynactin complex and phosphorylation of

JIP-1 alters KHC activation and also the direction of APP transport (Fu and Holzbaur, 2013). siRNA knockdown of calsyntenin-1 has also been shown to disrupt axonal transport of APP, suggesting that APP is co-transported with calsyntenin-1 through axons (Vagnoni et al., 2012).

A small heat shock protein, HSPB1, is a mutant in CMT disease and increases the stability of microtubules (Almeida-Souza et al., 2011). How exactly the increased stability can cause CMT is not known although it has been suggested that the stabilisation blocks remodeling of the cytoskeleton at synaptic sites (Conde and Caceres, 2009). Another possibility is that the mutant form of HSPB1 binds along the microtubule and sterically block transport (Dixit et al., 2008). Kif5A mutations have also been associated with Charcot-Marie-Tooth Type 2 (CMT2) (as well as Hereditary Spastic Paraplegia (HSP)) (Crimella et al., 2012). The mechanism of mutant Kif5A involvement in the progressive axonal degeneration characteristic of these diseases is not well understood. Campbell et al. show that mutation of Kif5Aa diminishes axonal mitochondrial density in peripheral sensory neurons, which correlates with axonal degeneration and decreased sensory function (Campbell et al., 2014).

Viruses as well as bacteria have been shown to hijack the cell's internal transport system through binding to these motor proteins (Dodding and Way, 2011, Boucrot et al., 2005). Dodding et al. showed that the vaccinia integral membrane protein, A36 interacts with KLC TPR domain through highly conserved tryptophan-acidic motifs and allows for the kinesin-1-dependent transport of the virus to the cell periphery (Dodding et al., 2011). Adenovirus subunit hexon binds directly to dynein through its intermediate and light intermediate chains and recruits dynein for transport to the nucleus (Bremner et al., 2009). Both kinesin-1 as well as dynein bind to the herpes simplex virus (HSV1) tegumented capsid using different inner tegument structures (Radtke et al., 2010). HSV1 tegument protein, US11 interacts with the C-terminal tail of KHC (Diefenbach et al., 2002b). However, virions that lack US11 have also been shown to bind to kinesin-1. Radtke et al. suggest that HSV1 uses different structural features of the inner tegument, such as pUS3, pUL36, pUL37, ICP0, pUL14, pUL16, and pUL21 to recruit dynein or kinesin-1 (Radtke et al., 2010). In the case of HIV-1, inhibition of dynein disrupts viral transport towards the nucleus during the early stages of infection (McDonald et al., 2002).

The PH domain of the kinesin-1 cargo SKIP binds the bacterial effector, SifA upon infection with salmonella (Boucrot et al., 2005). The SifA:SKIP interaction is required for the kinesin-1 dependent transport of vesicles that bud from the Salmonella-containing vacuole to the cell periphery (Dumont et al., 2010). Continued research into the molecular mechanisms involved in cargo recognition as well as activation should provide insights for future therapeutic approaches.

1.9 SKIP

SKIP (SifA and kinesin-interacting protein, also known as PLEKHM2) contains an N-terminal RPIP8, UNC-14, and NESCA (RUN) domain and a C-terminal pleckstrin homology (PH) domain (Boucrot et al., 2005)(Figure 1.9). SKIP contains a pair of W-acidic motifs centered at amino acid positions 207 and 208 (WD) and 236 and 237 (WE) that fall within the N-terminal kinesin-1 binding region (residues 1 to 310) that has been shown to interact with KLC (Rosa-Ferreira and Munro, 2011, Dumont et al., 2010).

The PH domain binds the bacterial effector, SifA upon infection with Salmonella (Boucrot et al., 2005). Replication of Salmonella occurs within the membrane-bound compartment called the Salmonella-containing vacuole (SCV) within cells (Boucrot et al., 2003). In infected cells, SifA contributes to the fission of vesicles from the bacterial SCV. The SifA:SKIP interaction is required for the kinesin-1 dependent transport of vesicles that bud from the SCV to the cell periphery (Dumont et al., 2010).

SKIP has been shown to be important in lysosomal trafficking to the cell periphery (Rosa-Ferreira and Munro, 2011). Recruitment of lysosomes to kinesin-1 occurs by the initial recruitment of the small GTPase Arl8 by the BORC complex, followed by the Arl8 dependent recruitment of SKIP via its RUN domain (Pu et al., 2015, Rosa-Ferreira and Munro, 2011). Arl8b associates with lysosomal membranes via its acetylated amino-terminal amphipathic helix (Hofmann and Munro, 2006). The acetylated N-terminal helix ensures tight membrane association of Arl8-GTP. GTP hydrolysis results in Arl8-GDP dissociating from the lysosomal membrane. (Bagshaw et al., 2006). SKIP interacts directly with kinesin-1 via KLC. Rosa-Ferreira et al. showed that when SKIP is co-expressed with Arl8b, there is a peripheral scattering of lysosomes. When a mutant form of SKIP where both tryptophan acidic motifs are mutated is

co-expressed with Arl8b, peripheral scattering of lysosomes is not induced. Instead there is an accumulation in the perinuclear region (Rosa-Ferreira and Munro, 2011). This demonstrates that the movement of lysosomes to the periphery is dependent on the ability of SKIP to bind kinesin-1. Dodding et al., 2011 showed that mutation of the separate tryptophan acidic motifs of SKIP resulted in a reduction in kinesin-1 dependent transport of vaccinia virus to the cell periphery with the first tryptophan acidic motif (WD) having a much greater effect than mutation of the second tryptophan acidic motif (WE) (Dodding et al., 2011).

This combination of clear interaction with kinesin-1 and convenient functional assays makes SKIP an ideal candidate to pursue further studies on the mechanisms underlying kinesin-1 cargo recognition.

1.10 Project aims

Despite the large diversity in kinesin-1 cargo, it is emerging that at least for KLC, there may be common underlying principles and molecular mechanisms that support cargo recognition. This must be intimately related to the control of the activity of the motor. For KLC, it seems clear that a crucial element of this is achieved by interaction of the TPR domain with short linear peptide motifs. The aim of this thesis is to further investigate these mechanisms with the goal of providing a framework for understanding the general principles of kinesin-1 cargo recognition. I have pursued this by attempting a detailed molecular dissection of the mechanism of recognition of the lysosomal cargo adaptor SKIP which carries a pair of W-acidic motifs, seeking to apply the knowledge gained to other kinesin-1 cargo.

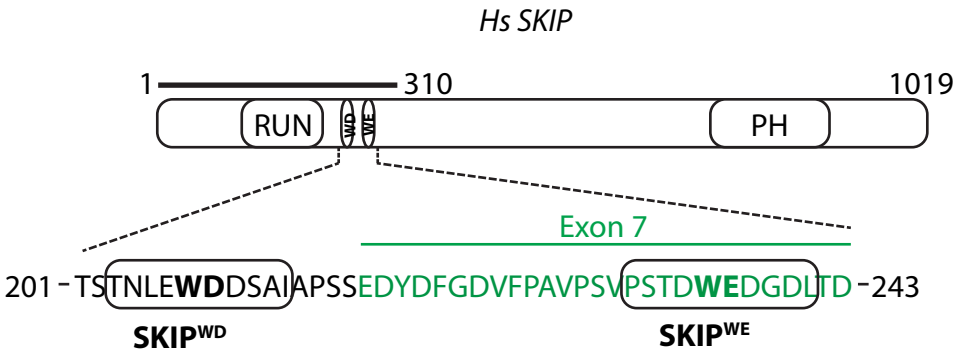

Figure 1.9. Schematic of human SKIP
The two Tryptophan-acidic motifs within the N-terminal kinesin-1 binding region (residues 1 to 310) are highlighted ($SKIP^{WD}$, $SKIP^{WE}$). The RUN domain and the C-terminal pleckstrin homology (PH) domain are also labeled. The region in green (exon 7) is not expressed in a certain splice variant of SKIP.

CHAPTER 2 . MATERIALS AND METHODS

2.1 Recombinant DNA

2.1.1 Polymerase chain reaction (PCR)

Polymerase chain reactions were carried out to amplify sections of DNA from plasmids. Taq plus precision polymerase (Agilent) was used in all cases. Primers were purchased from Sigma-Aldrich. A typical reaction consisted of 100ng template DNA, 0.5µl of each primer at 100µM, 1µl 10mM dNTP's, 10µl Polymerase buffer, and 1µl polymerase made up to 100µl with H_2O. Using a BioRad C1000 thermal cycler, reactions were subject to a 2 minute denaturing step at 95°C, followed by 25 cycles of 95°C for 30 seconds, 55°C for 1 minute and 72°C for 1 minute per kb of sequence to be amplified. Reactions were completed by a 7 minute incubation at 72°C.

2.1.2 Site-directed mutagenesis

Site directed mutagenesis was carried out according to the guidelines in the Quickchange mutagenesis kit (Stratagene). Complementary oligonucleotides were designed 20-40 nucleotides in length to target the region of interest whilst incorporating one or more nucleotide changes. A list of primers used is shown in Table 1. A typical reaction consisted of 100ng template plasmid DNA, 125ng of each primer, 1µl 10µM dNTP's, 1µl (2.5U) Native Pfu Polymerase, and 10µl 10x polymerase buffer made up to 100µl with H_2O. After 3 minute 95°C denaturing step, reactions were subjected to thermal cycling of 12-18 cycles of 1 minute at 95°C, 1 minute at 55°C and 1 minute per kilobase (kb) of template plasmid at 68°C. After thermal cycling, reactions were incubated for 20 minutes at 37°C in the presence of 1µl Dpn1 to digest methylated template DNA. 5µl of this reaction was used to transform Top 10 competent cells (Invitrogen). Colonies were picked after 24 hours and bacterial cultures prepared for small scale (mini prep) or large scale (midi prep). Plasmid integrity was verified by restriction enzyme digestion and the confirmation of the correct mutation by DNA sequencing.

Table 1. Primers

Lab name		Sequence
AS1	msKLC2 R251D F	5' CATCCTGGCACTGGTTTATGACGACCAGAATAAGTACAAG 3'
AS2	msKLC2 R251D R	5' CTTGTACTTATTCTGGTCGTCATAAACCAGTGCCAGGATG 3'
AS3	msKLC2 R312E F	5' GAGCACTGGAGATCGAGGAGAAGGTCCTG 3'
AS4	msKLC2 R312E R	5' CAGGACCTTCTCCTCGATCTCCAGTGCTC 3'
AS5	msKLC2 N287L F	5' CTGCGACCCTCAACCTTCTGGCTGTTCTC 3'
AS6	msKLC2 N287 R	5' GAGAACAGCCAGAAGGTTGAGGGTCGCAG 3'
AS7	msKLC2 L291D F	5' CAACAATCTGGCTGTTGACTACGGCAAACGGGG 3'
AS8	msKLC2 L291D R	5' CCCCGTTTGCCGTAGTCAACAGCCAGATTGTTG 3'
AS9	msKLC2 R312A F	5' CAAGAGAGCACTGGAGATCGCAGAGAAGGTCCTGGGCAA G 3'
AS10	msKLC2 R312A R	5' CTTGCCCAGGACCTTCTCTGCGATCTCCAGTGCTCTCTTG 3'
AS11	msKLC2 L333K F	5' CAACCTGGCCTTGAAGTGCCAGAACCAGG 3'
AS12	msKLC2 L333K R	5' CCTGGTTCTGGCACTTCAAGGCCAGGTTG 3'
AS13	msKLC2 V290K F	5' CCTCAACAATCTGGCTAAGCTCTACGGCAAACGGG 3'
AS14	msKLC2 V290K R	5' CCCGTTTGCCGTAGAGCTTAGCCAGATTGTTGAGG 3'
AS15	msKLC2 V290Y F	5' CCTCAACAATCTGGCTTATCTCTACGGCAAACGG 3'
AS16	msKLC2 V290Y R	5' CCGTTTGCCGTAGAGATAAGCCAGATTGTTGAGG 3'
AS17	msKLC2 K325E F	5' GTTTCACCCAGATGTGGCCGAACAGCTCAGCAACCTGGCC 3'
AS18	msKLC2 K325E R	5' GGCCAGGTTGCTGAGCTGTTCGGCCACATCTGGGTGAAA C 3'
AS19	msKLC2 K325A F	5' CCAGATGTGGCCGCGCAGCTCAGCAAC 3'
AS20	msKLC2 K325A R	5' GTTGCTGAGCTGCGCGGCCACATCTGG 3'
AS21	msKLC2 N329L F	5' CCAAGCAGCTCAGCTTACTGGCCTTGCTGTGC 3'
AS22	msKLC2 N329L R	5' GCACAGCAAGGCCAGTAAGCTGAGCTGCTTGG 3'
AS23	msKLC2 C305S F	5' GCTGAGCCACTGAGCAAGAGAGCAC 3'
AS24	msKLC2	5' GTGCTCTCTTGCTCAGTGGCTCAGC 3'

	C305S R	
AS25	msKLC2 V290A F	5' CAACAATCTGGCTGCTCTCTACGGCAAAC 3'
AS26	msKLC2 V290A R	5' GTTTGCCGTAGAGAGCAGCCAGATTGTTG 3'
AS27	msKLC2 L291T F	5' CAACAATCTGGCTGTTACCTACGGCAAACGGGG 3'
AS28	msKLC2 L291T R	5' CCCCGTTTGCCGTAGGTAACAGCCAGATTGTTG 3'
AS29	msKLC2 L291A F	5' CAATCTGGCTGTTGCCTACGGCAAACGGG 3'
AS30	msKLC2 L291A R	5' CCCGTTTGCCGTAGGCAACAGCCAGATTG 3'
AS31	msKLC2 L333D F	5' CTCAGCAACCTGGCCTTGGACTGCCAGAACCAGGGCAAA G 3'
AS32	msKLC2 L333D R	5' CTTTGCCCTGGTTCTGGCAGTCCAAGGCCAGGTTGCTGAG 3'
AS33	msKLC2 L286L F	5' GTGGCTGCGACCCTCCTAAATCTGGCTGTTCTC 3'
AS34	msKLC2 L286L R	5' GAGAACAGCCAGATTTAGGAGGGTCGCAGCCAC 3'
AS35	msKLC2 R270D F	5' GATGCCCTGGCTATCGACGAAAAGACACTGGGC 3'
AS36	msKLC2 L270D R	5' GCCCAGTGTCTTTTCGTCGATAGCCAGGGCATC 3'
AS37	msKLC2 R251A F	5' CCTGGCACTGGTTTATGCGGACCAGAATAAGTAC 3'
AS38	msKLC2 R251A R	5' GTACTTATTCTGGTCCGCATAAACCAGTGCCAGG 3'
AS62	JIP1(C11) Nde1 F	5'TATGTACACCTGCCCCACAGAAGATATCTACCTGGAGAC GGGGAGTACGGGGAGTACGGGGAGTACGGGGAGTCA 3'
AS63	JIP1(C11) Nde1 R	5'TATGACTCCCCGTACTCCCCGTACTCCCCGTACTCCCCG TCTCCAGGTAGATATCTTCTGTGGGGCAGGTGTACA 3'
AS66	rKIF5C Not1 S815 F	5' TATAGCGGCCGCATGAGTGTGGAGCTGGACAGCGACG 3'
AS67	rKIF5C Not1 V907 F	5' TATAGCGGCCGCATGGTGCGGGCCAAGAACATGGCC 3'
AS68	rKIF5C EcoRI K955 R	5' TATAGAATTCTTACTTCTGGTAGTGAGTGGAG 3'
AS72	rKIF5C Not 1 A827 F	5' TATAGCGGCCGCATGGCCGCCCAGAAGCAGAAGATC 3'
AS73	rKIF5C Not 1 K866 F	5' TATAGCGGCCGCATGAAGAGGCTCCGTGCTACTGCAG 3'
AS74	rKIF5C Not 1 K876 F	5' TATAGCGGCCGCATGAAGGCCTTGGAGAGTGCGCTC 3'
AS75	rKIF5C Not 1 M1	5' TATAGCGGCCGCATGGCGGATCCAGCCGAATGC 3'

	F	
AS76	rKIF5C EcoRI H917 R	5' TATAGAATTCTTAATGTGCCCTCCTGGCCATGTTC 3'
AS77	KHC 891_ F	5'GGCCGCAGGGACCGAAAGCGCTACCAGCAGGAAGTGGATCGCATCAAGGAGGCTGTGCGGGCCAAGAACATGGCCAGGAGGGCACATTAGG 3'
AS78	KHC 891_ R	5'AATTCCTAATGTGCCCTCCTGGCCATGTTCTTGGCCCGCACAGCCTCCTTGATGCGATCCACTTCCTGCTGGTAGCGCTTTCGGTCCCTGC 3'
AS79	KHC 899_ F	5'GGCCGCGAAGTGGATCGCATCAAGGAGGCTGTGCGGGCCAAGAACATGGCCAGGAGGGCACATTAGG 3'
AS80	KHC 899_ R	5'AATTCCTAATGTGCCCTCCTGGCCATGTTCTTGGCCCGCACAGCCTCCTTGATGCGATCCACTTCGC 3'
AS81	KHC 903_ F	5'GGCCGCATCAAGGAGGCTGTGCGGGCCAAGAACATGGCCAGGAGGGCACATTAGG 3'
AS82	KHC 903_ R	5'AATTCCTAATGTGCCCTCCTGGCCATGTTCTTGGCCCGCACAGCCTCCTTGATGC 3'
AS83	KHC R908_ F	5' CATCAAGGAGGCTGTGTAGGCCAAGAACATGGC 3'
AS84	KHC R908_ R	5' GCCATGTTCTTGGCCTACACAGCCTCCTTGATG 3'
AS85	KHC S918_ F	5' GGAGGGCACATTAGGCTCAGATCGC 3'
AS86	KHC S918_ R	5' GCGATCTGAGCCTAATGTGCCCTCC,3'
AS87	KHC A932_ F	5' CCAGGACACTATCCTTGATCATCTCCAACAGCC,3'
AS88	KHC A932_ R	5' GGCTGTTGGAGATGATCAAGGATAGTGTCCTGG,3'
AS89	KHC IAK921AAA F	5'GGGCACATTCGGCTCAGGCAGCAGCGCCCATCCGCCCAGGAC 3'
AS90	KHC IAK921AAA R	5'GTCCTGGGCGGATGGGCGCTGCTGCCTGAGCCGAATGTGCCC 3'
AS91	KHC_AAAAAARPG/AAAAAAAA_F	5'GCAGCAGCAGCAGCAGCCGCCGCCGCACACTATCCTGCATCATC 3'
AS92	KHC_AAAAAARPG/AAAAAAAA_R	5'GATGATGCAGGATAGTGTGCGGCGGCGGCTGCTGCTGCTGCTGC 3'
AS93	KHC_QAAAPI/AAA_F	5'GAGGGCACATTCGGCTGCAGCAGCAGCAGCAGCCCGCCCAGGACACTATC3'
AS94	KHC_QAAAPI/AAA_R	5'GATAGTGTCCTGGGCGGGCTGCTGCTGCTGCTGCAGCCGAATGTGCCCTC 3'
AS95	KHC907_917_NMAA F	5'GGCTGTGCGGGCCAAGGCAGCAGCCAGGAGGGCACATTC 3'
AS96	KHC907_917_NMAA R	5'GAATGTGCCCTCCTGGCTGCTGCCTTGGCCCGCACAGCC 3'

AS97	KHC907_917_RAKAAA F	5'CGCATCAAGGAGGCTGTGGCCGCCGCGAACATGGCCAGGAGGG 3'
AS98	KHC907_917_RAKAAA R	5'CCCTCCTGGCCATGTTCGCGGCGGCCACAGCCTCCTTGATGCG 3'
AS99	KHC907_917_RRAA F	5' GGCCAAGAACATGGCCGCAGCGGCACATTCGGCTCAG 3'
AS100	KHC907_917_RRAA R	5' CTGAGCCGAATGTGCCGCTGCGGCCATGTTCTTGGCC 3'
AS112	SKIP A277_ F	5' CTTCAACGAGGAGCCGTAAGAGACTGTGTCCTC 3'
AS113	SKIP A277_ R	5' GAGGACACAGTCTCTTACGGCTCCTCGTTGAAG 3'
AS114	SKIP A291_ F	5' CCCCCGTGCACACCTAATCTCAGGAGAAGGAG 3'
AS115	SKIP A291_ R	5' CTCCTTCTCCTGAGATTAGGTGTGCACGGGGG 3'
AS116	SKIP E217_ F	5' CGATTGCCCCATCTAGTTAGGATTATGATTTTGG 3'
AS117	SKIP E217_ R	5' CCAAAATCATAATCCTAACTAGATGGGGCAATCG 3'
AS118	SKIP F151_ F	5' CTAGAGTTCATTCGTTAAGAGCTGGATCTGGATGC 3'
AS119	SKIP F151_ R	5' GCATCCAGATCCAGCTCTTAACGAATGAACTCTAG 3'
AS120	SKIP K171_ F	5' GCCCGACTACTACTAACCTCAGTACCTG 3'
AS121	SKIP K171_ R	5' CAGGTACTGAGGTTAGTAGTAGTCGGGC 3'
AS122	SKIP T244_ F	5' GAGACCTCACAGACTAGGTCAGTGGTCCC 3'
AS123	SKIP T244_ R	5' GGGACCACTGACCTAGTCTGTGAGGTCTC 3'
AS124	SKIP T203_ F	5' CAACTCCGTCACCTCCTAAAACCTGGAGTGGGATG 3'
AS125	SKIP T203_ R	5' CATCCCACTCCAGGTTTTAGGAGGTGACGGAGTTG 3'

2.1.3 Agarose gel electrophoresis

DNA was added to 6x DNA loading buffer (Qiagen). Samples were loaded on a 1% (W/V) agarose gel containing 10µl SafeView (NBS Biologicals Ltd) Nucleic Acid Stain (NBS Biologicals Ltd). Hyper ladder 1 (Bioline) was used as a DNA marker.

2.1.4 Purification of DNA from agarose gels

Bands were excised and the DNA extracted using the QIAquick Gel Extraction Kit (Qiagen) according to the manufacturers guidelines. The gel slice was dissolved in QG buffer (300µl of Buffer QG per 100mg of gel) and incubated at 50°C for 10 minutes (or until the gel slice had completely dissolved). 1 gel volume of isopropanol was added to the sample and mixed. The sample was applied to the QIAquick column, and centrifuged at 13,000 rpm for 1 minute. The flow-through was discarded and the QIAquick column placed back in the same collection tube. 0.75 ml of Buffer PE was added to the QIAquick column and centrifuged for 1 minute. The flow-through was discarded and the QIAquick column centifuged for an additional 1 minute at 13,000 rpm. To elute DNA, 50µl of buffer EB or water was added to the center of the QIAquick membrane and centrifuged for 1 minute at 13,000 rpm.

2.1.5 Transformation of chemically competent bacteria

Chemically competent *E.coli* BL21(DE3) cells (BioLabs) or chemically competent *E.coli* TOP10 cells (Invitrogen) and DNA (typically 50µl and 5µl) were incubated with on ice for 30 minutes. This was followed by heat-shock at 42°C for 30 seconds and incubation on ice for 2 minutes. 250µl S.O.C medium was added to the transformation reaction. This was followed by incubation at 37°C, 250RMP for 1 hour. 30µl and 60µl were then plated on LB-agar plates containing appropriate antibiotic (either ampicillin or kanamycin (Sigma) at 50ug/ml) and incubated overnight at 37°C.

2.1.6 Purification of plasmid DNA from bacteria

Small scale purification by mini-prep:

A single bacterial colony was picked and grown overnight in 5ml LB broth (10g bacto-tryptone, 5g bacto- yeast extract, 10g NaCl in 1 litre, pH7.5) supplemented with the appropriate antibiotic (either ampicillin or kanamycin at

50µg/ml). Using the Plasmid Mini kit (Qiagen) according to manufacturers protocol.

Large scale purification by midi-prep:
Plasmid DNA picked from a single colony was grown overnight in 100ml LB broth supplemented with the appropriate antibiotic (either ampicillin or kanamycin at 50µg/ml). The DNA was purified using the Plasmid Midi Kit (Qiagen) according to manufacturers protocol.

2.1.7 Restriction enzyme digest of DNA

For sub-cloning or to confirm the identity of plasmids according to restriction digest profile, plasmid DNA was digested with the relevant restriction enzyme.
All enzymes were supplied by Roche and used in buffers recommended by the manufacturer. A typical reaction consisted of 1µg of plasmid DNA, 2.5µl 10x restriction buffer, 1µl restriction enzyme made up to 25µl with H_2O, incubated at 37°C for 2 hours. Reactions were subsequently analysed by agarose gel electrophoresis.

2.1.8 Annealing oligonucleotides

Oligonucleotides were obtained from Sigma 0.025µM Scale. Oligos were dissolved in 50µl H_2O. 1µl from each oligo (forward & reverse) was added to 48µl annealing buffer (100mM potassium acetate, 30mM HEPES-KOH pH7.4, 2mM Mg-acetate) and incubated at 95°C for 4 minutes followed by a 10 minute incubation at 70°C. The annealed oligos were cooled slowly to 4°C.

2.1.9 Phosphorylation of oligonucleotides

2µl of the annealed oligos, 1 µl DNA ligase buffer, 5µl H_2O and 1µl T4 polynucleotide kinase (BioLabs) were incubated at 37°C for 30 minutes followed by a 10 minute incubation at 70°C. The phosphorylated oligonucleotides were ligated into a restriction digested and CIP treated plasmid (see 2.1.10).

2.1.10 Dephosphorylation of plasmid

1µg plasmid DNA was restriction digested by relevant restriction enzymes and purified by gel purification and eluted in 35µl H_2O. 1µl Alkaline phosphatase,

Calf Intestinal (CIP) (BioLabs) and 3.5µl NEB (New England Biolabs) buffer 3 was added and incubated at 37°C for 30 minutes.

2.1.11 DNA ligation

Ligation reactions were carried out at 16°C for 16 hours using T4 DNA ligase (New England Biolabs) in 1x DNA ligase buffer. A typical reaction consisted of a 1:5 molar ratio of vector: insert and 1µl ligase made up to 20µl with H_2O.

2.1.12 DNA sequencing

DNA samples were sent at a concentration of 100µg/µl to be sequenced by Source Bioscience.

2.2 Protein expression an purification

2.2.1 Protein expression

Proteins were expressed in *E.coli* BL21(DE3) cells. Single bacterial colonies were picked and grown overnight in 5ml LB broth (10g bacto-tryptone, 5g bacto-yeast extract, 10g NaCl in 1 litre, pH7.5) supplemented with the appropriate antibiotic (either ampicillin or kanamycin at 50µg/ml). 2ml small-scale overnight bacterial cultures were used to inoculate 500ml LB broth supplemented with the appropriate antibiotic (either ampicillin or kanamycin at 50µg/ml). Cultures were incubated at 37°C until they reached an OD_{600} of 0.5. The temperature was then lowered to 16°C and protein synthesis was induced by the addition of 300µM Isopropyl β-D-1-thiogalactopyranoside (IPTG) for 16 hours. Cells were harvested by centrifugation at 5000 x g for 15 minutes at 4°C and resuspended in 20mM HEPES pH 7.5, 500mM NaCl, 20mM imidazole, 5mM β-mercaptoethanol supplemented with protease inhibitor cocktail (Roche).

2.2.2 Protein purification using Ni^{2+} column

Cell lysis was accomplished by sonication. Insoluble material was sedimented by centrifugation at 13000 rpm for 30 minutes at 4°C and the supernatant filtered using 0.22µm prior to loading on a His-trap HP column (GE Healthcare) pre-equilibrated with lysis buffer (in 20mM HEPES pH 7.5, 500mM NaCl, 20mM imidazole, 5mM β- mercaptoethanol). The protein was eluted with an imidazole gradient (20mM to 300mM Imidazole) and fractions containing the target protein collected and dialysed overnight against imidazole-free lysis buffer.

2.2.3 Size-exclusion chromatography (SEC)

The sample was applied to a HiLoad 16⁄600 Superdex 75 prep grade column (GE Healthcare) pre-equilibrated with sample buffer (20mM HEPES pH 7.5, 500mM NaCl, 5mM β- mercaptoethanol) and 2ml fractions collected using an AKTA prime plus. Typically a 4L bacterial culture yielded 25mg of purified protein after Ni^{2+} column purification followed by SEC.

2.2.4 Batch purification using GST beads

Cell lysis was accomplished by sonication. Insoluble material was sedimented by centrifugation at 13,000rpm for 30 minutes at 4°C and the supernatant filtered using a 0.22µm filter. The glutathione Sepharose 4 Fast Flow beads were washed 5 times with buffer (20mM HEPES pH 7.5, 500mM NaCl, 5mM β-mercaptoethanol) This was followed by incubation of the cell lysate with 0.5ml of glutathione Sepharose 4 Fast Flow beads (GEHealthcare life sciences) per 1L bacterial culture for 2 hours at 4°C with end-over-end rotation. This was followed by a further 5 washes. The GST fusion protein was eluted by adding 0.5 ml 50 mM Tris-HCl, 10mM reduced glutathione, pH 8.0 per 1 ml original slurry of glutathione Sepharose 4 Fast Flow. This was repeated for a total of three elutions. Typically a 2L bacterial culture yielded 10mg of purified protein after batch purification.

2.2.5 Thrombin cleavage

Thrombin cleavage was carried out using Novagen Thrombin cleavage capture kit according to the manufacturers guidelines. 1:25 dilution was made of thrombin in Thrombin Dilution/Storage Buffer. The dilution contained approximately 0.04 U enzyme per µl. Each reaction contained 1µl diluted thrombin/10ug target protein in 1X Thrombin Cleavage/Capture Buffer. The reactions were incubated at 4°C overnight.

Biotinylated thrombin was removed with streptavidin agarose (using a ratio of 16µl settled resin (32µl of the 50% slurry) per unit of enzyme. The desired amount of streptavidin beads was transferred to the reaction and incubated at room temperature for 30 minutes with gentle shaking and this was followed by the reaction being transferred to the sample cup of a Spin Filter and centrifuged at 500 x g for 5 minutes.

2.2.6 C3 cleavage

PreScission protease (GE Healthcare) was added to the target protein (in buffer: 20mM HEPES pH 7.5, 500mM NaCl, 5mM β-mercaptoethanol) at a 1 unit protease to 100µg target protein ratio. The reaction was incubated at 4°C overnight. The GST-HRV 3C protease, Cleaved GST as well as any uncleaved protein were removed by incubation with glutatione Sepharose 4 fast flow beads (GE healthcare) for 1 ½ hr.

2.3 SDS polyacrylamide gel electrophoresis (SDS-PAGE) and Western Blot

2.3.1 SDS/PAGE

Denaturing 10% or 12% polyacrylamide gels were cast using Novex cassettes (Novex Life Technologies). Running gels were made up to 10% or 12% acrylamide (30% stock Acrylamide/Bis-acrylamide (Sigma), 375mM Tris-HCL, pH 8.8, 0.1% SDS, 0.1% ammonium persulphate (APS), and 8ul TEMED. 2.5 ml stacking gels consisted of 5% acrylamide, 124mM Tris-HCl pH6.8, 0.1% SDS, 0.1% APS and 10uL TEMED. Samples were resuspended in1x (or diluted 5x) SDS loading buffer (1x (10% glycerol, 2% SDS(w/v) 60mM Tris pH 6.8, 0.001% bromophenol blue, 100mM DTT and heated to 100°C for 5 minutes. Gels were run at 180V for 1 hour in 1x SDS Running Buffer (1% SDS, 27.6mM Tris, 0.2M glycine pH 8.8) A 17- prestained protein ladder (Precision Plus Protein™) was used as a standard.

2.3.2 Transfer to PDVF membrane and western Blot

Protein samples that had been separated on SDS-PAGE gel were transferred to a PVDF membrane (Immobilon-P, Millipore). Membranes were prepared by wetting for 1 minute in methanol followed by 5 minutes in transfer buffer (25mM Tris, 192mM glycine, 10% methanol). Transfer was typically 1 hour at 100 volts.

2.3.3 Analysis of samples by western blot

The membrane was blocked overnight at 4 °C in 5% milk (skim milk powder (MERCK) in TBST (20mM Tris, 0.25M NaCl, 0.1% Tween-20, pH 7.5 with HCl). Membranes were probed with the appropriate antibodies at the concentration

indicated in Table 2. Membranes were washes 3 x in TBS-T prior to incubation with a horseradish peroxidase conjugated secondary antibody if required. This was followed by another 3 washes in TBST. The Clarity Western ECL substrate (Biorad) was used to detect the HRP- conjugated antibody.

Table 2. Antibodies used

Target/Purpose	Type	Manufacturer/ Reference	Dilution/Time WB	Dilution/Time IFA
Anti-His HRP	Mouse monoclonal	Novagen	1:2000 30 minutes	
Anti-GST	Rabbit monoclonal	Sigma	1:5000 20 minutes	
Anti-HA	Mouse monoclonal	Sigma	1:1000 16 hours	1:1000 2 hours
Anti-GFP	Mouse monoclonal	Sigma	1:1000 16 hours	
Anti-mouse HRP	Goat polyclonal	Dako	1:5000 30 minutes	
Anti-Rabbit HRP	Goat polyclonal	Dako	1:5000 30 minutes	
Anti-LAMP1	Rabbit monoclonal	Cell Signalling Technologies		1:200 2 hours
Anti-Myc	Mouse monoclonal	Sigma		1:1000 2 hours
Anti-mouse Alexa 488	Goat polyclonal	Novagen		1:250 30 minutes
Anti-rabbit Alexa 568	Goat polyclonal	Novagen		1:250 30 minutes
Anti-mouse Alexa 568	Goat polyclonal	Novagen		1:250 30 minutes
Anti-rabbit Alexa 633	Goat polyclonal	Novagen		1:250 30 minutes

2.4 Crystallisation

In order to obtain crystals that will diffract to a high resolution, the protein in solution must be pure and homogenous. During crystallisation a protein self assembles into a periodic lattice. For crystallization, the protein must be concentrated to supersaturation to allow for nucleation to occur and crystal formation (McPherson, 1990). This is illustrated in the phase diagram in Figure 2.1.

It is not predictable which conditions will yield well diffracting crystals. Many crystallisation trials involve varying reagents (such as buffers, precipitants and additives), concentrations of reagents, pH or temperature. Vapour diffusion is the most common technique used to obtain crystals. Both the hanging drop and the sitting drop techniques use evaporation to achieve supersaturation. This is illustrated in the diagram shown below. In the vapour diffusion method the protein solution is mixed with reservoir (precipitant) solution and is placed on the glass slide covering and sealing the reservoir in the case of the hanging drop technique and in a sub-well in the sitting drop technique. The protein-precipitant concentration in the hanging or sitting drop is much lower than that in the reservoir. As water evaporates from the drop into the reservoir the concentration of the protein is increased steadily until the solution becomes supersaturated allowing for nucleation to occur.

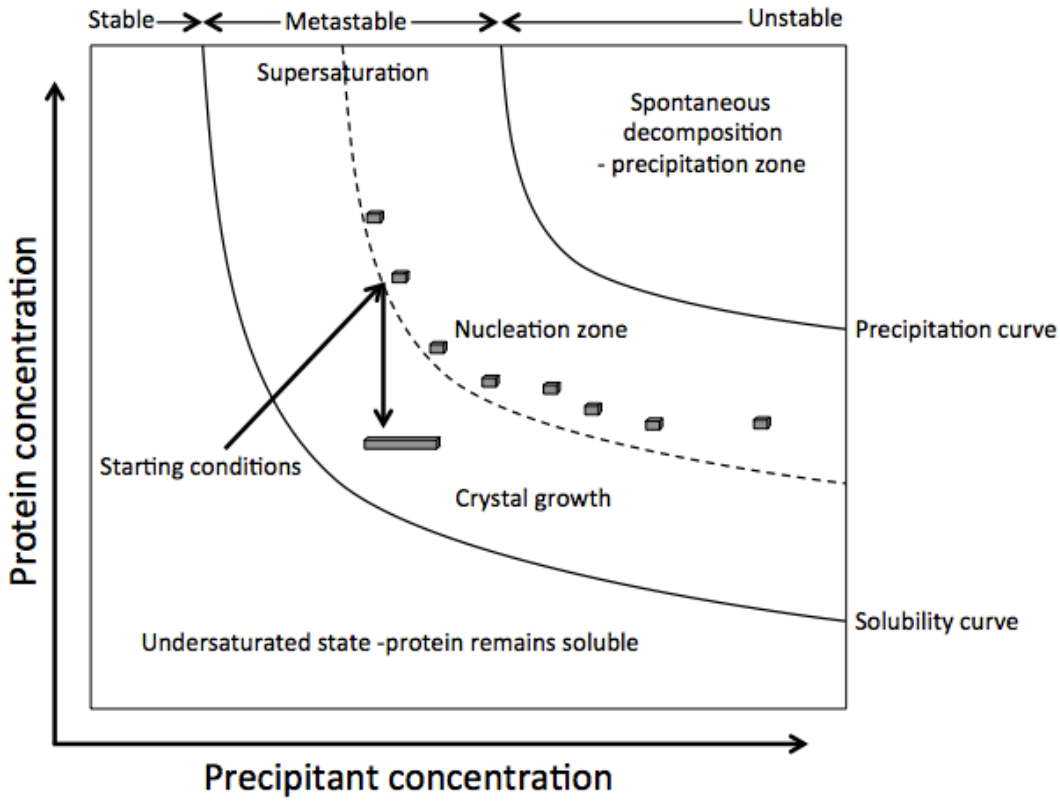

Figure 2.1. Phase diagram of crystal growth.
Nucleation is thought to occur in the nucleation zone followed by further growth in the metastable zone. If the protein concentration or the precipitant concentration is too high, the protein will precipitate out of solution. Adapted from (Rupp, 2009).

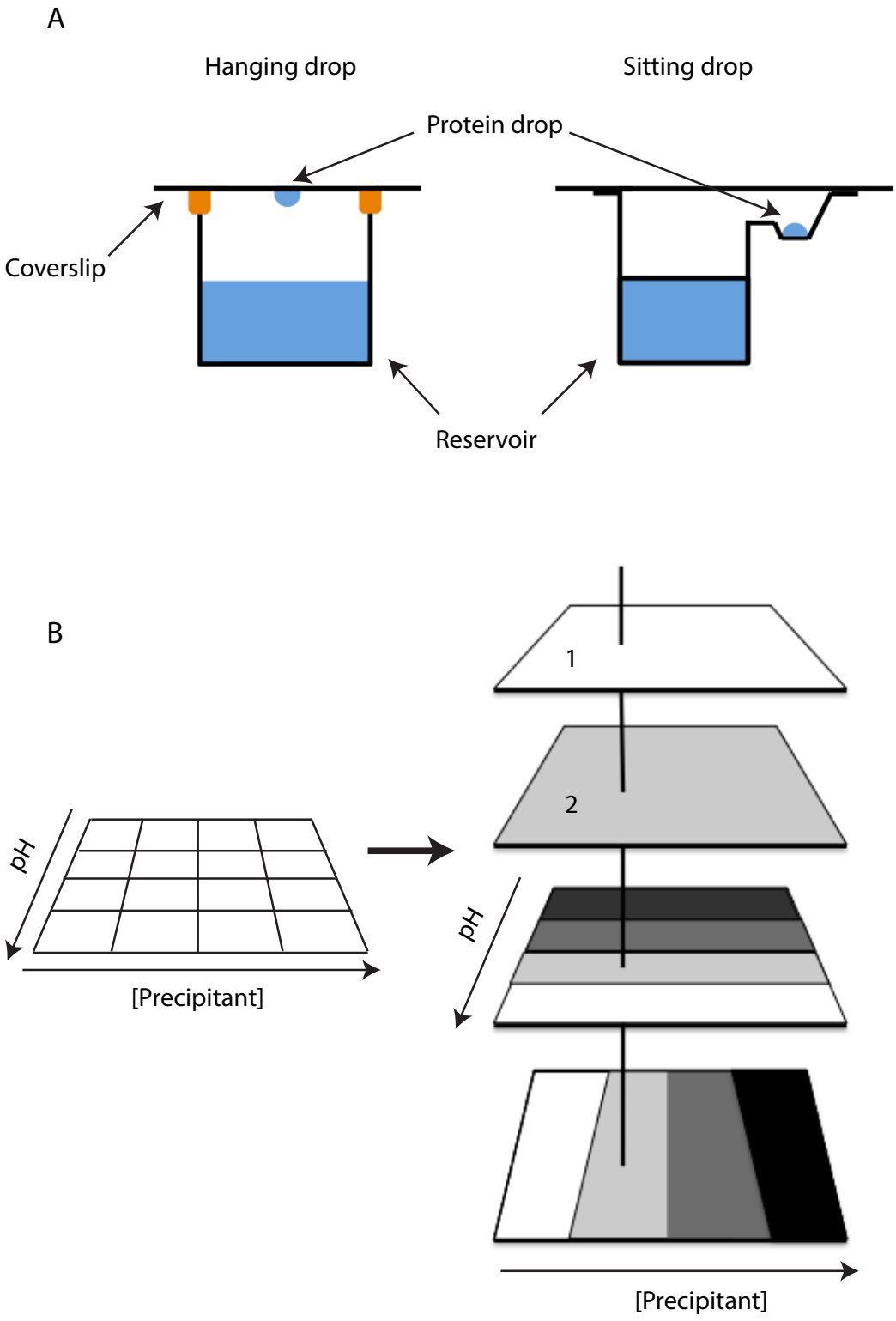

Figure 2.2. Schematic of crystallisation techniques
(A) Schematic of the hanging drop and sitting drop techniques. (B) Schematic of the optimisation grid set up for protein crystalisation. Components of the optimisation grid are shown separately. 1 and 2 represents components kept constant. Adapted from (McPherson and Cudney, 2014).

2.5 Crystalisation Method

2.5.1 Pre-Crystallisation Screen

A pre-crystallisation screen was carried out according to the guidelines in the Hampton Research user guide. Sample concentrations were between 5 and 20 mg/ml.

2.5.2 Crystallisation screens

96-well sitting drop vapour diffusion crystallisation screens were set up using a Mosquito (TTP Labtech) robotic crystallization device. Initial screens were set up using drops of 200nl of the protein sample (at the concentration determined by the pre-crystallisation screen ~ 5mg/ml) mixed in a 1:1 ratio with the reservoir in the top drop. In the lower drop, the drop was set up 133nl protein and 267nl reservoir. (1:2 ratio). The crystallisation screens used in trials were PGA, MIDAS, Proplex (Molecular Dimensions) and JCSG+ (Qiagen). Plates were sealed and stored at 18C. For optimisation of conditions that produced crystals, a grid screening around the condition was made in 96-well sitting drop plate.

2.6 Protein interaction assays

2.6.1 Fluorescence polarisation

Light polarized by passing through a vertical polarizing filter is absorbed by and excites fluorescent molecules that are oriented in the vertical polarized plane in the sample tube. These fluorescent molecules subsequently emit light. The emitted light is measured perpendicular and parallel to the plane of the excitation beam. Polarization is a measure of the extent of molecular rotation during the period between excitation and emission and is dependent upon fluorescent lifetime of the fluorophore. The polarization value, P, is a ratio of light intensities expressed in millipolarization units (1 Polarization Unit = 1000 mP Units). P = (F1 – F2)/ (F1 + F2) (F1= fluorescence intensity parallel to the excitation plane, F2= fluorescence intensity perpendicular to the excitation plane). Small molecules rotate quickly during the excited state and have low polarization values. Large molecules, caused by the binding of the fluorescent peptide to a second protein, rotate little during the excited state, and therefore have high polarization values.

N-terminal carboxytetramethylrhodamine (TAMRA) conjugated peptides used for fluorescence polarization measurements $SKIP^{WD}$: TAMRA- STNLEWDDSAI, TAMRA-$SKIP^{WE}$: TAMRA-VPSTDWEDGDL, TAMRA-$SKIP^{WDWE}$: TAMRA-STNLEWDDSAIAPSSEDYDFGDVFPAVPSVPSTDWEDGDL were supplied by BioSynthesis (Lewisville, TX, USA). Measurements were performed on a Horiba Fluoromax-4 spectrofluorometer at 20 °C by incubating 100nM TAMRA-labeled peptides with KLC2TPR (or KHC(866-917)) at increasing concentrations in 25mM Hepes pH 7.5, 5 mM β-mercaptoethanol and 150mM NaCl. Data analysis was performed using the Prism (GraphPad Software Inc., San Diego CA, USA) package. Data was fitted assuming first order kinetics, generating a binding curve from which a dissociation constant (Kd) and Bmax were calculated. Polarisation values for peptide with buffer alone was subtracted from polarization values and data was normalised to calculated Bmax. The data are presented are as normalised fluorescence polarisation.

2.6.2 GST Pull-down of purified protein

All samples were dialysed overnight into a buffer containing 20mM HEPES pH7.5, 150mM NaCl and 5mM β-mercaptoethanol (and 20mM imidazole if His-tagged protein was involved in the pull-down). 0.5nmoles GST/ GST fusion construct (1.6 µM) was incubated with 1.2µM target protein in a volume of 300µl for 1 ½ hours followed by a 1 ½ hour incubation with 20µl prewashed GST beads. Beads were centrifuged at 2000g for 2 minutes. This was followed by three wash steps with 1ml buffer: 20mM HEPES pH7.5, 150mM NaCl and 5mM β-mercaptoethanol (and 20mM imidazole if His-tagged protein was involved in the pull-down). The beads were transferred to a new microcentrifuge tube during the second wash step. Binding was analysed by gel electrophoresis followed by western blot analysis and coomassie staining.

2.6.3 GST Pull-down of protein expressed in 293T

0.25nmoles (0.83µM) purified GST /GST fusion protein was incubated with 20µl prewashed GST beads in a volume of 300µl for 90 minutes. Beads were centrifuged at 2000g for 2 minutes. This was followed by the removal of the supernatant and three wash steps with 1ml wash buffer (20mM HEPES pH7.5, 20mM imidazole, 150mM NaCl and 5mM β-mercaptoethanol)

293T cells were plated at a density of 1.5 x 10^5 per 10cm dish 5 hours prior to transfection. Cells were transfected with 2µg DNA (CB6 expression vectors) using Effectene transfection reagent (Qiagen). 10µl DNA (200ng/µl stock), 16µl Enhancer and 273µl buffer EC (that provides optimal salt conditions for efficient DNA condensation) were combined. Samples were vortexed for 1 second and incubated for a further 2 minutes at room temperature. 20µl Effectene Reagent was then added to the samples and the samples were vortexed for 30 seconds and the mixture was incubated for 20 minutes to allow Effectene-DNA complexes to form and added directly to the cells. The cells were then incubated at 37°C. After 16 hours, transfected cells were lysed in 1ml of 25 mM HEPES pH 7.5, 150 mM NaCl, 0.1% NP-40, 0.1X Triton-X 100 containing a protease inhibitor cocktail (Roche) for 10 minutes prior to centrifugation at 13 000g for 10 min at 4°C. The resulting supernatant was incubated with the 20µl GST beads described above for 90 minutes. 50µl of supernatant was retained for analysis of cell lysate. 10µl 6x loading buffer was added. Beads were washed four times and boiled in 60µl SDS-loading buffer. 20µl samples were subjected to SDS–PAGE and analysed by western blot.

2.6.4 Immunoprecipitation

293T cells were plated at a density of 1.5 x 10^5 per 10cm dish 5 hours prior to transfection. Cells were transfected with 2µg DNA (CB6 expression vectors) using Effectene transfection reagent (Qiagen). 10µl DNA (200ng/µl stock), 16µl Enhancer and 273µl buffer EC (that provides optimal salt conditions for efficient DNA condensation) were combined. Samples were vortexed for 1 second and incubated for a further 2 minutes at room temperature. 20µl Effectene Reagent was then added to the samples and the samples were vortexed for 30 seconds and the mixture was incubated for 20 minutes to allow Effectene-DNA complexes to form and added directly to the cells. The cells were then incubated at 37°C. After 16 hours, transfected cells were lysed in 1ml of 25 mM HEPES pH 7.5, 150 mM NaCl, 0.1% NP-40, 0.1X Trition-X 100 containing a protease inhibitor cocktail (Roche) for 10 minutes prior to centrifugation at 13 000g for 10 min at 4°C. The resulting supernatant was incubated with 15µl of prewashed GFPTrap beads (ChromoTek) for 90 minutes. 50µl of supernatant was retained for analysis of cell lysate. 10µl 6x loading buffer was added.

Beads were washed four times and boiled in 60µl SDS-loading buffer. 20µl samples were subjected to SDS–PAGE and analysed by western blot.

2.7 Immunofluorescence

Cells were plated at a density of 1.5 x 10^4 per well on fibronectin-coated glass cover slips in a 6 well plate 6 hours prior to transfection. Cells were transfected using Effectene transfection reagent (Qiagen). Cells were transfected with 0.8µg DNA (CB6 expression vectors) using Effectene transfection reagent (Qiagen). 4µl DNA (200ng/µl stock), 3.2µl Enhancer and 92.8µl buffer EC (that provides optimal salt conditions for efficient DNA condensation) were combined. Samples were vortexed for 1 second and incubated for a further 2 minutes at room temperature. 5µl Effectene Reagent was then added to the samples and the samples were vortexed for 30 seconds and the mixture was incubated for 20 minutes to allow Effectene-DNA complexes to form and added directly to the cells. The cells were then incubated at 37°C for 16 hours.

Cells were fixed for 10 minutes at room temperature in 4% paraformaldehyde (PFA). To allow entry of antibodies, cells were permeabilised with 0.2% Triton X in PBS for 10 minutes at room temperature prior to blocking with 1% BSA in PBS for 20 minutes. Alternatively, cells were fixed at -20°C with 100% methanol for 10 minutes. Cells were washed three times with PBS. Cells were then probed with the appropriate antibody diluted in blocking solution 1% BSA in PBS). After 2 hours at room temperature, cells were washed three times for 5 minutes each with PBS followed by incubation with a secondary fluorescent conjugated antibody (in blocking solution) for 30 minutes. Coverslips were washed 3 more times with PBS, placed cell side down in fluor save reagent (Calbiochem). Widefield fluorescence images were collected using a Zeiss Olympus IX-81 microscope with a 40x objective running Metamorph. Confocal images were collected using a Nikon A1 system with a 100x objective running NIS Elements.

2.8 Quantification of lysosome distribution

To quantify lysosome distribution, widefield images were acquired at a 40x magnification. The cell perimeter was defined by thresholding equivalent saturated images and the area was scaled at 10% decrements using ImageJ.

The image was binarised and the cumulative LAMP-1 distribution (relative to the whole cell) was then plotted for increasing incremental deciles. Data points are from a minimum of 15 cells in 3 replicates and are representative of at least 3 independent experiments. For analysis of the resulting curves, the non-linear regression function in Graphpad Prism was used to fit a centered 6^{th} order polynominal. R^2 values were all above 0.8. To compare models and assess the statistical significance of differences in distribution profiles, the extra sum of F-squares test was applied. P values for particular comparisons are indicated on the graphs. T-test was also used for statistical analysis at the 60^{th} centile.

CHAPTER 3 . EXPRESSION, PURIFICATION AND CRYSTALLISATION OF KLC2TPR BOUND TO SKIP

Despite many examples of robust biochemical experiments that clearly demonstrate interactions between microtubule motors and many cargo proteins, no structural information is available that describes these interfaces. This holds back our understanding of these crucial transport processes. Recent reports from several groups have uncovered that a significant component of the kinesin-1 cargo mechanism involves binding of short, charged, peptides by the KLC TPR domain with low micromolar affinity. There are numerous examples of TPR-domain peptide X-ray crystal structures with similar properties. Therefore, at least in the case of kinesin-1, it appeared that this problem may be tractable using structural approaches. This chapter describes experiments that aimed to solve an X-ray crystal structure of a tryptophan-acidic motif in complex with the KLC2 TPR domain, focusing on the pair of motifs found within the lysosomal cargo adaptor SKIP, which in several complementary reports have been found to play a role in kinesin-1 dependent microtubule transport (Dumont et al., 2010, Rosa-Ferreira and Munro, 2011). These reports have shown that the N-terminal domain of SKIP (amino acids 1-310, with W-acidic motifs located at 207-208 and 236-237) is both necessary and sufficient for binding to kinesin-1.

3.1 Determination of the relative importance of the two tryptophan acidic motifs of SKIP.

To begin to determine the best approach for X-ray crystallography a GFP-TRAP immuno-precipitation strategy was used to determine the relative contribution of each motif to KLC2 binding, reasoning that the motif that made the biggest contribution to binding was most likely to be successful in downstream applications. HeLa cells were co-transfected with plasmids designed to express N-terminally hemagglutinin (HA) tagged KLC2 (HA-KLC2) and N-terminally green fluorescent protein (GFP) tagged SKIP(1-310) (either wild-type, carrying alanine substitution at residues 207-208 (WD), 236-237 (WE) or both WD and WE), or with amino acids 219 to 238 deleted (ΔExon7). GFP-SKIP(1-310) was immunoprecipitated with GFP-TRAP beads and the amount of co-immunoprecipitated HA-KLC2 was assessed by western blot (Figure 3.1).

Disruption of the WD motif essentially eliminated the GFP-SKIP interaction with HA-KLC2, whereas equivalent mutations in the WE motif had relatively little effect. When both tryptophan-acidic motifs were mutated, the reduction in binding was similar to the WD mutation alone. Deletion of Exon7 (DelEx7), which encompasses the WE motif and surrounding residues, did considerably reduce binding, suggesting some contribution from these residues in binding to KLC2. It was notable that in experiments where an interaction did occur, there was an apparent increase in HA-KLC2 expression in the cell extract, compared to the GFP control, although the extent of this tended to vary between repeats of experiments. This may is due to some level of SKIP dependent stabilisation of KLC2 in this over expression system. Taken together, these data suggest that this first W-acidic acidic motif of SKIP is the primary determinant of interaction with KLC2 but that the second motif and intervening residues may also make a contribution to binding.

3.2 Fluorescence polarization analysis of the SKIP-KLC2 interaction.

To validate these findings *in vitro* and further biophysically characterise the interactions between KLC2 TPR and SKIP W-acidic motifs, fluorescent polarisation assays were carried out in collaboration with Dr. Stefano Pernigo, Steiner group, KCL (see methods for details). These assays should ideally be performed with the most pure recombinant proteins possible.

To allow comparison with data from Zhu et al., 2012 who performed isothermal titration calorimetry (ITC) based characterisation of similar W-acidic motifs binding to KLC2, the KLC2 TPR chosen for these experiments consisted of residues 219-480, and does not include the first helix of TPR1. The authors found that deletion of this helix stabilised the protein and improved crystal quality (PDB code 3CEQ). KLC2 TPR was expressed in *E.coli* as an N-terminally His_6-tagged protein and was first purified by Ni^{2+}-affinity chromatography followed by size exclusion chromatography (SEC). KLC2 TPR eluted as a single peak at 66.57 ml during SEC with very few low molecular weight impurities (Figure 3.2).

N-terminal carboxytetramethylrhodamine (TAMRA) conjugated peptides that centered on the first W-acidic motif of SKIP (SKIP^{WD}: STNLEWDDSAI), or

the second motif ($SKIP^{WE}$: VPSTDWEDGDL) (comparable to peptides used by Zhu et al.), as well as a long peptide encompassing the entire region were obtained from Biosynthesis Inc. at >95% purity.

Peptides were added at 100nM concentration to increasing concentrations of KLC2 TPR in saturation binding experiments (in triplicate) and analysed using a spectrophotometer. Binding of the protein to the peptide at equilibrium is associated with an increase in the polarisation of emitted light (see methods). Fitting the data assuming first order kinetics, enables a binding curve to be generated from which a dissociation constant (Kd) and Bmax can be calculated. Following subtraction of polarisation values for peptide with buffer alone and normalising to calculated Bmax, the data are presented as normalised fluorescence polarisation.

Whilst it was not possible to achieve saturation in all three cases, these fluorescence polarisation measurements clearly show that the first SKIP tryptophan-acidic motif ($SKIP^{WD}$) has a higher affinity for the TPR domain of KLC2 than the second motif ($SKIP^{WE}$). ($SKIP^{WD}$ = 24 μM, $SKIP^{WE}$ above 110 μM) (Figure 3.3). The longer peptide containing both tryptophan-acidic motifs as well as including Exon7 yielded a Kd of 4.9μM. These low micromolar affinities (for $SKIP^{WD}$ and $SKIP^{WDWE}$) are broadly comparable to similar measurements made by Zhu et al. using ITC. Importantly, they strongly reinforce the conclusions of the immunoprecipitation experiment above that suggests that the first W-acidic motif of SKIP makes the key contribution to binding and was therefore the best candidate for downstream crystallographic approaches. They do however also suggest that incorporation of both motifs (or further residues C-terminal to $SKIP^{WD}$) can also contribute to binding.

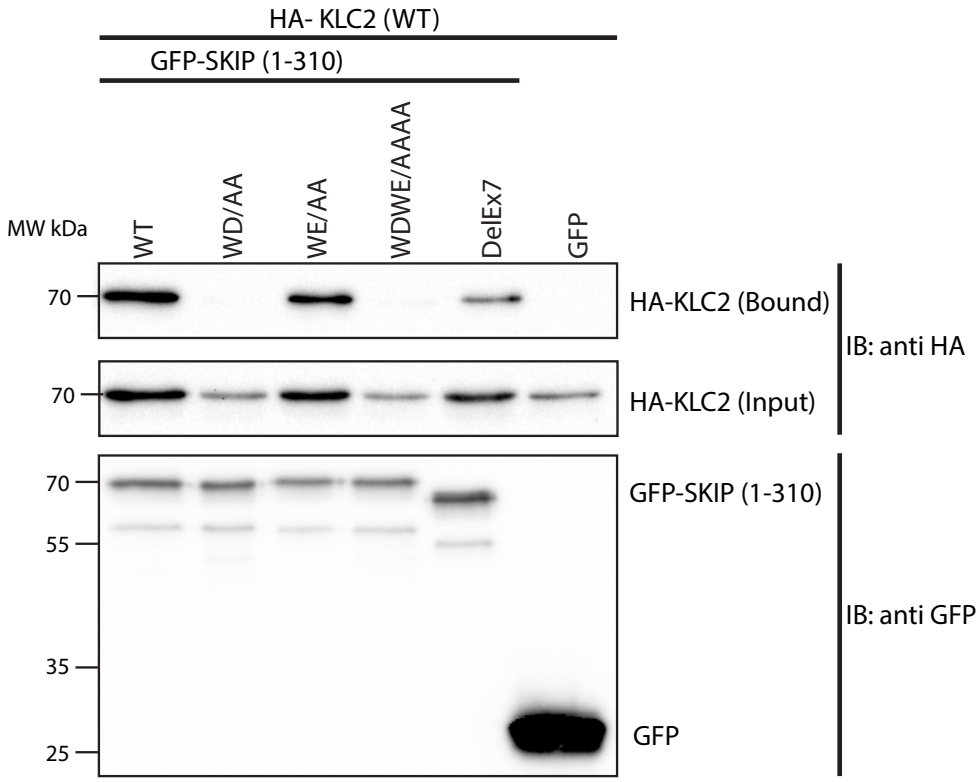

Figure 3.1. Alanine substitution of the first W-acidic motif (SKIP^{WD}) abrogates SKIP:KLC2 binding, whereas the same substitution in the second motif (SKIP^{WE}) has a smaller effect.

GFP-Trap of HA-KLC2 (70.0 kDa) with GFP-SKIP (62.1 kDa), mutants of SKIP (WD/AA (61.9 kDa), WE/AA (61.9 kDa), WEWD/AAAA (61.7 kDa)), SKIP containing a deletion of exon 7(DelEx7)(59.8 kDa) or GFP (26.9 kDa) control expressed in HeLa cells. Input lysates and co-immunoprecipitated HA-KLC2 (bound) were blotted for KLC2 using an anti-HA mouse monoclonal antibody. GFP and GFP-SKIP were blotted for using an anti-GFP mouse monoclonal antibody. A goat polyclonal anti-mouse HRP antibody was used as a secondary antibody to allow for detection using the Clarity Western ECL substrate. The blot is representative of three experiments involving three independent repeat transfections followed by co-immunoprecipitation.

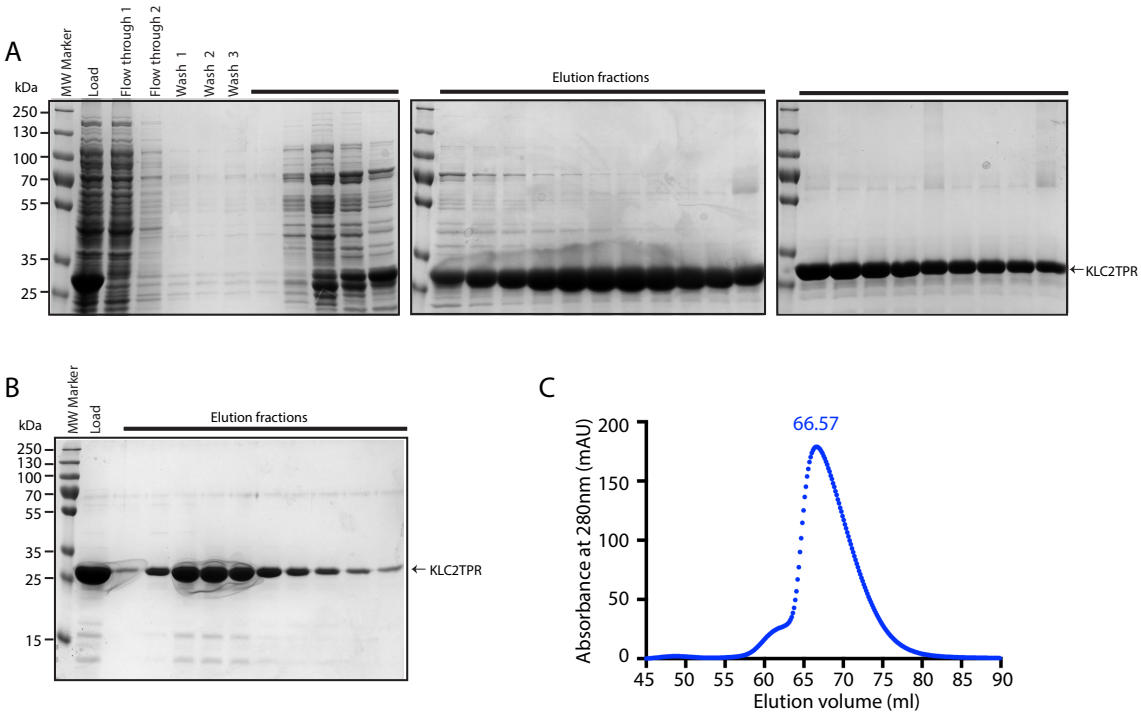

Figure 3.2. Purification of KLC2TPR.
(A) Coomassie stained SDS-PAGE gel showing collected fractions of Ni^{2+} column purification. The soluble cell lysate is labeled load. The flow through as well as the wash buffer were collected after passing through the column (flowthrough 1,2 and wash 1, 2, 3 respectively). KLC2TPR (32.1kDa) was eluted with an imidazole gradient and fractions containing the target protein collected. (B) Coomassie stained gel of fractions eluted during size exclusion chromatography using a HiLoad 16⁄600 Superdex 75pg column. (C) Size exclusion chromatogram showing absorbance measurements at 280nm of eluted fractions shown in B.

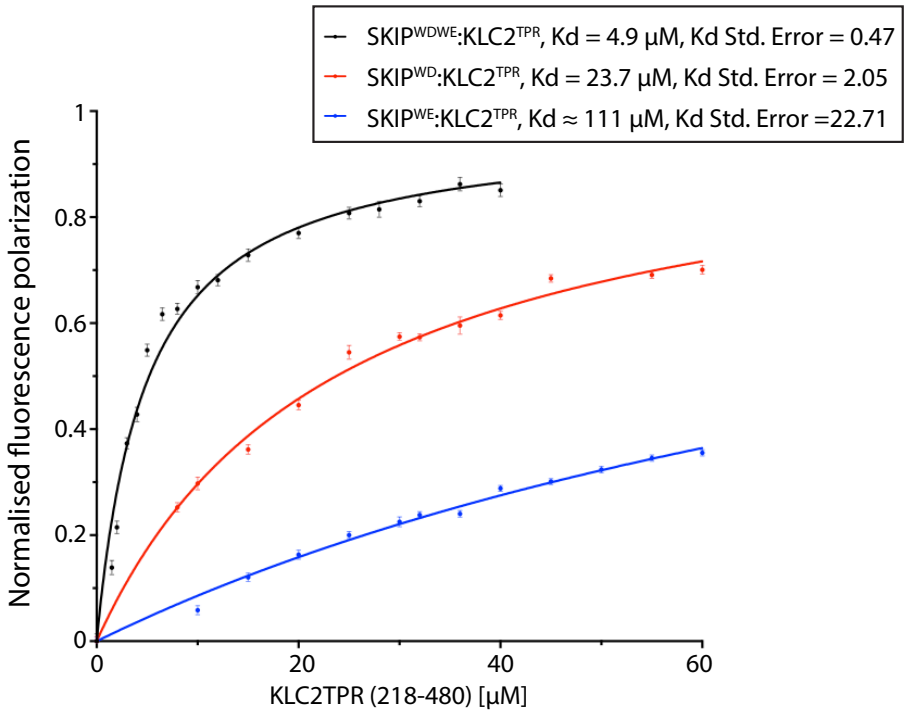

Figure 3.3. SKIP^{WD} has a higher binding affinity for KLC2 than SKIP^{WE}. Fluorescence polarisation measurements of increasing concentrations of KLC2TPR with 100nM N-terminal carboxytetramethylrhodamine (TAMRA) conjugated peptides (SKIP^{WE} (blue), SKIP^{WD}(red), and SKIP^{WDWE}(black)) in 25mM Hepes pH 7.5, 5 mM β-mercaptoethanol and 150mM NaCl. Calculated values for dissociation constants are shown in the box. The graph shows average values from three independent experiments utilising the same KLC2TPR(218-480) preparation and TAMRA conjugated peptide stock solutions. Measurements were performed on a Horiba Fluoromax-4 spectrofluorometer at 20 °C. A one site - specific binding curve was fitted to the data: Y = Bmax*X/(Kd + X). Experiment carried out in collaboration with Dr. Stefano Pernigo, Steiner group, KCL.

3.3 Construct design

Previous attempts in the group and by others at crystallising the KLC2 TPR domain and W-acidic peptides had proven unsuccessful. The data described in the previous section suggested that this may in part be due to the relatively low affinity of the KLC2 TPR – W-acidic interaction. Further fluorescence polarisation experiments by Dr. Pernigo had also suggested that this interaction may be highly sensitive to the salt concentration in the buffer. In an attempt to overcome these potential obstacles, the approach of Pellegrini et al. was adopted where a peptide from Rad51 was fused to BRCA2 in a chimeric construct. This enabled crystallisation and structural determination for the complex construct (Pellegrini et al., 2002). Thus, the first W-acidic motif of SKIP (identified as binding with the highest affinity) was fused via a flexible TGS(4) linker to the TPR domain of KLC2 (lacking the first helix of TPR1). Fusing the peptide and the KLC2 TPR domain brings them in close proximity, and may make the interaction more likely to occur in the often high salt conditions of crystallisation experiments (Figure 3.4) The KLC2 TPR consisted of residues 219-480 and did not include the first helix of the first TPR, as this is the section that has previously been crystallised (PDB code 3CEQ) and so was thought most likely to be successful (Zhu et al., 2012). The $SKIP^{WD}$ (10aa) and the TGS(4) linker sequence were introduced by annealing oligos and inserting at an NdeI site prior to the TPR region in the 219-480 construct described earlier.

3.4 Cloning and expression of $SKIP^{WD}$_KLC2TPR

$SKIP^{WD}$_KLC2TPR was expressed in *E.coli* as an N-terminally His_6-tagged protein and was first purified by Ni^{2+}-affinity chromatography followed by size exclusion chromatography (SEC). $SKIP^{WD}$_KLC2TPR eluted as a single tailing peak at 55.01ml. The tailing could be caused by the presence of an impurity that is slightly smaller and therefore eluted slightly after $SKIP^{WD}$_KLC2TPR (Figure 3.5). The most pure samples were pooled and concentrated to 5mg/ml for crystallisation trials.

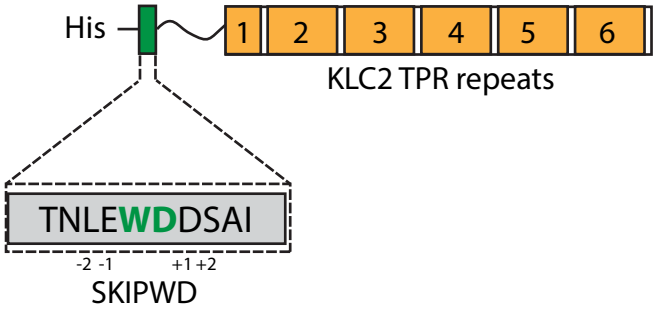

Figure 3.4. Schematic of SKIP^{WD}_KLC2TPR construct design.
The SKIP^{WD} peptide (green) is fused N-Terminal to KLC2TPR residues 219-480 (orange) via a flexible TGS(4) linker.

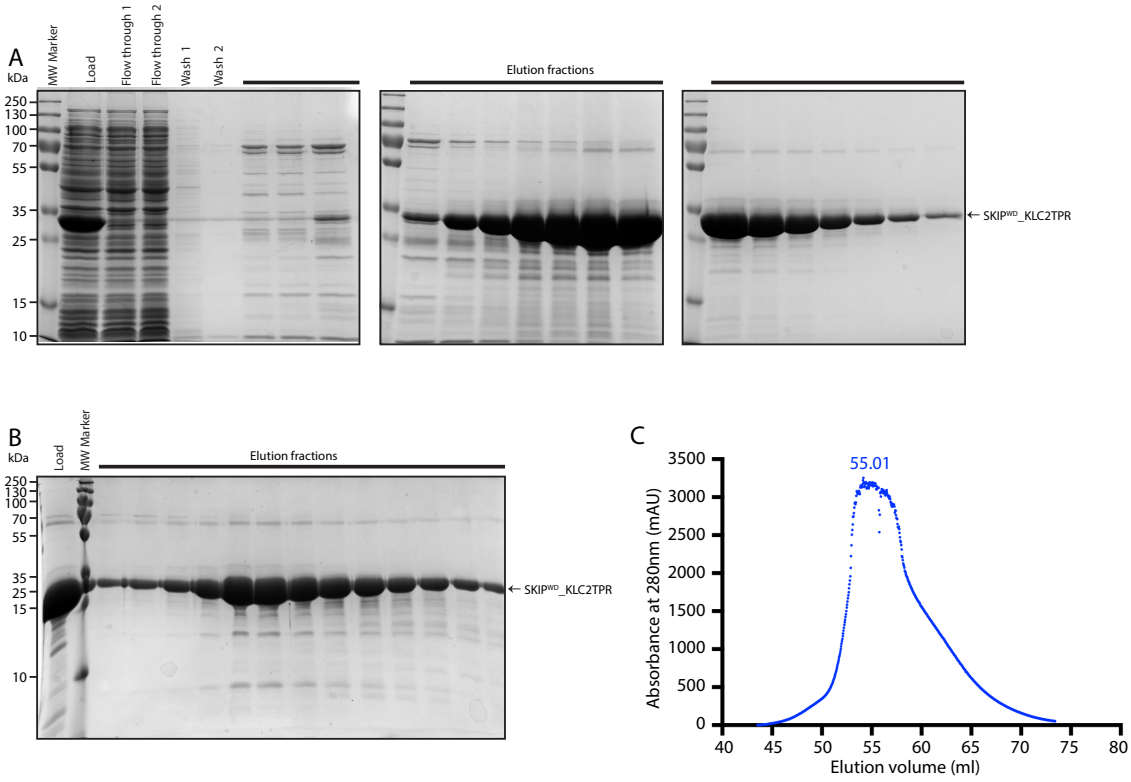

Figure 3.5. Purification of SKIP^{WD}_KLC2TPR.
(A) Coomassie stained gel of the collected fractions of Ni^{2+} column purification. The soluble cell lysate is labeled load. The flow through as well as the wash buffer were collected after passing through the column (flow through 1,2 and wash 1, 2 respectively). The SKIP^{WD}_ KLC2TPR chimera (34.5kDa) was eluted with an imidazole gradient and fractions containing the target protein collected. (B) Coomassie stained gel of fractions eluted during size exclusion chromatography. A size exclusion chromatography column (HiLoad 16⁄600 Superdex 75pg) was used. (C) Size exclusion chromatogram showing absorbance measurements at 280nm of eluted fractions shown in B.

3.5 Crystallisation of SKIP^{WD}_KLC2TPR

Initial screening experiments were set up using the histidine tagged SKIP^{WD}_ KLC2TPR. The crystallisation screens used in trials were PGA, MIDAS, and ProComplex and JCSG+ (Qiagen). Hits were obtained in the poly-γ- glutamic acid (PGA) screen and also in ammonium sulphate based conditions of the ProComplex screen (Figure 3.7). The most frequent crystallising agent for the un-cleaved construct was PGA. The nature of the precipitant clearly influenced the morphology of the resulting crystals. More needle shaped crystals grew in the presence of ammonium sulphate while more single separated crystals grew using PGA as a precipitant (Figure 3.6). The presence of potassium bromide also resulted in more needle like crystals. The optimal pH at which SKIPWD_KLC2TPR crystals grew was centered on 6.5. For all of the conditions in Figure 3.7 apart from number 4 the drops remained clear for 3 days, after which small singular crystals appeared. Nucleation took a relatively short period of time, but once the nucleation process was accomplished the crystals grew relatively slowly. Nucleation took a week longer in condition number 4.

For a second set of screens, the N-terminal histidine affinity purification tag was removed by thrombin cleavage (Figure 3.8A). Western blot analysis using an anti-His antibody confirmed highly efficient proteolytic processing. However, following size exclusion chromatography, the resultant product eluted with two peaks. This could be due to the histidine cleaved SKIP^{WD}_KLC2TPR existing in two different conformations in solution. The fraction containing the highest concentration of the protein that eluted at 55.89 ml was concentrated to 5mg/ml for crystallisation screens. Whilst some crystals were obtained, these were judged to be smaller and less promising and so further work with the tag-free protein was not pursued.

Optimisation screens were set up for the conditions that yielded crystals for the un-cleaved SKIP^{WD}_KLC2TPR construct. Three screens were set up each with a pH vs PGA gradient (pH(5-9) vs PGA concentration (3-13%)) keeping the concentration of the respective additive (potassium bromide, magnesium chloride or L-proline) constant. Another screen was set up with a pH and ammonium sulphate gradient (pH(5-9) vs ammonium sulphate concentration (0.2-1)). Figure 3.7B shows the conditions from the optimisation screens from which SKIP^{WD}_KLC2TPR crystals were chosen for data collection due to their larger dimensions and sharp edges. The crystal that produced the

best diffraction pattern for highest resolution was obtained using 0.10 M MES pH 6.5, 0.2 L-proline, 7% PGA. A complete data set was collected at 2.9 Å resolution at the I24 beamline of Diamond Light Source (Didcot, Oxford, UK) by Dr. Stefano Pernigo, Steiner group, KCL.

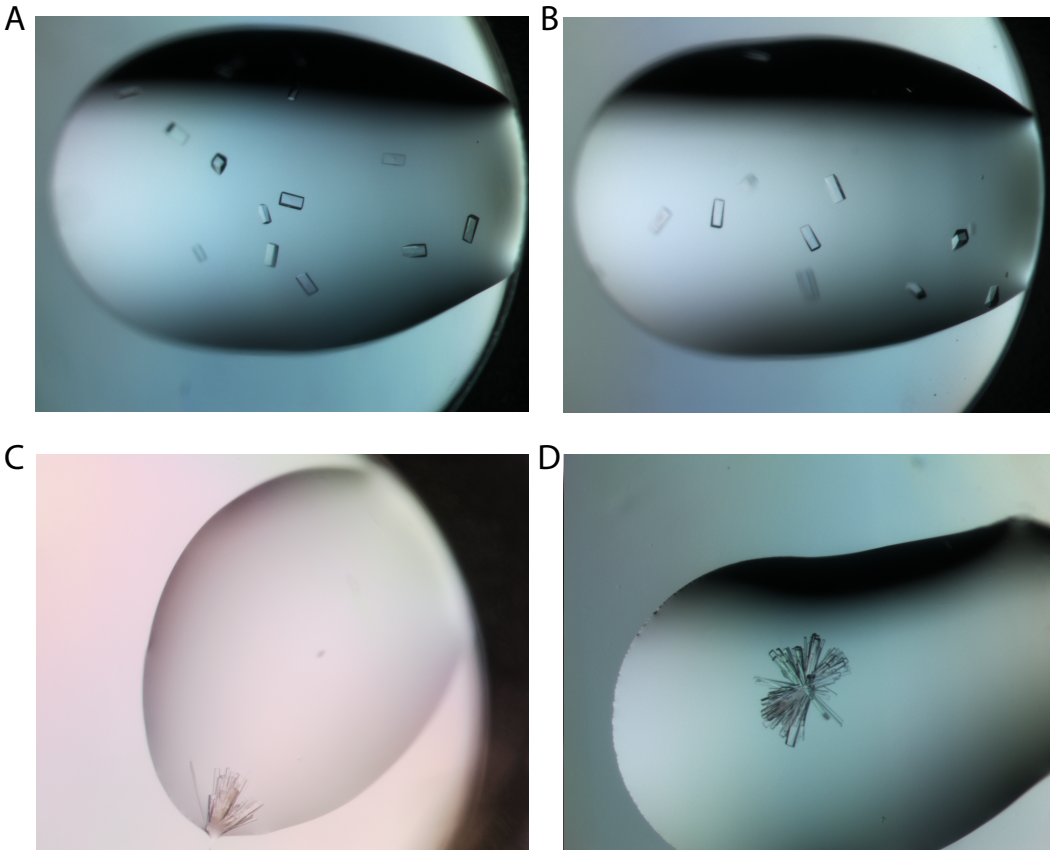

Figure 3.6. Examples of SKIP^{WD}_KLC2TPR crystals.
Images of singular as well as needle like SKIP^{WD}_KLC2TPR crystals. Single separated crystals: (A) 0.1M MES pH6, 0.2M L-proline, 9% PGA, (B) 0.1M MES pH6, 0.2M L-proline, 10% PGA. Needle like crystals: (C) 0.1M Sodium Cacodylate pH6.5, 0.45 ammonium sulphate, (D) 0.1M sodium cacodylate pH6.5, 0.55 ammonium sulphate.

A

No	Buffer	pH	Precipitating Agent	Additive
1	0.1M Sodium cacodylate	6.5	8% w/v PGA	0.3M Potassium bromide
2	0.1M Sodium cacodylate	6.5	8% w/v PGA	0.2M Magnesium chloride
3	0.1M Sodium cacodylate	6.5	8% w/v PGA	0.2M L-Proline
4	0.1M MES	6.5	0.5M (NH4)2 SO4	
5	0.1M MES	6	8% w/v PEG 6000	0.1M Magnesium chloride

B

No	Buffer	pH	Precipitating Agent	Additive
1	0.1M MES	6	7% w/v PGA	0.2M L-Proline
2	0.1M MES	6	8% w/v PGA	0.2M L-Proline
3	0.1M MES	6	10% w/v PGA	0.2M L-Proline
4	0.1M MES	6.5	8% w/v PGA	0.2M L-Proline
5	0.1M MES	6.5	10% w/v PGA	0.2M L-Proline
6	0.1M MES	6	3% w/v PGA	0.3M Potassium bromide
7	0.1M MES	6	4% w/v PGA	0.3M Potassium bromide
8	0.1M MES	6	11% w/v PGA	0.3M Potassium bromide
9	0.1M MES	6.5	0.3 M Ammonium sulphate	
10	0.1M MES	6.5	0.6 M Ammonium sulphate	
11	0.1M HEPES	7	0.4 M Ammonium sulphate	

Figure 3.7. Conditions that produced SKIP^{WD}_ KLC2TPR crystals.
(A) List of the conditions from the initial crystal screens that produced crystals (no.1-3: PGA, No.4,5: ProPlex). (B) List of the conditions from the optimisation screens that produced crystals. Optimization screens that produced crystals were pH(5-9) vs PGA concentration (3-13%) with 0.2M L-proline, pH(5-9) vs PGA concentration (3-13%) with 0.3M potassium bromide and pH pH(5-9) vs ammonium sulphate concentration (0.2-1 M).

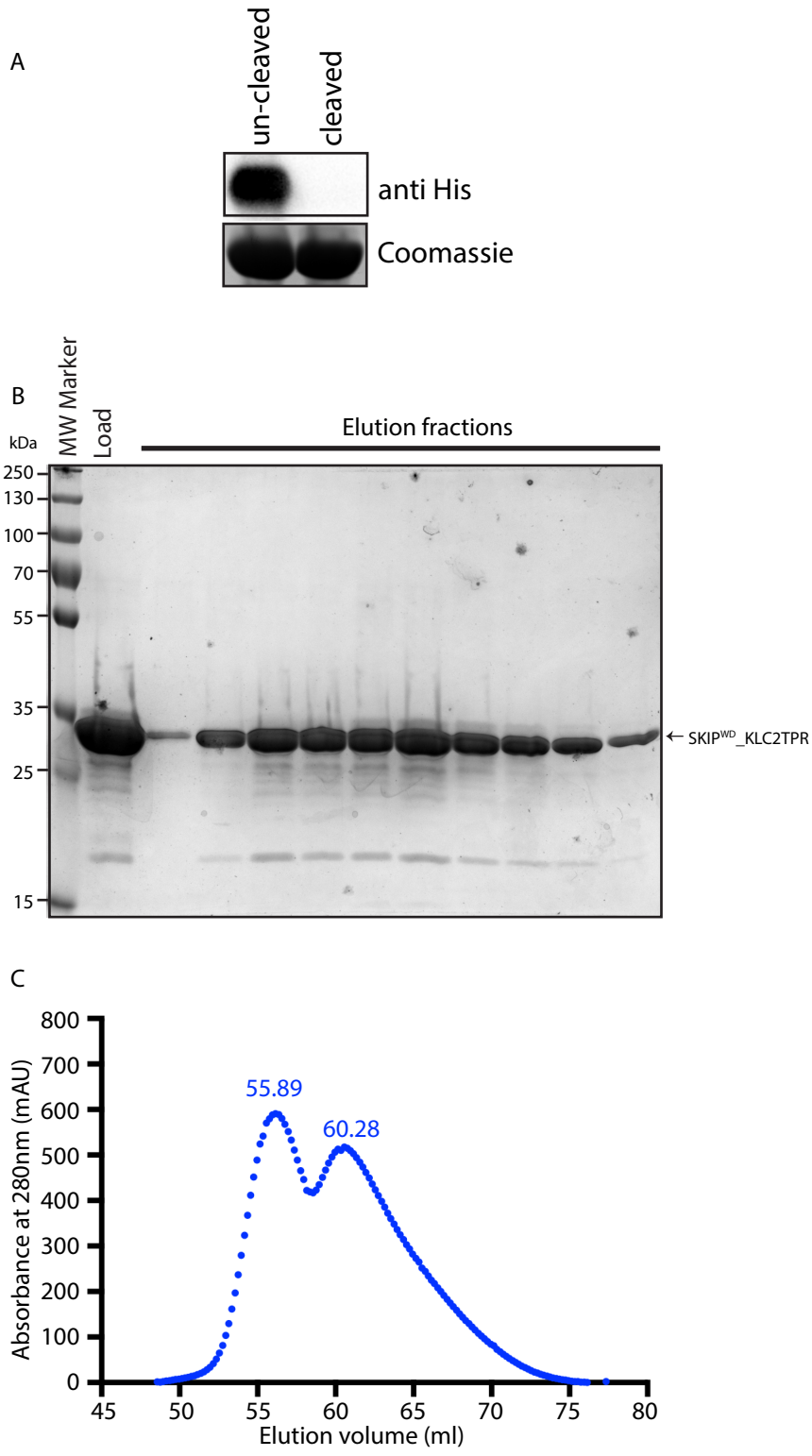

Figure 3.8. Thrombin cleavage of Histidine tag.
(A) Coomassie stained gel and western-blot (blotting with a monoclonal HRP conjugated anti His antibody) of the thrombin cleaved (32.6kDa) and un-cleaved $SKIP^{WD}$_KLC2TPR (34.5kDa). (B) Coomassie stained gel of fractions eluted during size exclusion chromatography (C) Size exclusion chromatogram showing absorbance measurements at 280nm of eluted fractions shown in B.

3.6 Structural determination

Using molecular replacement for phase information, the structure of the tryptophan-acidic motif containing peptide from SKIP in complex with the KLC2 TPR ($SKIP^{WD}$_KLC2TPR) was solved by Dr. Stefano Pernigo and Dr. Roberto Steiner and the figures of the structure presented here were created by them and the structure is deposited in the PDB under code 3ZFW (Figure 3.9 and Figure 3.10). The R_{factor}/R_{free} gives an indication as to whether the structure that was solved agrees with the data collected. The R-value can range from zero (for perfect agreement between calculated and observed) to approximately 60% for a random model compared to an experimental data set. An R_{factor} of 20% is desirable for a protein model refined with data to 2.5Å. 20.27% is therefore a good R_{factor} value for a model refined to 2.9Å. The R_{free} value enables the assessment of possible overmodelling of the data and validate the extent to which the model explains the diffraction data. The R_{free} value was calculated against 5% of the total reflections that are set apart during scaling and is not used for refinement. This aids in reducing model bias and over fitting of data. Iterative model fitting and refinement cycles results in model improvement and both R_{factor} and R_{free} values dropping (Brunger, 1992). The molprobity score is a log-weighted combination of the clashscore, percentage Ramachandran not favored and percentage bad side-chain rotamers, giving one number that reflects the crystallographic resolution at which those values would be expected (Chen et al., 2010). Since the molprobity score is lower than its actual crystallographic resolution, the quality of the structure modelled is thought to be better than the average structure solved at that resolution (Figure 3.10).

The $SKIP^{WD}$_KLC2TPR structure shows the KLC2 TPR domain (orange) consisting of TPR motifs 2-6 as a concave alpha helical structure similar to that found by (Zhu et al., 2012). The construct includes the external helix of TPR1, however the residues could not be assigned, so the KLC2TPR starts from TPR2. Each TPR motif consists of two anti-parallel alpha helices, one that is internal to the TPR domain and one external. This is denoted by or I or E for the helix at the center of the TPR domain (internal) and the outer helix (external) respectively. The SKIP peptide (green) spans the length of the TPR domain and residues throughout the peptide interact via H-bonds and salt bridges with the TPR domain. When comparing the cargo free KLC2 TPR (3CEQ) (grey) domain and the cargo bound KLC2 TPR (orange), the N-terminal TPR2-3 appears to

fold around the SKIP peptide (Figure 3.9). The SKIP peptide is highly negatively charged and the electrostatic surface representation of the binding pocket shows the surface to be largely positive in charge (blue) suggesting that recognition of cargo is partly achieved by charge complementarity (Figure 3.11).

The tryptophan sits within a relatively hydrophobic leucine-rich pocket in the centre of the structure, interacting with residues on TPR2 (L248, R251, L263) and TPR3 (N287, L290, L291). The aspartic acid (SKIP D208) and the glutamic acid (SKIP E206) point in the opposite direction and face the TPR3-4 side of KLC2TPR groove. The carboxylate side chain of SKIP D208 form a network of salt bridges and H-bonds with the positively charged R312 and K325 side-chains and SKIP E206 is stabilized by ionic interactions with K325 of KLC2 TPR. The leucine at the -2 position is common for W-acidic motif containing proteins and the structure shows that SKIP L205 is buried in a pocket between TPR3 and TPR4, involving V290, C305 (from TPR3) and N329, L332, and L333 (from TPR4).

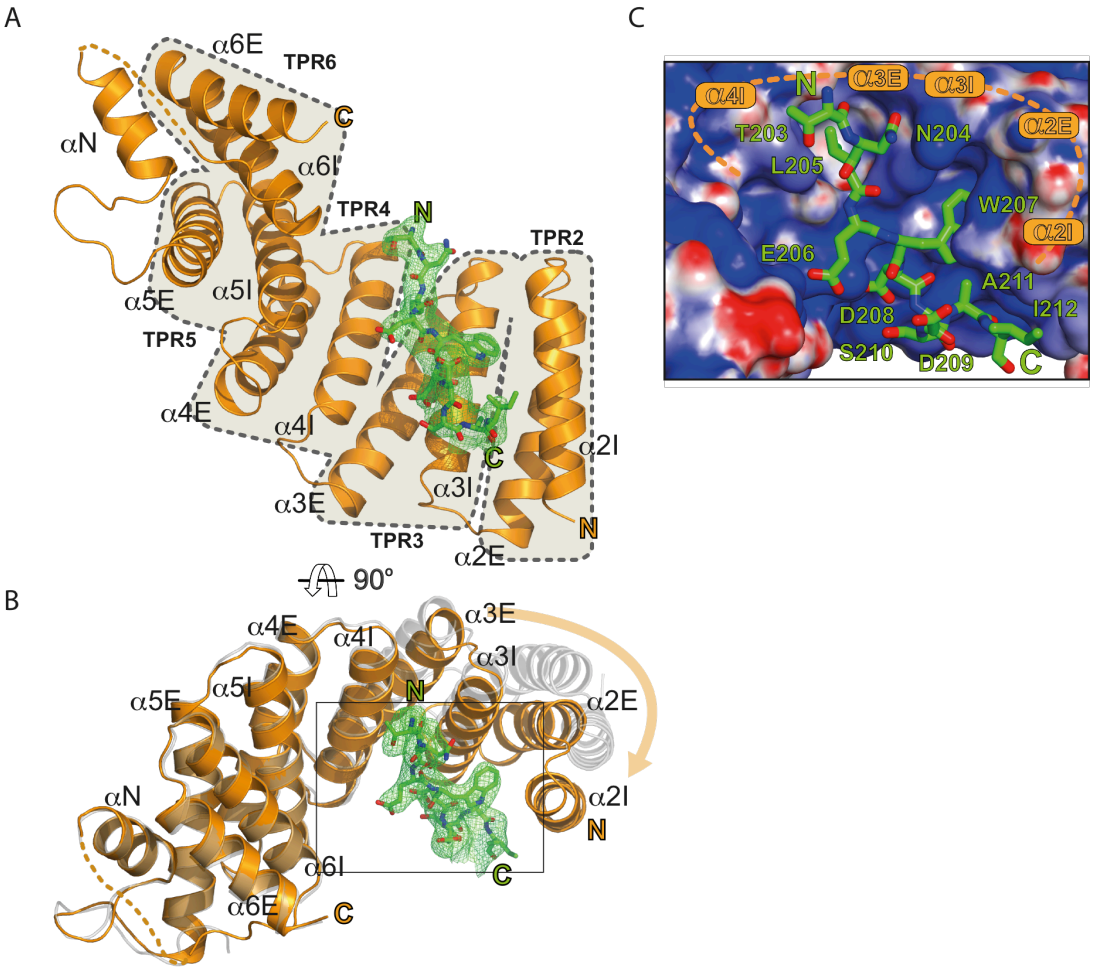

Figure 3.9. Structure of the SKIP^{WD}_KLC2TPR cargo complex.
(A and B) Illustrated representations of the SKIPWD motif (displayed as stickmodel in green) bound to KLC2TPR domain (orange) in two orthogonal orientations. Simulated annealing (Fo-Fc) omit map for the W-acidic cargo motif is contoured at the 3s level. Individual TPR repeats composed by helix-turn-helix elements ("I" and "E" for internal and external, respectively) are highlighted in (A). A non-TPR helix (αN) is between TPR5 and TPR6. (B) also shows the cargofree KLC2TPR structure (gray transparent), with an orange arrow indicating the movement of the TPR2-TPR3 region with respect to the common TPR4-TPR6 reference frame. (C) Electrostatic potential surface representation of KLC2TPR with its SKIPWD-bound cargo. Positive and negative potential is shown in blue and red, respectively. Cargo recognition is achieved by a combination of charge complementarity and sequence specificity. (Figure supplied by Dr. Roberto Steiner).

Data set	$SKIP^{WD}$-$KLC2^{TPR}$
Data collection	
Beamline	I24 (DLS)
Wavelength (Å)	0.9686
Resolution range (Å)/Highest res. bin (Å)	52.42-2.90/(2.98-2.90)
Space group	$P2_12_12$
Cell dimensions (Å)	87.81, 90.86, 94.04
Unique reflections	17034
Overall redundancy	5.60/(5.04)
Completeness, (%)	99.0/(98.2)
Wilson B ($Å^2$)	95.4
R_{symm} (%)	7.1/(70.0)
$\langle I/\sigma(I) \rangle$	10.5/(2.4)
Refinement	
PDB code	3ZFW
R_{factor} (%)/R_{free}(%)	20.27/24.48
# non-H atoms	3751
Mean B value ($Å^2$)	108.7
rmsd bond lengths (Å)	0.009
rmsd bond angles (°)	1.03
Molprobity score	1.89 (99% percentile)

Figure 3.10. Data collection and refinement statistics.
(Figure supplied by Dr. Roberto Steiner).

3.7 Verification of the binding pocket

3.7.1 Co-immunoprecipitation

To verify the structural model and to examine the importance of the main residues found within the binding pocket of the KLC2 TPR domain in cargo recognition, a series of key residues that appeared to interact with the SKIPWD peptide were mutated. Both charge reversal mutations as well as mutations not affecting charge were made; for example R to E and R to A. A GFP-TRAP immunoprecipitation assay was used to determine the effect of making mutations of key residues within the KLC2 binding pocket. HeLa cells were co-transfected with plasmids designed to express N-terminally hemagglutinin (HA) tagged KLC2 and mutants of KLC2 (R251D, N287L, V290K, L291D, R312E, R312A, K325E, L333K) and N-terminally green fluorescent protein (GFP) tagged SKIP(1-310). GFP and GFP-SKIPWEWD (Both WE and WD mutated) were also included as negative controls. GFP/GFP-SKIP(1-310) was immunoprecipitated with GFP-TRAP beads and the amount of co-immunoprecipated HA-KLC2 was assessed by western blot. Binding was significantly reduced or lost completely for all of the mutations made. The charge reversal mutations give an indication of the large part that electrostatic interactions play in cargo binding. Mutating R251, R312, K325 of KLC2 to acidic residues resulted in substantial loss of binding to SKIP (Figure 3.11B). The R312E mutation had the largest impact; supporting the fact that this residue is directly involved in forming salt bridges with the side chain of the aspartic acid (of the tryptophan-acidic motif) on the cargo. The R312E mutation had a greater impact than R312A, illustrating that the interaction is not only due to sequence specificity but also due to charge complementarity (Figure 3.11B).

3.7.2 Fluorescence polarisation analysis of key mutations

To further validate the structure in a biophysical assay, the effect of making the KLC2 point mutations (N287L, R251D or R312E) on the affinity of the SKIP:KLC interaction, fluorescence polarisation assays were carried out in collaboration with Dr. Stefano Pernigo, Steiner group, KCL. N287L, R251D and R312E were chosen because N287 and R251 make direct interactions with the tryptophan and R312 interacts with the aspartic acid flanking the tryptophan (D-208) in the tryptophan-acidic motif (WD).

As described earlier, N-terminal carboxytetramethylrhodamine (TAMRA) conjugated peptide ($SKIP^{WD}$) was added at 100nM concentration to increasing concentrations of wildtype KLC2 TPR(219-480) and proteins containing a point mutations (N287L, R251D or R312E). This enabled binding curves to be generated from which dissociation constants (Kd) could be calculated. These fluorescence polarization measurements confirm that upon making mutations of key residues within the KLC2 binding pocket, binding is significantly reduced.

3.7.3 Immunofluorescence

When full length SKIP and its small guanosine triphosphatase binding partner Arl8 are co-expressed in cells they associate strongly with lysosomes and promote their trafficking to the cell periphery (Rosa-Ferreira and Munro, 2011). When co-expressed, GFP-KLC2 associates with the same lysosomes (Figure 3.11, top). Thus, this provides a convenient assay to determine whether the mutations defined by the structure impact upon cargo binding *in vivo.* This association does not occur upon making the KLC2 mutations (R251D, N287L, and R312E) (Figure 3.12), providing further validation of the model in a cellular context where full length SKIP is present.

3.7.4 Disruption of the SKIP:KLC interface disrupts the association of SKIP with the kinesin-1 tetramer

The experiments described above confirm that mutational disruption of the KLC TPR – W-acidic interface prevents SKIP interaction with the light chain in biochemical, biophysical and cell based assays. However, they do not demonstrate that this interface is crucial for binding the kinesin-1 tetramer. If this interface is crucial for kinesin-1 cargo recognition then it would be expected that the same mutations would also inhibit this interaction.

To test this, GST-tagged SKIP (1-310) was purified from E.coli and bound to glutathione coated beads. GST-SKIP beads (or control GST beads) were incubated with 293T cell extracts expressing N-terminally citrulline (Cit) tagged KHC alone or Cit-KHC co-expressed with wildtype and mutant HA-KLC2 constructs. As expected, both HA-KLC2 and Cit-KHC were pulled down robustly by GST-SKIP (but not GST) from extracts with wildtype KLC2. KHC expressed alone was not pulled down by GST-SKIP. It was also notable that co-expression of light chain appeared to enhance expression of KHC. More importantly

however, mutation of the W-acidic binding site using N287L or R251D dramatically reduced binding of both the heavy and light chains. Taken together, these data confirm the importance of the W-acidic interface defined in the structural model in kinesin-1 – SKIP recognition.

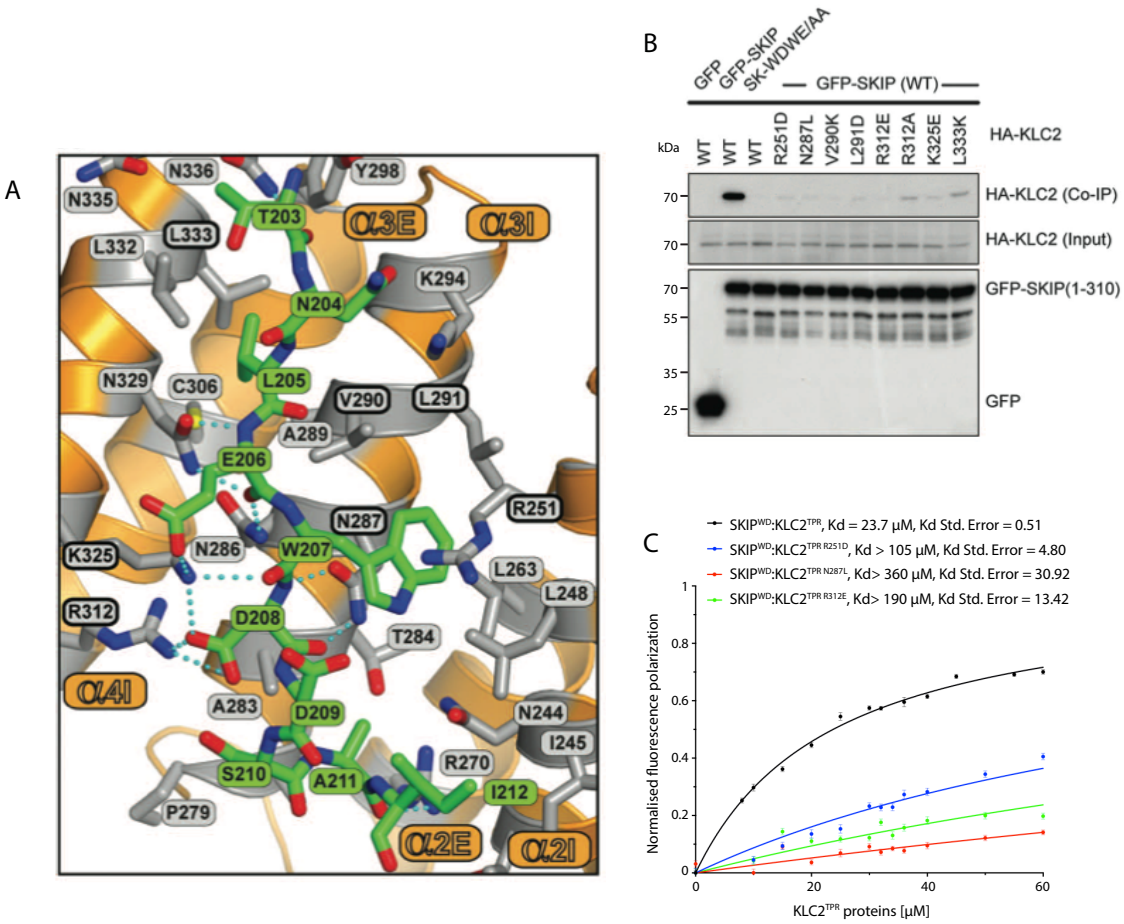

Figure 3.11. Mutations in the SKIP^{WD}:KLC2TPR interface disrupt binding. (A) Details of the SKIP^{WD}:KLC2TPR interface. KLCTPR side chains stabilising the SKIP^{WD} cargo peptide (green) are shown as gray sticks emanating from the orange model. Non-carbon elements are nitrogen, dark blue; oxygen, red; and sulfur, yellow. Hydrogen bonds are represented by dotted light blue lines. (Figure supplied by Steiner group) (B) Co-immunoprecipitation of HA-KLC2TPR (70.0 kDa) and KLC2TPR containing mutations at the SKIP^{WD}:KLC2TPR interface with GFP-SKIP (62.1 kDa) or GFP (29.9 kDa) control. Input lysates and co-immunoprecipitated HA-KLC2 (bound) were blotted for KLC2 using an anti-HA mouse monoclonal antibody. GFP and GFP-SKIP were blotted for using an anti-GFP mouse monoclonal antibody. A goat polyclonal anti-mouse HRP antibody was used as a secondary antibody to allow for detection using Clarity Western ECL substrate. The blot is representative of three experiments involving three independent repeat transfections followed by co-immunoprecipitation (C) Fluorescence polarization measurements showing that R251D, N287L, and R312E mutations in KLC2 dramatically reduce the affinity of the TPR domain for the SKIP^{WD} peptide. The graph shows average values from three independent experiments utilising the same KLC2TPR/mutant preparation and TAMRA conjugated peptide stock solutions. Measurements were performed on a Horiba Fluoromax-4 spectrofluorometer at 20 °C. A one site - specific binding curve was fitted to the data: Y = Bmax*X/(Kd + X). Kd values reported here were calculated at 150 mM NaCl.

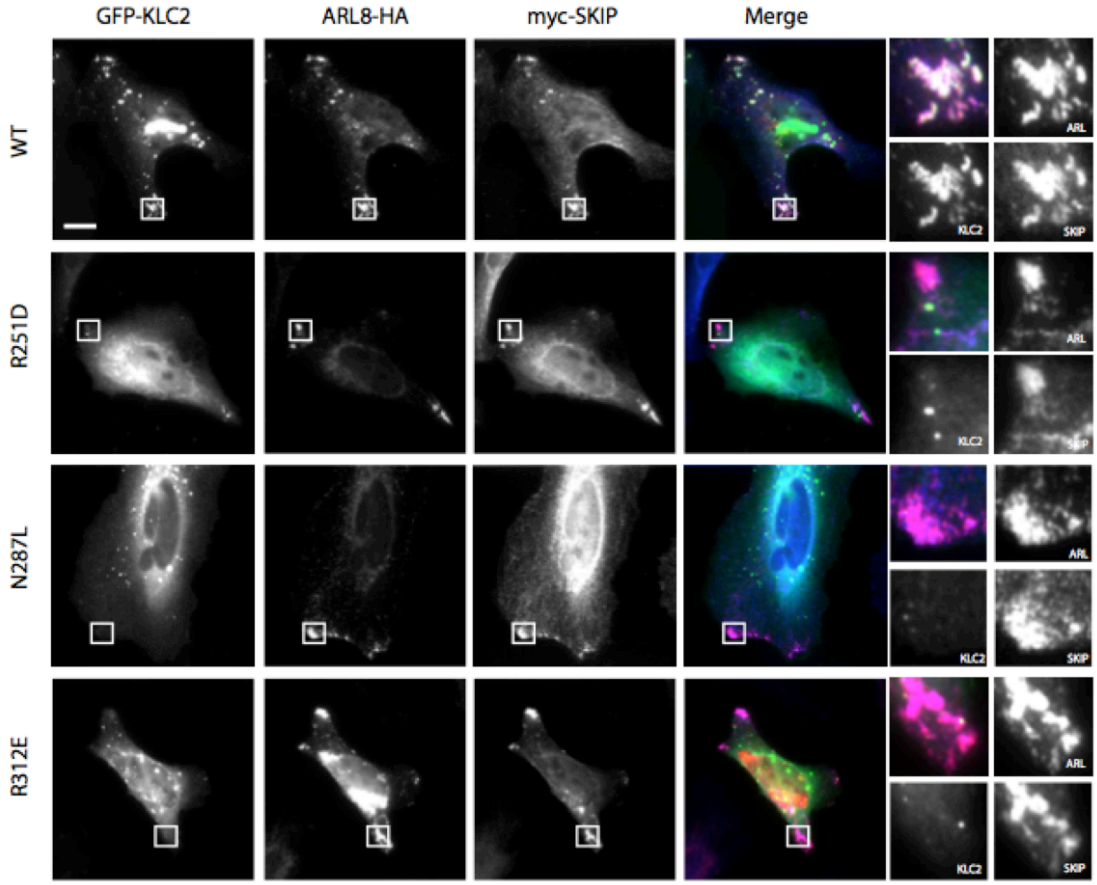

Figure 3.12. Replacement of key KLC2TPR residues results in loss of GFP-KLC2 association with Arl8/SKIP– positive lysosomal membranes.
Representative confocal fluorescence images showing HeLa cells transfected with GFP-KLC2 or KLC2 mutant (N287L, R251D or R312E), Arl8-HA and myc-SKIP. The primary antibodies used were a rabbit polyclonal anti-HA antibody and a mouse monoclonal anti-myc antibody. The secondary antibodies were Alexa 633 goat anti-rabbit antibody and Alexa 568 goat anti-mouse antibody probing for Arl8-HA and myc-SKIP respectively. In merge panels, GFP-KLC2, Arl8, and SKIP are shown in green, red, and blue, respectively. N=3 Scale bar = 10μm.

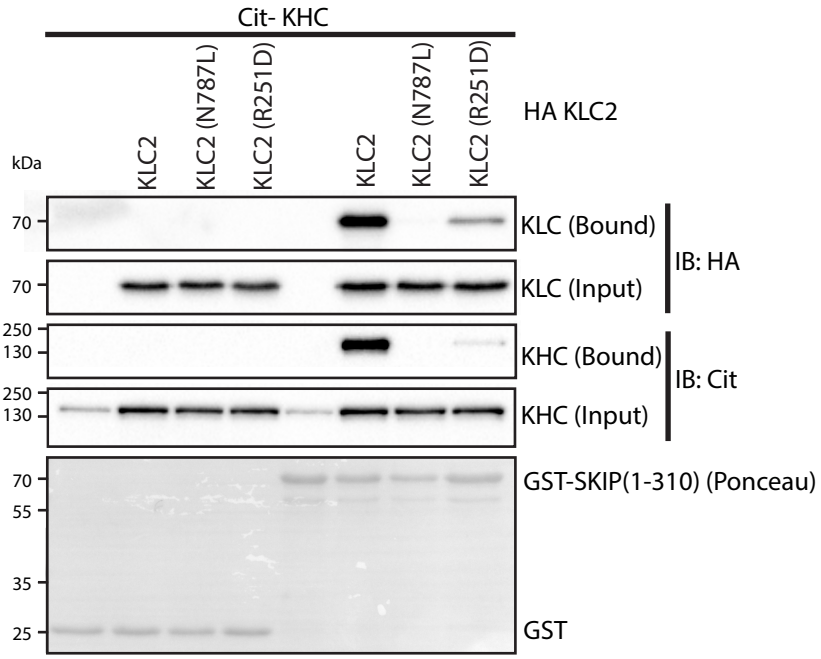

Figure 3.13. KLC2 TPR domain mutations prevent binding to the kinesin-1 tetramer.

Pull-down of Cit-KHC(135.6 kDa) and HA-KLC2 (70.0 kDa) (or HA-KLC2 mutants N287L or R251D) from 293T cell lysate using GST-SKIP(1-310) (61.8 kDa) or GST (25.5 kDa) as control. Input lysates were blotted for HA-KLC2 (or HA-KLC2 mutants N287L or R251D) and Cit-KHC as control using a mouse monoclonal anti-HA antibody and a mouse monoclonal anti-GFP (detecting the citrulline tag). A goat polyclonal anti-mouse HRP antibody was used as a secondary antibody to allow for detection using Clarity Western ECL substrate. GST and GST-SKIP(1-310) were visualized by ponceau staining. The blot is representative of three experiments involving three independent repeat transfections followed by GST-pulldown with the same GST/GST-SKIP protein preparations.

3.8 Discussion

The aim of the experiments in this chapter was to determine an X-ray crystal structure of a W-acidic motif in complex with the TPR domain of KLC2 in order to shed much needed light on the molecular mechanisms underlying the kinesin-1 cargo recognition. This was achieved through the careful characterisation of the determinants of the SKIP – KLC interaction and development of a suitable crystallisation strategy. Validation of the resulting structure was achieved with a series of biochemical, biophysical and cell based assays. Specific recognition is achieved though a combination of sequence specific and electrostatic interactions.

Fluorescent polarisation assays show that the KLC2 TPR domain specifically recognises the tryptophan acidic motif(s) in SKIP and that they make different contributions to KLC2 binding (Figure 3.1 and Figure 3.3). Consistent with this, significantly more binding is lost when the first motif is replaced by alanine compared to the second motif (Figure 3.1). This appears to parallel the situation in vaccinia A36R protein where one motif makes a much more important contribution than the other (Dodding et al. 2011). In that same study, replacement of the cytoplasmic domain of A36 with the kinesin binding region of SKIP (aa157–264) was sufficient for kinesin-1 recruitment and transport. This was dependent upon both W-acidic motifs in SKIP. However, supporting the data shown here, the first motif of SKIP plays a bigger role (Dodding et al. 2011), but does perhaps suggest that the second motif is still important.

Extension of the peptide in FP experiments to encompass both W-acidic motifs resulted in a substantial increase in binding affinity compared to either motif alone. Two hypotheses have the potential to explain this effect. Firstly, it may be the case that co-operativity and/or avidity effects operating between the motifs contribute to an increase in apparent affinity. Alternatively, residues in the intervening sequence may directly contribute to binding. Some experimental evidence that the second mechanism may at least make a contribution is suggested by the larger effect of the exon 7 deletion on KLC binding than the WE mutation alone, however further (although likely very costly) studies using mutated peptides may provide a more definitive answer. The SKIP peptide: KLC TPR domain interaction is of a relatively low affinity. Whether this interaction alone is sufficient for transport through the cell remains to be

established. The TPR construct used in the fluorescence polarisation experiments did not include the first helix of the first TPR and as a result the binding affinity quantified may also not be representative for the full length TPR domain.

Calsyntenin-1 contains two tryptophan-acidic motifs where both motifs contribute to similar degrees to binding to KLC1 (Konecna et al., 2006). In line with this, both motifs contribute to similar extents in a vaccinia virus transport assay (Dodding et al. 2011). Further work on this by Dr. Dodding and Dr. Perngio confirmed that both Calsyntenin-1 motif peptides bind KLC with comparable and high affinities (10μM) and that binding is inhibited by the mutations defined in this thesis (Pernigo et al. 2013), suggesting that the pocket defined here may be universal for these motifs. However a single Calsyntenin-1 motif is sufficient to mediate some degree of kinesin-1 activity and transport when fused to a TM domain (Kawano et al., 2012), suggesting that the relationship between cargo containing two tryptophan acidic-motifs and kinesin-1 can vary depending on context and sequence. Indeed, since publication of this work, the Holzbaur group discovered a single W-acidic motif in Nesprin-2 that contributes to nuclear positioning in myotubes (Wilson and Holzbaur, 2015). Further validating the findings here, the mutations defined in this chapter also inhibit interaction with Nesprin-2.

Dodding et al. identify more than 1360 motifs as potential KLC binding partners based on bioinformatics analysis of a loose consensus W-acidic sequence. Given the difference in affinity between very similar motifs studied here, more effort will be needed to further understand the reasons for these differences to refine this consensus before more accurate predictions can be made. However, it seems likely that number is an overestimate.

In this chapter, the binding pocket for tryptophan-acidic motifs is observed in the structure of the KLC2TPR domain in complex with the tryptophan-acidic motif containing peptide from SKIP (Figure 3.9). The KLC2TPR concave groove is highly positively charged and complements the highly negatively charged SKIP peptide. This suggests that recognition of cargo is partly achieved by charge complementarity (Figure 3.11). Upon SKIP binding to the KLC2 TPR domain the N-terminal TPR2-3 appears to fold around the SKIP peptide. This structural change is not typical for TPR domains and may be responsible for the transduction of a signal to activate kinesin-1. The key

residues identified from the crystal structure to be involved in interacting with SKIP, was verified through mutagenesis, co-immunoprecipitation, fluorescence polarisation as well as immunofluorescence.

Amino acid substitution tested within the KLC2TPR groove significantly reduced binding to SKIP(1-310). The importance of electrostatic interactions in cargo recognition is highlighted by the charge-reversal mutations. Replacement of R251, R312, K325 by acidic residues, results in substantial loss of binding. Less “extreme” mutations for example R312A also significantly impairs binding, but to a lesser extent than R312E. Fluorescence polarization also showed complete abrogation of binding upon making three key mutations within KLC2 TPR domain (R251D, N287L, or R312E). This was verified *in vivo*, showing that KLC2 containing the mutations (R251D, N287L, or R312E) do not associate with lysosomes at the cell periphery.

The structure suggests that the highly conserved leucine in the -2 position from the tryptophan in the tryptophan-acidic motif plays an important part in cargo recognition as it occupies a relatively hydrophobic binding pocket on the TPR. This is supported by the fact that the $SKIP^{WE}$ peptide which does not have a leucine in the -2 position (but instead has a threonine residue) makes a lower affinity interaction with KLC2. The leucine in the -2 position of the second tryptophan-acidic motif of Calsyntenin-1 has also been shown to be essential for binding to KLC as mutation of the leucine to alanine abrogates binding to KLC1 (Kawano et al., 2012). The first tryptophan acidic motif from Calsyntenin-1 also contains a related methionine at the -2 position and binds to KLC1 with comparable affinity (Konecna et al., 2006, Pernigo et al., 2013). The constraints used by Dodding et al., 2011 to identify possible tryptophan-acidic motif containing binding partners did not include a leucine/methionine in the -2 position. There are therefore likely to be far fewer higher affinity tryptophan-acidic motifs than predicted. It is likely that this will have a significant impact on the real number of W-acidic cargoes in mammalian cells.

Despite this, there are examples of cargo that also bind to KLC TPR domain that do not have a tryptophan acidic motif. Zhu et al. suggest that the acidic C-terminal peptide of JIP1 that also contains aromatic and hydrophobic residues (sequence EYTCPTEDIYLE) binds within the same positively charged groove (although perhaps making more important contacts with TPR3). It seems possible that the general principle of sequence specific and electrostatic

interactions established here may support the recognition of more diverse sequences, with peptides of different composition taking different paths through the charged groove. Further attempts to address this question are described in chapter 6.

CHAPTER 4 . SKIP BINDS DIRECTLY TO KINESIN HEAVY CHAIN.

Chapter 3 has provided a greater understanding of how cargo recognition is achieved by KLC, through the crystallisation and solving of the structure of the first kinesin-cargo interface. Over expression experiments in cells suggest that SKIP has an intrinsic capacity to bind and activate kinesin-1 as transfection of full-length SKIP promotes kinesin-1 dependent lysosome dispersion. A number of reports suggested that full activation of kinesin-1 requires binding to the heavy chain in addition to contacts with the light chain (Blasius et al., 2007). Indeed, JIP-1 binds both the heavy and light chains (Fu and Holzbaur, 2013). Given this potent capacity of SKIP to drive lysosome dispersion, it seemed possible that SKIP may also possess a similar capacity to bind to both KHC and KLC. Experiments in this chapter test this hypothesis and show just a variety of biochemical and biophysical assays that SKIP does indeed have the capacity to interact directly with KHC. Further work fine maps the respective binding sites on both molecules.

4.1 SKIP binds to KHC

To determine whether SKIP binds directly to the cargo binding domain of KHC, a GST pulldown experiment was carried out using *E.coli* expressed GST tagged C-terminal tail region of KHC (Kif5C) (amino acid residues 815-955) and SKIP (amino acid residues 1-310). The C-terminal tail region of KHC was expressed as a GST fusion and eluted in a batch purification method with glutathione Sepharose 4 fast flow beads. GST-SKIP(1-310) was expressed and purified in the same way. The GST tag was then cleaved from SKIP(1-310) using the C3 protease and the bulk of free GST or uncleaved GST-SKIP were removed by a second incubation with glutathione coated beads. This enabled the study of the KHC:SKIP interaction by GST pulldown (Figure 4.1A).

Saturation binding experiments were carried out by incubating 1.6μM of GST-KHC(815-955) with increasing concentrations of SKIP(1-310), followed by pulldown with glutathione coated beads and analysis by SDS-PAGE (Figure 4.1B). Binding was monitored by band densitometry that indicated that binding tends toward saturation. The binding curve appeared sigmoidal in character,

perhaps suggesting some degree of co-operativity. Although such a non-equilibrium experiment is not ideal for the determination of Kd, fitting binding data from three independent experiment suggested that the Kd is on the order of 1.5μM with a Hill coefficient of 2. This Hill coefficient is indicative of some co-operativity. Due to the high concentration of GST-KHC(815-955) used, the calculated Kd should be treated with caution. At the lower concentrations of SKIP, SKIP is not in excess, which may cause the sigmoidal curve observed. This effect may be overcome by using a lower GST-KHC(815-955) concentration to pull down SKIP. However to enable binding to be seen by coomassie staining a high concentration of KHC was used. Within an equilibrium binding experiment, the concentration of the receptor is usually kept constant and below the Kd (R/Kd < 0.1 or lower). Higher receptor concentrations may lead to ligand depletion due to the binding of significant amounts of ligand. In Figure 4.6 a much lower concentration of receptor (TAMRA-SKIP (202-241)) is used than ligand KHC (866-917) which suggests that the shape of the curve is not due to ligand depletion, but may result from cooperative binding.

Confirming the statistical significance of the level of binding observed, comparison of SKIP bound at a concentration of 3.5μM bound significantly less to GST than GST-KHC (815-955) ($p<0.001$) (Figure 4.1C). The GST cleaved SKIP(1-310) used for the pulldown contains a series of breakdown products and some higher molecular weight impurities. It seems likely that that SKIP* and SKIP** highlighted in Figure 4.1B could be uncleaved SKIP and SKIP*** may be a breakdown product of an uncleaved SKIP as all of these contaminants bind GST-KHC in a concentration dependent manner but do not bind to GST alone. The KHC breakdown products (KHC* and KHC**), as expected, remain constant as a fixed concentration of KHC was used. Taken together, these data suggest that SKIP may interact directly with the KHC C-terminal tail.

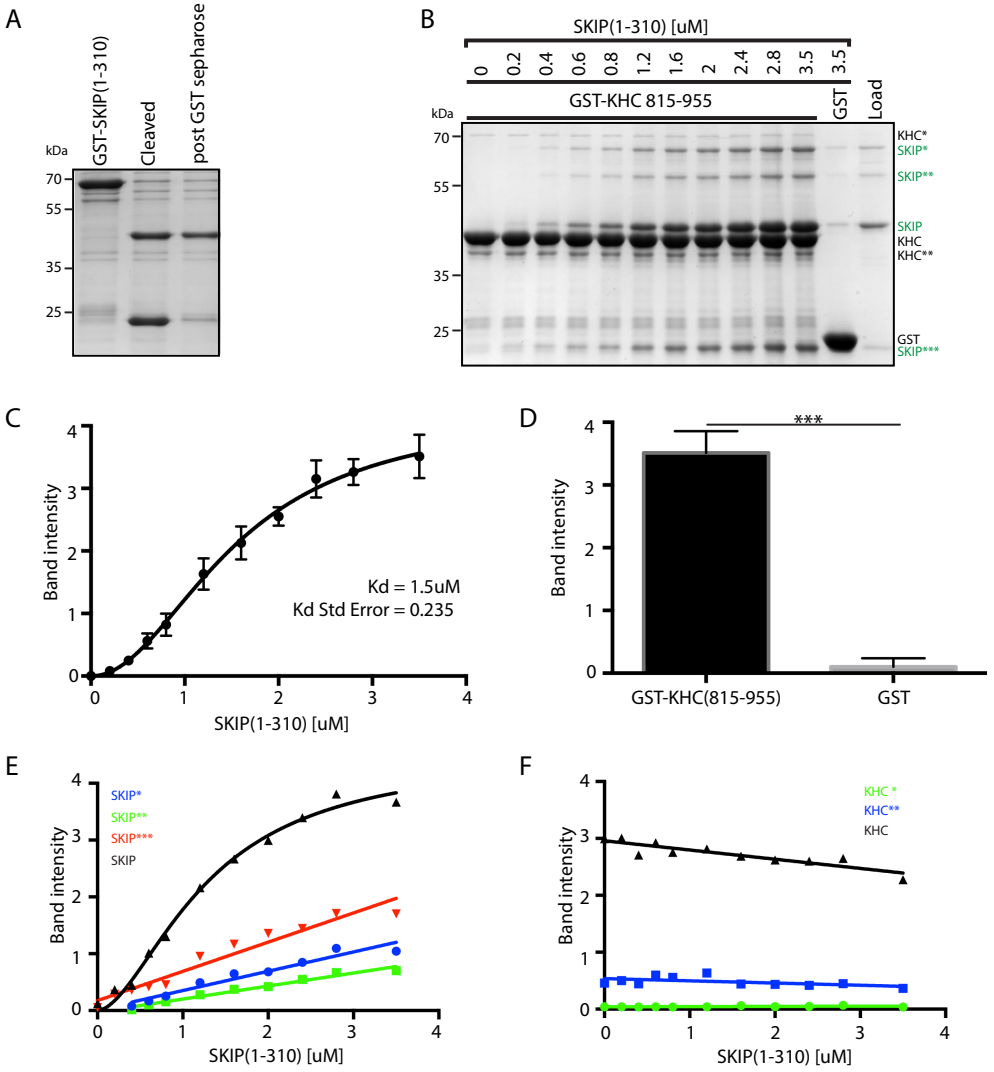

Figure 4.1. SKIP(1-310) tends toward saturable binding to GST-KHC (815-955).

(A) Coomassie stained gel of C3 cleavage of GST tag from GST-SKIP(1-310) (61.8 kDa). Lanes from left show uncleaved protein, protein sample after cleavage (35.3 kDa) and cleaved protein sample after removal of GST by GST Sepharose beads. (B) Coomassie stained gel of pull-down of SKIP(1-310) using GST-KHC(815-955) (42.6 kDa) or GST (25.5 kDa) as control. The concentrations of SKIP(1-310) indicated were incubated with 0.5nmoles GST-KHC(815-955) or GST in a volume of 300µl (1.6µM). (C) Graph of the band intensity of SKIP(1-310) against concentration of SKIP(1-310) incubated with GST-KHC(815-955). Hill coefficient (h) = 2, h standard error=0.339. The graph is based on quantification from three experiments with the same protein preparations. A one site - specific binding curve with a hill slope was fitted to the data: Y=Bmax*X^h/(Kd^h + X^h). (D) Comparison of band intensity of SKIP(1-310) incubated at 3.5µM with GST-KHC(815-955) and GST. ***P<0.001 (two-tailed T-test). (E) Representative graph of one experiment showing the band intensities of SKIP(1-310) and the SKIP breakdown products (SKIP*, SKIP** and SKIP***). (F) Representative graph of one experiment showing the band intensities of KHC the KHC breakdown products (KHC* and KHC**).

4.2 SKIP binding to the C-terminal tail of KHC requires amino acids 876-917

To map where SKIP binds on the KHC tail a series of GST tagged C-terminal KHC fragments were expressed in *E.coli* (Figure 4.2A and Figure 4.2B) and purified by batch purification with glutathione Sepharose 4 fast flow beads. GST-SKIP(1-310) was expressed and purified in the same way and the tag cleaved as described in the previous section. SKIP(1-310) was incubated at the subsaturating concentration of 1.2μM with 1.6μM GST-KHC(815-955), GST alone or GST-KHC fragments (815-907, 815-917, 815-931, and 907-955) in a volume of 300μl. A subsaturation concentration of SKIP was used to allow for subtle variation in binding to be observed. Figure 4.2B shows the purified protein used in the GST-pulldown in Figure 4.2C. Truncating the C-terminal tail from 815-955 to 815-917 has no effect on binding (compare lane 5 with lanes 3 and 4). However, removing an additional 10 amino acids by truncating KHC 815-917 to 815-907, binding to SKIP(1-310) is completely lost. This suggests that the region between 907 and 917 is essential for binding to KHC. The KHC fragment 907-955 however does not bind to SKIP(1-310) (Figure 4.2C lane 6 and D). This suggests that although the 907-917 region of KHC is essential for binding to SKIP(1-310) it is not sufficient. These observations were supported by quantification of band densities from 3 independent experiments (Figure 4.2C). These data suggested that further residues from the final coiled-coil of KHC are also required for the interaction.

The 907-917 construct was extended at the amino terminal end further into the coiled-coil region of the KHC C-terminal tail to amino acids 903, 899 and 891 (Figure 4.3A). However, no binding was seen extending the KHC construct as far as residue 891 into the coiled coil region (Figure 4.3B and C). A region prior to 891 is essential for binding to KHC. Expressing further GST-KHC fragments extending further into the coiled coil region showed that the region 876-917 is sufficient for binding to SKIP(1-310) although some incremental binding is observed with further N-terminal extension to residue 815. Figure 4.3C and E show a coomassie stained gel of the purified proteins used in Figure 4.3B and D.

Given the apparent importance of residues in 907-917, a GST-pulldown was carried out mutating residues in triplicate between 907-917 to alanine in an

attempt to further map the SKIP(1-310) binding site on KHC. SKIP(1-310) was incubated at a concentration of 1.2µM with 0.5nmoles GST-KHC(815-955), GST-KHC(915-955) with mutations RAK, NMA or RRA to alanine and GST as control in a volume of 300µl (1.6µM) (Figure 4.4). However, these mutations did not have an appreciable affect binding. This may be caused by the other binding regions compensating for the disruption in binding of three amino acid residues. It may be that mutation or deletion of more residues is required to disrupt binding.

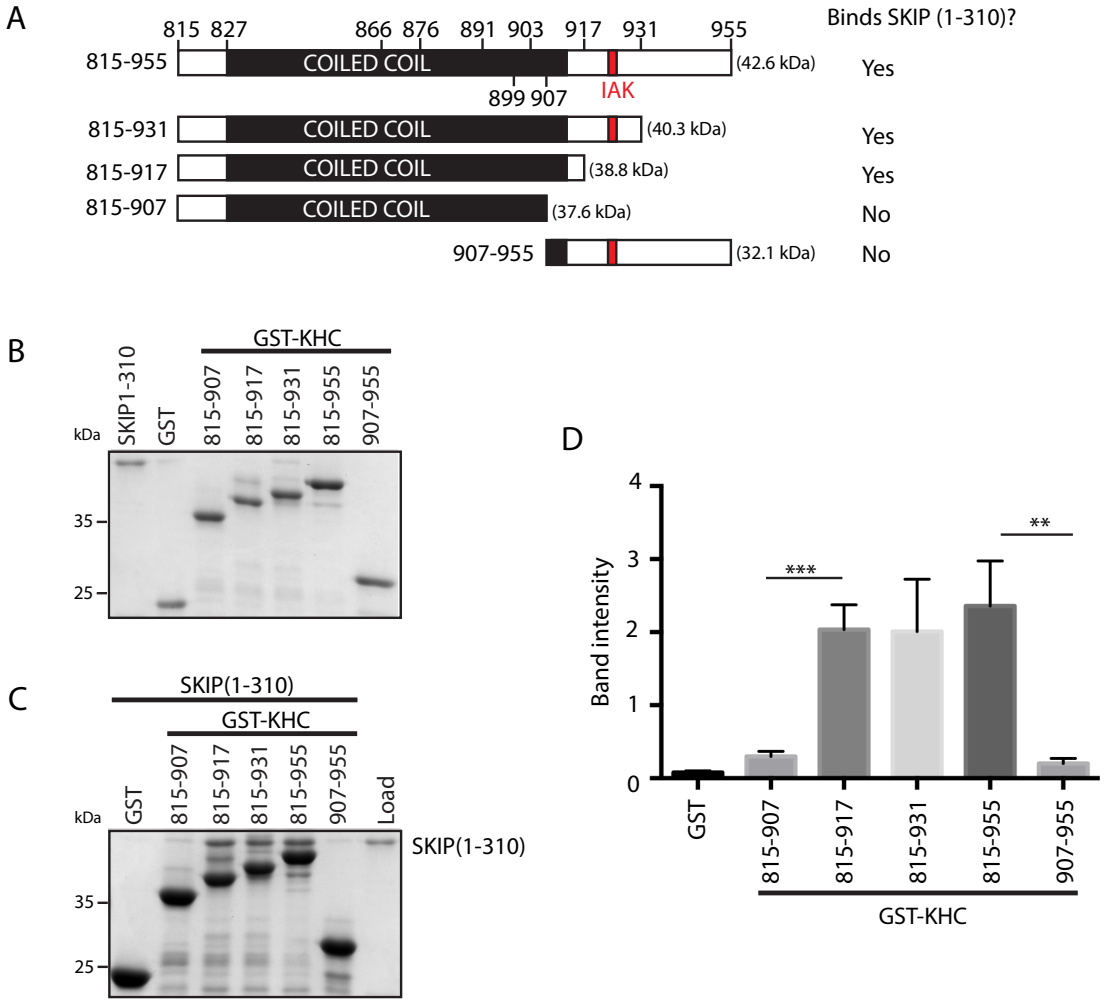

Figure 4.2. KHC residues 907-917 are essential for binding to (SKIP1-310) but not sufficient.

(A) Schematic representation of rat KHC fragments used in this experiment. The predicted coiled-coil region as well as the IAK autoinhibitory sequence are highlighted. Molecular Weights are shown in brackets. (B) Coomassie stained gel of pulldown of SKIP(1-310) (35.3 kDa) at 1.2μM using GST-KHC fragments or GST as control at 0.5nmoles in a volume of 300μl (1.6μM). (C) Coomassie stained gel showing purity of samples used in B. (D) Comparison of bound band densities of SKIP (1-310) incubated at 1.2μM with GST-KHC fragments and GST. The graph shows data from three independent experiments with the same protein preparations. ***P<0.001 (two-tailed T-test)

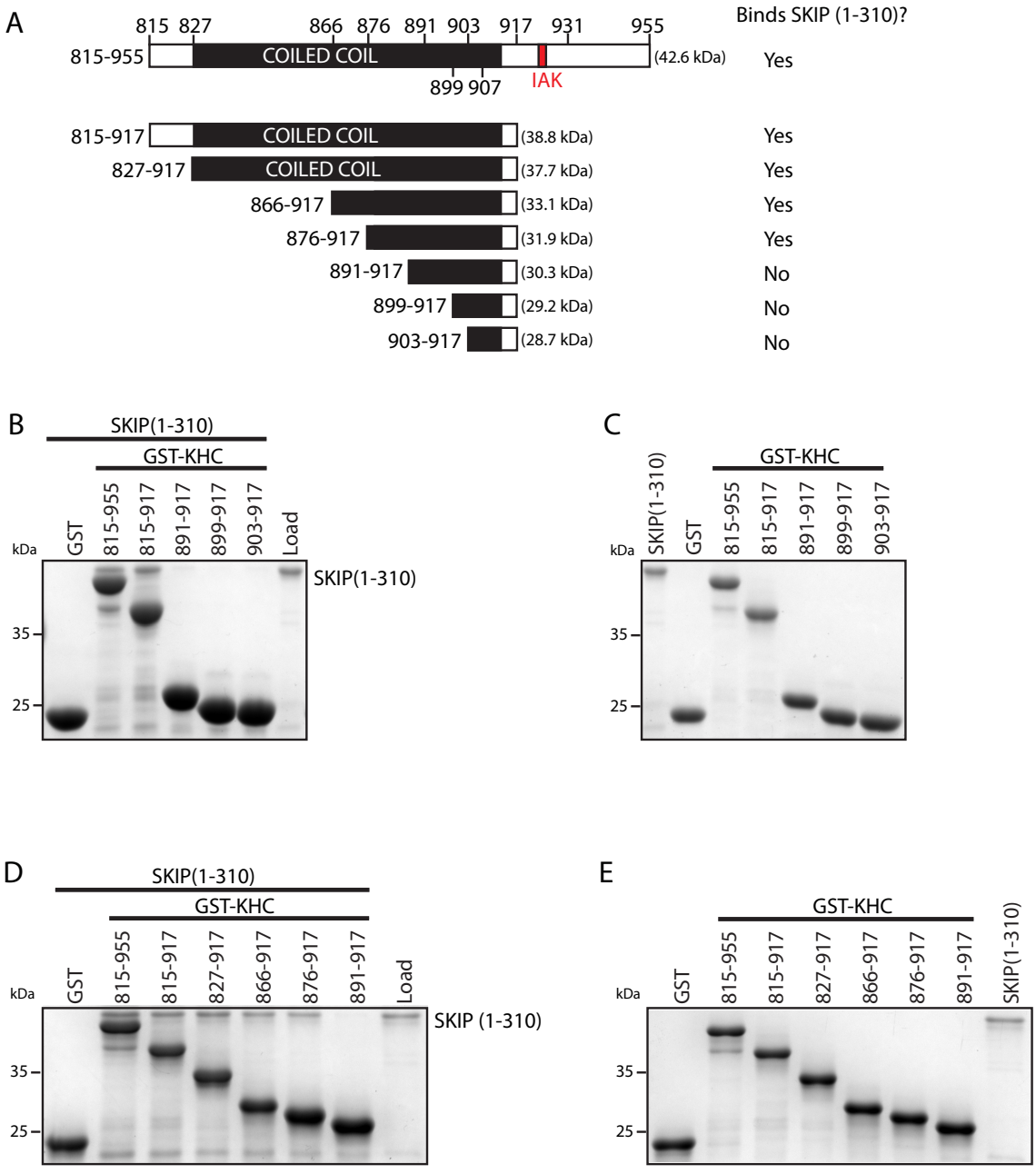

Figure 4.3. The minimal SKIP(1-310) binding site on KHC is 876-917.
(A) Schematic representation of additional rat KHC fragments expressed in this study. The coiled coil region as well as the IAK autoinhibitory sequence are highlighted. Molecular Weights are shown in brackets. (C) and (E) Coomassie stained gel showing purity of samples used in B and D respectively. (B) and (D) Coomassie stained gel of pulldown of SKIP(1-310) (35.3 kDa) at 1.2µM using GST-KHC fragments or GST as control at 0.5nmoles in a volume of 300µl (1.6µM) (n=3). Pull-downs were repeated using the same protein preparations.

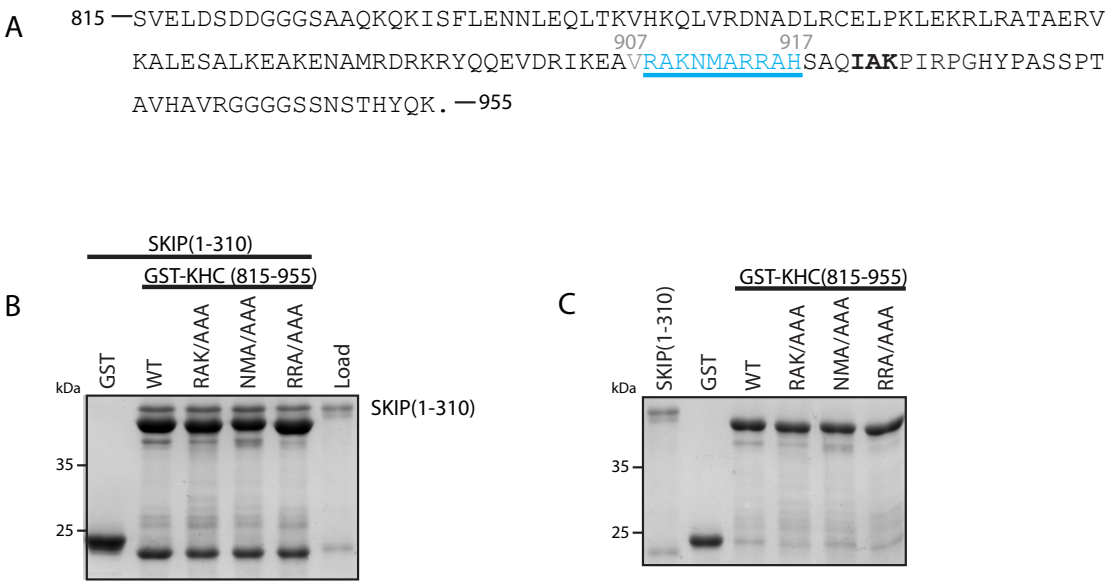

Figure 4.4. Mutation of residues within the essential binding region 907-917.

(A) Sequence of KHC(815-955) with essential binding region highlighted in blue and autoinhibitory sequence (IAK) highlighted in bold. (B) Coomassie stained gel of pull-down of SKIP(1-310) at 1.2μM using GST-KHC(815-955) (42.2kDa) and GST(815-955) with amino acid residues in the 907-917 region mutated in triplicate (RAK, NMA, RRA) (42.5 kDa) to alanine or GST (25.5kDa) as control at 0.5nmoles in a volume of 300μl (1.6μM) (n=3) Pull-down was repeated using the same protein preparations. (C) Coomassie stained gel showing purity of samples used in B.

4.3 KHC binds to an extended region of SKIP

Having mapped the minimal SKIP binding site on KHC to amino acid residues 876-917, the next task was to determine the KHC binding site on SKIP (1-310). SKIP 1-310 and a series of C-terminal truncations of SKIP (1-276,1-260, 1-243,1-216 and 1-202) shown in Figure 4.5A were expressed in *E.coli* as N-terminally His_6-tagged proteins and were purified by Ni^{2+}-affinity chromatography. The purity of the proteins expressed is shown in the Coomassie stained gel in Figure 4.5B. Due to the similar molecular weights of GST/GST-KHC and His-SKIP proteins, results were analysed by anti-His western blot rather than coomassie staining. GST-KHC is shown by ponceau staining of the same membrane. Consistent with the previous assays indicating a direct interaction between KHC and SKIP, His-SKIP (1-310) was pulled down by GST-KHC but not GST alone (Figure 4.5C). Interestingly, C-terminal truncation of SKIP to amino acid 276 appeared to enhance binding with a slight reduction in binding when that construct was truncated to amino acid 243. Strikingly however, binding was dramatically reduced when this construct was further truncated to residue 216 which removes both W-acidic motifs of SKIP and further diminished by truncation to residue 202. These data suggest that an extended region of SKIP, encompassing the W-acidic motifs may be required for KHC binding. However, this interpretation may be complicated by the similar size of the His-SKIP (1-310) and GST-KHC proteins. In some cases, the relatively large amount of one protein can interfere with antibody binding to another protein that migrates at a similar position on the gel and so occupies the same area of membrane. To investigate this, the assay was adapted to pull down GFP-tagged SKIP proteins expressed in 293T cell extract which have higher molecular weights resulting from the inclusion of a 26kDa GFP tag. GST-KHC did not pull down GFP alone but did efficiently pull down GFP-SKIP (Figure 4.5D). Broadly supportive of the conclusions from the direct binding experiments, C-terminal truncation of SKIP 1-310 did appear to enhance binding. Similarly, truncation from residue 243 to 216 essentially eliminated binding further supporting a role for the SKIP W-acidic motif region.

4.4 The SKIP binding region of KHC interacts with the SKIP^{WDWE} peptide (202-241) in fluorescence polarisation assays

The data described above suggested a crucial role for the region of SKIP that includes the two W-acidic motifs. To verify these findings using another assay and to understand whether this region is sufficient to mediate an interaction, a fluorescence polarization assay was carried out using KHC amino acids 866-917 and the TAMRA conjugated SKIP^{WDWE} peptide (described in the previous chapter) adding a 100nM TAMRA conjugated SKIP^{WDWE} peptide to increasing concentrations of KHC (866-917)(Figure 4.6). The concentration dependent increase in polarisation suggests that the protein and peptide interact. Similar to that observed in pull down analyses, the binding curve is sigmoidal in character. Curve fitting indicated a Kd of 7.8 µM and a Hill co-efficient of 4. Whilst the Kd is slightly lower than that calculated in figure 4.1, these data do indicate that this region make a significant contribution to the SKIP KHC interaction.

4.5 *In vitro*, KHC and KLC compete for overlapping binding sites on SKIP

Since both tryptophan-acidic motifs (WD and WE) are present in the minimal SKIP binding region, the contribution of these residues to KHC binding was also investigated. Pull-down of GFP-SKIP and SKIP mutants (WD, WE, and both WD and WE) from 293T cell lysates using GST-KHC(815-955) or GST as control show that binding is dramatically reduced upon making alanine substitutions in either of the tryptophan acidic motifs. This suggests that both tryptophan-acidic motifs contribute to KHC binding (Figure 4.7A). It is possible, (although unlikely given the typically low expression of KLCs in non neuronal cells when compared to exogenous, over expressed protein) that this interpretation may be confounded by endogenous KLC in the cell lysates. To verify that this does indeed occur in direct binding experiments when both proteins are produced in *E.coli, a* GST-pulldown assay of His-SKIP and SKIP mutants (WD, WE, and both WD and WE) with GST-KHC(815-955) or GST was performed. This again showed that binding is significantly reduced upon making the alanine substitutions in the tryptophan-acidic motifs (Figure 4.7B).

Since both KHC and KLC appear to share the same binding region it was important to determine whether KLC binding could compete with KHC binding to SKIP(1-310) in a concentration dependent manner. GST pull-down of GFP-SKIP from 293T cell lysates using GST-KHC(815-955) or GST as control in the presence of increasing concentrations of KLC2 TPR (produced in *E.coli)* show that upon increasing the concentration of KLC2 TPR, binding between KHC and SKIP is reduced (Figure 4.8A). KLC2 TPR binding to SKIP can compete off KHC binding. To verify that this is due to KLC2 TPR binding to SKIP, the N287L KLC2 mutant (shown to abrogate KLC:SKIP binding) was also added at increasing concentrations. Consistent with this interpretation, this did not have any effect on KHC: SKIP binding (Figure 4.8B).

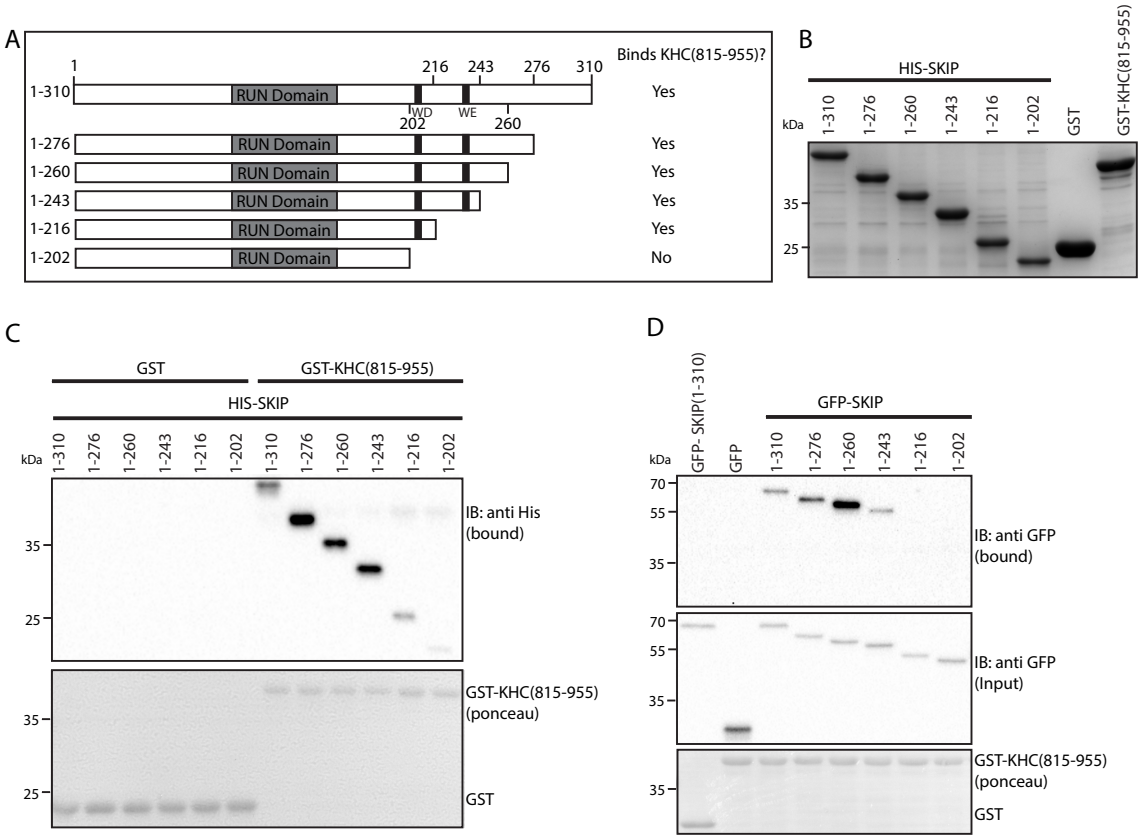

Figure 4.5. Extended region of SKIP is required for KHC binding.
(A) Schematic representation of the SKIP fragments expressed in this study. The RUN domain and the tryptophan-acidic residues (WD and WE) are highlighted (B) Coomassie stained gel showing purity of samples used in (C) (His-SKIP(1-310): 37.8 kDa, His-SKIP(1-276): 34.2k Da, His-SKIP(1-260): 32.4 kDa, His-SKIP(1-243): 30.7 kDa, His-SKIP(1-216): 27.7kDa, His-SKIP(1-202): 26.3 kDa, GST; 25.5 kDa, GST-KHC(815-955): 42.6 kDa). (C) Western blot of pull-down of His-SKIP(1-310) and truncations of SKIP at 1.2μM using GST-KHC(815-955) or GST as control at 0.25nmoles in a volume of 300μl (0.83μM). His-SKIP was blotted for using a mouse monoclonal anti-His HRP conjugated antibody to allow for detection using Clarity Western ECL substrate. GST and GST-KHC(815-955) were visualized by ponceau staining. (n=3) Repeats involved three independent repeat transfections followed by pulldown using the same protein preparations. (D) Pull-down of GFP-SKIP(1-310) and SKIP truncations from 293T cell lysate using GST-KHC(815-955) or GST as control. Input lysates were blotted for GFP-SKIP and SKIP truncations as control using a mouse monoclonal anti-GFP antibody. A goat polyclonal anti-mouse HRP antibody was used as a secondary antibody to allow for detection using Clarity Western ECL substrate (GFP-SKIP(1-310): 62.1 kDa, GFP-SKIP(1-276): 58.5 k Da, GFP-SKIP(1-260): 56.6 kDa, GFP-SKIP(1-243): 55.0 kDa, GFP-SKIP(1-216): 52.0 kDa, GFP -SKIP(1-202): 50.5 kDa, GFP; 26.9 kDa). GST and GST-KHC(815-955) were visualized by ponceau staining. (n=3) Pull-downs were repeated using the same protein preparations.

SKIP(202-241): TAMRA-STNLEWDDSAIAPSSEDYDFGDVFPAVPSVPSTDWEDGDL

KHC (866-917): KRLRATAERVKALESALKEAKENAMRDRKRYQQEVDRIKEAVRAKNMARRAH

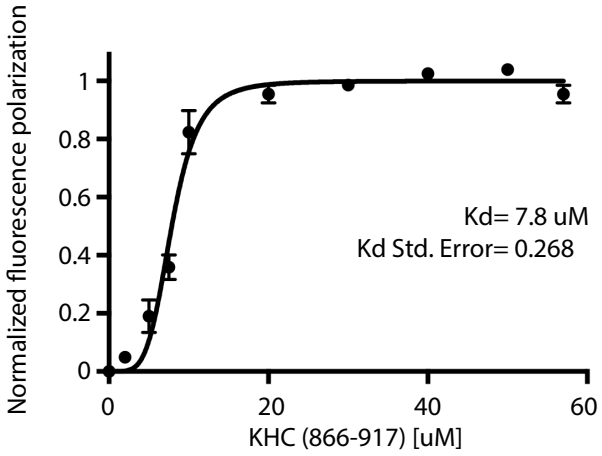

Figure 4.6. The minimal SKIP binding region on KHC interacts with SKIP(202-241) peptide.

Fluorescence polarisation measurements of increasing concentrations of KHC(866-917) with 100nM N-terminal carboxytetramethylrhodamine (TAMRA) conjugated peptide SKIP(202-241) in 25mM Hepes pH 7.5, 5 mM β-mercaptoethanol and 150mM NaCl. Measurements were performed on a Horiba Fluoromax-4 spectrofluorometer at 20 °C. A one site - specific binding curve with a hill slope was fitted to the data: Y=Bmax*X^h/(Kd^h + X^h).

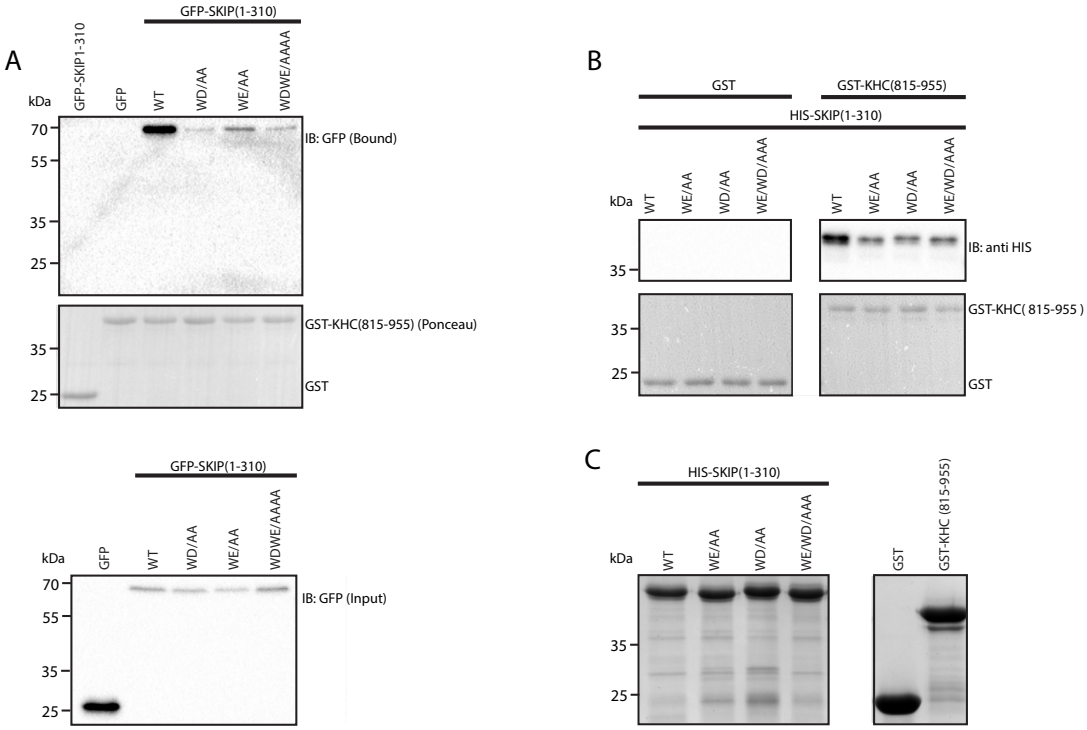

Figure 4.7. Light chain binding motifs are also required for heavy chain interaction.

(A) Pull-down of GFP-SKIP(1-310) (62.1 kDa) and SKIP mutants (WD, WE, and both WD and WE) (61.9 kDa) from 293T cell lysate using GST-KHC(815-955) (42.6 kDa) or GST (25.5 kDa) as control. Input lysates were blotted for GFP-SKIP(1-310) and SKIP mutants as control using a mouse monoclonal anti-GFP antibody. A goat polyclonal anti-mouse HRP antibody was used as a secondary antibody to allow for detection using Clarity Western ECL substrate. GST and GST-KHC(815-955) were visualized by ponceau staining. (n=3) Repeats involved three independent repeat transfections followed by pulldown using the same protein preparations. (B) Western-blot of pull-down of His-SKIP(1-310) and SKIP mutants (WD/AA, WE/AA, and WDWE/AAAA) (37.8 kDa) at 1.2μM using 0.25nmoles GST-KHC(815-955) or GST as control in 300μl (0.83μM). His-SKIP was blotted for using a mouse monoclonal anti-His HRP conjugated antibody to allow for detection using Clarity Western ECL substrate (n=3). Repeats involved three independent repeat transfections followed by pulldown using the same protein preparations. (C) Coomassie stained gel showing purity of samples used in B.

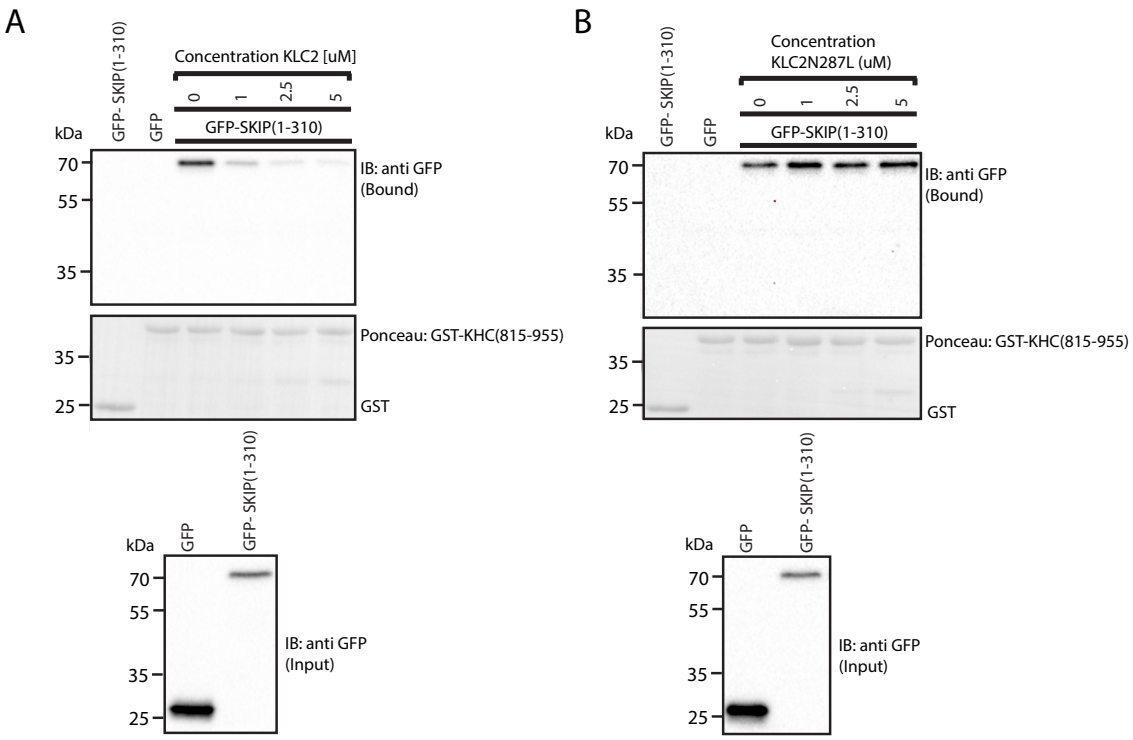

Figure 4.8. Increasing KLC2 concentration reduces KHC binding to SKIP. Pull-down of GFP-SKIP (1-310) (62.1 kDa) from 293T cell lysate using GST-KHC (815-955) (42.6 kDa) or GST (25.5 kDa) as control in the presence of increasing concentrations of (A) KLC2 and (B) KLC2 N287L mutant. Input lysates were blotted for GFP-SKIP(1-310) and SKIP mutants as control using a mouse monoclonal anti-GFP antibody. A goat polyclonal anti-mouse HRP antibody was used as a secondary antibody to allow for detection using Clarity Western ECL substrate. GST and GST-KHC(815-955) were visualized by ponceau staining. (n=3). Repeats involved three independent repeat transfections followed by pulldown using the same protein preparations. Single KLC2 and KLC2 N287L preparations were also used in repeats.

4.6 Discussion

This chapter has described experiments aimed at determining whether SKIP interacts directly with KHC and demonstrate that SKIP(1-310) binds directly to the C-terminal tail of KHC. The region to which SKIP(1-310) binds on KHC has been mapped to amino acid residues 876-917. N and C terminal deletions from this construct show that the KHC regions 876-891 (KALESALKEAKENAM) and 907-917 (VRAKNMARRAH) are essential for SKIP binding although neither is sufficient for binding on their own (Figure 4.2 and Figure 4.3). The bulk of this minimal binding region is predicted to be composed of coiled-coil (although the final 10 amino acids may be less structured). It may be that the formation and stability of this coiled-coil dimer requires these extended N- and C- terminal regions. Since truncations were used to map the binding sites, there is the possibility that through truncation the tertiary and quaternary structure of the protein in question is affected. The KHC truncations used in mapping the SKIP binding site are expected to be dimeric in nature due to the length of the predicted coiled coil region. The shorter constructs with a shorter coiled coil region may however not be dimeric and extending the construct further into the coiled coil region may enable dimerization of the longer constructs. Extending the KHC construct from 891-917 to 876-917, into the coiled coil region, may be required for dimerization and may not be an essential SKIP binding region itself, but through dimerization allow for SKIP to make a series of contacts along the length of KHC that is dependent upon dimerization.

Mapping of the KHC binding site on SKIP reveals that whilst an extended region of SKIP appears to be important, the W-acidic containing region and the motifs themselves play a key role. Mutation of these motifs impairs binding to KHC and at high concentrations KLC is capable of competing for the same site(s). Given the unstructured nature of the SKIP peptide, it is tempting to speculate that this peptide may make multiple specific contacts along the length of the coiled-coil. The 876-917 region of KHC is highly basic (pI 10.37) and the SKIP peptide is highly acidic (pI 2.74), so it is also likely that electrostatic interactions also make an important contribution. Thus, the data here suggest that both KHC and KLC may recognise similar features within cargo proteins.

When the binding sites of different cargo are compared, the region encompassing the sequence ALKEAKE (Kif5C(877-887)) of KHC appears not

only to be required for SKIP binding but also the binding of TRAK2 and the Kv3 (Shaw) voltage-gated K+ channel T1 domain (Kv1.3 T1) (Figure 4.9)(Barry et al., 2013, Randall et al., 2013). This is not the sole binding region for any of the three, and each has other regions of KHC that are required for binding. However, the fact that the pI of the Kv1.3 T1 domain is relatively low at 4.39 and the TRAK2 kinesin binding region (124-283)(Brickley et al., 2005), has a pI of 4.52) may suggest that charge-charge interactions may play a general role. Consistent with this, Barry et al. show the residues $R^{892}K^{893}R^{894}$ to be essential for the binding of KHC to Kv3.1 T1 (Barry et al., 2013). Figure 4.3B shows that upon extending the KHC C-terminal tail from 899-917 to 891-917 (which contains the RKR sequence) binding is not achieved. Since it has been shown that multiple contacts are required for binding to be seen, this region may also be involved in binding to SKIP but not be sufficient for binding. Thus the precise mode of binding likely differs from cargo-to-cargo but similar underlying molecular principles may still apply.

In the case of SKIP, whilst the W-acidic motifs appear to be central to the KHC interaction, a more extended region of SKIP appears to be able to modulate this interaction. Surprisingly, with both recombinant protein and pull down from cell extracts, shortening of the SKIP 1-310 construct appears to enhance binding to KHC. Whilst this may be an artifact of the truncations used, this could also point to an auto-inhibitory regulatory mechanism within SKIP itself that may control its propensity to associate with kinesin-1.

In this chapter, SKIP is shown to have overlapping binding sites for KLC and KHC. The KHC binding site has been mapped to SKIP(202-241) and mutation of both tryptophan acidic motifs to alanine within this region significantly reduces KHC binding (Figure 4.5 and Figure 4.7). In contrast to this, KLC binding is significantly reduced by mutation of the first tryptophan-acidic motif, whereas mutation of the second tryptophan acidic motif has very little effect on KLC binding (Figure 3.1). This suggests that although the binding regions overlap, the relative importance of the residues within this region in binding to KLC and KHC varies. SKIP is also unlikely to be bound to both KHC and KLC simultaneously as residues involved in KLC binding are also required in KHC binding for example the first tryptophan acidic motif (WD). KLC2 is also shown to compete with KHC for the binding site on SKIP (Figure 4.8), which suggests that binding may be mutually exclusive.

Thus, having established using a series of assays that KHC interacts with SKIP, the next task is to establish what if any is the functional role of this interaction in SKIP/kinesin-1 mediated cargo transport.

Figure 4.9. C-terminal KHC cargo binding region.
An alignment of the amino acid sequences of the rat Kif5A (Protein accession number: NP_997688), Kif5B (Protein accession number: NP_476550) and Kif5C (Protein accession number: NP_001101200) cargo binding domains. Binding regions of TRAK2 on Kif5C (black), TRAK2 on Kif5A(blue text and underlined), Kv3.1 (green) and SKIP (red) is shown on the respective Kif5 (Barry et al., 2013, Randall et al., 2013, Xu et al., 2010).

CHAPTER 5 . FUNCTIONAL ROLES OF THE KLC: CARGO AND THE KHC:CARGO INTERACTIONS IN KINESIN-1 RECRUITMENT AND ACTIVATION.

Data presented in the previous chapters have shown that SKIP, in addition to being able to interact with KLC, can also interact with the C-terminal tail of KHC. Whilst it is clear that cargo binding is important for activation of transport, the relative contributions of KLC and KHC binding in cargo recognition and activation of transport are not fully understood.

Data presented in Chapter 3 showed that the SKIP:KLC interaction is required for recruitment. Specific disruption of the SKIP:KLC interface through making mutations (N287L, R251D) in the KLC cargo-binding pocket essentially eliminates the ability of SKIP to associate with the kinesin-1 tetramer. Moreover, full length KHC expressed alone in cells did not interact with SKIP(1-310). What the functional role is of the SKIP:KHC interaction remains to be established.

Since the KHC and KLC binding sites on SKIP were shown to overlap answering this question requires the capacity to mutationally separate these two interactions and assess the functional consequences. The experiments described in this chapter aimed to firstly further dissect the determinants of the SKIP:KHC interaction, as well as examining its relationship to the SKIP:KLC interaction and thus also understand its function.

5.1 SKIP only binds to KHC when autoinhibition is relieved

The data in Chapter 4 described how the C-terminal tail of KHC (KHC-815-955) produced in *E.coli* is able to interact with either GFP-SKIP(1-310) expressed in cell extracts or recombinant protein. However, in the context of the kinesin-1 tetramer, disruption of the KLC:SKIP interaction is sufficient to prevent association of SKIP and KHC (Figure 3.13). In addition, full length KHC expressed alone in cells did not interact with GST-SKIP(1-310) (Figure 3.12). Thus, despite the fact that KHC and SKIP interact directly, the binding site may not be accessible in the context of the full length protein. Moreover, this may imply a role for the light chain in making that site accessible. As the SKIP binding site is proximal to the residues involved in mediating autoinhibition, it may be that this discrepancy is caused by inaccessibility of this binding site in

the autoinhibited state. To test this hypothesis, 9 residues of the autoinhibitory 'IAK' sequence (QIAKPIRPG/AAAAAAAA) were mutated to alanine to disrupt the binding of the C-terminal tail to the motor domain of KHC and prevent autoinhibition (Dietrich et al., 2008, Hackney and Stock, 2000). HA-KHC constructs were expressed in 293T cells and binding to SKIP(1-310) analysed by GST-pulldown. Consistent with the hypothesis proposed above, when the "IAK' sequence is disrupted, GST-SKIP(1-310) is capable of interaction with full length KHC. The C-terminal tail of KHC is also pulled down to a similar extent in the same context.

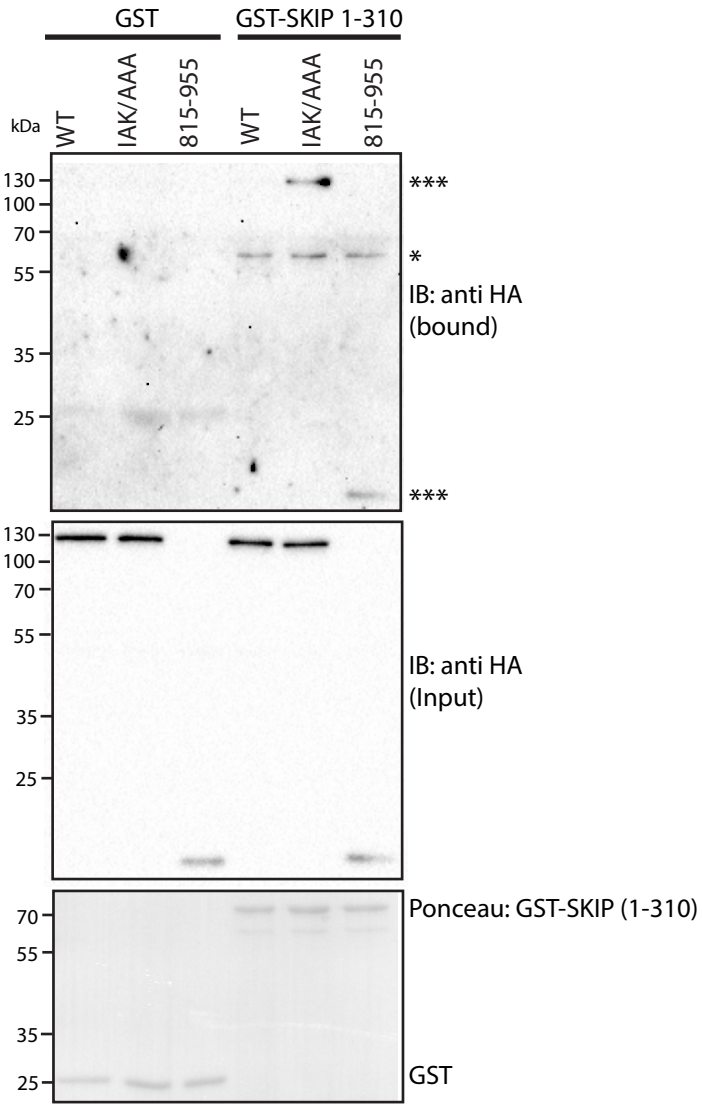

Figure 5.1. SKIP only binds to full length KHC when autoinhibition is relieved.

Western blot of pull-down of HA-KHC (109.2 kDa), HA-KHC with QIAKPIRPG mutated to alanine (110.5 kDa) and HA-KHC(815-955) (17.3 kDa) (bands highlighted with ***) from 293T cell lysate using 0.25nmoles GST-SKIP(1-310) (61.8 kDa) or GST(25.5 kDa) as control in a volume of 300µl (0.84µM). (Bands highlighted with * is GST-SKIP(1-310) and cross reactivity with the HA antibody.) Input lysates were blotted for HA-KHC, HA-KHC with QIAKPIRPG mutated to alanine and HA-KHC(815-955) as control using a mouse monoclonal anti-HA antibody. A goat polyclonal anti-mouse HRP antibody was used as a secondary antibody to allow for detection using Clarity Western ECL substrate. GST and GST-SKIP(1-310) were visualized by ponceau staining. (n=3). Repeats involved three independent repeat transfections followed by pulldown using the same protein preparations.

5.2 Mutation of key residues in SKIP disrupt KHC:SKIP binding without affecting KLC:SKIP interaction.

Data presented in Chapter 3 and Chapter 4 have demonstrated that amino acid residues 202-241 of SKIP contain both KLC and KHC binding sites. KHC and KLC binding to SKIP were shown in Chapter 4 to share some determinants, because mutation of the first tryptophan acidic motif (WD) in SKIP not only disrupts KLC binding but also disrupts SKIP binding to KHC. However, some indication that these binding sites may also contain distinct determinants came from data showing that the WE residues of SKIP are largely dispensable for the KLC interaction, whereas it does make a significant contribution to KHC binding. A naturally occurring splice variant of SKIP, where exon 7 is deleted, results in the residues highlighted in green (amino acid residues 219 to 238) in Figure 5.2A to not be expressed. This splice variant, that does not promote lysosome dispersion (Rosa-Ferreira and Munro, 2011) and also lacks the WE motif, was further impaired in its ability to interact with KHC suggesting that other KHC specific binding determinants may exist within this region.

To determine whether this was the case, amino acid residues within exon 7 were mutated in triplicate to alanine as indicated in Figure 5.2A. 293T cells were transfected with plasmids designed to express green fluorescent protein (GFP) tagged SKIP, SKIP mutants (WD, EDY, DFG, DVF, PAV, PSV, PSTD, WE, DGD, LTD) or splice variant with exon 7 deleted (DelEx7). Pulldown of GFP-SKIP, SKIP mutants (WD, EDY, DFG, DVF, PAV, PSV, PSTD, WE, DGD, LTD) or splice variant DelEx7 from 293T cell lysate using GST-KHC(815-955) or GST as control is shown in Figure 5.2B. Expression levels between the different GFP-SKIP mutants tended to vary in these small scale screening pull down experiments and therefore, for quantitative purposes, binding was normalized to SKIP (1-310) input levels in this screen. Normalised binding from three independent experiments is shown in Figure 5.2C. This analysis suggested that as well as the WD and WE motifs of SKIP, the EDY, DFG, and DGD triplets located within exon 7 also contributed to SKIP binding (Figure 5.2C and Figure 5.2D). These results were confirmed in larger scale pulldowns (which tended to be affected less by variation in expression level) (Figure 5.2D).

To determine whether the mutations that were identified to disrupt SKIP binding to KHC were also important in KLC binding, a GFP-TRAP

immunoprecipitation strategy was used. 293T cells were co-transfected with plasmids designed to express N-terminally hemagglutinin (HA) tagged KLC2 and N-terminally green fluorescent protein (GFP) tagged SKIP(1-310) (either wild-type, carrying alanine substitution at residues EDY, DFG, WE, DGD) or with amino acids 219 to 238 deleted (DelEx7). GFP-SKIP(1-310) was immunoprecipitated with GFP-TRAP beads and the amount of co-immunoprecipated HA-KLC2 was assessed by western blot (Figure 5.3). Consistent with data presented in Chapter 3 (Figure 3.1) mutation of the WD motif to alanine essentially eliminated the GFP-SKIP interaction with HA-KLC2, whereas equivalent mutations in the WE motif had no effect. Deletion of exon 7, which encompasses the WE motif and surrounding residues did considerably reduce binding, suggesting some contribution from these residues in binding to KLC2. However, specific mutation of EDY, DFG, DGD had no effect on the interaction between SKIP and KLC, confirming that KLC and KHC binding capacity in SKIP is mutationally separable.

5.3 Disruption of KHC:SKIP interaction reduces SKIP:kinesin-1 tetramer interaction

In order to examine the effect of independently disrupting SKIP:KHC binding on association of SKIP with the kinesin-1 tetramer, 293T cells were co-transfected with plasmids designed to express N-terminally hemagglutinin (HA) tagged KLC2 and N-terminally HA tagged KHC. Pulldown of HA-KLC and HA-KHC from 293T cell lysates using GST-SKIP (1-310) or GST-SKIP containing alanine substitutions (EDY, DFG, WE, DGD) or GST as control is shown in Figure 5.4. Consistent with data presented in Figure 5.2D, these experiments revealed a key role for the EDY or DFG residues of SKIP in binding of the kinesin-1 tetramer, although the effect of mutating the WE or DGD residues was less striking. Collectively, these experiments show that the capacity for SKIP to interact specifically with KHC is important for maintaining a stable interaction with the entire kinesin-1 tetramer under conditions where light chain binding is unperturbed.

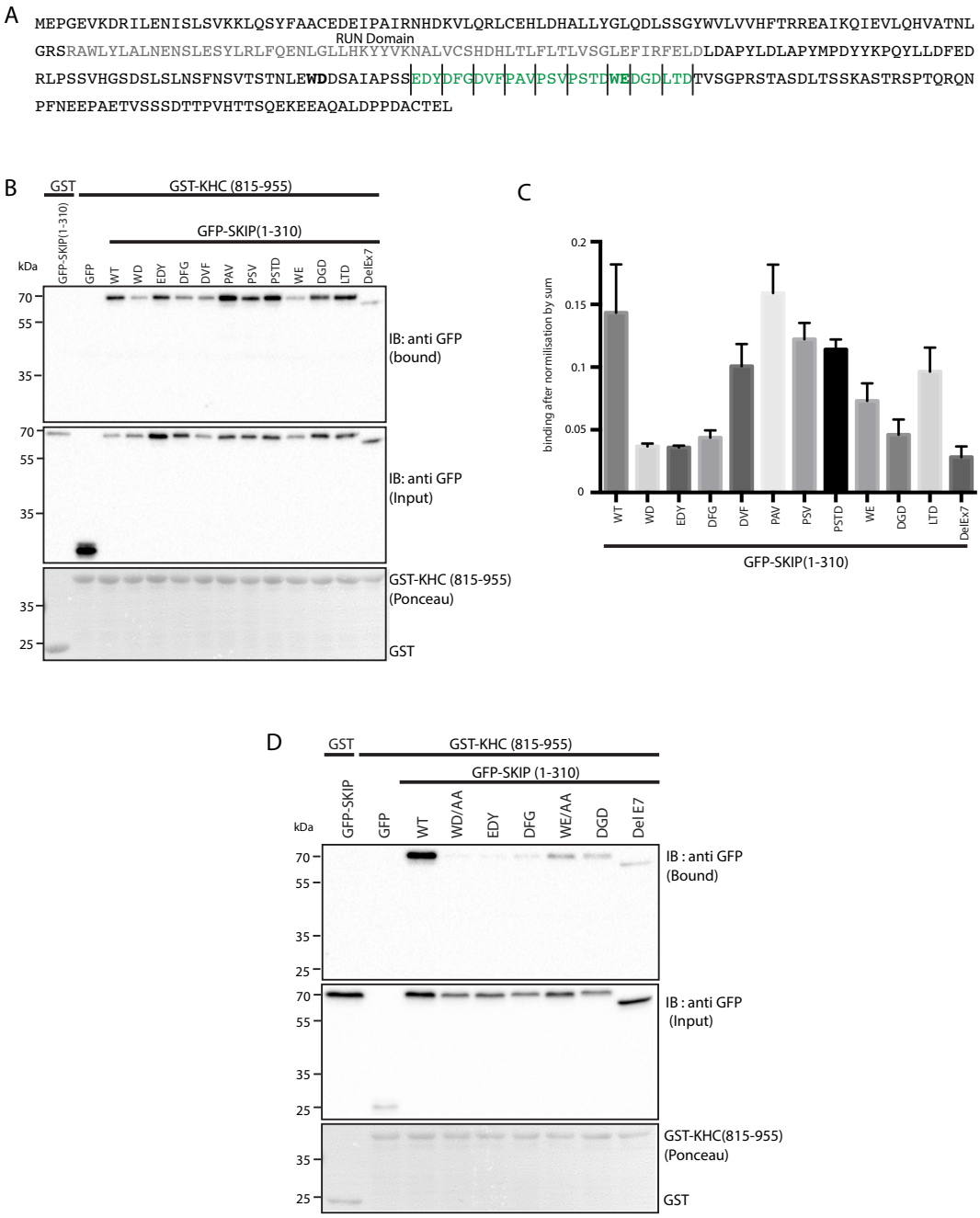

Figure 5.2. Mutation of amino acid residues within exon 7 disrupts KHC binding.

(A) Amino acid sequence of SKIP(1-310). Run domain is highlighted in grey and the amino acids translated when exon 7 is not deleted is shown in green. The vertical lines indicate the triplets of alanine mutations. (B) Pull-down of GFP-SKIP and SKIP mutants (WD, EDY, DFG, DVF, PAV, PSV, PSTD, WE, DGD, LTD) as well as splice variant where exon 7 is deleted (DelEx7) from 293T cell lysate using GST-KHC(815-955) (42.6 kDa) or GST (25.5 kDa) as control. Input lysates were blotted for GFP-SKIP(1-310) and SKIP mutants as control using a mouse monoclonal anti-GFP antibody. A goat polyclonal anti-mouse HRP antibody was used as a secondary antibody to allow for detection using Clarity Western ECL substrate. GST and GST-KHC(815-955) were visualized by

ponceau staining. (n=3). Repeats involved three independent repeat transfections followed by pulldown using the same protein preparations. (C) Graph of fraction of GFP-SKIP(1-310) binding normalised to total GFP-SKIP(1-310) binding. (D) Pull-down of GFP-SKIP and SKIP mutants (WD, EDY, DFG, WE, DGD) as well as splice variant DelEx7 from 293T cell lysates using GST-KHC(815-955) or GST as control (n=3). Repeats involved three independent repeat transfections followed by pulldown using the same protein preparations.

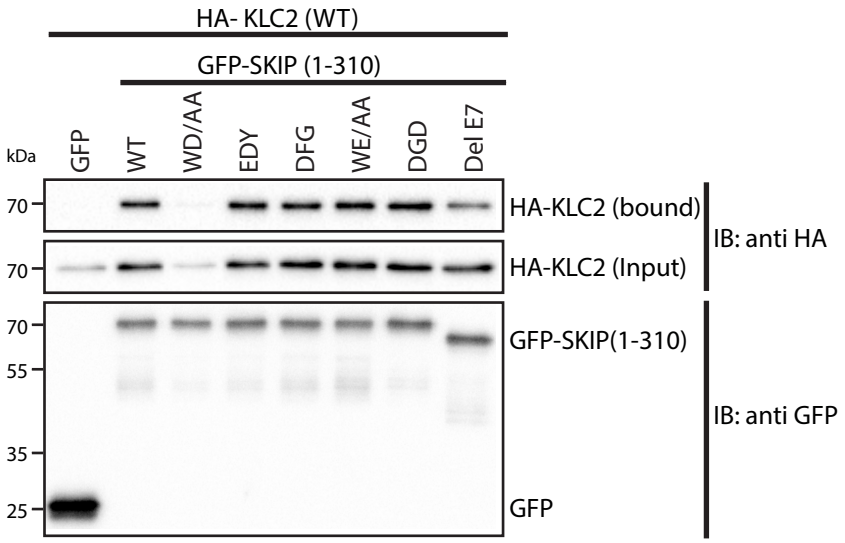

Figure 5.3. Alanine replacement of key residues shown to be involved in KHC binding does not affect KLC binding.

Co-immunoprecipitation of HA-KLC2 (70.0 kDa) with GFP-SKIP(1-310) (62.1 kDa), mutants of SKIP (WD, EDY, WE, DGD), SKIP containing a deletion of exon 7 (59.8 kDa) or GFP (26.9 kDa) control. Input lysates and co-immunoprecipitated HA-KLC2 (bound) were blotted for KLC2 using an anti-HA mouse monoclonal antibody. GFP and GFP-SKIP were blotted for using an anti-GFP mouse monoclonal antibody. A goat polyclonal anti- mouse HRP antibody was used as a secondary antibody to allow for detection using Clarity Western ECL substrate. The blot is representative of three experiments involving three independent repeat transfections.

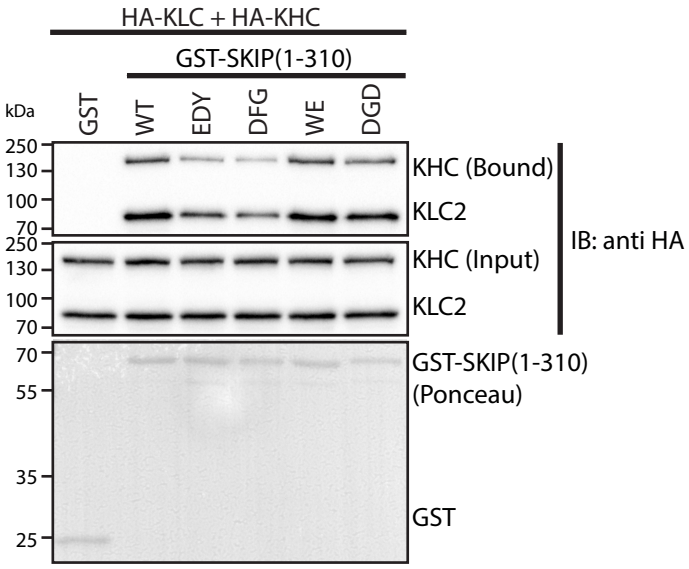

Figure 5.4. Alanine replacement of key residues shown to be involved in KHC binding reduces binding to the kinesin-1 tetramer.

Pull-down of HA-KLC2 (70.0 kDa) and HA-KHC (109.2 kDa) from 293T cell lysate using GST-SKIP(1-310) (61.8 kDa) and SKIP mutants (WD, EDY, DFG, WE, DGD) or GST(25.5 kDa) as control. Input lysates were blotted for HA-KLC2 and HA-KHC as control using a mouse monoclonal anti-HA antibody. A goat polyclonal anti-mouse HRP antibody was used as a secondary antibody to allow for detection using Clarity Western ECL substrate. GST and GST-SKIP(1-310) were visualized by ponceau staining. The blot is representative of three experiments involving three independent repeat transfections followed by GST-pulldown with the same GST/GST-SKIP protein preparations.

5.4 Specific disruption of SKIP binding to KHC results in a reduced capacity to promote lysosomal transport to the cell periphery.

Identification of the residues that independently disrupted SKIP binding to KHC offered an opportunity to determine their functional role. Expression of full-length SKIP in HeLa promotes kinesin-1 dependent lysosome transport to the cell periphery (Rosa-Ferreira and Munro, 2011). This provides a useful assay to assess SKIP function. Consistent with Rosa-Ferreira and Munro, 2011, transfection of HeLa cells with full-length SKIP promoted dispersion of lysosomes and accumulation at the cell periphery (Figure 5.5A). To quantify this in an unbiased manner, the cell was segmented into scaled percentile regions and cumulative LAMP-1 distribution determined (Figure 5.5B, see methods). The graph in Figure 5.5C shows the effect of SKIP expression (compared to non transfected) on cumulative LAMP-1 distribution relative to the whole cell. SKIP promotes a relative shift in the curve to the right indicating dispersion. In contrast, expression of the dynein adaptor RILP (that promotes lysosome transport to the MTOC) accumulation promoted a left shift confirming the utility of this assay. The non-linear regression function in Graphpad Prism was used to fit a centered 6th order polynominal to the cumulative LAMP-1 distribution. To compare models to assess the statistical significance of differences in distribution profiles, the extra sum of F-squares test was applied. This analysis confirms a statistical significant difference between non-transfected and SKIP as well as non-transfected and RILP. Non-transfected and GFP is shown to not be statistically significantly different. P values are shown in Figure 5.5C. The cumulative distribution at the 60th centile is shown in Figure 5.5D. Whilst this data can be statistically analysed at any point on the curve, further analysis at the point of widest control/SKIP separation (60th centile) revealed that this change in distribution is statistically significant and was used as a benchmark for future analysis of mutants. In order to determine the effect of making SKIP mutations that were shown to disrupt KHC binding to SKIP (without affecting KLC binding) on the distribution of lysosomes, HeLa were transfected with myc-SKIP or mutants of SKIP (EDY, DFG, WE, DGD) or splice variant DelEx7 as well as non transfected as control and stained for LAMP-1. Representative

confocal fluorescence images of the lysosomal distribution are presented in Figure 5.6A. This is quantified in Figure 5.6B-F. The non-linear regression function in Graphpad Prism was used to fit a centered 6th order polynominal to the cumulative LAMP-1 distribution. To compare models so assess the statistical significance of differences in distribution profiles, the extra sum of F-squares test was applied. Transfection with the KHC specific EDY, DFG or DGD mutations significantly affected lysosomal distribution when compared to SKIP (P values are shown on the graphs in Figure 5.6B-F). Figure 5.6G also shows the reduced capacity of EDY, DFG and EDY mutations in promoting lysosome dispersion (as measured at the 60^{th} centile) showing that capacity to interact with KHC as well as KLC is important for SKIP function.

A

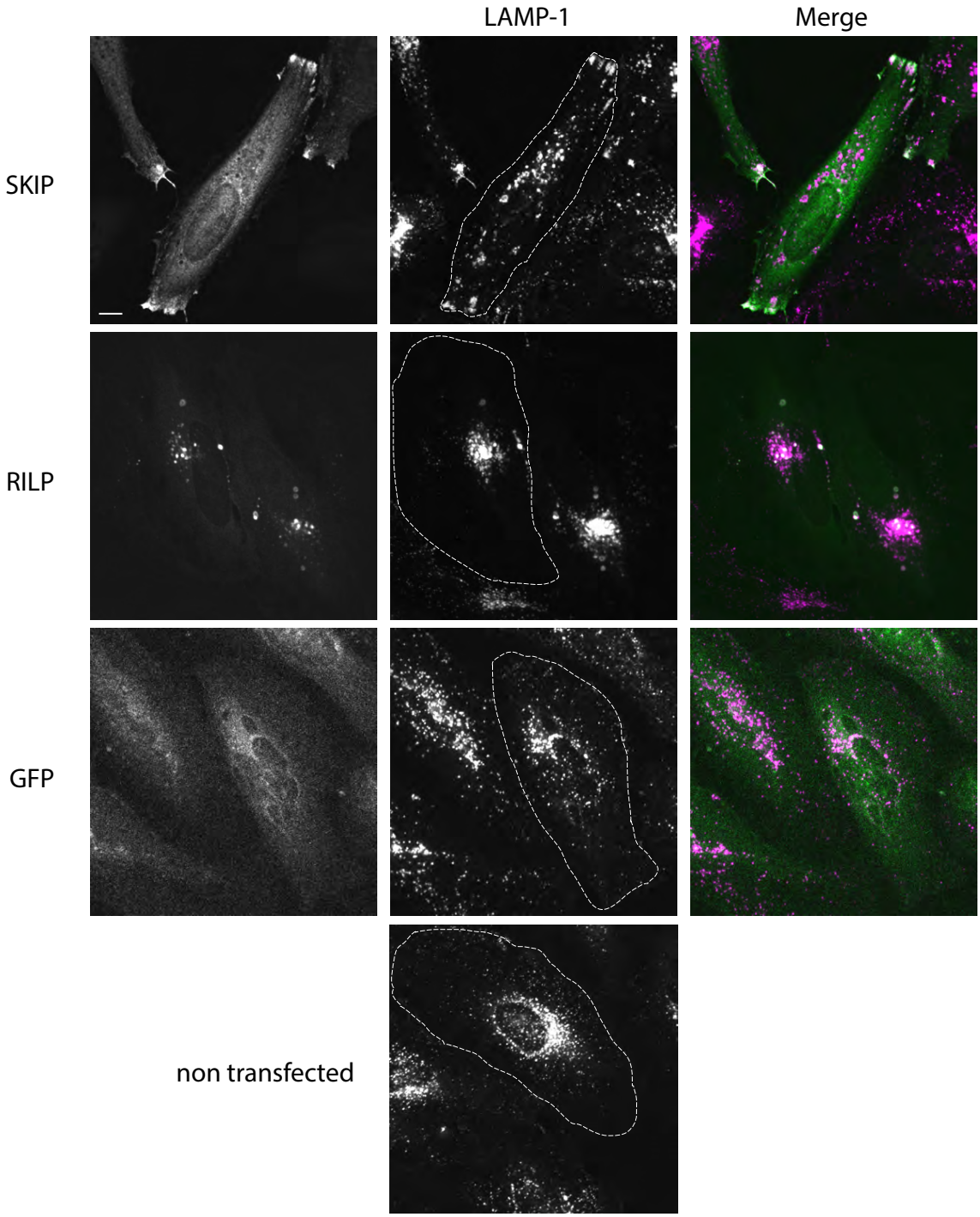

B

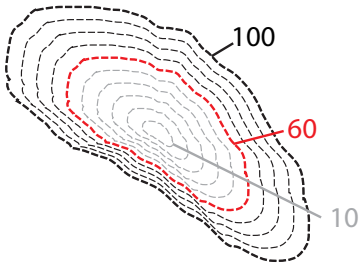
100
60
10

C

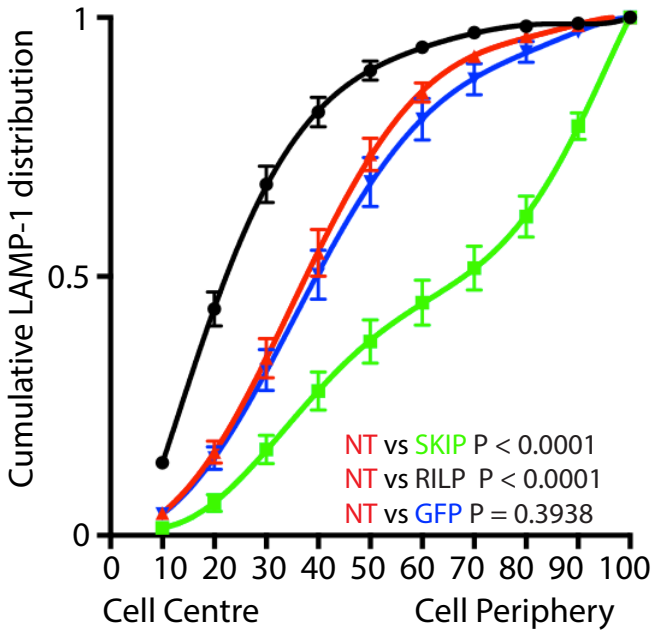
Cumulative LAMP-1 distribution
1
0.5
0
0 10 20 30 40 50 60 70 80 90 100
Cell Centre
Cell Periphery
NT vs SKIP P < 0.0001
NT vs RILP P < 0.0001
NT vs GFP P = 0.3938

D

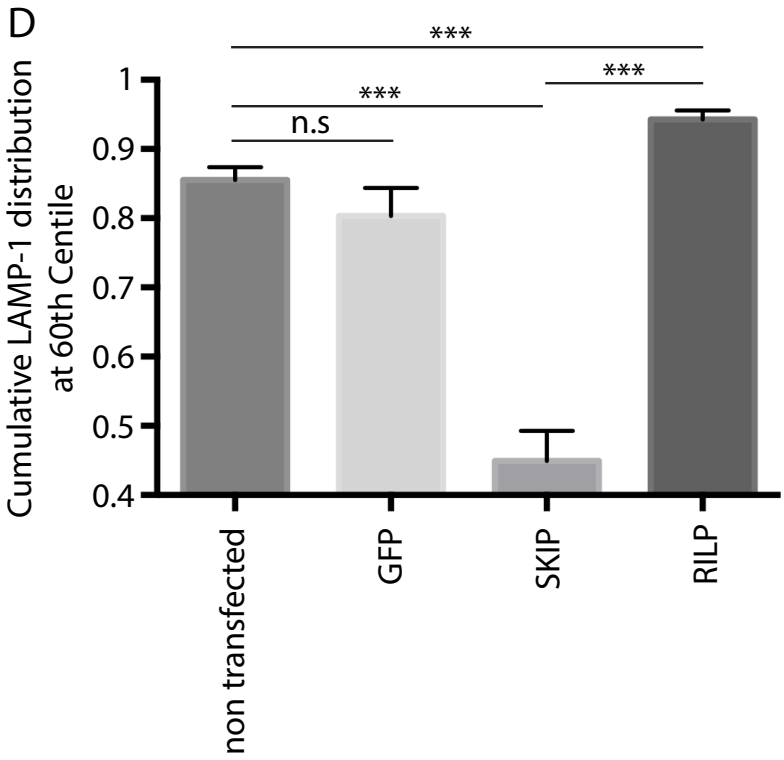
Cumulative LAMP-1 distribution at 60th Centile
1
0.9
0.8
0.7
0.6
0.5
0.4
***
***
***
n.s
non transfected
GFP
SKIP
RILP

Figure 5.5. The assay used to study lysosomal distribution.
(A) Representative confocal fluorescence images showing methanol fixed HeLa cells transfected with either myc-SKIP, GFP-RILP or GFP and stained for LAMP-1. Scale bar = 10μm The primary antibodies used were rabbit monoclonal anti-LAMP-1 and a mouse monoclonal anti-myc antibody. The secondary antibodies were Alexa 568 goat anti-rabbit antibody and Alexa 488 goat anti-mouse antibody probing for LAMP-1 and myc-SKIP respectively. (B) The circumference of the non transfected cell in (A) was used to highlight the 10% increments used to calculate the cumulative LAMP-1 intensity. The 60^{th} centile is shown in red. (C) Graph showing the cumulative of LAMP-1 distribution for myc-SKIP, GFP-RILP, GFP or non transfected (NT). A centered 6th order polynominal was fitted to the cumulative LAMP-1 distribution: Y=B0 + B1*X + B2*X^2 + B3*X^3 + B4*X^4 + B5*X^5 + B6*X^6. To compare models to assess the statistical significance of differences in distribution profiles, the extra sum of F-squares test was applied (D) Graph showing the cumulative distribution of LAMP-1 intensity at the 60^{th} centile. ***P<0.001 (Two-tailed T-test). Error bars show S.E.M from 15 cells in 3 replicates.

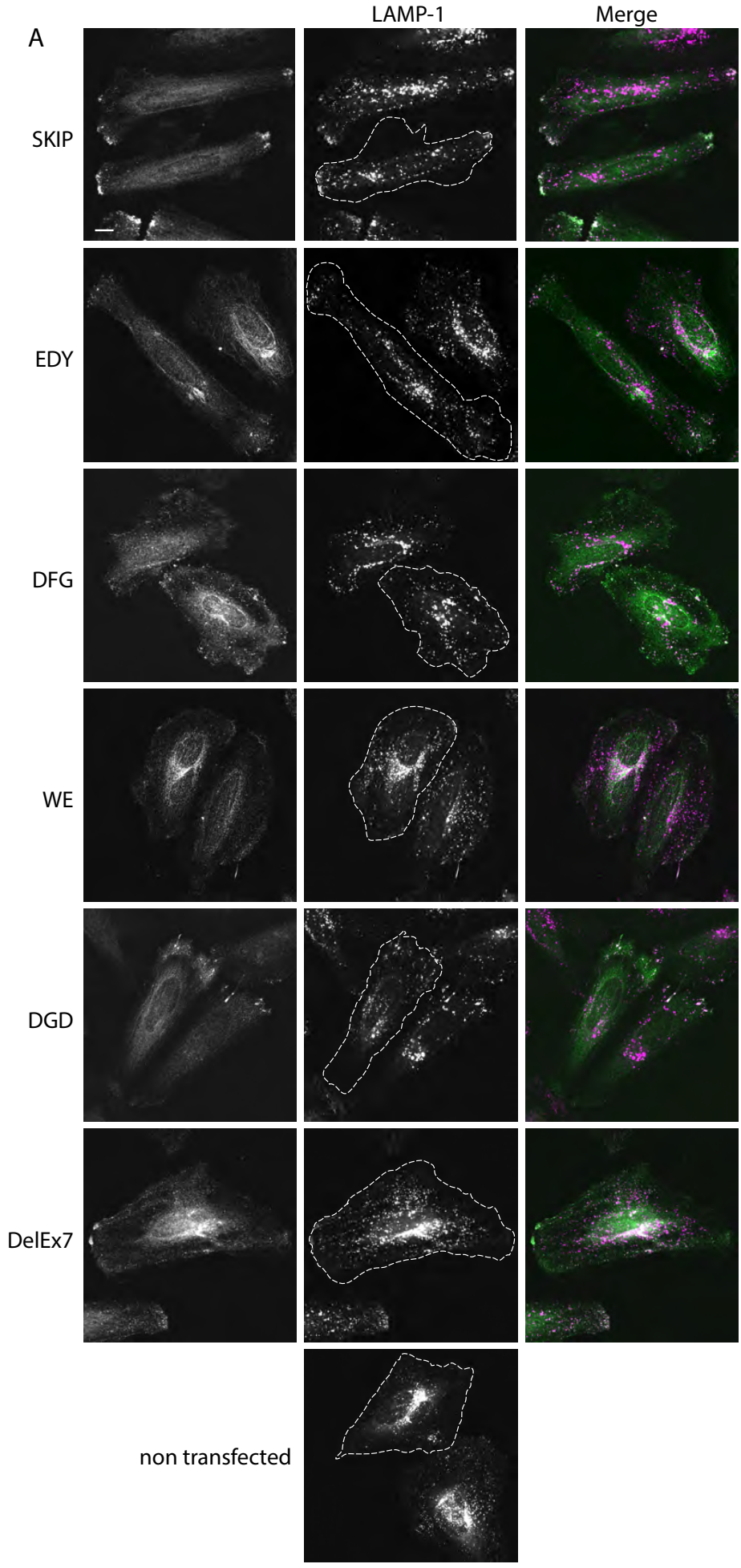
A
LAMP-1
Merge
SKIP
EDY
DFG
WE
DGD
DelEx7
non transfected

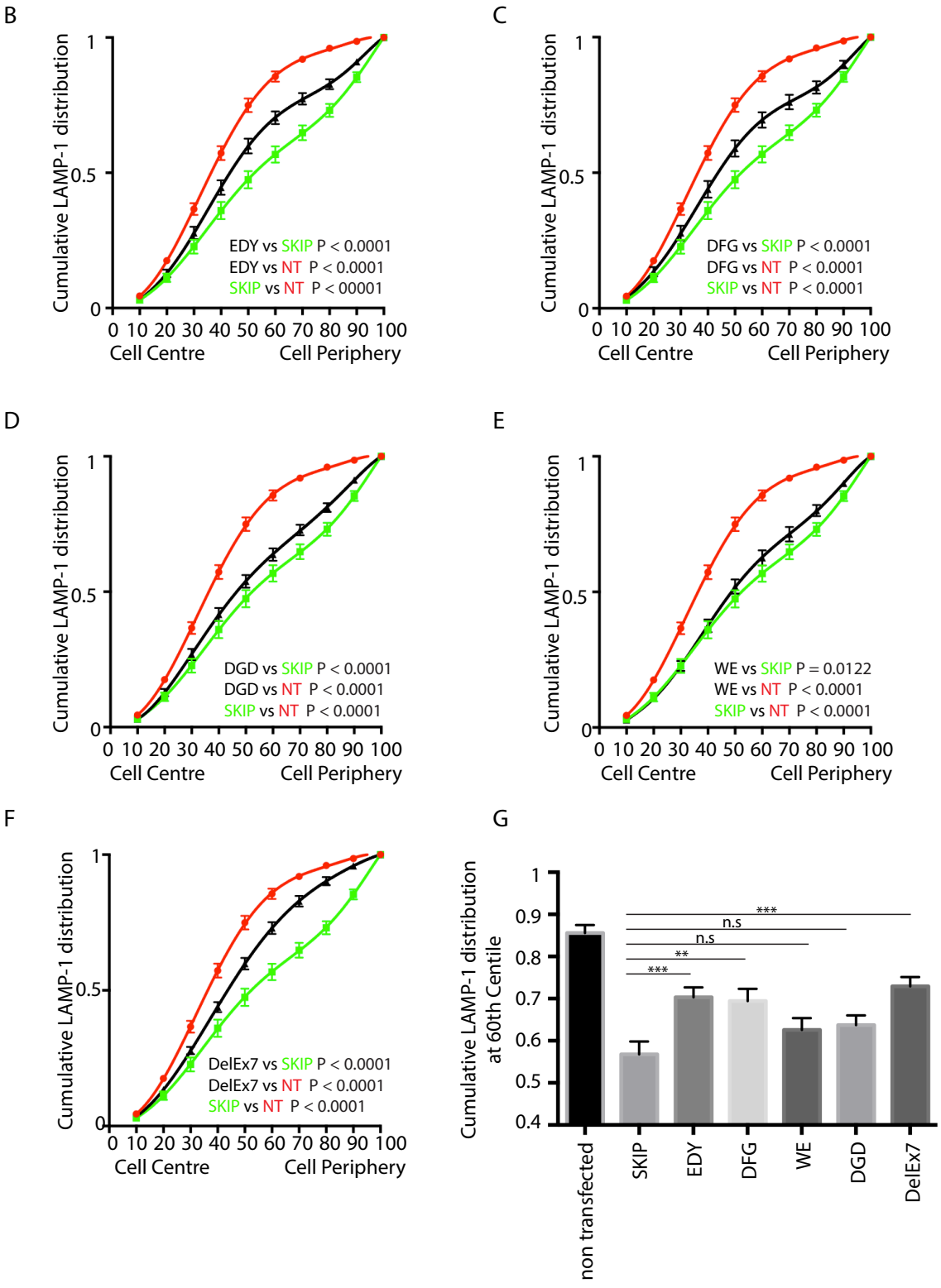
B
Cumulative LAMP-1 distribution
1
0.5
0
0 10 20 30 40 50 60 70 80 90 100
Cell Centre
Cell Periphery
EDY vs SKIP P < 0.0001
EDY vs NT P < 0.0001
SKIP vs NT P < 00001
C
Cumulative LAMP-1 distribution
DFG vs SKIP P < 0.0001
DFG vs NT P < 0.0001
SKIP vs NT P < 0.0001
D
Cumulative LAMP-1 distribution
DGD vs SKIP P < 0.0001
DGD vs NT P < 0.0001
SKIP vs NT P < 0.0001
E
Cumulative LAMP-1 distribution
WE vs SKIP P = 0.0122
WE vs NT P < 0.0001
SKIP vs NT P < 0.0001
F
Cumulative LAMP-1 distribution
DelEx7 vs SKIP P < 0.0001
DelEx7 vs NT P < 0.0001
SKIP vs NT P < 0.0001
G
Cumulative LAMP-1 distribution at 60th Centile
1
0.9
0.8
0.7
0.6
0.5
0.4
***
n.s
n.s
**
***
non transfected
SKIP
EDY
DFG
WE
DGD
DelEx7

Figure 5.6. Disruption of KHC:SKIP interaction results in reduction in lysosomal transport to the cell periphery.

(A) Representative confocal fluorescence images showing methanol fixed HeLa cells transfected with either myc-SKIP, or mutants of SKIP (EDY, DFG, WE, DGD) or SKIP with Exon 7 deleted (DelEx7) or non transfected (NT) and stained for LAMP-1. Scale bar= 10μm The primary antibodies used were rabbit monoclonal anti-LAMP-1 and a mouse monoclonal anti-myc antibody. The secondary antibodies were Alexa 568 goat anti-rabbit antibody and Alexa 488 goat anti-mouse antibody probing for LAMP-1 and myc-SKIP respectively. (B-F) Graphs showing the cumulative distribution of LAMP-1 for myc-SKIP, mutants of SKIP (EDY, DFG, WE, DGD) and SKIP with Exon 7 deleted (DelEx7). A centered 6th order polynominal was fitted to the cumulative LAMP-1 distribution: Y=B0 + B1*X + B2*X^2 + B3*X^3 + B4*X^4 + B5*X^5 + B6*X^6. To compare models to assess the statistical significance of differences in distribution profiles, the extra sum of F-squares test was applied. (C) Graph showing the cumulative distribution of LAMP-1 distribution at the 60^{th} centile. ***P<0.001 (Two-tailed T-test) Error bars show S.E.M from 45 cells in 3 replicates.

5.5 Discussion

The experiments described in this chapter aimed to investigate further the determinants of the SKIP:KHC interaction, examine its relationship to the SKIP:KLC interaction and thus also separate the function of the KLC:SKIP and KHC :SKIP interaction in cargo recognition and transport.

Figure 3.13 shows that KLC is important in recruitment of SKIP and that association with KHC can only occur once SKIP has bound to KLC TPR domain via its tryptophan acidic (WD) motif. SKIP is also only able to bind to KHC once autoinhibition has been relieved. This was shown through mutation of the 9 residues of the autoinhibitory 'IAK' sequence (QIAKPIRPG/AAAAAAAA) allowing for KHC binding to SKIP (Figure 5.1).

Since KHC and KLC binding sites appear to overlap, SKIP mutations were identified that separate KHC binding from KLC binding (Figure 5.2 and Figure 5.3) Disruption of the KHC:SKIP interaction (through mutation of EDY or DFG residues in SKIP) reduced binding of the kinesin-1 tetramer to SKIP suggesting that heavy chain binding is required for the stable interaction of SKIP to the kinesin-1 tetramer (Figure 5.4). Disruption of the KHC:SKIP interaction is shown to hinder transport of lysosomes to the cell periphery, suggesting the KHC:SKIP interaction is important in transport (Figure 5.6). Whether transport of cargo is triggered by KHC binding or whether the increased cargo transport observed results only from a more stable cargo:kinesin-1 tetramer interaction cannot be established from the data presented here. The presence of low level transport of lysosomes to the periphery seen when the SKIP:KHC interaction is disrupted may suggest that the latter is the case, however the transport of some lysosomes to the cell periphery may occur due to the presence of endogenous SKIP within HeLa. Taken together, these data suggest that KLC has some capacity to gate access to the heavy chain cargo binding site.

Kawano et al. shows that a 10 residue peptide from Calsyntenin-1 centering on the tryptophan acidic motif is sufficient for at least partial activation of Kinesin-1 and vesicle transport when fused to a transmembrane domain (Kawano et al., 2012). Pu et al. also gives further evidence that KLC binding is sufficient for transport. Expression of a Lamp-GFP construct containing three copies of the tryptophan- acidic motifs form SKIP (TNLEWDDSAI) links lysosomes to Kinesin-1 and results in the peripheral accumulation of lysosomes

(Pu et al., 2015). It is not clear whether three motifs were absolutely required or whether this simply made the process more efficient. It may be the case that three tryptophan acidic motifs from SKIP were perhaps used as more than one interaction with kinesin-1 is required for the stable association and transport of lysosomes. The fact that KLC binding alone can result in transport suggests that perhaps the latter model is the true model, where binding to KHC enables a more stable kinesin-1:cargo interaction resulting in more efficient transport.

The cumulative distribution of LAMP-1 intensity at the 60th centile gives a clear indication of the proportion of lysosomes in the centre 60% of the cell compared to the periphery (40%). This method of quantification assumes that the mTOC is in the centre of the cell, and when there is perinuclear clustering of lysosomes that this clustering would occur in the centre of the cell. Accumulation of lysosomes do not always occur completely in the centre of the cell, which reduces the perinuclear clustering effect when quantified using this method compared to what is observed in cells. A clear difference could however still be seen between RILP and control, suggesting that although the method of quantification might reduce the effect seen, it is still possible to distinguish between transport to the periphery and perinuclear clustering. Another method could involve plating individual HeLa cells on a micropatterned array in order to quantify lysosomal distribution over a fixed cell shape as used by (Rosa-Ferreira and Munro, 2011).

The results presented in this chapter is summarised in Figure 5.7. Cargo first interacts with KLC, via its W-acidic motif, triggering a conformational change in kinesin-1, resulting in the autoinhibition to be at least partially relieved. Transport either commences when cargo interacts with the KHC binding site or more likely more efficient transport occurs due to a more stable kinesin-1 tetramer cargo interaction. Further experiments to investigate the effect of disruption of KHC binding on transport of cargo to the cell periphery will be discussed in Chapter 7.

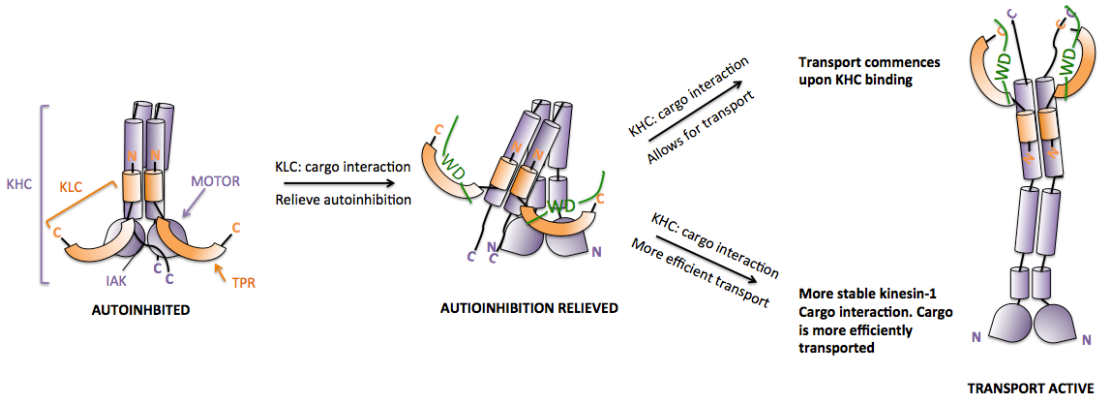

Figure 5.7. Model of activation.
Kinesin-1 is found in an autoinhibited state in the cell where the C-terminal tail of KHC binds to the motor domain. Cargo interaction with KLC via its W-acidic motif relieves autoinhibition as the interaction with KLC triggers a conformational change in kinesin-1. Transport either commences when cargo interacts with the KHC binding site or more efficient transport occurs due to a more stable kinesin-1 tetramer cargo interaction.

CHAPTER 6 . EXPRESSION, PURIFICATION AND CRYSTALLISATION OF KLC1TPR BOUND TO JIP1.

Cargo binding to kinesin-1 is not restricted to those containing a tryptophan-acidic motif. JNK-interacting protein-1 (JIP1) is an example of a kinesin-1 cargo protein that does not contain a tryptophan-acidic motif. The 11 amino acid at the C terminus of JIP1 (JIP1(C11) has been shown to bind preferentially to KLC1 and does not bind to KLC2 (Zhu et al., 2012).

Progress has been made in understanding the determinants of this apparent specificity. Data from isothermal titration experiments demonstrated that N343 of KLC1-TPR and the equivalent residue S328 in KLC2-TPR are crucial determinants of the different binding properties of the two TPR domains. This residue resides on the fourth TPR repeat and is distinct from the residues on TPR2/3 that primarily comprise the W-acidic motif binding site. JIP1 was unable to bind the KLC1-N343S mutant, but was able to bind KLC2-S328N mutant. Mutation of these residues did not affect binding to the tryptophan acidic motif containing peptide from CSTN. This agrees with the structural data provided in Chapter 1, where this residue is outside the W-acidic binding site. Taken together, these data suggest that the groove of the TPR domain can bind other peptides of different sequence at at least one other distinct site.

In order to have a greater understanding of the cargo recognition process of KLC and to determine the importance of the residues within the TPR domain in binding to a non-tryptophan acidic motif containing cargo, crystallisation was attempted of the TPR domain of KLC1 in complex with the 11 reside C-terminal region of JIP1 using similar approaches to those presented in Chapter 3.

6.1 Construct design

A chimeric construct was engineered in a similar way as for SKIPWD_KLC2TPR in which the C-terminal 11 residues of JIP1 were fused N-terminal to KLC1TPR via a flexible (TGS)4 linker (JIP1(C11)_KLC1TPR) (Figure 6.1). The KLC1TPR consisted of residues 229-491 and did not include the first helix of the first TPR, as this is the section that has previously been successfully crystallised (PDB code 3NF1). A histidine tag was fused N-Terminal to JIP1(C11)_KLC1TPR to aid in purification. Again, the advantage of this

approach is that the stoichiometry is defined and the interaction is more favorable than if the protein and peptide were not attached. Fusing the peptide and the KLC1TPR domain brings them in close proximity, making the interaction more likely.

6.2 Expression and purification of JIP1(C11)_KLC1TPR

JIP1(C11)_KLC1TPR was expressed in *E.coli* as an N-terminally His^6-tagged protein and was first purified by Ni^{2+}-affinity chromatography (Figure 6.2A) followed by size exclusion chromatography (SEC). JIP1(C11)_KLC1TPR eluted as a single symmetric peak at 61.64ml (Figure 6.2B and Figure 6.2C). The most pure samples were pooled and concentrated to 5mg/ml for crystallisation screens.

6.3 Crystallisation of JIP1(C11)_KLC1TPR

Initial screening experiments were set up using the histidine tagged JIP1(C11)_KLC1TPR. The crystallisation screens used in trials were PGA, MIDAS, and ProComplex and JCSG+ (Qiagen). No crystals formed under the conditions within these screens. To determine whether the N-terminal histidine tag had a detrimental effect on crystallisation, the tag was removed by thrombin cleavage.

6.4 Thrombin cleavage of JIP1(C11)_KLC1TPR

To increase the efficiency of the thrombin cleavage of the His-tag, the cleavage condition was optimised. An overnight incubation at 4°C with a 1:25 dilution of the biotinylated thrombin stock (at a concentration of approx 1 U/µl, Novagen) showed the best cleavage efficiency (Figure 6.3A). Figure 6.3B shows that the thrombin cleavage of JIP1(C11)_KLC1TPR was efficient with no uncleaved histidine tagged JIP1(C11)_KLC1TPR detectable by western blot (Figure 6.3B). The elution profile from SEC show that JIP1(C11)_KLC1TPR eluted in a single symmetric peak at 70.98ml (Figure 0.3D). The sample contains a very small fraction of lower and higher molecular weight impurities (Figure 6.3C). The crystallisation screens set up were JCSG+, MIDAS, PGA, PaCT Premier and Structure screen 1&2 (molecular dimensions) and ProComplex Suite (Qiagen). The un-tagged JIP1(C11)_KLC1TPR did not crystallise.

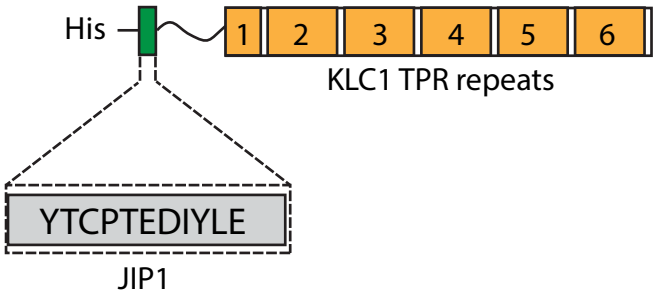

Figure 6.1. Schematic of JIP1(C11)_KLC1TPR construct design.
The JIP1(C11) peptide (green) is fused N-Terminal to KLC1TPR residues 229-491 (orange) via a flexible (TGS)4 linker.

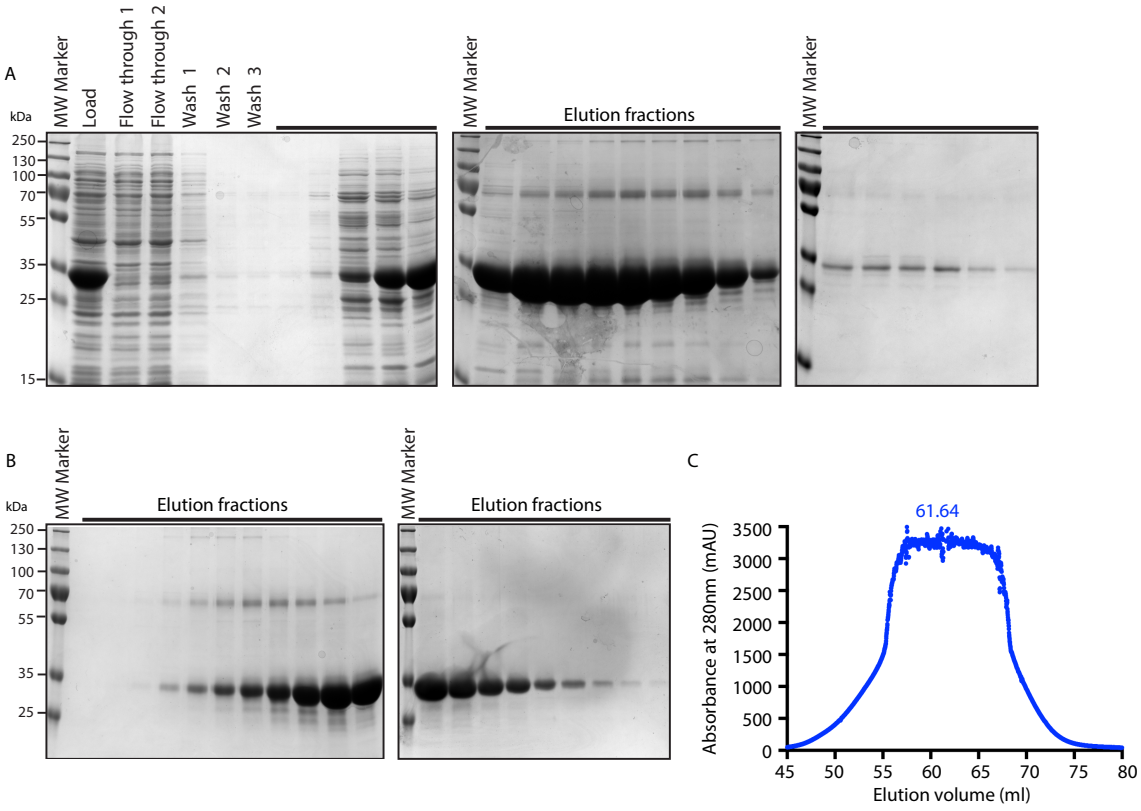

Figure 6.2. Purification of His-JIP1(C11)_KLC1TPR.
(A) Coomassie stained gel of the collected fractions of Ni^{2+} column purification. The soluble cell lysate is labeled load. The flow through as well as the wash buffer were collected after passing through the column (flow through 1,2 and wash 1, 2, 3 respectively). The JIP1(C11)_KLC1TPR (34.6 kDa) chimera was eluted with an imidazole gradient and fractions containing the target protein collected. (B) Coomassie stained gel of fractions eluted during size exclusion chromatography. A size exclusion chromatography column (HiLoad 16⁄600 Superdex 75pg) was used. (C) Size exclusion chromatogram showing absorbance measurements at 280nm of eluted fractions shown in B.

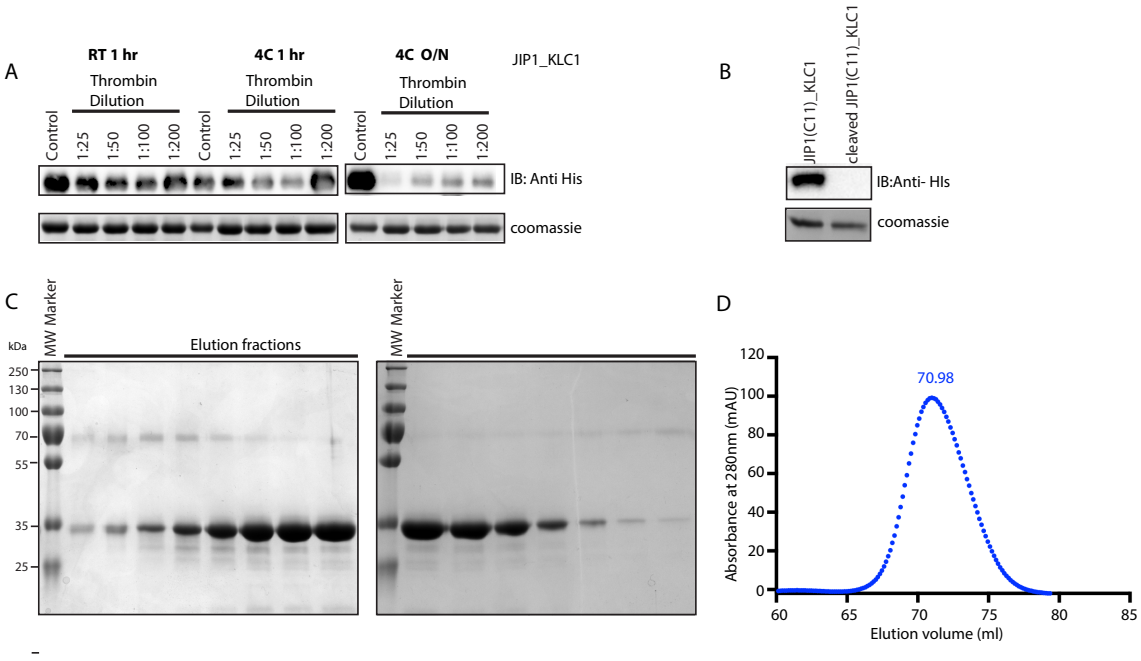

Figure 6.3. Thrombin cleavage and purification of un-tagged JIP1(C11)_KLC1TPR.

(A) Histidine tagged JIP1(C11)_KLC1TPR was incubated with a serial dilution of the Thrombin stock (1:25, 1:50,1:100,1:200), for 1hr at room temperature, 1hour at 4°C and overnight at 4°C. The amount of histidine tagged protein is shown by western blot and the protein load by coomassie stain (B) Western-blot of histidine tagged JIP1(C11)_KLC1TPR (34.6 kDa) and un-tagged JIP1(C11)_KLC1TPR (32.8 kDa) (C) Coomassie stained gel of fractions eluted during size exclusion chromatography. A size exclusion chromatography column (HiLoad 16⁄600 Superdex 75pg) was used. (D) Size exclusion chromatogram showing absorbance measurements at 280nm of eluted fractions shown in B.

6.5 Cloning C terminal fusion constructs

The work carried out by Zhu et al. suggest that a polar patch (TPR4-5) in the KLC1TPR domain is involved in JIP1 binding, whereas another polar patch (TPR3-4) is involved in the tryptophan acidic motif containing protein, CSTN binding (Zhu et al., 2012). The JIP1 binding site is therefore suggested to be closer to the C-terminal end of the TPR domain than CSTN. As an alternative strategy, a similar construct was designed where the JIP1(C11) peptide is fused at the C-terminus of the KLC1TPR domain (KLC1TPR_JIP(C11) (Figure 6.4A) . An additional construct was designed that also incorporated the first helix of the first TPR motif as this may play a role in stabilising the complex and so its presence may aid in crystal formation. Another C-terminal fusion was therefore designed where the JIP(C11) peptide was fused to the C-terminus of the full length KLC1TPR domain (KLC1TPR(FL)_JIP(C11) (Figure 6.4B). The KLC1TPR(FL)_JIP(C11) containing the full length KLC1TPR domain, with JIP1(C11) fused at the C terminus of the protein was ordered from Genscript. The KLC1TPR_JIP(C11) construct was cloned from the Genscript construct shortening the first TPR motif (including KLC1 residues 229-491) so that the TPR domain is the same length as in the JIP1(C11)_KLC1TPR construct (Figure 6.4B).

6.6 Expression and Purification of KLC1TPR_JIP(C11)

KLC1TPR_JIP(C11) was expressed in *E.coli* as an N-terminally His_6-tagged protein and was first purified by Ni^{2+}-affinity chromatography followed by size exclusion chromatography (SEC). KLC1TPR_JIP(C11) eluted 59.64ml. The elution volume suggests that KLC1TPR_JIP1(C11) is slightly more extended than JIP1(C11)_KLC1TPR. The protein eluted with an impurity very close in succession making it difficult to separate the impurity form JIP1(C11)_KLC1TPR. Using the coomassie stained gel the purest fraction was selected and used for crystallisation.

6.7 Crystallisation screens of KLC1TPR_JIP(C11)

Initial screening experiments were set up using the histidine tagged KLC1TPR_JIP(C11). The crystallisation screens used in trials were JCSG+,

MIDAS, PGA, PaCT Premier and Structure screen 1&2 (molecular dimensions) and ProComplex Suite (Qiagen). None of the initial screens were successful.

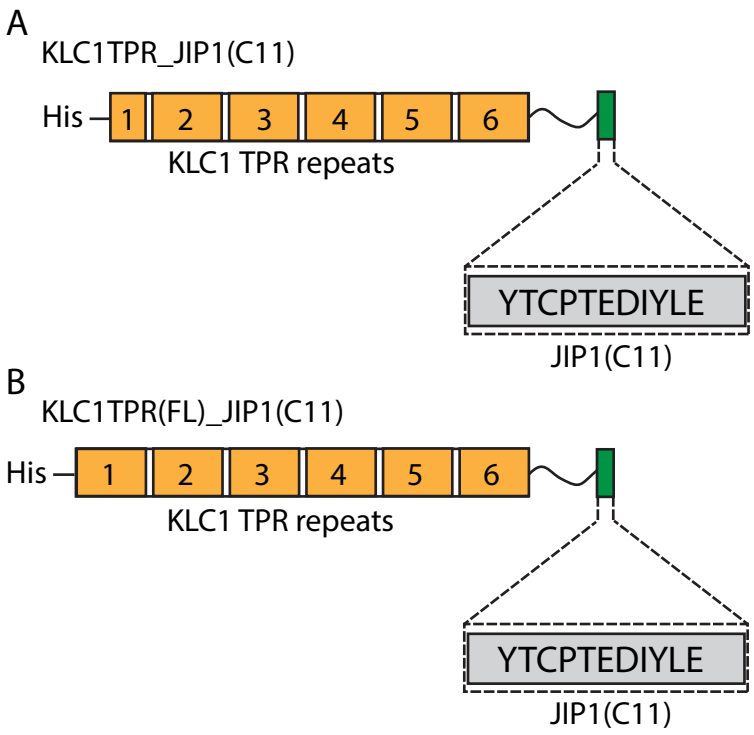

Figure 6.4. Schematic of KLC1TPR_JIP(C11) and KLC1TPR(FL)_JIP(C11) construct design.

(A) KLC1TPR_JIP(C11): The JIP1(C11) peptide (green) is fused C-terminal to KLC1TPR residues 229-491 (orange) via a flexible (TGS)4 linker. (B) KLC1TPR(FL)_JIP(C11): The JIP1(C11) peptide (green) is fused C-terminal to KLC1TPR residues 207-480 (orange) via a flexible (TGS)4 linker.

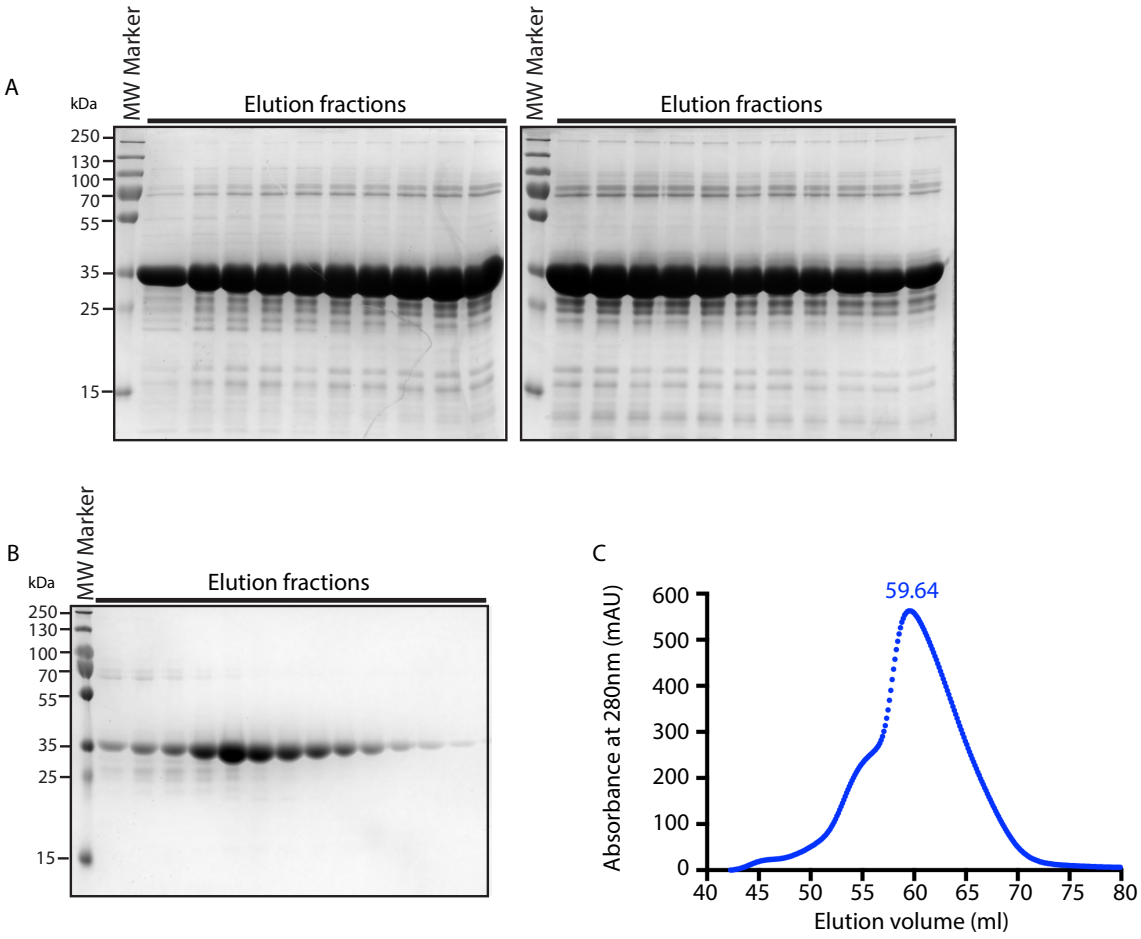

Figure 6.5. Purification of KLC1TPR_JIP1(C11).
(A) Coomassie stained gel of the collected fractions of Ni^{2+} column purification. KLC1TPR_JIP(C11) (34.7 kDa) chimera was eluted with an imidazole gradient and fractions containing the target protein collected. (B) Coomassie stained gel of fractions eluted during size exclusion chromatography. A size exclusion chromatography column (HiLoad 16⁄600 Superdex 75pg) was used. (C) Size exclusion chromatogram showing absorbance measurements at 280nm of eluted fractions shown in B.

6.8 Expression and Purification of KLC1TPR(FL)_JIP(C11)

KLC1TPR(FL)_JIP(C11) was expressed in *E.coli* as an N-terminally His6-tagged protein and was first purified by Ni^{2+}-affinity chromatography followed by size exclusion chromatography (SEC) (Figure 6.6A and Figure 6.6B/C) KLC1TPR(FL)_JIP(C11) eluted as a single peak at 65.07ml with a slight tail (Figure 6.6C). The most pure samples were pooled and concentrated to 5mg/ml for crystallisation trials.

6.9 Crystallisation screens of KLC1TPR(FL)_JIP(C11)

Initial screening experiments were set up using the histidine tagged KLC1TPR(FL)_JIP(C11). The crystallisation screens used in trials were JCSG+, MIDAS, PGA, PaCT Premier and Structure screen 1&2 (molecular dimensions) and ProComplex Suite (Qiagen). Figure 6.7A shows the conditions where initial crystals formed. Optimisation screens were set up for condition 1 and 5 shown in Figure 6.7A due to the larger dimensions of the crystals. A screen was set up based on condition 1 centering on 5% PEG8000 and 3%PGA with a PEG8000 (0-10%) vs PGA gradient (0-6%) keeping the concentration of the additive (potassium bromide and potassium thiocyanate) constant. This screen did not yield any crystals, with the drops remaining clear. Three screens were set up based on condition 5 shown in Figure 6.7A one at pH4.5, pH5 and pH5.5, each with a PEG8000 (0-10%) vs PGA gradient (0-6%) keeping the concentration of the additive (0.1M ammonium sulphate and 0.3M sodium formate) constant. The pH5.5 screen did not produce any crystals. The crystals that formed in the pH5 grid centered on 9% PEG and 1% PGA. Another screen was therefore set up with a narrower PGA range (0-4%) and the PEG8000 concentration shifted to a higher percentage (5-15%) centering the new optimisation grid on 9% PEG8000 and 1% PGA. The conditions that yielded crystals in the pH4.5 and pH5 conditions are illustrated in Figure 6.7B, with examples of crystals shown in Figure 6.9. The crystals formed were all pentagonal in shape. The crystals yielded a diffraction pattern that showed it was protein, but was not sufficient for structure determination (acquisition of data was carried out by Dr. Stefano Pernigo, Steiner group KCL). In an attempt to enable the crystals to form in a different crystal shape, the screens were attempted at PEGMME 2K, PEG3350, as well as PEG6K. The three screens involved using a 0-4% PGA gradient vs a

5-15% gradient of the respective PEG (PEGMME 2000, PEG3350, or PEG6000) keeping the concentration of the additive (0.1M ammonium sulphate and 0.3M sodium formate) constant. PEG3350 and PEG6000 yielded crystals of a similar shape to PEG8000. An additive screen was also used based on condition 5 in Figure 6.7 to aid in slowing down crystal formation. This also did not yield crystals that were sufficient for data collection. Examples of crystals are shown in Figure 6.10.

This was followed by the removal of the histidine tag. To increase the efficiency of the thrombin cleavage of the histidine tag, the cleavage condition was optimised. An overnight incubation at 4°C with a 1:25 dilution of the biotinylated thrombin stock (at a concentration of approx. 1 U/µl, Novagen) showed the best cleavage efficiency (Figure 6.8A). Figure 6.8B shows that the thrombin cleavage of KLC1TPR(FL)_JIP(C11) was efficient with no uncleaved histidine tagged KLC1TPR(FL)_JIP(C11) detectable by western blot. The elution profile from SEC shows that JIP1(C11)_KLC1TPR eluted in a single symmetric peak at 68.38ml . The sample contains a very small fraction of lower and higher molecular weight impurities. The crystallisation screens set up were JCSG+, MIDAS, PGA, PaCT Premier and Structure screen 1&2 (molecular dimensions) and ProComplex Suite (Qiagen). The un-tagged KLC1TPR(FL)_JIP(C11) did not crystallise.

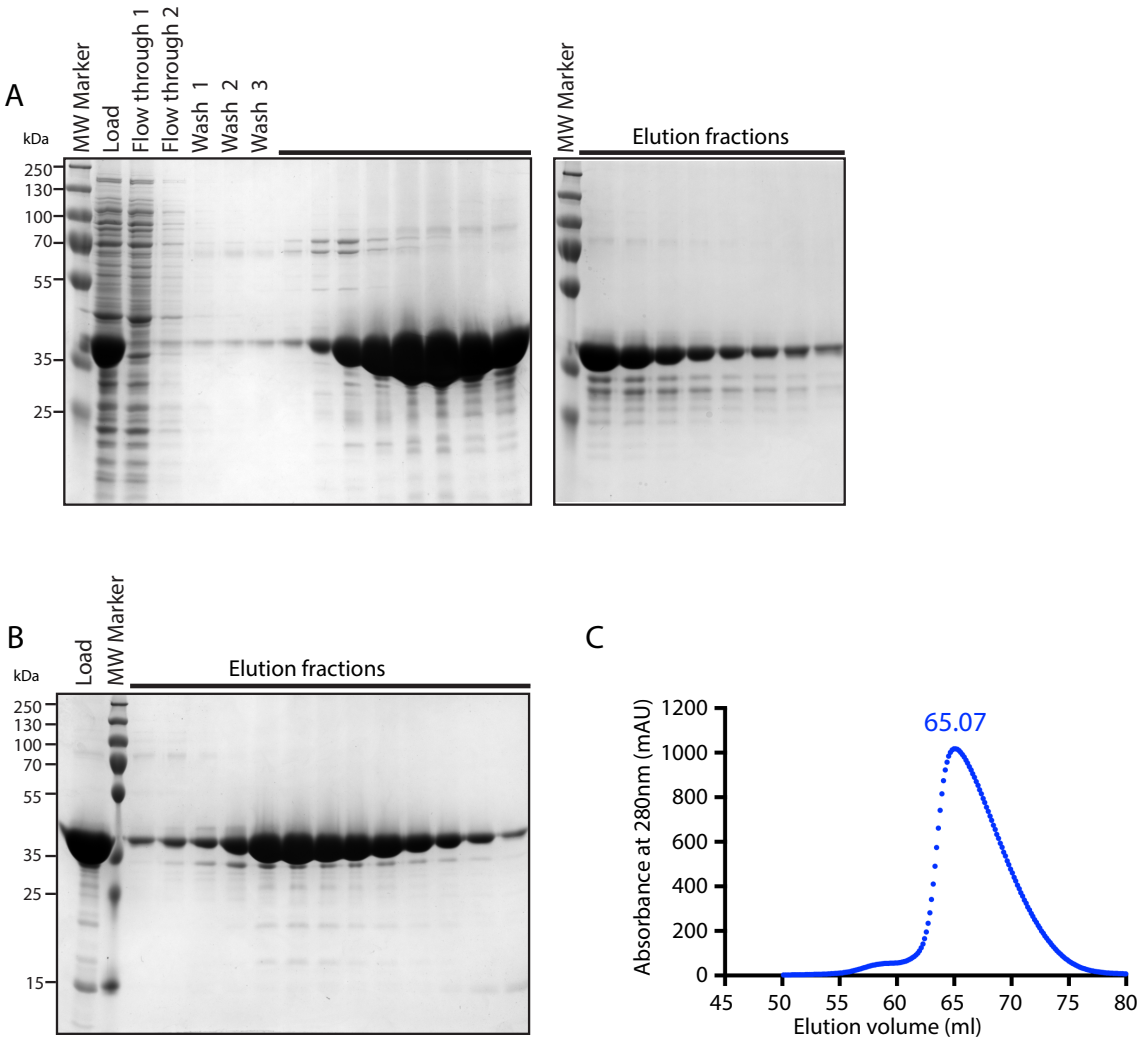

Figure 6.6. Purification of KLC1TPR(FL)_JIP(C11).
(A) Coomassie stained gel of the collected fractions of Ni^{2+} column purification. The soluble cell lysate is labeled load. The flow through as well as the wash buffer were collected after passing through the column (flow through 1,2 and wash 1, 2, 3 respectively). KLC1TPR(FL)_JIP(C11) (37.9 kDa) chimera was eluted with an imidazole gradient and fractions containing the target protein collected. (B) Coomassie stained gel of fractions eluted during size exclusion chromatography. A size exclusion chromatography column (HiLoad 16⁄600 Superdex 75pg) was used. (C) Size exclusion chromatogram showing absorbance measurements at 280nm of eluted fractions shown in B.

A

No	Buffer	pH	Precipitating Agent	Additive
1	0.1M Sodium acetate	5	3% w/v PGA 5% w/v PEG8000	0.2M Potassium bromide 0.2M Potassium thiocyanate
2	0.1M Sodium acetate	5	3% w/v PGA 20% v/v PEG500MME	0.1M Ammonium sulphate 0.3 M Sodium formate
3	0.1M Sodium acetate	5	3% w/v PGA 10% PEG2000MME	0.1M Ammonium sulphate 0.3 M Sodium formate
4	0.1M Sodium acetate	5	3% w/v PGA 5% w/v PEG3350	0.1M Ammonium sulphate 0.3 M Sodium formate
5	0.1M Sodium acetate	5	3% w/v PGA 5% w/v PEG8000	0.1M Ammonium sulphate 0.3 MSodium formate

B

No	Buffer	pH	Precipitating Agent	Additive
1	0.1M Sodium acetate	4.5	2-4% w/v PGA 5% w/v PEG8000	0.1M Ammonium sulphate 0.3 M Sodium formate
2	0.1M Sodium acetate	5	0.5-2% w/v PGA 5-10% w/v PEG8000	0.1M Ammonium sulphate 0.3 M Sodium formate
3	0.1M Sodium acetate	5	1% w/v PGA 10% w/v PEG8000	0.1M Ammonium sulphate 0.3 M Sodium formate 0.01 M Strontium chloride hexahydrate
4	0.1M Sodium acetate	5	1% w/v PGA 10% w/v PEG8000	0.1M Ammonium sulphate 0.3 M Sodium formate 4% v/v 1-Propanol
5	0.1M Sodium acetate	5	1-1.5% w/v PGA 10% w/v PEG3350	0.1M Ammonium sulphate 0.3 M Sodium formate
6	0.1M Sodium acetate	5	1.5-3% w/v PGA 7% w/v PEG3350	0.1M Ammonium sulphate 0.3 M Sodium formate
7	0.1M Sodium acetate	5	2-4% w/v PGA 8-9% w/v PEG3350	0.1M Ammonium sulphate 0.3 M Sodium formate
8	0.1M Sodium acetate	5	3% w/v PGA 6% w/v PEG3350	0.1M Ammonium sulphate 0.3 M Sodium formate
9	0.1M Sodium acetate	5	3% w/v PGA 6% w/v PEG3350	0.1M Ammonium sulphate 0.3 M Sodium formate
10	0.1M Sodium acetate	5	5-9% w/v PGA 1-2% w/v PEG6000	0.1M Ammonium sulphate 0.3 M Sodium formate
11	0.1M Sodium acetate	5	10-14% w/v PGA 1% w/v PEG6000	0.1M Ammonium sulphate 0.3 M Sodium formate
12	0.1M Sodium acetate	5	13-15% w/v PGA 0.5% w/v PEG6000	0.1M Ammonium sulphate 0.3 M Sodium formate
13	0.1M Sodium acetate	5	5-7% w/v PGA 3% w/v PEG6000	0.1M Ammonium sulphate 0.3 M Sodium formate

Figure 6.7. Conditions that produced KLC1TPR(FL)_JIP1(C11) crystals.
(A) List of the conditions from the initial crystal screens that produced crystals. (All the crystals were from the PGA screen (Molecular Dimensions). B) List of the conditions from the optimisation screens that produced crystals.

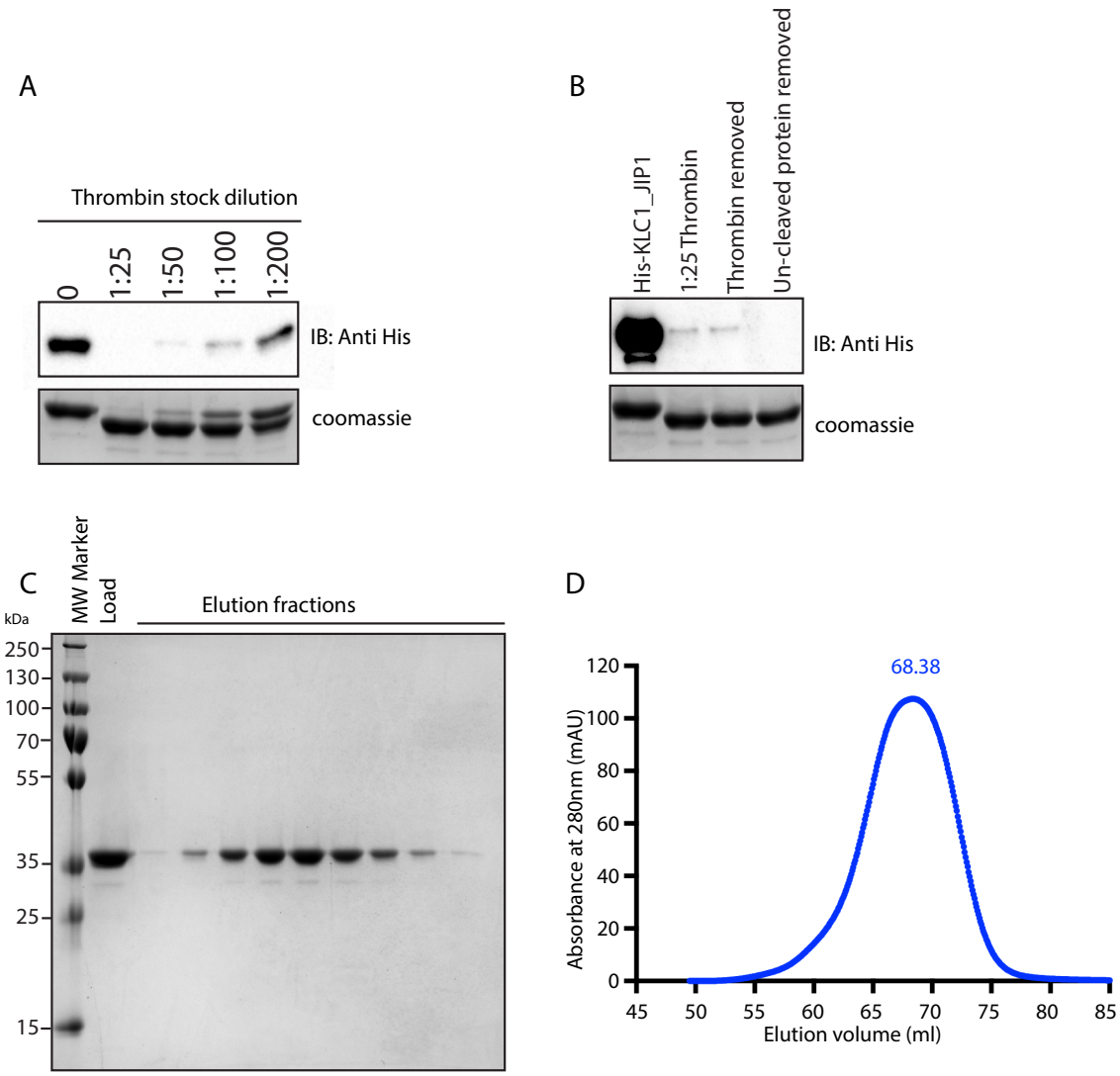

Figure 6.8. Thrombin cleavage and purification of KLC1TPR(FL)_ JIP1(C11).

(A) Histidine tagged KLC1TPR(FL)_JIP1(C11) (37.9kDa) was incubated with a serial dilution of the Thrombin stock (1:25, 1:50,1:100,1:200), overnight at 4°C. The amount of histidine tagged protein is shown by western blot and the protein load by coomassie stained gel (B) 1:25 dilution of thrombin stock was used to cleave the histidine tag, thrombin was removed by incubation with streptavidin beads followed by removal of the histidine tag and any uncleaved protein by NiNTA beads. (C) Coomassie stained gel of fractions eluted during size exclusion chromatography (un-tagged KLC1TPR(FL)_JIP1(C11): 36.0 kDa). A size exclusion chromatography column (HiLoad 16/600 superdex 75pg) was used. (D) Size exclusion chromatogram showing absorbance measurements at 280nm of eluted fractions shown in B.

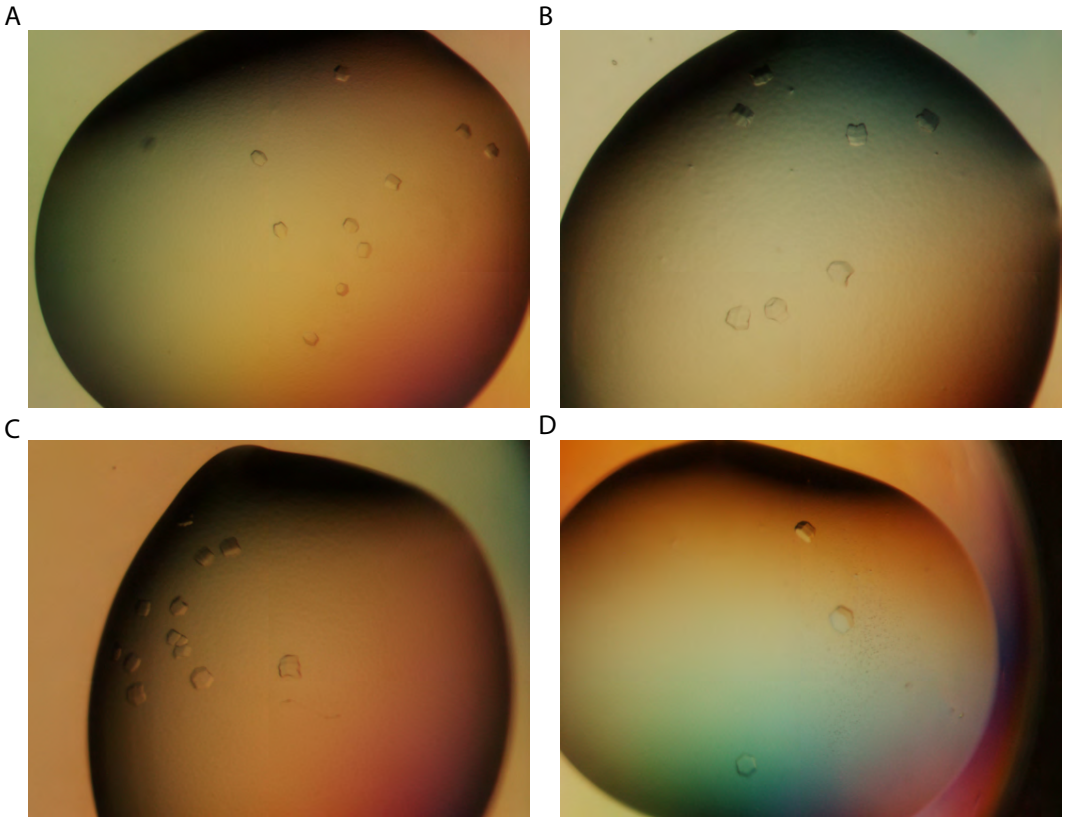

Figure 6.9. Examples of KLC1TPR(FL)_JIP1(C11) crystals.
The crystals shown above formed under the following conditions: (A) 0.1M ammonium sulphate, 0.3M sodium formate, 1M sodium acetate pH5 1%PGA, 5%w/v PEG8000, (1:3 protein: well ratio) (B) 0.1M ammonium sulphate, 0.3M sodium formate, 1M sodium acetate pH5 1%PGA, 6%w/v PEG8000, (1:2 protein: well ratio) (C) 0.1M ammonium sulphate, 0.3M sodium formate, 1M sodium acetate pH5 1.5%PGA, 5%w/v PEG8000, (D) 0.1M ammonium sulphate, 0.3M sodium formate, 1M sodium acetate pH5 1%PGA, 5%w/v PEG8000, (1:2 protein: well ratio)

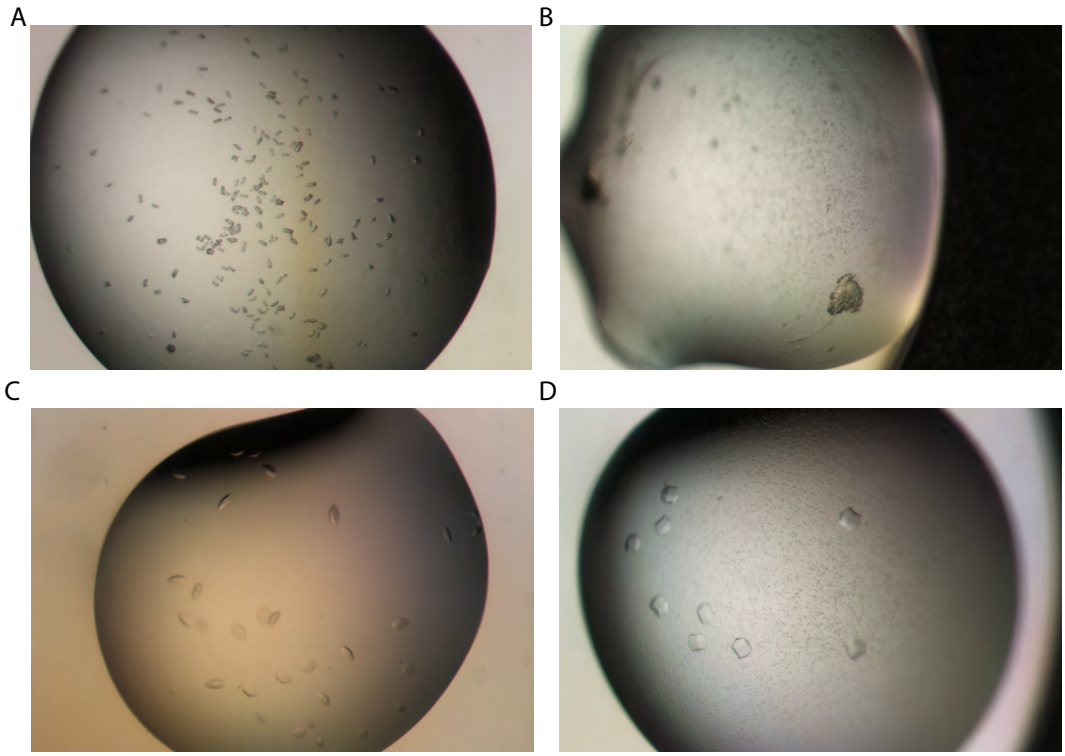

Figure 6.10. Examples of optimised KLC1TPR(FL)_JIP1(C11) crystals.
(A and B) Crystals yielded from the additive screen. Crystals were formed under the following conditions 0.1M ammonium sulphate, 0.3M sodium formate, 1M sodium acetate pH5, 1%PGA, 10%w/v PEG8000, with 0.01M strontium chloride hexahydrate in A or 4% v/v 1-Propanol in B, (C) 0.1M ammonium sulphate, 0.3M sodium formate, 1M sodium acetate pH5, 2%PGA, 7%w/v PEG6000, (D) 0.1M ammonium sulphate, 0.3M sodium formate, 1M sodium acetate pH5, 3%PGA, 8%w/v PEG3350.

6.10 Discussion

In this chapter the aim was to crystallise KLC1 TPR domain in complex with the C-terminal 11 residues of JIP (JIP(C11). Crystals that were obtained however did not yield a diffraction pattern that was sufficient for data collection.

Initial crystal hits for KLC1(FL)_JIP1 were obtained in a pH5 buffer. A lower or higher pH resulted in precipitation. The first optimisation screen was therefore not pH v precipitant, but varying the relative concentrations of the two precipitants (PGA vs PEG8000). This screen was set up at pH4.5 and pH5.5 in order to allow for slight changes in pH to affect crystal formation. The pH5 screen yielded larger crystals and so this was further optimised centering on the conditions that yielded crystals and reducing the range of PGA and PEG. The largest crystals in the optimisation screen were in the following condition:0.1M sodium acetate pH5, 0.1M ammonium sulphate, 0.3M sodium formate, 10% PEG8K, 1% PGA. The KLC1(FL)_JIP1 crystal morphology was poor, therefore an additive screen was used to aid in the packing of the crystals. The addition of additives may enable different crystal forms to appear (Larson et al., 2007). Additives may enable crosslinking within the crystal (McPherson and Cudney, 2006).

Since the initial crystal hits involved different types of PEG, varying the PEG may allow for the crystal to stack better and also form different shaped crystals. PEG2000MME, PEG3350 as well as PEG6000 were used in PGA vs PEG screens at pH5.

Due to the time requirement for further optimisation, crystallisation of JIP1(C11) in complex with KLC1 TPR domain was further pursued by the Steiner group. Optimisation at PEG3350 yielded crystals that appeared as though it may have a different morphology as well as having larger dimensions. Further KLC1TPR(FL)_JIP1 optimisation by the Steiner group involved crystal seeding. Seeding techniques were applied in order to aid in creasing the size and quality of crystals (Bergfors, 2003). Crystal seeding involves using a seed stock produced using a ‘seed-bead’ method (Luft and DeTitta, 1999). Crystals from G4 from initial screens were placed in 50µl of the reservoir condition and homogenised by vortexing. These seeds were stored at 20°C and used for seeding experiments.

Seeding experiments included varying seed stock dilution vs PEG3350 concentration, pH vs precipitant concentration as well as PGA concentration vs

PEG3350 concentration. None of these screens yielded crystals that were appropriate for data collection. A microseed matrix-screen approach was also taken to aid in improving the packing of crystals (D'Arcy et al., 2007, Ireton and Stoddard, 2004). This method could allow for crystallisation where little or no nucleation is normally observed.

Other approaches used to aid in improving the packing of the crystals involved the addition of a lysozyme tag as well as the addition of maltose binding protein (MBP), both of which have been used to aid crystallisation of other proteins (Moon et al., 2010, Zhao et al., 2011, Cherezov et al., 2007). The lysozyme tagged KLC1TPR(FL)_JIP1 was insoluble and the tagging of maltose binding protein yielded no crystals in the initial commercial screens.

Currently camelid heavy chain antibodies (VHHs, also called 'nanobodies') are being used in crystallisation attempts in collaboration with the Steiner group. Nanobodies are one of many protein chaperones used to aid in the formation of well diffracting crystals. Chaperones minimise the heterogeneity in the target protein conformation as it binds to a specific conformation. It also facilitates contacts between molecules in the crystal lattice, reducing the contacts that the protein of interest is required to make in order for crystallisation (Bukowska and Grutter, 2013, Koide, 2009).

Other approaches to crystallisation could include changing the construct. This may involve the cloning of a construct that has a longer linker, since KLC2TPR_SKIPWD crystallised as a dimer with the SKIPWD peptide binding across to another KLC2TPR_SKIPWD. This construct may have crystallised in this way if the linker was too short to allow the SKIPWD to fold back round and crystallise as a monomer. Extending the linker length may allow the JIP1C11 to reach the groove more easily and perhaps crystallise as a monomer. A too long linker will on the other hand negatively affect crystallisation due to the flexibility of the linker. Crystallisation could also be attempted using KLC1 TPR with purified JIPC11 peptides.

Once the structure is determined, the binding site could be verified by biophysical analysis including fluorescent polarisation.

CHAPTER 7 DISCUSSION

In this thesis, the molecular basis of the KLC:cargo interaction as well as the KHC:cargo interaction were investigated using SKIP as a model cargo. The independent functional roles of the KLC:cargo and KHC:cargo interactions in cargo recognition and activation of transport were also investigated.

7.1 Kinesin-1 cargo recognition

7.1.1 KLC : Cargo interaction

7.1.1.1 KLC TPR domain tryptophan acidic binding pocket

Data presented in this thesis has shown that the tryptophan-acidic SKIP peptide binds within a distinct highly positively charged groove of the KLC TPR domain. Early experiments showing that kinesin-1 is able to transport negatively charged beads (Vale et al., 1985b, Terasaki et al., 1995) gave an indication that kinesin-1; cargo recognition is partly achieved through electrostatic interactions and charge complementarity and so these new data are consistent with this. The highly positively charged inner concave surface of the TPR domain complements the highly negatively charged tryptophan-acidic motif containing SKIP peptide (TNLE**WD**DSAIT). The SKIP peptide binds in an extended conformation making a series of contacts along the length of the TPR groove. The TPR domain appears to fold around the cargo upon binding. Whilst the importance of this conformational change is not yet determined, it seems possible that this structural change may transduce the signal that cargo has bound contributing in the relief of autoinhibition. This binding pocket is likely to be a universal binding pocket as another tryptophan-acidic motif containing protein, CSTN was shown to interact via its tryptophan acidic motifs with the same pocket of the TPR domain (Pernigo et al., 2013). The structure presented in this thesis also establishes key residues within the binding pocket of KLC (KLC2 N287, R251, R312) to be responsible for interacting with tryptophan-acidic motif containing proteins. These have since been used by the Holzbaur group, confirming that mutation of these residues disrupt the interaction with a similar W-acidic motif in Nesprin-2 (Wilson and Holzbaur, 2015).

Not all kinesin-1 cargos contain tryptophan-acidic motifs. JIP1 is an example of a cargo that also interacts with the TPR domain of KLC, but has a

unique sequence. JIP1 is also highly negatively charged which complements the positively charged KLC TPR domain. Work by Zhu et al. suggests that JIP1 binds within a different groove of the TPR domain, contributed to by residues from TPR 4-5 (Zhu et al., 2012). Structural determination would aid in further characterisation of the KLC TPR domain interactions with cargo.

7.1.1.2 Tryptophan acidic motif recognition by KLC TPR domain

Tryptophan-acidic motifs were identified within cargo as being responsible for binding specifically to the TPR domain of KLC (Konecna et al., 2006, Araki et al., 2007, Aoyama et al., 2009, Schmidt et al., 2009). Dodding et al. identified that hydrophilic residues (D, E, N or Q) preceded the tryptophan residue at the –1 position and was also found at the +2 position residue in known KLC binding proteins. Using this information the RefSeq database was searched for expressed human proteins for the presence of four combinations of bipartite motifs: W(DENQ)—W(DENQ)(DENQ); W(DENQ)—(DENQ) W(DENQ); W(DENQ) (DENQ)—W(DENQ) and (DENQ) W(DENQ)—W(DENQ) to identify potential kinesin-1 interacting proteins (Dodding et al., 2011).

The SKIP(WD)_KLC2TPR structure presented in this thesis reveals a key role for a leucine residue at the W-2 position within the cargo binding motif. Further work in collaboration with the Steiner group also established that a methionine at the -2 position in tryptophan acidic motif containing cargo also binds to the same groove within the KLC TPR domain (Pernigo et al., 2013). Although bipartite motifs where both motifs are involved in KLC binding have been identified (in for example CSTN), for many cargo only one motif has been shown experimentally to be important in binding. In Chapter 3 mutation of the second tryptophan acidic motif of SKIP is also shown to have very little effect on KLC binding. The search for other possible cargo (that can interact with KLC) that contain tryptophan-acidic motifs can therefore likely be further constrained to those that have a methionine or leucine at the -2 position as well as acidic residues (an aspartic acid or a glutamic acid residue) at the -1 and +1 positions (M/L, E/D, W, E/D).

7.1.2 KHC: Cargo interaction

In Chapter 4, SKIP (1-310) is shown to bind to an extended region of the C-terminal tail of KHC (867-917) making multiple contacts along the length of

KHC. Two main regions were identified as essential for binding: 876-891 (KALESALKEAKENAM) and 907-917 (VRAKNMARRAH) although neither is sufficient for binding on their own (Figure 4.2 and Figure 4.3). Other kinesin-1 cargos exhibit similar binding properties and bind to an extended region of the C-terminal tail region of KHC (Barry et al., 2013, Randall et al., 2013). The cargo binding sites of other kinesins have also been shown to be located at the C-terminal tail. Seeger and Rice show that the C-terminal tail within the majority of kinesin motors is highly intrinsically disordered and is responsible for binding to multiple cargos (Seeger and Rice, 2013).

Kinesin-1 is found in an autoinhibited state within the cell and the SKIP binding site appears to flank the auto inhibitory sequence (IAK). As shown in Chapter 4, SKIP is able to bind to the truncated C-terminal tail of KHC directly, but is unable to bind to the full length KHC in the absence of KLC (Figure 3.13 and Figure 5.1). This may be because the SKIP binding site is inaccessible if autoinhibition is not relieved. Unlike SKIP, other cargos are able to bind to the full-length motor in the absence of KLC. This may be due to the recognition of additional regions of KHC that are accessible in the autoinhibited state. JIP-1 for example binds to both the tail and the stalk region of KHC (Fu and Holzbaur, 2013).

7.1.3 Overlapping KHC and KLC binding sites on SKIP

In this thesis, the binding determinant for KLC and KHC in SKIP were shown to overlap. The KHC binding site has been mapped to SKIP(202-241) and mutation of both tryptophan acidic motifs to alanine within this region significantly reduces KHC binding (Figure 4.5 and Figure 4.7). In contrast to this, KLC binding is significantly reduced by mutation of the first tryptophan-acidic motif, whereas mutation of the second tryptophan acidic motif has very little effect on KLC binding (Chapter 3). This suggests that although the binding regions overlap the relative importance of the residues within this region in binding to KLC and KHC varies.

Mutational analysis of the KHC binding region on SKIP illustrates that a relatively extended region of SKIP is also required for KHC binding (Figure 5.2). Further characterisation of the interaction through perhaps crystallisation of KHC (866-917) bound to the SKIP(202-241) should further define the underlying mechanisms of KHC-cargo recognition.

7.2 Proposed mechanism for cargo binding

Since the KHC and KLC binding regions appear to overlap, KHC and KLC binding to SKIP are unlikely to occur simultaneously. Either SKIP binds to KLC, which opens the motor allowing for two more SKIP molecules to bind, or SKIP is transferred from KLC to KHC. Recent work in the Dodding group indicates that KLC is itself found in an autoinhibited state, where a highly conserved (leucine-phenylalanine-proline (LFP)) motif and flanking acidic residues in the disordered region that links the heptad repeat to the TPR domain, itself binds to the concave groove of the TPR. A manuscript describing this work to which I made an early stage contribution is appended to this thesis. This interaction occludes the W-acidic binding site. Upon W-acidic cargo binding, this intramolecular interaction is displaced. Incorporating this data into my analysis, it seems possible that under this circumstance, KLC may rebind the highly conserved LFP motif upon transfer of cargo to KHC. This is likely to reduce the possible obstruction caused by KLC upon cargo transport if the cargo is transferred to KHC. This is illustrated in Figure 7.1. The exact mechanism of cargo binding needs to be established further.

7.3 Independent functional roles of the KLC:cargo and KHC: cargo interactions in cargo recognition and activation of transport.

In Chapter 3 it is reported that KLC is important in recruitment of SKIP and that association with KHC can only occur once SKIP has bound to KLC TPR domain via its tryptophan acidic (TNLE**WD**DSAIT) motif (Figure 3.13). SKIP is also only able to bind to KHC once autoinhibition has been relieved. This was shown through mutation of the 9 residues of the autoinhibitory 'IAK' sequence (QIAKPIRPG/AAAAAAAA) allowing for KHC binding to SKIP (Figure 5.1).

Disruption of the KHC:SKIP interaction (through mutation of EDY or DFG residues on SKIP) reduced binding of the kinesin-1 tetramer to SKIP suggesting that heavy chain binding is required for the stable interaction of SKIP to kinesin-1. Disruption of the KHC: SKIP interaction is also shown to hinder transport of lysosomes to the cell periphery, suggesting the KHC: SKIP interaction is important in transport.

The increased cargo transport observed is likely to occur due to a more stable cargo:kinesin-1 tetramer interaction as discussed in Chapter 5. Blasius et al. proposed another model where the autoinhibitory effects of both KHC as well as KLC must be relieved for activation to occur and transport to commence. JIP1 was shown to bind to KLC1, but requires the binding of a cofactor (FEZ1) to KHC to activate Kinesin-1 (Blasius et al., 2007). Both models may be true as JIP1 interacts with a different region of KLC and may therefore not transduce the signal to allow for autoinhibition to be relieved in the absence of KHC binding.

In this thesis it is shown that KLC as well as KHC binding are required for efficient transport. The requirement of cargo to bind to KHC as well as KLC for full activation would allow for additional regulation of the cargo that is transported. This would also aid in explaining how such a large variety of cargo is able to bind to kinesin-1.

7.4 Brief comparison of principles of kinesin-1: cargo recognition with cytoplasmic dynein-1 and myosin- V

Kinesin-1 cargo recognition is partly achieved through electrostatic interactions and charge complementarity as well as involving sequence specific determinants. Although cytoplasmic dynein and myosin V also transport several cargo, consensus sequences for recognition have not been identified. However several dynein adaptor proteins (BICD2, Hook3 and Spindly FIP3, HAP1, RILP, Snapin, and TRAK1) have been shown to contain long coiled coil regions (>20nm) and are thought that they may interact with dynein and dynactin via these coiled coil regions as is seen for BicD2 (Cianfrocco et al., 2015, Urnavicius et al., 2015). The globular cargo binding tail of myosin-V has been shown to contain several non-overlapping recognition sites for binding to its cargoes (for example melanophillin, RILPL2 and and vesicle-bound GTPase Rab11) (Lu et al., 2014, Pylypenko et al., 2013). Whether there are consensus sequences for these recognition sites remains to be established.

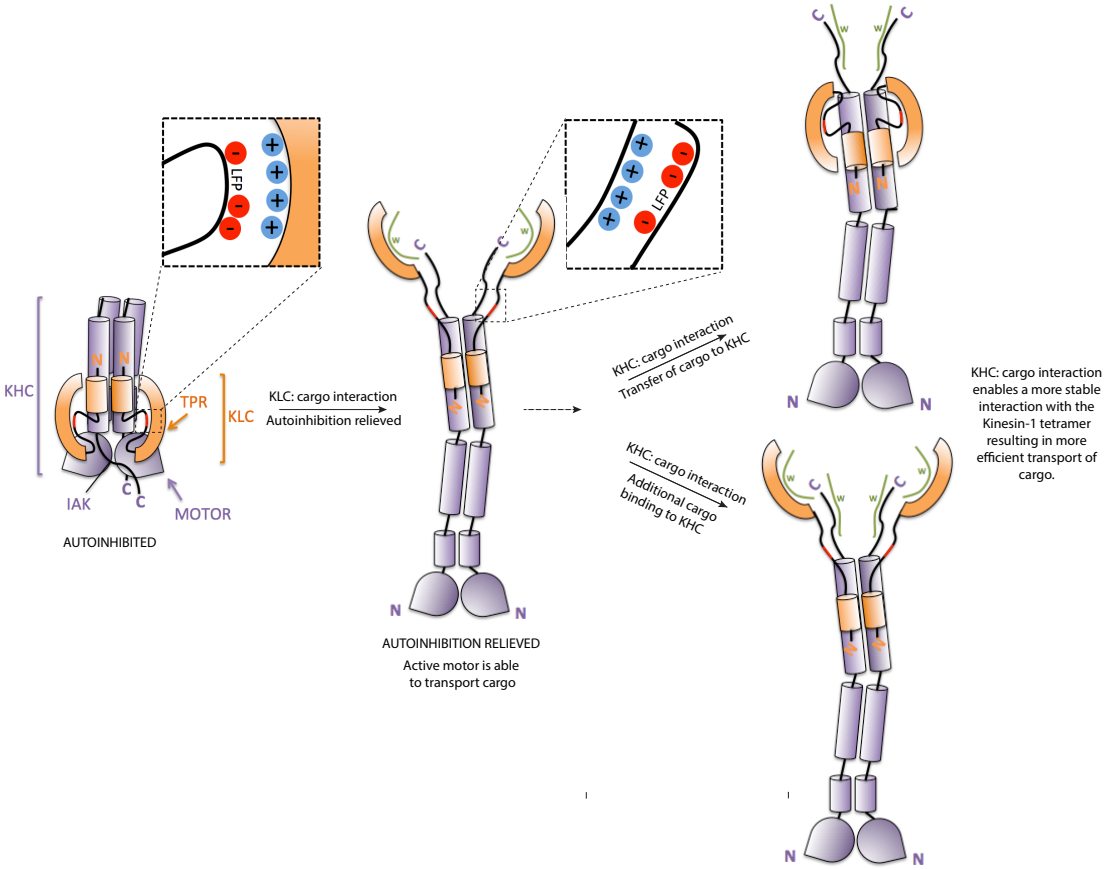

Figure 7.1. Proposed model of activation for Kinesin-1.
Kinesin-1 is found in an autoinhibited state in the cell. Upon Tryptophan- acidic motif containing cargo interacting with KLC TPR domain, autoinhibition is relieved. KHC:cargo binding results in more efficient cargo transport. Either SKIP binds to KLC, which opens the motor allowing for two more SKIP molecules to bind, or SKIP is transferred from KLC to KHC. Boxed regions show a universally conserved LFP motif and flanking acidic residues (red), located within the otherwise divergent linker region of KLC interacting with the positive groove of the TPR domain. When this intramolecular interaction is displaced by cargo binding, the LFP interacts with a positively charged region of KHC.

7.5 Further work

7.5.1 Mechanism of cargo binding

The model described in Figure 7.1 attempting to describe the mechanism of cargo binding is not complete. To establish whether cargo is transferred from KLC to KHC or whether KLC binding allows for more SKIP binding could be further investigated through GST-pulldown or immunoprecipitation assays.

7.5.2 Functional role of KHC: cargo interaction

The KHC: cargo interaction is shown to be important in a more stable Kinesin-1: cargo interaction. The effect that this might have on amount of transport, rate of transport or the distance of transport need to be further investigated. In order to investigate the effect of disruption of KHC binding on transport of cargo to the cell periphery further, TIRF microscopy could be used to visualise KHC dependent transport of SKIP along microtubules *in vitro* in the presence of KLC. The number of motile events, velocity and run length could be established using this method. The ATPase rate of kinesin-1 (KHC and KLC) in the presence of increasing concentrations of SKIP (wild type or mutant disrupting KHC binding) could also be investigated to more fully grasp the effect of the KHC cargo interaction on transport.

7.5.3 Targeting the motor:cargo interface with small molecules

The data presented in Chapter 3 gave the first structural and biophysical characterisation of a microtubule motor/cargo interface. This opened up the opportunity to answer a key question that has so far not been addressed for any motor. Can we modulate the motor-cargo interaction using small molecules?

As a result a time-resolved fluorescent resonance energy transfer (TRFRET) assay that will allow high-throughout screening of small molecules for their capacity to modulate the motor-cargo interaction interface, has been established and optimised within the Dodding group. This assay format is routinely used in drug discovery. The long fluorescence lifetime of terbium chelates allows signals to be read in a time-resolved manner reducing assay interference and a ratiometric approach decreases well-to-well variability. This assay involves using Lanthascreen reagents (Life Technologies), a highly stable, highly pure KLC2TPR domain construct (amino acids 161-480) purified

on Ni-NTA resin and by size-exclusion chromatography labeled with a terbium chelate compound on surface amine residues at a low molar ratio (one label per ten TPR molecules). This serves as a FRET donor. An N-terminally Cy5 labeled WD motif peptide from SKIP (5% labeled) is used as an acceptor. TRFRET is measured as a ratio of donor emission at 620 nm and acceptor emission at 665 nm. The specificity of this interaction has been shown by competitive inhibition using unlabeled KLC2TPR. This assay could allow for the identification of compounds with the capacity to inhibit W-acidic/KLC2TPR FRET.

REFERENCES

AKAMATSU, R., ISHIDA-KITAGAWA, N., AOYAMA, T., OKA, C. & KAWAICHI, M. 2015. BNIP-2 binds phosphatidylserine, localizes to vesicles, and is transported by kinesin-1. *Genes Cells,* 20**,** 135-52.

ALLY, S., LARSON, A. G., BARLAN, K., RICE, S. E. & GELFAND, V. I. 2009. Opposite-polarity motors activate one another to trigger cargo transport in live cells. *J Cell Biol,* 187**,** 1071-82.

ALMEIDA-SOUZA, L., ASSELBERGH, B., D'YDEWALLE, C., MOONENS, K., GOETHALS, S., DE WINTER, V., AZMI, A., IROBI, J., TIMMERMANS, J. P., GEVAERT, K., REMAUT, H., VAN DEN BOSCH, L., TIMMERMAN, V. & JANSSENS, S. 2011. Small heat-shock protein HSPB1 mutants stabilize microtubules in Charcot-Marie-Tooth neuropathy. *J Neurosci,* 31**,** 15320-8.

AOYAMA, T., HATA, S., NAKAO, T., TANIGAWA, Y., OKA, C. & KAWAICHI, M. 2009. Cayman ataxia protein caytaxin is transported by kinesin along neurites through binding to kinesin light chains. *J Cell Sci,* 122**,** 4177-85.

ARAKI, Y., KAWANO, T., TARU, H., SAITO, Y., WADA, S., MIYAMOTO, K., KOBAYASHI, H., ISHIKAWA, H. O., OHSUGI, Y., YAMAMOTO, T., MATSUNO, K., KINJO, M. & SUZUKI, T. 2007. The novel cargo Alcadein induces vesicle association of kinesin-1 motor components and activates axonal transport. *EMBO J,* 26**,** 1475-86.

ASBURY, C. L., FEHR, A. N. & BLOCK, S. M. 2003. Kinesin moves by an asymmetric hand-over-hand mechanism. *Science,* 302**,** 2130-4.

ASENJO, A. B., WEINBERG, Y. & SOSA, H. 2006. Nucleotide binding and hydrolysis induces a disorder-order transition in the kinesin neck-linker region. *Nat Struct Mol Biol,* 13**,** 648-54.

AYLOO, S., LAZARUS, J. E., DODDA, A., TOKITO, M., OSTAP, E. M. & HOLZBAUR, E. L. 2014. Dynactin functions as both a dynamic tether and brake during dynein-driven motility. *Nat Commun,* 5**,** 4807.

AZIMZADEH, J. & BORNENS, M. 2007. Structure and duplication of the centrosome. *J Cell Sci,* 120**,** 2139-42.

BAGSHAW, C. R. & TRENTHAM, D. R. 1974. The characterization of myosin-product complexes and of product-release steps during the magnesium ion-dependent adenosine triphosphatase reaction. *Biochem J,* 141**,** 331-49.

BAGSHAW, R. D., CALLAHAN, J. W. & MAHURAN, D. J. 2006. The Arf-family protein, Arl8b, is involved in the spatial distribution of lysosomes. *Biochem Biophys Res Commun,* 344**,** 1186-91.

BARRY, J., GU, Y., JUKKOLA, P., O'NEILL, B., GU, H., MOHLER, P. J., RAJAMANI, K. T. & GU, C. 2014. Ankyrin-G directly binds to kinesin-1 to transport voltage-gated Na+ channels into axons. *Dev Cell,* 28**,** 117-31.

BARRY, J., XU, M., GU, Y., DANGEL, A. W., JUKKOLA, P., SHRESTHA, C. & GU, C. 2013. Activation of conventional kinesin motors in clusters by Shaw voltage-gated K+ channels. *J Cell Sci,* 126**,** 2027-41.

BARTOLINI, F. & GUNDERSEN, G. G. 2006. Generation of noncentrosomal microtubule arrays. *J Cell Sci,* 119**,** 4155-63.

BERGFORS, T. 2003. Seeds to crystals. *J Struct Biol,* 142**,** 66-76.

BLASIUS, T. L., CAI, D., JIH, G. T., TORET, C. P. & VERHEY, K. J. 2007. Two binding partners cooperate to activate the molecular motor Kinesin-1. *J Cell Biol,* 176**,** 11-7.

BLOCK, S. M., GOLDSTEIN, L. S. & SCHNAPP, B. J. 1990. Bead movement by single kinesin molecules studied with optical tweezers. *Nature,* 348**,** 348-52.

BOUCROT, E., BEUZON, C. R., HOLDEN, D. W., GORVEL, J. P. & MERESSE, S. 2003. Salmonella typhimurium SifA effector protein requires its membrane-anchoring C-terminal hexapeptide for its biological function. *J Biol Chem,* 278**,** 14196-202.

BOUCROT, E., HENRY, T., BORG, J. P., GORVEL, J. P. & MERESSE, S. 2005. The intracellular fate of Salmonella depends on the recruitment of kinesin. *Science,* 308**,** 1174-8.

BOWMAN, A. B., KAMAL, A., RITCHINGS, B. W., PHILP, A. V., MCGRAIL, M., GINDHART, J. G. & GOLDSTEIN, L. S. 2000. Kinesin-dependent axonal transport is mediated by the sunday driver (SYD) protein. *Cell,* 103**,** 583-94.

BRACALE, A., CESCA, F., NEUBRAND, V. E., NEWSOME, T. P., WAY, M. & SCHIAVO, G. 2007. Kidins220/ARMS is transported by a kinesin-1-based mechanism likely to be involved in neuronal differentiation. *Mol Biol Cell,* 18**,** 142-52.

BREMNER, K. H., SCHERER, J., YI, J., VERSHININ, M., GROSS, S. P. & VALLEE, R. B. 2009. Adenovirus transport via direct interaction of cytoplasmic dynein with the viral capsid hexon subunit. *Cell Host Microbe,* 6**,** 523-35.

BRICKLEY, K., POZO, K. & STEPHENSON, F. A. 2011. N-acetylglucosamine transferase is an integral component of a kinesin-directed mitochondrial trafficking complex. *Biochim Biophys Acta,* 1813**,** 269-81.

BRICKLEY, K., SMITH, M. J., BECK, M. & STEPHENSON, F. A. 2005. GRIF-1 and OIP106, members of a novel gene family of coiled-coil domain proteins: association in vivo and in vitro with kinesin. *J Biol Chem,* 280**,** 14723-32.

BROUHARD, G. J. & RICE, L. M. 2014. The contribution of alphabeta-tubulin curvature to microtubule dynamics. *J Cell Biol,* 207**,** 323-34.

BRUNGER, A. T. 1992. Free R value: a novel statistical quantity for assessing the accuracy of crystal structures. *Nature,* 355**,** 472-5.

BUKOWSKA, M. A. & GRUTTER, M. G. 2013. New concepts and aids to facilitate crystallization. *Curr Opin Struct Biol,* 23**,** 409-16.

CAI, D., HOPPE, A. D., SWANSON, J. A. & VERHEY, K. J. 2007. Kinesin-1 structural organization and conformational changes revealed by FRET stoichiometry in live cells. *J Cell Biol,* 176**,** 51-63.

CAI, Q., GERWIN, C. & SHENG, Z. H. 2005. Syntabulin-mediated anterograde transport of mitochondria along neuronal processes. *J Cell Biol,* 170**,** 959-69.

CAI, Y., SINGH, B. B., ASLANUKOV, A., ZHAO, H. & FERREIRA, P. A. 2001. The docking of kinesins, KIF5B and KIF5C, to Ran-binding protein 2 (RanBP2) is mediated via a novel RanBP2 domain. *J Biol Chem,* 276**,** 41594-602.

CAMPBELL, P. D., SHEN, K., SAPIO, M. R., GLENN, T. D., TALBOT, W. S. & MARLOW, F. L. 2014. Unique function of Kinesin Kif5A in localization of mitochondria in axons. *J Neurosci,* 34**,** 14717-32.

CARLIER, M. F., HILL, T. L. & CHEN, Y. 1984. Interference of GTP hydrolysis in the mechanism of microtubule assembly: an experimental study. *Proc Natl Acad Sci U S A,* 81**,** 771-5.

CAVISTON, J. P., ROSS, J. L., ANTONY, S. M., TOKITO, M. & HOLZBAUR, E. L. 2007. Huntingtin facilitates dynein/dynactin-mediated vesicle transport. *Proc Natl Acad Sci U S A,* 104**,** 10045-50.

CECCARINI, M., TORRERI, P., LOMBARDI, D. G., MACCHIA, G., MACIOCE, P. & PETRUCCI, T. C. 2005. Molecular basis of dystrobrevin interaction with kinesin heavy chain: structural determinants of their binding. *J Mol Biol,* 354**,** 872-82.

CHEN, V. B., ARENDALL, W. B., 3RD, HEADD, J. J., KEEDY, D. A., IMMORMINO, R. M., KAPRAL, G. J., MURRAY, L. W., RICHARDSON, J. S. & RICHARDSON, D. C. 2010. MolProbity: all-atom structure validation for macromolecular crystallography. *Acta Crystallogr D Biol Crystallogr,* 66**,** 12-21.

CHEN, Y. & HANCOCK, W. O. 2015. Kinesin-5 is a microtubule polymerase. *Nat Commun,* 6**,** 8160.

CHEREZOV, V., ROSENBAUM, D. M., HANSON, M. A., RASMUSSEN, S. G., THIAN, F. S., KOBILKA, T. S., CHOI, H. J., KUHN, P., WEIS, W. I., KOBILKA, B. K. & STEVENS, R. C. 2007. High-resolution crystal structure of an engineered human beta2-adrenergic G protein-coupled receptor. *Science,* 318**,** 1258-65.

CHO, C., RECK-PETERSON, S. L. & VALE, R. D. 2008. Regulatory ATPase sites of cytoplasmic dynein affect processivity and force generation. *J Biol Chem,* 283**,** 25839-45.

CHO, K. I., CAI, Y., YI, H., YEH, A., ASLANUKOV, A. & FERREIRA, P. A. 2007. Association of the kinesin-binding domain of RanBP2 to KIF5B and KIF5C determines mitochondria localization and function. *Traffic,* 8**,** 1722-35.

CIANFROCCO, M. A., DESANTIS, M. E., LESCHZINER, A. E. & RECK-PETERSON, S. L. 2015. Mechanism and regulation of cytoplasmic dynein. *Annu Rev Cell Dev Biol,* 31**,** 83-108.

CLANCY, B. E., BEHNKE-PARKS, W. M., ANDREASSON, J. O., ROSENFELD, S. S. & BLOCK, S. M. 2011. A universal pathway for kinesin stepping. *Nat Struct Mol Biol,* 18**,** 1020-7.

CLIFF, M. J., HARRIS, R., BARFORD, D., LADBURY, J. E. & WILLIAMS, M. A. 2006. Conformational diversity in the TPR domain-mediated interaction of protein phosphatase 5 with Hsp90. *Structure,* 14**,** 415-26.

COLIN, E., ZALA, D., LIOT, G., RANGONE, H., BORRELL-PAGES, M., LI, X. J., SAUDOU, F. & HUMBERT, S. 2008. Huntingtin phosphorylation acts as a molecular switch for anterograde/retrograde transport in neurons. *EMBO J,* 27**,** 2124-34.

CONDE, C. & CACERES, A. 2009. Microtubule assembly, organization and dynamics in axons and dendrites. *Nat Rev Neurosci,* 10**,** 319-32.

COY, D. L., HANCOCK, W. O., WAGENBACH, M. & HOWARD, J. 1999. Kinesin's tail domain is an inhibitory regulator of the motor domain. *Nat Cell Biol,* 1**,** 288-92.

CREVEL, I. M., NYITRAI, M., ALONSO, M. C., WEISS, S., GEEVES, M. A. & CROSS, R. A. 2004. What kinesin does at roadblocks: the coordination mechanism for molecular walking. *EMBO J,* 23**,** 23-32.

CRIMELLA, C., BASCHIROTTO, C., ARNOLDI, A., TONELLI, A., TENDERINI, E., AIROLDI, G., MARTINUZZI, A., TRABACCA, A., LOSITO, L., SCARLATO, M., BENEDETTI, S., SCARPINI, E., SPINICCI, G., BRESOLIN, N. & BASSI, M. T. 2012. Mutations in the motor and stalk domains of KIF5A in spastic paraplegia type 10 and in axonal Charcot-Marie-Tooth type 2. *Clin Genet,* 82**,** 157-64.

D'ANDREA, L. D. & REGAN, L. 2003. TPR proteins: the versatile helix. *Trends Biochem Sci,* 28**,** 655-62.

D'ARCY, A., VILLARD, F. & MARSH, M. 2007. An automated microseed matrix-screening method for protein crystallization. *Acta Crystallogr D Biol Crystallogr,* 63**,** 550-4.

DAVID-PFEUTY, T., ERICKSON, H. P. & PANTALONI, D. 1977. Guanosinetriphosphatase activity of tubulin associated with microtubule assembly. *Proc Natl Acad Sci U S A,* 74**,** 5372-6.

DE VOS, K. J., GRIERSON, A. J., ACKERLEY, S. & MILLER, C. C. 2008. Role of axonal transport in neurodegenerative diseases. *Annu Rev Neurosci,* 31**,** 151-73.

DEBOER, S. R., YOU, Y., SZODORAI, A., KAMINSKA, A., PIGINO, G., NWABUISI, E., WANG, B., ESTRADA-HERNANDEZ, T., KINS, S., BRADY, S. T. & MORFINI, G. 2008. Conventional kinesin holoenzymes are composed of heavy and light chain homodimers. *Biochemistry,* 47**,** 4535-43.

DELUCA, J. G., NEWTON, C. N., HIMES, R. H., JORDAN, M. A. & WILSON, L. 2001. Purification and characterization of native conventional kinesin, HSET, and CENP-E from mitotic hela cells. *J Biol Chem,* 276**,** 28014-21.

DESAI, A., VERMA, S., MITCHISON, T. J. & WALCZAK, C. E. 1999. Kin I kinesins are microtubule-destabilizing enzymes. *Cell,* 96**,** 69-78.

DIBELLA, L. M. & KING, S. M. 2001. Dynein motors of the Chlamydomonas flagellum. *Int Rev Cytol,* 210**,** 227-68.

DIEFENBACH, R. J., DIEFENBACH, E., DOUGLAS, M. W. & CUNNINGHAM, A. L. 2002a. The heavy chain of conventional kinesin interacts with the SNARE proteins SNAP25 and SNAP23. *Biochemistry,* 41**,** 14906-15.

DIEFENBACH, R. J., MACKAY, J. P., ARMATI, P. J. & CUNNINGHAM, A. L. 1998. The C-terminal region of the stalk domain of ubiquitous human

kinesin heavy chain contains the binding site for kinesin light chain. *Biochemistry,* 37**,** 16663-70.

DIEFENBACH, R. J., MIRANDA-SAKSENA, M., DIEFENBACH, E., HOLLAND, D. J., BOADLE, R. A., ARMATI, P. J. & CUNNINGHAM, A. L. 2002b. Herpes simplex virus tegument protein US11 interacts with conventional kinesin heavy chain. *J Virol,* 76**,** 3282-91.

DIETRICH, K. A., SINDELAR, C. V., BREWER, P. D., DOWNING, K. H., CREMO, C. R. & RICE, S. E. 2008. The kinesin-1 motor protein is regulated by a direct interaction of its head and tail. *Proc Natl Acad Sci U S A,* 105**,** 8938-43.

DIXIT, R., ROSS, J. L., GOLDMAN, Y. E. & HOLZBAUR, E. L. 2008. Differential regulation of dynein and kinesin motor proteins by tau. *Science,* 319**,** 1086-9.

DODDING, M. P., MITTER, R., HUMPHRIES, A. C. & WAY, M. 2011. A kinesin-1 binding motif in vaccinia virus that is widespread throughout the human genome. *EMBO Journal,* 30**,** 4523-38.

DODDING, M. P. & WAY, M. 2011. Coupling viruses to dynein and kinesin-1. *EMBO J,* 30**,** 3527-39.

DOGAN, M. Y., CAN, S., CLEARY, F. B., PURDE, V. & YILDIZ, A. 2015. Kinesin's front head is gated by the backward orientation of its neck linker. *Cell Rep,* 10**,** 1967-73.

DRISKELL, O. J., MIRONOV, A., ALLAN, V. J. & WOODMAN, P. G. 2007. Dynein is required for receptor sorting and the morphogenesis of early endosomes. *Nat Cell Biol,* 9**,** 113-20.

DUMONT, A., BOUCROT, E., DREVENSEK, S., DAIRE, V., GORVEL, J. P., POUS, C., HOLDEN, D. W. & MERESSE, S. 2010. SKIP, the host target of the Salmonella virulence factor SifA, promotes kinesin-1-dependent vacuolar membrane exchanges. *Traffic,* 11**,** 899-911.

ECHARD, A., JOLLIVET, F., MARTINEZ, O., LACAPERE, J. J., ROUSSELET, A., JANOUEIX-LEROSEY, I. & GOUD, B. 1998. Interaction of a Golgi-associated kinesin-like protein with Rab6. *Science,* 279**,** 580-5.

ENCALADA, S. E., SZPANKOWSKI, L., XIA, C. H. & GOLDSTEIN, L. S. 2011. Stable kinesin and dynein assemblies drive the axonal transport of mammalian prion protein vesicles. *Cell,* 144**,** 551-65.

ENDOW, S. A., KANG, S. J., SATTERWHITE, L. L., ROSE, M. D., SKEEN, V. P. & SALMON, E. D. 1994. Yeast Kar3 is a minus-end microtubule motor

protein that destabilizes microtubules preferentially at the minus ends. *EMBO J,* 13**,** 2708-13.

ENGELENDER, S., SHARP, A. H., COLOMER, V., TOKITO, M. K., LANAHAN, A., WORLEY, P., HOLZBAUR, E. L. & ROSS, C. A. 1997. Huntingtin-associated protein 1 (HAP1) interacts with the p150Glued subunit of dynactin. *Hum Mol Genet,* 6**,** 2205-12.

ESPENEL, C., ACHARYA, B. R. & KREITZER, G. 2013. A biosensor of local kinesin activity reveals roles of PKC and EB1 in KIF17 activation. *J Cell Biol,* 203**,** 445-55.

ESPEUT, J., GAUSSEN, A., BIELING, P., MORIN, V., PRIETO, S., FESQUET, D., SURREY, T. & ABRIEU, A. 2008. Phosphorylation relieves autoinhibition of the kinetochore motor Cenp-E. *Mol Cell,* 29**,** 637-43.

EVANS, L., MITCHISON, T. & KIRSCHNER, M. 1985. Influence of the centrosome on the structure of nucleated microtubules. *J Cell Biol,* 100**,** 1185-91.

FRANSSON, S., RUUSALA, A. & ASPENSTROM, P. 2006. The atypical Rho GTPases Miro-1 and Miro-2 have essential roles in mitochondrial trafficking. *Biochem Biophys Res Commun,* 344**,** 500-10.

FRIEDMAN, D. S. & VALE, R. D. 1999. Single-molecule analysis of kinesin motility reveals regulation by the cargo-binding tail domain. *Nat Cell Biol,* 1**,** 293-7.

FU, M. M. & HOLZBAUR, E. L. 2013. JIP1 regulates the directionality of APP axonal transport by coordinating kinesin and dynein motors. *J Cell Biol,* 202**,** 495-508.

FU, M. M. & HOLZBAUR, E. L. 2014. Integrated regulation of motor-driven organelle transport by scaffolding proteins. *Trends Cell Biol,* 24**,** 564-574.

GAN, K. J., MORIHARA, T. & SILVERMAN, M. A. 2015. Atlas stumbled: kinesin light chain-1 variant E triggers a vicious cycle of axonal transport disruption and amyloid-beta generation in Alzheimer's disease. *Bioessays,* 37**,** 131-41.

GARNHAM, C. P. & ROLL-MECAK, A. 2012. The chemical complexity of cellular microtubules: tubulin post-translational modification enzymes and their roles in tuning microtubule functions. *Cytoskeleton (Hoboken),* 69**,** 442-63.

GATTO, G. J., JR., GEISBRECHT, B. V., GOULD, S. J. & BERG, J. M. 2000. Peroxisomal targeting signal-1 recognition by the TPR domains of human PEX5. *Nat Struct Biol,* 7**,** 1091-5.

GAUTHIER, L. R., CHARRIN, B. C., BORRELL-PAGES, M., DOMPIERRE, J. P., RANGONE, H., CORDELIERES, F. P., DE MEY, J., MACDONALD, M. E., LESSMANN, V., HUMBERT, S. & SAUDOU, F. 2004. Huntingtin controls neurotrophic support and survival of neurons by enhancing BDNF vesicular transport along microtubules. *Cell,* 118**,** 127-38.

GIBBONS, I. R. 1981. Cilia and flagella of eukaryotes. *J Cell Biol,* 91**,** 107s-124s.

GILL, S. R., SCHROER, T. A., SZILAK, I., STEUER, E. R., SHEETZ, M. P. & CLEVELAND, D. W. 1991. Dynactin, a conserved, ubiquitously expressed component of an activator of vesicle motility mediated by cytoplasmic dynein. *J Cell Biol,* 115**,** 1639-50.

GINDHART, J. G., CHEN, J., FAULKNER, M., GANDHI, R., DOERNER, K., WISNIEWSKI, T. & NANDLESTADT, A. 2003. The kinesin-associated protein UNC-76 is required for axonal transport in the Drosophila nervous system. *Mol Biol Cell,* 14**,** 3356-65.

GLATER, E. E., MEGEATH, L. J., STOWERS, R. S. & SCHWARZ, T. L. 2006. Axonal transport of mitochondria requires milton to recruit kinesin heavy chain and is light chain independent. *J Cell Biol,* 173**,** 545-57.

GROSS, S. P. 2004. Hither and yon: a review of bi-directional microtubule-based transport. *Phys Biol,* 1**,** R1-11.

GUILLAUD, L., WONG, R. & HIROKAWA, N. 2008. Disruption of KIF17-Mint1 interaction by CaMKII-dependent phosphorylation: a molecular model of kinesin-cargo release. *Nat Cell Biol,* 10**,** 19-29.

GUPTA, M. L., JR., CARVALHO, P., ROOF, D. M. & PELLMAN, D. 2006. Plus end-specific depolymerase activity of Kip3, a kinesin-8 protein, explains its role in positioning the yeast mitotic spindle. *Nat Cell Biol,* 8**,** 913-23.

GYOEVA, F. K., BYBIKOVA, E. M. & MININ, A. A. 2000. An isoform of kinesin light chain specific for the Golgi complex. *J Cell Sci,* 113 (Pt 11)**,** 2047-54.

GYOEVA, F. K., SARKISOV, D. V., KHODJAKOV, A. L. & MININ, A. A. 2004. The tetrameric molecule of conventional kinesin contains identical light chains. *Biochemistry,* 43**,** 13525-31.

HACKNEY, D. D. 1988. Kinesin ATPase: rate-limiting ADP release. *Proc Natl Acad Sci U S A,* 85**,** 6314-8.

HACKNEY, D. D. 1995. Highly processive microtubule-stimulated ATP hydrolysis by dimeric kinesin head domains. *Nature,* 377**,** 448-50.

HACKNEY, D. D., LEVITT, J. D. & SUHAN, J. 1992. Kinesin undergoes a 9 S to 6 S conformational transition. *J Biol Chem,* 267**,** 8696-701.

HACKNEY, D. D. & STOCK, M. F. 2000. Kinesin's IAK tail domain inhibits initial microtubule-stimulated ADP release. *Nat Cell Biol,* 2**,** 257-60.

HAMMER, J. A., 3RD & SELLERS, J. R. 2012. Walking to work: roles for class V myosins as cargo transporters. *Nat Rev Mol Cell Biol,* 13**,** 13-26.

HAMMOND, J. W., CAI, D., BLASIUS, T. L., LI, Z., JIANG, Y., JIH, G. T., MEYHOFER, E. & VERHEY, K. J. 2009. Mammalian Kinesin-3 motors are dimeric in vivo and move by processive motility upon release of autoinhibition. *PLoS Biol,* 7**,** e72.

HAMMOND, J. W., HUANG, C. F., KAECH, S., JACOBSON, C., BANKER, G. & VERHEY, K. J. 2010. Posttranslational modifications of tubulin and the polarized transport of kinesin-1 in neurons. *Mol Biol Cell,* 21**,** 572-83.

HANCOCK, W. O. 2014. Bidirectional cargo transport: moving beyond tug of war. *Nat Rev Mol Cell Biol,* 15**,** 615-28.

HARRELL, J. M., MURPHY, P. J., MORISHIMA, Y., CHEN, H., MANSFIELD, J. F., GALIGNIANA, M. D. & PRATT, W. B. 2004. Evidence for glucocorticoid receptor transport on microtubules by dynein. *J Biol Chem,* 279**,** 54647-54.

HENDRICKS, A. G., HOLZBAUR, E. L. & GOLDMAN, Y. E. 2012. Force measurements on cargoes in living cells reveal collective dynamics of microtubule motors. *Proc Natl Acad Sci U S A,* 109**,** 18447-52.

HENDRICKS, A. G., PERLSON, E., ROSS, J. L., SCHROEDER, H. W., 3RD, TOKITO, M. & HOLZBAUR, E. L. 2010. Motor coordination via a tug-of-war mechanism drives bidirectional vesicle transport. *Curr Biol,* 20**,** 697-702.

HIROKAWA, N., NIWA, S. & TANAKA, Y. 2010. Molecular motors in neurons: transport mechanisms and roles in brain function, development, and disease. *Neuron,* 68**,** 610-38.

HIROKAWA, N., NODA, Y., TANAKA, Y. & NIWA, S. 2009. Kinesin superfamily motor proteins and intracellular transport. *Nat Rev Mol Cell Biol,* 10**,** 682-96.

HIROKAWA, N., PFISTER, K. K., YORIFUJI, H., WAGNER, M. C., BRADY, S. T. & BLOOM, G. S. 1989. Submolecular domains of bovine brain kinesin identified by electron microscopy and monoclonal antibody decoration. *Cell,* 56**,** 867-78.

HISANAGA, S., MUROFUSHI, H., OKUHARA, K., SATO, R., MASUDA, Y., SAKAI, H. & HIROKAWA, N. 1989. The molecular structure of adrenal medulla kinesin. *Cell Motil Cytoskeleton,* 12**,** 264-72.

HOFMANN, I. & MUNRO, S. 2006. An N-terminally acetylated Arf-like GTPase is localised to lysosomes and affects their motility. *J Cell Sci,* 119**,** 1494-503.

HOWARD, J., HUDSPETH, A. J. & VALE, R. D. 1989. Movement of microtubules by single kinesin molecules. *Nature,* 342**,** 154-8.

HUANG, J. D., BRADY, S. T., RICHARDS, B. W., STENOLEN, D., RESAU, J. H., COPELAND, N. G. & JENKINS, N. A. 1999. Direct interaction of microtubule- and actin-based transport motors. *Nature,* 397**,** 267-70.

HUNTER, A. W., CAPLOW, M., COY, D. L., HANCOCK, W. O., DIEZ, S., WORDEMAN, L. & HOWARD, J. 2003. The kinesin-related protein MCAK is a microtubule depolymerase that forms an ATP-hydrolyzing complex at microtubule ends. *Mol Cell,* 11**,** 445-57.

IKEGAMI, K., HEIER, R. L., TARUISHI, M., TAKAGI, H., MUKAI, M., SHIMMA, S., TAIRA, S., HATANAKA, K., MORONE, N., YAO, I., CAMPBELL, P. K., YUASA, S., JANKE, C., MACGREGOR, G. R. & SETOU, M. 2007. Loss of alpha-tubulin polyglutamylation in ROSA22 mice is associated with abnormal targeting of KIF1A and modulated synaptic function. *Proc Natl Acad Sci U S A,* 104**,** 3213-8.

IMANISHI, M., ENDRES, N. F., GENNERICH, A. & VALE, R. D. 2006. Autoinhibition regulates the motility of the C. elegans intraflagellar transport motor OSM-3. *J Cell Biol,* 174**,** 931-7.

IRETON, G. C. & STODDARD, B. L. 2004. Microseed matrix screening to improve crystals of yeast cytosine deaminase. *Acta Crystallogr D Biol Crystallogr,* 60**,** 601-5.

JORDENS, I., FERNANDEZ-BORJA, M., MARSMAN, M., DUSSELJEE, S., JANSSEN, L., CALAFAT, J., JANSSEN, H., WUBBOLTS, R. & NEEFJES, J. 2001. The Rab7 effector protein RILP controls lysosomal transport by inducing the recruitment of dynein-dynactin motors. *Curr Biol,* 11**,** 1680-5.

JUNCO, A., BHULLAR, B., TARNASKY, H. A. & VAN DER HOORN, F. A. 2001. Kinesin light-chain KLC3 expression in testis is restricted to spermatids. *Biol Reprod,* 64**,** 1320-30.

KAAN, H. Y., HACKNEY, D. D. & KOZIELSKI, F. 2011. The structure of the kinesin-1 motor-tail complex reveals the mechanism of autoinhibition. *Science,* 333**,** 883-5.

KAMAL, A., STOKIN, G. B., YANG, Z., XIA, C. H. & GOLDSTEIN, L. S. 2000. Axonal transport of amyloid precursor protein is mediated by direct binding to the kinesin light chain subunit of kinesin-I. *Neuron,* 28**,** 449-59.

KAMM, C., BOSTON, H., HEWETT, J., WILBUR, J., COREY, D. P., HANSON, P. I., RAMESH, V. & BREAKEFIELD, X. O. 2004. The early onset dystonia protein torsinA interacts with kinesin light chain 1. *J Biol Chem,* 279**,** 19882-92.

KANAI, Y., OKADA, Y., TANAKA, Y., HARADA, A., TERADA, S. & HIROKAWA, N. 2000. KIF5C, a novel neuronal kinesin enriched in motor neurons. *J Neurosci,* 20**,** 6374-84.

KARDON, J. R. & VALE, R. D. 2009. Regulators of the cytoplasmic dynein motor. *Nat Rev Mol Cell Biol,* 10**,** 854-65.

KASEDA, K., HIGUCHI, H. & HIROSE, K. 2003. Alternate fast and slow stepping of a heterodimeric kinesin molecule. *Nat Cell Biol,* 5**,** 1079-82.

KAWAGUCHI, K. 2008. Energetics of kinesin-1 stepping mechanism. *FEBS Lett,* 582**,** 3719-22.

KAWANO, T., ARASEKI, M., ARAKI, Y., KINJO, M., YAMAMOTO, T. & SUZUKI, T. 2012. A small peptide sequence is sufficient for initiating kinesin-1 activation through part of TPR region of KLC1. *Traffic,* 13**,** 834-48.

KELKAR, N., STANDEN, C. L. & DAVIS, R. J. 2005. Role of the JIP4 scaffold protein in the regulation of mitogen-activated protein kinase signaling pathways. *Mol Cell Biol,* 25**,** 2733-43.

KHODJAKOV, A., LIZUNOVA, E. M., MININ, A. A., KOONCE, M. P. & GYOEVA, F. K. 1998. A specific light chain of kinesin associates with mitochondria in cultured cells. *Mol Biol Cell,* 9**,** 333-43.

KIMURA, T., WATANABE, H., IWAMATSU, A. & KAIBUCHI, K. 2005. Tubulin and CRMP-2 complex is transported via Kinesin-1. *J Neurochem,* 93**,** 1371-82.

KING, S. J. & SCHROER, T. A. 2000. Dynactin increases the processivity of the cytoplasmic dynein motor. *Nat Cell Biol,* 2**,** 20-4.

KLUMPP, L. M., HOENGER, A. & GILBERT, S. P. 2004. Kinesin's second step. *Proc Natl Acad Sci U S A,* 101**,** 3444-9.

KODERA, N., YAMAMOTO, D., ISHIKAWA, R. & ANDO, T. 2010. Video imaging of walking myosin V by high-speed atomic force microscopy. *Nature,* 468**,** 72-6.

KOIDE, S. 2009. Engineering of recombinant crystallization chaperones. *Curr Opin Struct Biol,* 19**,** 449-57.

KON, T., NISHIURA, M., OHKURA, R., TOYOSHIMA, Y. Y. & SUTOH, K. 2004. Distinct functions of nucleotide-binding/hydrolysis sites in the four AAA modules of cytoplasmic dynein. *Biochemistry,* 43**,** 11266-74.

KONECNA, A., FRISCHKNECHT, R., KINTER, J., LUDWIG, A., STEUBLE, M., MESKENAITE, V., INDERMUHLE, M., ENGEL, M., CEN, C., MATEOS, J. M., STREIT, P. & SONDEREGGER, P. 2006. Calsyntenin-1 docks vesicular cargo to kinesin-1. *Mol Biol Cell,* 17**,** 3651-63.

KRENDEL, M. & MOOSEKER, M. S. 2005. Myosins: tails (and heads) of functional diversity. *Physiology (Bethesda),* 20**,** 239-51.

KULL, F. J., SABLIN, E. P., LAU, R., FLETTERICK, R. J. & VALE, R. D. 1996. Crystal structure of the kinesin motor domain reveals a structural similarity to myosin. *Nature,* 380**,** 550-5.

KUZNETSOV, S. A., VAISBERG, E. A., SHANINA, N. A., MAGRETOVA, N. N., CHERNYAK, V. Y. & GELFAND, V. I. 1988. The quaternary structure of bovine brain kinesin. *EMBO J,* 7**,** 353-6.

KWOK, B. H., KAPITEIN, L. C., KIM, J. H., PETERMAN, E. J., SCHMIDT, C. F. & KAPOOR, T. M. 2006. Allosteric inhibition of kinesin-5 modulates its processive directional motility. *Nat Chem Biol,* 2**,** 480-5.

LAPOUGE, K., SMITH, S. J., WALKER, P. A., GAMBLIN, S. J., SMERDON, S. J. & RITTINGER, K. 2000. Structure of the TPR domain of p67phox in complex with Rac.GTP. *Mol Cell,* 6**,** 899-907.

LARSON, S. B., DAY, J. S., CUDNEY, R. & MCPHERSON, A. 2007. A novel strategy for the crystallization of proteins: X-ray diffraction validation. *Acta Crystallogr D Biol Crystallogr,* 63**,** 310-8.

LAWRENCE, C. J., DAWE, R. K., CHRISTIE, K. R., CLEVELAND, D. W., DAWSON, S. C., ENDOW, S. A., GOLDSTEIN, L. S., GOODSON, H. V., HIROKAWA, N., HOWARD, J., MALMBERG, R. L., MCINTOSH, J. R., MIKI, H., MITCHISON, T. J., OKADA, Y., REDDY, A. S., SAXTON, W. M., SCHLIWA, M., SCHOLEY, J. M., VALE, R. D., WALCZAK, C. E. & WORDEMAN, L. 2004. A standardized kinesin nomenclature. *J Cell Biol,* 167**,** 19-22.

LAZAROV, O., MORFINI, G. A., LEE, E. B., FARAH, M. H., SZODORAI, A., DEBOER, S. R., KOLIATSOS, V. E., KINS, S., LEE, V. M., WONG, P. C., PRICE, D. L., BRADY, S. T. & SISODIA, S. S. 2005. Axonal transport, amyloid precursor protein, kinesin-1, and the processing apparatus: revisited. *J Neurosci,* 25**,** 2386-95.

LIGON, L. A., TOKITO, M., FINKLESTEIN, J. M., GROSSMAN, F. E. & HOLZBAUR, E. L. 2004. A direct interaction between cytoplasmic dynein and kinesin I may coordinate motor activity. *J Biol Chem,* 279**,** 19201-8.

LU, Q., LI, J. & ZHANG, M. 2014. Cargo recognition and cargo-mediated regulation of unconventional myosins. *Acc Chem Res,* 47**,** 3061-70.

LUDERS, J. & STEARNS, T. 2007. Microtubule-organizing centres: a re-evaluation. *Nat Rev Mol Cell Biol,* 8**,** 161-7.

LUFT, J. R. & DETITTA, G. T. 1999. A method to produce microseed stock for use in the crystallization of biological macromolecules. *Acta Crystallogr D Biol Crystallogr,* 55**,** 988-93.

MACASKILL, A. F., RINHOLM, J. E., TWELVETREES, A. E., ARANCIBIA-CARCAMO, I. L., MUIR, J., FRANSSON, A., ASPENSTROM, P., ATTWELL, D. & KITTLER, J. T. 2009. Miro1 is a calcium sensor for glutamate receptor-dependent localization of mitochondria at synapses. *Neuron,* 61**,** 541-55.

MACIOCE, P., GAMBARA, G., BERNASSOLA, M., GADDINI, L., TORRERI, P., MACCHIA, G., RAMONI, C., CECCARINI, M. & PETRUCCI, T. C. 2003. Beta-dystrobrevin interacts directly with kinesin heavy chain in brain. *J Cell Sci,* 116**,** 4847-56.

MALIGA, Z., JUNQUEIRA, M., TOYODA, Y., ETTINGER, A., MORA-BERMUDEZ, F., KLEMM, R. W., VASILJ, A., GUHR, E., IBARLUCEA-BENITEZ, I., POSER, I., BONIFACIO, E., HUTTNER, W. B., SHEVCHENKO, A. & HYMAN, A. A. 2013. A genomic toolkit to investigate kinesin and myosin motor function in cells. *Nat Cell Biol,* 15**,** 325-34.

MALLIK, R., CARTER, B. C., LEX, S. A., KING, S. J. & GROSS, S. P. 2004. Cytoplasmic dynein functions as a gear in response to load. *Nature,* 427**,** 649-52.

MANSER, C., GUILLOT, F., VAGNONI, A., DAVIES, J., LAU, K. F., MCLOUGHLIN, D. M., DE VOS, K. J. & MILLER, C. C. 2012. Lemur tyrosine kinase-2 signalling regulates kinesin-1 light chain-2 phosphorylation and binding of Smad2 cargo. *Oncogene,* 31**,** 2773-82.

MARTIN, M., IYADURAI, S. J., GASSMAN, A., GINDHART, J. G., JR., HAYS, T. S. & SAXTON, W. M. 1999. Cytoplasmic dynein, the dynactin complex, and kinesin are interdependent and essential for fast axonal transport. *Mol Biol Cell,* 10**,** 3717-28.

MAURER, S. P., FOURNIOL, F. J., BOHNER, G., MOORES, C. A. & SURREY, T. 2012. EBs recognize a nucleotide-dependent structural cap at growing microtubule ends. *Cell,* 149**,** 371-82.

MAVLYUTOV, T. A., CAI, Y. & FERREIRA, P. A. 2002. Identification of RanBP2- and kinesin-mediated transport pathways with restricted neuronal and subcellular localization. *Traffic,* 3**,** 630-40.

MAYR, M. I., HUMMER, S., BORMANN, J., GRUNER, T., ADIO, S., WOEHLKE, G. & MAYER, T. U. 2007. The human kinesin Kif18A is a motile microtubule depolymerase essential for chromosome congression. *Curr Biol,* 17**,** 488-98.

MCCART, A. E., MAHONY, D. & ROTHNAGEL, J. A. 2003. Alternatively spliced products of the human kinesin light chain 1 (KNS2) gene. *Traffic,* 4**,** 576-80.

MCDONALD, D., VODICKA, M. A., LUCERO, G., SVITKINA, T. M., BORISY, G. G., EMERMAN, M. & HOPE, T. J. 2002. Visualization of the intracellular behavior of HIV in living cells. *J Cell Biol,* 159**,** 441-52.

MCGUIRE, J. R., RONG, J., LI, S. H. & LI, X. J. 2006. Interaction of Huntingtin-associated protein-1 with kinesin light chain: implications in intracellular trafficking in neurons. *J Biol Chem,* 281**,** 3552-9.

MCPHERSON, A. 1990. Current approaches to macromolecular crystallization. *Eur J Biochem,* 189**,** 1-23.

MCPHERSON, A. & CUDNEY, B. 2006. Searching for silver bullets: an alternative strategy for crystallizing macromolecules. *J Struct Biol,* 156**,** 387-406.

MCPHERSON, A. & CUDNEY, B. 2014. Optimization of crystallization conditions for biological macromolecules. *Acta Crystallogr F Struct Biol Commun,* 70**,** 1445-67.

MEHTA, A. D., ROCK, R. S., RIEF, M., SPUDICH, J. A., MOOSEKER, M. S. & CHENEY, R. E. 1999. Myosin-V is a processive actin-based motor. *Nature,* 400**,** 590-3.

MILLECAMPS, S. & JULIEN, J. P. 2013. Axonal transport deficits and neurodegenerative diseases. *Nat Rev Neurosci,* 14**,** 161-76.

MILLER, P. M., FOLKMANN, A. W., MAIA, A. R., EFIMOVA, N., EFIMOV, A. & KAVERINA, I. 2009. Golgi-derived CLASP-dependent microtubules control Golgi organization and polarized trafficking in motile cells. *Nat Cell Biol,* 11**,** 1069-80.

MITCHISON, T. & KIRSCHNER, M. 1984. Dynamic instability of microtubule growth. *Nature,* 312**,** 237-42.

MOON, A. F., MUELLER, G. A., ZHONG, X. & PEDERSEN, L. C. 2010. A synergistic approach to protein crystallization: combination of a fixed-arm carrier with surface entropy reduction. *Protein Sci,* 19**,** 901-13.

MOORES, C. A., YU, M., GUO, J., BERAUD, C., SAKOWICZ, R. & MILLIGAN, R. A. 2002. A mechanism for microtubule depolymerization by KinI kinesins. *Mol Cell,* 9**,** 903-9.

MORFINI, G., PIGINO, G., SZEBENYI, G., YOU, Y., POLLEMA, S. & BRADY, S. T. 2006. JNK mediates pathogenic effects of polyglutamine-expanded androgen receptor on fast axonal transport. *Nat Neurosci,* 9**,** 907-16.

MORFINI, G., SZEBENYI, G., ELLURU, R., RATNER, N. & BRADY, S. T. 2002. Glycogen synthase kinase 3 phosphorylates kinesin light chains and negatively regulates kinesin-based motility. *EMBO J,* 21**,** 281-93.

MORIHARA, T., HAYASHI, N., YOKOKOJI, M., AKATSU, H., SILVERMAN, M. A., KIMURA, N., SATO, M., SAITO, Y., SUZUKI, T., YANAGIDA, K., KODAMA, T. S., TANAKA, T., OKOCHI, M., TAGAMI, S., KAZUI, H., KUDO, T., HASHIMOTO, R., ITOH, N., NISHITOMI, K., YAMAGUCHI-KABATA, Y., TSUNODA, T., TAKAMURA, H., KATAYAMA, T., KIMURA, R., KAMINO, K., HASHIZUME, Y. & TAKEDA, M. 2014. Transcriptome analysis of distinct mouse strains reveals kinesin light chain-1 splicing as an amyloid-beta accumulation modifier. *Proc Natl Acad Sci U S A,* 111**,** 2638-43.

MORITZ, M., BRAUNFELD, M. B., SEDAT, J. W., ALBERTS, B. & AGARD, D. A. 1995. Microtubule nucleation by gamma-tubulin-containing rings in the centrosome. *Nature,* 378**,** 638-40.

MULLER, M. J., KLUMPP, S. & LIPOWSKY, R. 2008. Tug-of-war as a cooperative mechanism for bidirectional cargo transport by molecular motors. *Proc Natl Acad Sci U S A,* 105**,** 4609-14.

NAVONE, F., NICLAS, J., HOM-BOOHER, N., SPARKS, L., BERNSTEIN, H. D., MCCAFFREY, G. & VALE, R. D. 1992. Cloning and expression of a human kinesin heavy chain gene: interaction of the COOH-terminal domain with cytoplasmic microtubules in transfected CV-1 cells. *J Cell Biol,* 117**,** 1263-75.

NEUWALD, A. F., ARAVIND, L., SPOUGE, J. L. & KOONIN, E. V. 1999. AAA+: A class of chaperone-like ATPases associated with the assembly, operation, and disassembly of protein complexes. *Genome Res,* 9**,** 27-43.

NEWTON, C. N., WAGENBACH, M., OVECHKINA, Y., WORDEMAN, L. & WILSON, L. 2004. MCAK, a Kin I kinesin, increases the catastrophe frequency of steady-state HeLa cell microtubules in an ATP-dependent manner in vitro. *FEBS Lett,* 572**,** 80-4.

NGUYEN, Q., LEE, C. M., LE, A. & REDDY, E. P. 2005. JLP associates with kinesin light chain 1 through a novel leucine zipper-like domain. *J Biol Chem,* 280**,** 30185-91.

ODRONITZ, F. & KOLLMAR, M. 2007. Drawing the tree of eukaryotic life based on the analysis of 2,269 manually annotated myosins from 328 species. *Genome Biol,* 8**,** R196.

ONG, L. L., LIM, A. P., ER, C. P., KUZNETSOV, S. A. & YU, H. 2000. Kinectin-kinesin binding domains and their effects on organelle motility. *J Biol Chem,* 275**,** 32854-60.

PALACIOS, I. M. & ST JOHNSTON, D. 2002. Kinesin light chain-independent function of the Kinesin heavy chain in cytoplasmic streaming and posterior localisation in the Drosophila oocyte. *Development,* 129**,** 5473-85.

PELLEGRINI, L., YU, D. S., LO, T., ANAND, S., LEE, M., BLUNDELL, T. L. & VENKITARAMAN, A. R. 2002. Insights into DNA recombination from the structure of a RAD51-BRCA2 complex. *Nature,* 420**,** 287-93.

PERNIGO, S., LAMPRECHT, A., STEINER, R. A. & DODDING, M. P. 2013. Structural basis for kinesin-1:cargo recognition. *Science,* 340**,** 356-9.

PFISTER, K. K., SHAH, P. R., HUMMERICH, H., RUSS, A., COTTON, J., ANNUAR, A. A., KING, S. M. & FISHER, E. M. 2006. Genetic analysis of the cytoplasmic dynein subunit families. *PLoS Genet,* 2**,** e1.

PILLING, A. D., HORIUCHI, D., LIVELY, C. M. & SAXTON, W. M. 2006. Kinesin-1 and Dynein are the primary motors for fast transport of mitochondria in Drosophila motor axons. *Mol Biol Cell,* 17**,** 2057-68.

PU, J., SCHINDLER, C., JIA, R., JARNIK, M., BACKLUND, P. & BONIFACINO, J. S. 2015. BORC, a Multisubunit Complex that Regulates Lysosome Positioning. *Dev Cell,* 33**,** 176-88.

PYLYPENKO, O., ATTANDA, W., GAUQUELIN, C., LAHMANI, M., COULIBALY, D., BARON, B., HOOS, S., TITUS, M. A., ENGLAND, P. & HOUDUSSE, A. M. 2013. Structural basis of myosin V Rab GTPase-dependent cargo recognition. *Proc Natl Acad Sci U S A,* 110**,** 20443-8.

RADTKE, K., KIENEKE, D., WOLFSTEIN, A., MICHAEL, K., STEFFEN, W., SCHOLZ, T., KARGER, A. & SODEIK, B. 2010. Plus- and minus-end directed microtubule motors bind simultaneously to herpes simplex virus capsids using different inner tegument structures. *PLoS Pathog,* 6**,** e1000991.

RAHMAN, A., FRIEDMAN, D. S. & GOLDSTEIN, L. S. 1998. Two kinesin light chain genes in mice. Identification and characterization of the encoded proteins. *J Biol Chem,* 273**,** 15395-403.

RAI, A. K., RAI, A., RAMAIYA, A. J., JHA, R. & MALLIK, R. 2013. Molecular adaptations allow dynein to generate large collective forces inside cells. *Cell,* 152**,** 172-82.

RANDALL, T. S., MOORES, C. & STEPHENSON, F. A. 2013. Delineation of the TRAK binding regions of the kinesin-1 motor proteins. *FEBS Lett,* 587**,** 3763-9.

RECK-PETERSON, S. L., YILDIZ, A., CARTER, A. P., GENNERICH, A., ZHANG, N. & VALE, R. D. 2006. Single-molecule analysis of dynein processivity and stepping behavior. *Cell,* 126**,** 335-48.

REED, N. A., CAI, D., BLASIUS, T. L., JIH, G. T., MEYHOFER, E., GAERTIG, J. & VERHEY, K. J. 2006. Microtubule acetylation promotes kinesin-1 binding and transport. *Curr Biol,* 16**,** 2166-72.

RICE, S., LIN, A. W., SAFER, D., HART, C. L., NABER, N., CARRAGHER, B. O., CAIN, S. M., PECHATNIKOVA, E., WILSON-KUBALEK, E. M., WHITTAKER, M., PATE, E., COOKE, R., TAYLOR, E. W., MILLIGAN, R. A. & VALE, R. D. 1999. A structural change in the kinesin motor protein that drives motility. *Nature,* 402**,** 778-84.

RIEF, M., ROCK, R. S., MEHTA, A. D., MOOSEKER, M. S., CHENEY, R. E. & SPUDICH, J. A. 2000. Myosin-V stepping kinetics: a molecular model for processivity. *Proc Natl Acad Sci U S A,* 97**,** 9482-6.

RIVERO, S., CARDENAS, J., BORNENS, M. & RIOS, R. M. 2009. Microtubule nucleation at the cis-side of the Golgi apparatus requires AKAP450 and GM130. *EMBO J,* 28**,** 1016-28.

ROBERTS, A. J., NUMATA, N., WALKER, M. L., KATO, Y. S., MALKOVA, B., KON, T., OHKURA, R., ARISAKA, F., KNIGHT, P. J., SUTOH, K. & BURGESS, S. A. 2009. AAA+ Ring and linker swing mechanism in the dynein motor. *Cell,* 136**,** 485-95.

ROSA-FERREIRA, C. & MUNRO, S. 2011. Arl8 and SKIP act together to link lysosomes to kinesin-1. *Dev Cell,* 21**,** 1171-8.

ROSENFELD, S. S., JEFFERSON, G. M. & KING, P. H. 2001. ATP reorients the neck linker of kinesin in two sequential steps. *J Biol Chem,* 276**,** 40167-74.

ROUX, K. J., CRISP, M. L., LIU, Q., KIM, D., KOZLOV, S., STEWART, C. L. & BURKE, B. 2009. Nesprin 4 is an outer nuclear membrane protein that

can induce kinesin-mediated cell polarization. *Proc Natl Acad Sci U S A,* 106**,** 2194-9.

RUPP, B. 2009. *Biomolecular Crystallography: Principles, Practice, and Application to Structural Biology*, Garland Science

SAOTOME, M., SAFIULINA, D., SZABADKAI, G., DAS, S., FRANSSON, A., ASPENSTROM, P., RIZZUTO, R. & HAJNOCZKY, G. 2008. Bidirectional Ca2+-dependent control of mitochondrial dynamics by the Miro GTPase. *Proc Natl Acad Sci U S A,* 105**,** 20728-33.

SATO-YOSHITAKE, R., YORIFUJI, H., INAGAKI, M. & HIROKAWA, N. 1992. The phosphorylation of kinesin regulates its binding to synaptic vesicles. *J Biol Chem,* 267**,** 23930-6.

SATPUTE-KRISHNAN, P., DEGIORGIS, J. A., CONLEY, M. P., JANG, M. & BEARER, E. L. 2006. A peptide zipcode sufficient for anterograde transport within amyloid precursor protein. *Proc Natl Acad Sci U S A,* 103**,** 16532-7.

SCHEINFELD, M. H., RONCARATI, R., VITO, P., LOPEZ, P. A., ABDALLAH, M. & D'ADAMIO, L. 2002. Jun NH2-terminal kinase (JNK) interacting protein 1 (JIP1) binds the cytoplasmic domain of the Alzheimer's beta-amyloid precursor protein (APP). *J Biol Chem,* 277**,** 3767-75.

SCHEUFLER, C., BRINKER, A., BOURENKOV, G., PEGORARO, S., MORODER, L., BARTUNIK, H., HARTL, F. U. & MOAREFI, I. 2000. Structure of TPR domain-peptide complexes: critical elements in the assembly of the Hsp70-Hsp90 multichaperone machine. *Cell,* 101**,** 199-210.

SCHIEF, W. R., CLARK, R. H., CREVENNA, A. H. & HOWARD, J. 2004. Inhibition of kinesin motility by ADP and phosphate supports a hand-over-hand mechanism. *Proc Natl Acad Sci U S A,* 101**,** 1183-8.

SCHMIDT, M. R., MARITZEN, T., KUKHTINA, V., HIGMAN, V. A., DOGLIO, L., BARAK, N. N., STRAUSS, H., OSCHKINAT, H., DOTTI, C. G. & HAUCKE, V. 2009. Regulation of endosomal membrane traffic by a Gadkin/AP-1/kinesin KIF5 complex. *Proc Natl Acad Sci U S A,* 106**,** 15344-9.

SCHNITZER, M. J. & BLOCK, S. M. 1997. Kinesin hydrolyses one ATP per 8-nm step. *Nature,* 388**,** 386-90.

SCHROER, T. A. 2004. Dynactin. *Annu Rev Cell Dev Biol,* 20**,** 759-79.

SCHROER, T. A., STEUER, E. R. & SHEETZ, M. P. 1989. Cytoplasmic dynein is a minus end-directed motor for membranous organelles. *Cell,* 56**,** 937-46.

SEEGER, M. A. & RICE, S. E. 2010. Microtubule-associated protein-like binding of the kinesin-1 tail to microtubules. *J Biol Chem,* 285**,** 8155-62.

SEEGER, M. A. & RICE, S. E. 2013. Intrinsic Disorder in the Kinesin Superfamily. *Biophys Rev,* 5.

SETOU, M., SEOG, D. H., TANAKA, Y., KANAI, Y., TAKEI, Y., KAWAGISHI, M. & HIROKAWA, N. 2002. Glutamate-receptor-interacting protein GRIP1 directly steers kinesin to dendrites. *Nature,* 417**,** 83-7.

SHAH, J. V., FLANAGAN, L. A., JANMEY, P. A. & LETERRIER, J. F. 2000. Bidirectional translocation of neurofilaments along microtubules mediated in part by dynein/dynactin. *Mol Biol Cell,* 11**,** 3495-508.

SINDELAR, C. V. & DOWNING, K. H. 2010. An atomic-level mechanism for activation of the kinesin molecular motors. *Proc Natl Acad Sci U S A,* 107**,** 4111-6.

SMITH, M. J., POZO, K., BRICKLEY, K. & STEPHENSON, F. A. 2006. Mapping the GRIF-1 binding domain of the kinesin, KIF5C, substantiates a role for GRIF-1 as an adaptor protein in the anterograde trafficking of cargoes. *J Biol Chem,* 281**,** 27216-28.

SOPPINA, V., RAI, A. K., RAMAIYA, A. J., BARAK, P. & MALLIK, R. 2009. Tug-of-war between dissimilar teams of microtubule motors regulates transport and fission of endosomes. *Proc Natl Acad Sci U S A,* 106**,** 19381-6.

STOCK, M. F., GUERRERO, J., COBB, B., EGGERS, C. T., HUANG, T. G., LI, X. & HACKNEY, D. D. 1999. Formation of the compact confomer of kinesin requires a COOH-terminal heavy chain domain and inhibits microtubule-stimulated ATPase activity. *J Biol Chem,* 274**,** 14617-23.

STOWERS, R. S., MEGEATH, L. J., GORSKA-ANDRZEJAK, J., MEINERTZHAGEN, I. A. & SCHWARZ, T. L. 2002. Axonal transport of mitochondria to synapses depends on milton, a novel Drosophila protein. *Neuron,* 36**,** 1063-77.

SUN, F., ZHU, C., DIXIT, R. & CAVALLI, V. 2011. Sunday Driver/JIP3 binds kinesin heavy chain directly and enhances its motility. *EMBO J,* 30**,** 3416-29.

SVOBODA, K., SCHMIDT, C. F., SCHNAPP, B. J. & BLOCK, S. M. 1993. Direct observation of kinesin stepping by optical trapping interferometry. *Nature,* 365**,** 721-7.

SWEENEY, H. L. & HOUDUSSE, A. 2010. Structural and functional insights into the Myosin motor mechanism. *Annu Rev Biophys,* 39**,** 539-57.

TALAPATRA, S. K., HARKER, B. & WELBURN, J. P. 2015. The C-terminal region of the motor protein MCAK controls its structure and activity through a conformational switch. *Elife,* 4.

TEIXIDO-TRAVESA, N., ROIG, J. & LUDERS, J. 2012. The where, when and how of microtubule nucleation - one ring to rule them all. *J Cell Sci,* 125**,** 4445-56.

TERASAKI, M., SCHMIDEK, A., GALBRAITH, J. A., GALLANT, P. E. & REESE, T. S. 1995. Transport of cytoskeletal elements in the squid giant axon. *Proc Natl Acad Sci U S A,* 92**,** 11500-3.

TOBA, S., WATANABE, T. M., YAMAGUCHI-OKIMOTO, L., TOYOSHIMA, Y. Y. & HIGUCHI, H. 2006. Overlapping hand-over-hand mechanism of single molecular motility of cytoplasmic dynein. *Proc Natl Acad Sci U S A,* 103**,** 5741-5.

TODA, H., MOCHIZUKI, H., FLORES, R., 3RD, JOSOWITZ, R., KRASIEVA, T. B., LAMORTE, V. J., SUZUKI, E., GINDHART, J. G., FURUKUBO-TOKUNAGA, K. & TOMODA, T. 2008. UNC-51/ATG1 kinase regulates axonal transport by mediating motor-cargo assembly. *Genes Dev,* 22**,** 3292-307.

TWELVETREES, A. E., YUEN, E. Y., ARANCIBIA-CARCAMO, I. L., MACASKILL, A. F., ROSTAING, P., LUMB, M. J., HUMBERT, S., TRILLER, A., SAUDOU, F., YAN, Z. & KITTLER, J. T. 2010. Delivery of GABAARs to synapses is mediated by HAP1-KIF5 and disrupted by mutant huntingtin. *Neuron,* 65**,** 53-65.

URNAVICIUS, L., ZHANG, K., DIAMANT, A. G., MOTZ, C., SCHLAGER, M. A., YU, M., PATEL, N. A., ROBINSON, C. V. & CARTER, A. P. 2015. The structure of the dynactin complex and its interaction with dynein. *Science,* 347**,** 1441-6.

VAGNONI, A., PERKINTON, M. S., GRAY, E. H., FRANCIS, P. T., NOBLE, W. & MILLER, C. C. 2012. Calsyntenin-1 mediates axonal transport of the amyloid precursor protein and regulates Abeta production. *Hum Mol Genet,* 21**,** 2845-54.

VAGNONI, A., RODRIGUEZ, L., MANSER, C., DE VOS, K. J. & MILLER, C. C. 2011. Phosphorylation of kinesin light chain 1 at serine 460 modulates binding and trafficking of calsyntenin-1. *J Cell Sci,* 124**,** 1032-42.

VALE, R. D. 2003. The molecular motor toolbox for intracellular transport. *Cell,* 112**,** 467-80.

VALE, R. D., REESE, T. S. & SHEETZ, M. P. 1985a. Identification of a novel force-generating protein, kinesin, involved in microtubule-based motility. *Cell,* 42**,** 39-50.

VALE, R. D., SCHNAPP, B. J., REESE, T. S. & SHEETZ, M. P. 1985b. Organelle, bead, and microtubule translocations promoted by soluble factors from the squid giant axon. *Cell,* 40**,** 559-69.

VARGA, V., HELENIUS, J., TANAKA, K., HYMAN, A. A., TANAKA, T. U. & HOWARD, J. 2006. Yeast kinesin-8 depolymerizes microtubules in a length-dependent manner. *Nat Cell Biol,* 8**,** 957-62.

VERHEY, K. J. & HAMMOND, J. W. 2009. Traffic control: regulation of kinesin motors. *Nat Rev Mol Cell Biol,* 10**,** 765-77.

VERHEY, K. J., LIZOTTE, D. L., ABRAMSON, T., BARENBOIM, L., SCHNAPP, B. J. & RAPOPORT, T. A. 1998. Light chain-dependent regulation of Kinesin's interaction with microtubules. *J Cell Biol,* 143**,** 1053-66.

VERHEY, K. J., MEYER, D., DEEHAN, R., BLENIS, J., SCHNAPP, B. J., RAPOPORT, T. A. & MARGOLIS, B. 2001. Cargo of kinesin identified as JIP scaffolding proteins and associated signaling molecules. *J Cell Biol,* 152**,** 959-70.

WALKER, M. L., BURGESS, S. A., SELLERS, J. R., WANG, F., HAMMER, J. A., 3RD, TRINICK, J. & KNIGHT, P. J. 2000. Two-headed binding of a processive myosin to F-actin. *Nature,* 405**,** 804-7.

WANG, X. & SCHWARZ, T. L. 2009. The mechanism of Ca2+ -dependent regulation of kinesin-mediated mitochondrial motility. *Cell,* 136**,** 163-74.

WANG, Z. & SHEETZ, M. P. 2000. The C-terminus of tubulin increases cytoplasmic dynein and kinesin processivity. *Biophys J,* 78**,** 1955-64.

WARSHAW, D. M., KENNEDY, G. G., WORK, S. S., KREMENTSOVA, E. B., BECK, S. & TRYBUS, K. M. 2005. Differential labeling of myosin V heads with quantum dots allows direct visualization of hand-over-hand processivity. *Biophys J,* 88**,** L30-2.

WELLS, A. L., LIN, A. W., CHEN, L. Q., SAFER, D., CAIN, S. M., HASSON, T., CARRAGHER, B. O., MILLIGAN, R. A. & SWEENEY, H. L. 1999. Myosin VI is an actin-based motor that moves backwards. *Nature,* 401**,** 505-8.

WILKIE, G. S. & DAVIS, I. 2001. Drosophila wingless and pair-rule transcripts localize apically by dynein-mediated transport of RNA particles. *Cell,* 105**,** 209-19.

WILSON, M. H. & HOLZBAUR, E. L. 2015. Nesprins anchor kinesin-1 motors to the nucleus to drive nuclear distribution in muscle cells. *Development,* 142**,** 218-28.

WONG, Y. C. & HOLZBAUR, E. L. 2014. The regulation of autophagosome dynamics by huntingtin and HAP1 is disrupted by expression of mutant huntingtin, leading to defective cargo degradation. *J Neurosci,* 34**,** 1293-305.

WONG, Y. L. & RICE, S. E. 2010. Kinesin's light chains inhibit the head- and microtubule-binding activity of its tail. *Proc Natl Acad Sci U S A,* 107**,** 11781-6.

WOZNIAK, M. J. & ALLAN, V. J. 2006. Cargo selection by specific kinesin light chain 1 isoforms. *EMBO J,* 25**,** 5457-68.

XIA, C., RAHMAN, A., YANG, Z. & GOLDSTEIN, L. S. 1998. Chromosomal localization reveals three kinesin heavy chain genes in mouse. *Genomics,* 52**,** 209-13.

XU, M., GU, Y., BARRY, J. & GU, C. 2010. Kinesin I transports tetramerized Kv3 channels through the axon initial segment via direct binding. *J Neurosci,* 30**,** 15987-6001.

YILDIZ, A., TOMISHIGE, M., VALE, R. D. & SELVIN, P. R. 2004. Kinesin walks hand-over-hand. *Science,* 303**,** 676-8.

YONEKURA, H., NOMURA, A., OZAWA, H., TATSU, Y., YUMOTO, N. & UYEDA, T. Q. 2006. Mechanism of tail-mediated inhibition of kinesin activities studied using synthetic peptides. *Biochem Biophys Res Commun,* 343**,** 420-7.

YOUNG, A., DICTENBERG, J. B., PUROHIT, A., TUFT, R. & DOXSEY, S. J. 2000. Cytoplasmic dynein-mediated assembly of pericentrin and gamma tubulin onto centrosomes. *Mol Biol Cell,* 11**,** 2047-56.

ZHAO, M., CASCIO, D., SAWAYA, M. R. & EISENBERG, D. 2011. Structures of segments of alpha-synuclein fused to maltose-binding protein suggest intermediate states during amyloid formation. *Protein Sci,* 20**,** 996-1004.

ZHENG, Y., WONG, M. L., ALBERTS, B. & MITCHISON, T. 1995. Nucleation of microtubule assembly by a gamma-tubulin-containing ring complex. *Nature,* 378**,** 578-83.

ZHU, H., LEE, H. Y., TONG, Y., HONG, B. S., KIM, K. P., SHEN, Y., LIM, K. J., MACKENZIE, F., TEMPEL, W. & PARK, H. W. 2012. Crystal structures of the tetratricopeptide repeat domains of kinesin light chains: insight into cargo recognition mechanisms. *PLoS One,* 7**,** e33943.

APPENDIX - PUBLICATIONS

7.6 Appendix 1: Structural Basis for kinesin-1:cargo recognition

PERNIGO, S., LAMPRECHT, A., STEINER, R. A. & DODDING, M. P. 2013. Structural basis for kinesin-1:cargo recognition. *Science,* 340**,** 356-9.

This paper derived predominantly from data described Chapter 3 provides the first structural description of a kinesin-cargo interface.

7.7 Appendix 2: The light chains of kinesin-1 are autoinhibited

YIP, Y. Y., PERNIGO, S., SANGER, A., XU, M., PARSONS, M., STEINER, R. A. & DODDING, M. P. 2016. The light chains of kinesin-1 are autoinhibited. Proc Natl Acad Sci U S A, 113, 2418-23.

This paper describes a novel intramolecular interaction within KLC2. I made the initial constructs used for this study before focusing on the SKIP-KHC interaction.

functional parallels to mismatch repair: After mismatch targeting through helix-correlated sliding and 3D steps, the ABC transporter family MutS enzymes use a two-step conformational change to adopt a sliding clamp configuration that displays accelerated, helix-uncorrelated 1D diffusion (*23*–*25*). This transition requires a sole ADP-to-ATP exchange, contrasting with EcoP15I that hydrolyzes many ATPs upon initiation (fig. S1). Together this shows that ATP-triggered sliding is a general function that has evolved in different ATPase kingdoms.

References and Notes

1. M. R. Singleton, M. S. Dillingham, D. B. Wigley, *Annu. Rev. Biochem.* **76**, 23 (2007).
2. J. Park *et al.*, *Cell* **142**, 544 (2010).
3. L. K. Stanley *et al.*, *EMBO J.* **25**, 2230 (2006).
4. Y. Zhang *et al.*, *Mol. Cell* **24**, 559 (2006).
5. D. T. Dryden, N. E. Murray, D. N. Rao, *Nucleic Acids Res.* **29**, 3728 (2001).
6. N. K. Raghavendra, S. Bheemanaik, D. N. Rao, *Front. Biosci.* **17**, 1094 (2012).
7. A. Meisel, T. A. Bickle, D. H. Krüger, C. Schroeder, *Nature* **355**, 467 (1992).
8. K. van Aelst *et al.*, *Proc. Natl. Acad. Sci. U.S.A.* **107**, 9123 (2010).
9. A. Meisel, P. Mackeldanz, T. A. Bickle, D. H. Krüger, C. Schroeder, *EMBO J.* **14**, 2958 (1995).
10. S. P. Ramanathan *et al.*, *Proc. Natl. Acad. Sci. U.S.A.* **106**, 1748 (2009).
11. N. Crampton *et al.*, *EMBO J.* **26**, 3815 (2007).
12. H. Brutzer, F. W. Schwarz, R. Seidel, *Nano Lett.* **12**, 473 (2012).
13. F. W. Schwarz, K. van Aelst, J. Tóth, R. Seidel, M. D. Szczelkun, *Nucleic Acids Res.* **39**, 8042 (2011).
14. F. Ruhnow, D. Zwicker, S. Diez, *Biophys. J.* **100**, 2820 (2011).
15. P. C. Blainey *et al.*, *Nat. Struct. Mol. Biol.* **16**, 1224 (2009).
16. Y. K. Gupta *et al.*, *J. Mol. Biol.* **420**, 261 (2012).
17. M. R. Webb, *Mol. Biosyst.* **3**, 249 (2007).
18. S. E. McClelland, D. T. F. Dryden, M. D. Szczelkun, *J. Mol. Biol.* **348**, 895 (2005).
19. A. Revyakin, C. Liu, R. H. Ebright, T. R. Strick, *Science* **314**, 1139 (2006).
20. J. Tóth, K. van Aelst, H. Salmons, M. D. Szczelkun, *Nucleic Acids Res.* **40**, 6752 (2012).
21. S. E. Halford, *Biochem. Soc. Trans.* **37**, 343 (2009).
22. B. A. Kelch, D. L. Makino, M. O'Donnell, J. Kuriyan, *Science* **334**, 1675 (2011).
23. W.-K. Cho *et al.*, *Structure* **20**, 1264 (2012).
24. J. Gorman *et al.*, *Proc. Natl. Acad. Sci. U.S.A.* **109**, E3074 (2012).
25. R. Qiu *et al.*, *EMBO J.* **31**, 2528 (2012).

Acknowledgments: This work was supported by The Wellcome Trust (084086), the Deutsche Forschungsgemeinschaft (DFG, SE 1646/1-1, SE 1646/7-1), a starting grant of the European Research Council (261224), and the Dresden International Graduate School for Biomedicine and Bioengineering, funded by the DFG (to F.W.S.). We thank N. Savery and S. Halford for comments on the manuscript. The authors declare no conflict of interest.

Supplementary Materials

www.sciencemag.org/cgi/content/full/340/6130/353/DC1
Materials and Methods
Supplementary Text
Figs. S1 to S12
References (*26*–*49*)

Movie S1

4 October 2012; accepted 22 February 2013
10.1126/science.1231122

Structural Basis for Kinesin-1:Cargo Recognition

Stefano Pernigo,* Anneri Lamprecht,* Roberto A. Steiner,† Mark P. Dodding†

Kinesin-mediated cargo transport is required for many cellular functions and plays a key role in pathological processes. Structural information on how kinesins recognize their cargoes is required for a molecular understanding of this fundamental and ubiquitous process. Here, we present the crystal structure of the tetratricopeptide repeat domain of kinesin light chain 2 in complex with a cargo peptide harboring a "tryptophan-acidic" motif derived from SKIP (SifA-kinesin interacting protein), a critical host determinant in *Salmonella* pathogenesis and a regulator of lysosomal positioning. Structural data together with biophysical, biochemical, and cellular assays allow us to propose a framework for intracellular transport based on the binding by kinesin-1 of W-acidic cargo motifs through a combination of electrostatic interactions and sequence-specific elements, providing direct molecular evidence of the mechanisms for kinesin-1:cargo recognition.

The plus-end–directed motor kinesin-1 plays a critical role in the intracellular transport of diverse protein, ribonuclear protein complexes, and membrane compartments on microtubules (*1*). Its functions are also usurped by bacteria and viruses to aid in their replication (*2*, *3*). Kinesin-1 can perform this diverse range of functions by virtue of its ability to interact with many different cargo proteins (*4*). Diversity of cargo recognition is accomplished largely through the kinesin light chains (KLCs), which harbour a tetratricopeptide repeat (TPR) domain, a versatile protein interaction platform (*5*, *6*). The KLC^{TPR} domain can recognize short peptide stretches within relatively disordered regions of its targets. These peptides are characterized by a tryptophan residue flanked by acidic residues (such as EWD) and are found in a growing list of KLC-binding proteins (*7*–*16*). [Single-letter abbreviations for the amino acid residues are as follows: A, Ala; C, Cys; D, Asp; E, Glu; F, Phe; G, Gly; H, His; I, Ile; K, Lys; L, Leu; M, Met; N, Asn; P, Pro; Q, Gln; R, Arg; S, Ser; T, Thr; V, Val; W, Trp; and Y, Tyr. In the mutants, other amino acids were substituted at certain locations; for example, R251D indicates that arginine at position 251 was replaced by aspartic acid.] Although W-acidic motifs often occur in pairs, single motifs are also functional and can support microtubule-based transport even when explanted from their host protein (*7*, *12*, *17*).

We set out to solve the structure of a KLC^{TPR} domain bound to a cargo W-acidic motif. We focused our attention on the SifA-kinesin interacting protein (SKIP) cargo for its importance in *Salmonella* pathogenesis. SKIP contains a pair of W-acidic motifs centered at amino acid positions 207 and 208 (WD) and 236 and 237 (WE) that fall within the N-terminal kinesin-1 binding region (residues 1 to 310) (Fig. 1A) (*3*, *7*, *13*). To assess the relative importance of the SKIP W-acidic motifs for KLC binding, we cotransfected HeLa cells with wild-type and WD/WE mutant constructs expressing green fluorescent protein (GFP)–SKIP(1-310) and hemagglutinin (HA)–KLC2 (Fig. 1B).

Disruption of the WD motif reduced GFP-SKIP interaction with HA-KLC2, whereas abrogation of the WE motif had no obvious effects. A double mutant with both motifs disrupted displayed HA-KLC2 binding similar to the single WD mutant. Thus, the WE motif has a very low affinity for KLC2. Indeed, a 10-amino-acid-long peptide centered on the WD motif (SKIP^{WD}) (Fig. 1A) bound to KLC2^{TPR} with a dissociation constant (K_d) of 24 μM, whereas the affinity of the equivalent SKIP^{WE} peptide was above 110 μM (Fig. 1C). The presence of both motifs improves the affinity for KLC2^{TPR} because a 40-amino-acid-long peptide SKIP^{WDWE} that encompasses the W-acid pair sequence bound with an apparent affinity higher than that of the single SKIP^{WD} motif (K_d = 4.9 μM). Binding affinity measurements at varying NaCl concentrations showed that electrostatic interactions play an important role in the recognition process (fig. S1).

For structural studies, we focused on the SKIP^{WD} motif, and to facilitate the crystallization process, we engineered a chimeric construct in which the SKIP^{WD} peptide was fused N-terminal to KLC2^{TPR} via a flexible $(TGS)_4$ linker (*18*). Crystals of SKIP^{WD}-KLC2^{TPR} were grown by using vapor diffusion techniques and diffracted at 2.9 Å by using synchrotron radiation. The final model of the cargo complex is characterized by R and R_{free} values of 20.3 and 24.5%, respectively (table S1). KLC2^{TPR} consists of six TPR repeats (TPR1 to TPR6), each contributed by a classical helix-turn-helix structural motif arranged in a right-handed super-helical conformation, with a non-TPR helix

Randall Division of Cell and Molecular Biophysics, King's College London, London SE1 1UL, UK.

*These authors contributed equally to this work.
†Corresponding authors. E-mail: mark.dodding@kcl.ac.uk (M.P.D.); roberto.steiner@kcl.ac.uk (R.A.S.)

positioned between TPR5 and TPR6 (*14*). The structure of SKIP^{WD}-KLC2^{TPR} revealed the cargo peptide bound in an extended conformation at the N-terminal portion of the KLC2^{TPR} concave surface, with a direction parallel to the external helix of the repeat (Fig. 2, A and B, and fig. S2). Although our construct includes the external helix of TPR1, this region, as well as other flexible stretches, could not be unambiguously interpreted in the electron density. Thus, KLC2^{TPR} starts from TPR2 in our model.

A comparison between cargo-free KLC2^{TPR} (3CEQ) and cargo-bound KLC2^{TPR} revealed structural differences considered to arise from a rigid jaw movement of the N-terminal TPR2-3 region, which closes upon cargo recognition engendering the binding surface and pockets for the SKIP^{WD} peptide. (Fig. 2B and fig. S3). An analysis performed by using the Protein Interfaces, Surfaces and Assemblies (PISA) algorithm (*19*) indicates that all residues of the SKIP^{WD} peptide are involved in formation of the complex, which is stabilized by residues from TPR2-TPR3 and the internal helix of TPR4 (Fig. 2C). This concave groove surface displays a positive electrostatic charge ideally poised to complement the negatively charged W-acidic cargo motifs (Fig. 2C and fig. S4). Overall, the interface area of the SKIP^{WD}-KLC2^{TPR} complex is ~770 Å^2, stabilized by a mixture of H-bonds, salt bridges, and hydrophobic interactions (Fig. 3A).

The W residue central to the motif is generally flanked by amino acids bearing a carboxylate side chain. SKIP^{W207} (position 0, *p*0) is buried within a leucine-rich pocket positioned roughly in the middle along the TPR length and contributed by side chains from TPR2 (L248, R251, and L263) and TPR3 (N287, L290, and L291). In particular, the side-chain of N287 is in a conformation so that it serves the dual purpose of stabilizing SKIP^{W207} indole group by lining one side of the pocket while engaging at the same time in hydrogen bonds with the main chain amide and carbonyl oxygen of the residue at *p*+1. The latter position is almost invariably occupied by a glutamic or aspartic acid residue (*7*). The carboxylate side-chain of SKIP^{D208} points in the opposite direction to that of SKIP^{W207}, engaging in a network of salt bridges and H-bonds with the positively charged R312 and K325 side chains of α3E and α4I, respectively. An acidic side chain at position *p*-1 (SKIP^{E206}) of the motif is also very conserved in other W-acidic motifs. Like SKIP^{D208}, the carboxylate side-chain of SKIP^{E206} faces the TPR3-TPR4 side of the KLC2^{TPR} recognition groove, where it is stabilized by an ionic interaction with K325. Position *p*-2 of SKIP^{WD} features a leucine residue (SKIP^{L205}). The hydrophobic side chain of SKIP^{L205} is deeply buried in a hydrophobic pocket formed by residues from TPR3 and TPR4. The side chain of N329 plays a similar dual role as that of N287. Although lining the SKIP^{L205} pocket, it also H-bonds with the main chain at position *p*-1. Together, N287 and N329 act like a clamp on opposite sides of SKIP^{WD}, providing 4 of the 10 hydrogen bonds that stabilize the complex. Residues at positions *p*-(3,4) are less important for complex stability consistent with their general lack of sequence conservation amongst W-acidic motif cargo (*7*). The C-terminal stretch of SKIP^{WD} encompassing *p*+(2,3,4,5)

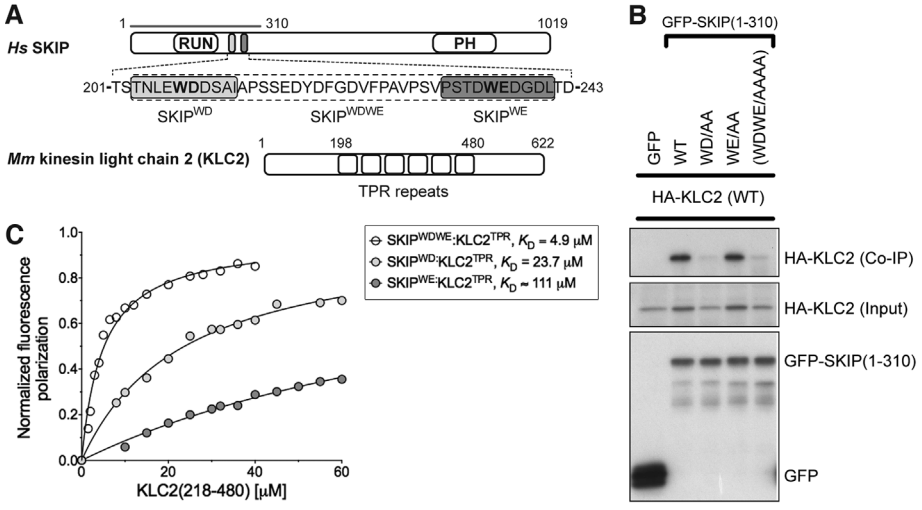

Fig. 1. Binding of SKIP to KLC2. (A) Scheme of SKIP and KLC2. The two W-acidic motifs and KLC2 TPR repeats are highlighted. **(B)** Coimmunoprecipitation shows that alanine replacement in the first W-acidic motif (WD) abrogates SKIP:KLC2 binding, whereas the same substitution in the second motif (WE) has virtually no effect. **(C)** Fluorescence polarization measurements confirm that the first SKIP W-acidic motif (SKIP^{WD}) has a higher affinity for the TPR domain of KLC2 than that of the second one (SKIP^{WE}). A peptide encompassing both motifs (SKIP^{WDWE}) binds with higher affinity than the best single motif. K_d values reported here were calculated at 150 mM NaCl. Binding affinity values at varying ionic strength values are given in fig. S1.

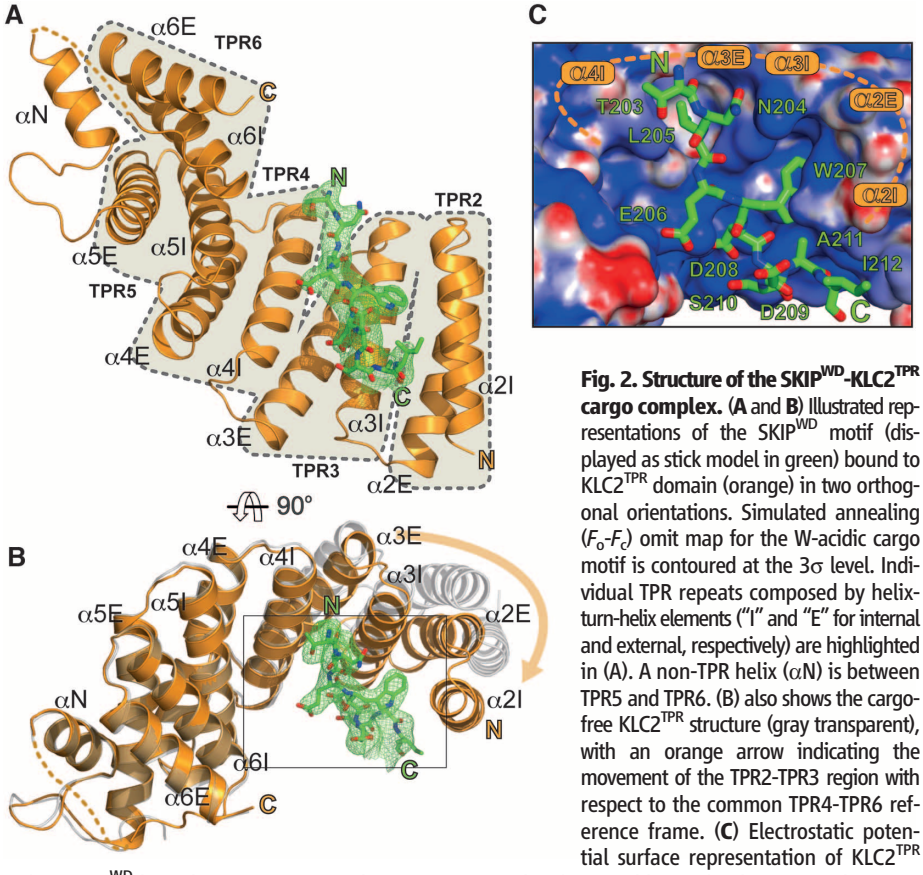

Fig. 2. Structure of the SKIP^{WD}-KLC2^{TPR} cargo complex. (A and **B)** Illustrated representations of the SKIP^{WD} motif (displayed as stick model in green) bound to KLC2^{TPR} domain (orange) in two orthogonal orientations. Simulated annealing (F_o-F_c) omit map for the W-acidic cargo motif is contoured at the 3σ level. Individual TPR repeats composed by helix-turn-helix elements ("I" and "E" for internal and external, respectively) are highlighted in (A). A non-TPR helix (αN) is between TPR5 and TPR6. (B) also shows the cargo-free KLC2^{TPR} structure (gray transparent), with an orange arrow indicating the movement of the TPR2-TPR3 region with respect to the common TPR4-TPR6 reference frame. **(C)** Electrostatic potential surface representation of KLC2^{TPR} with its SKIP^{WD}-bound cargo. Positive and negative potential is shown in blue and red, respectively. Cargo recognition is achieved by a combination of charge complementarity and sequence specificity.

is observed in a more compact, turn-like conformation, with SKIP^{D209,S210} at *p*+(2,3) making very minor contacts with the groove. As for the N-terminal peripheral region of SKIP^{WD}, the exact nature of the amino acids at *p*+(4,5) does not seem critical for complex stability. Alternative side chains can be positioned at this topological position, possibly involving a rearrangement of the main chain.

To investigate the effect of amino acid replacements within the KLC2^{TPR} region on the interaction with SKIP, we used immunoprecipitation as described above. All amino acid substitutions tested resulted in abrogation or near-abrogation of complex formation between KLC2 and SKIP (Fig. 3, B and C). The importance of electrostatic interactions in cargo recognition is underscored by charge-reversal mutations (Fig. 3, B and C). When coexpressed in cells, SKIP and its small guanosine triphosphatase–binding partner Arl8 associate strongly with lysosomes and promote their trafficking to the cell periphery. GFP-KLC2 associates with the same lysosomes (Fig. 3D and fig. S5) (*13*). This is essentially abolished by KLC2 mutations (R251D, N287L, and R312E) (Fig. 3D and fig. S5). The same mutations strongly inhibited the binding of KLC2^{TPR} to the WD motif peptide (Fig. 3C). We conclude that optimal SKIP:KLC2 stability critically depends on a very conserved cargo recognition-interaction groove. We extended our analysis to the well-characterized Calsyntenin-1 (CSTN-1) cargo, which also exhibits two W-acidic motifs (*9*, *11*, *12*). Differently from SKIP, both CSTN-1 motifs bound to KLC2^{TPR} with similar affinity (fig. S6). However, the mutations in the KLC2-binding groove that disrupted SKIP^{WD} binding also abrogated recognition of CSTN-1 (fig. S6). A sequence alignment shows total conservation of the KLC^{TPR} residues interacting with the cargo across the kinesin light chain family (fig. S7). Thus, the concave groove within the TPR domain where the SKIP^{WD} peptide binds is likely to be the primary site of interaction for W-acidic cargo motifs in general. However, we cannot exclude that secondary sites also exist.

In the context of intracellular transport in which kinesin-1 functions as a tetramer containing two KLCs held together by a coiled-coil region and both SKIP motifs contribute to transport (*7*, *13*), it is tempting to speculate that both chains can contribute to the binding of the W-acidic cargo pair. For SKIP, the higher-affinity WD motif would direct the first binding event to one of the KLC^{TPR}, with avidity effect promoting the association of the WE motif to the other KLC (*20*, *21*). It will be important to determine this

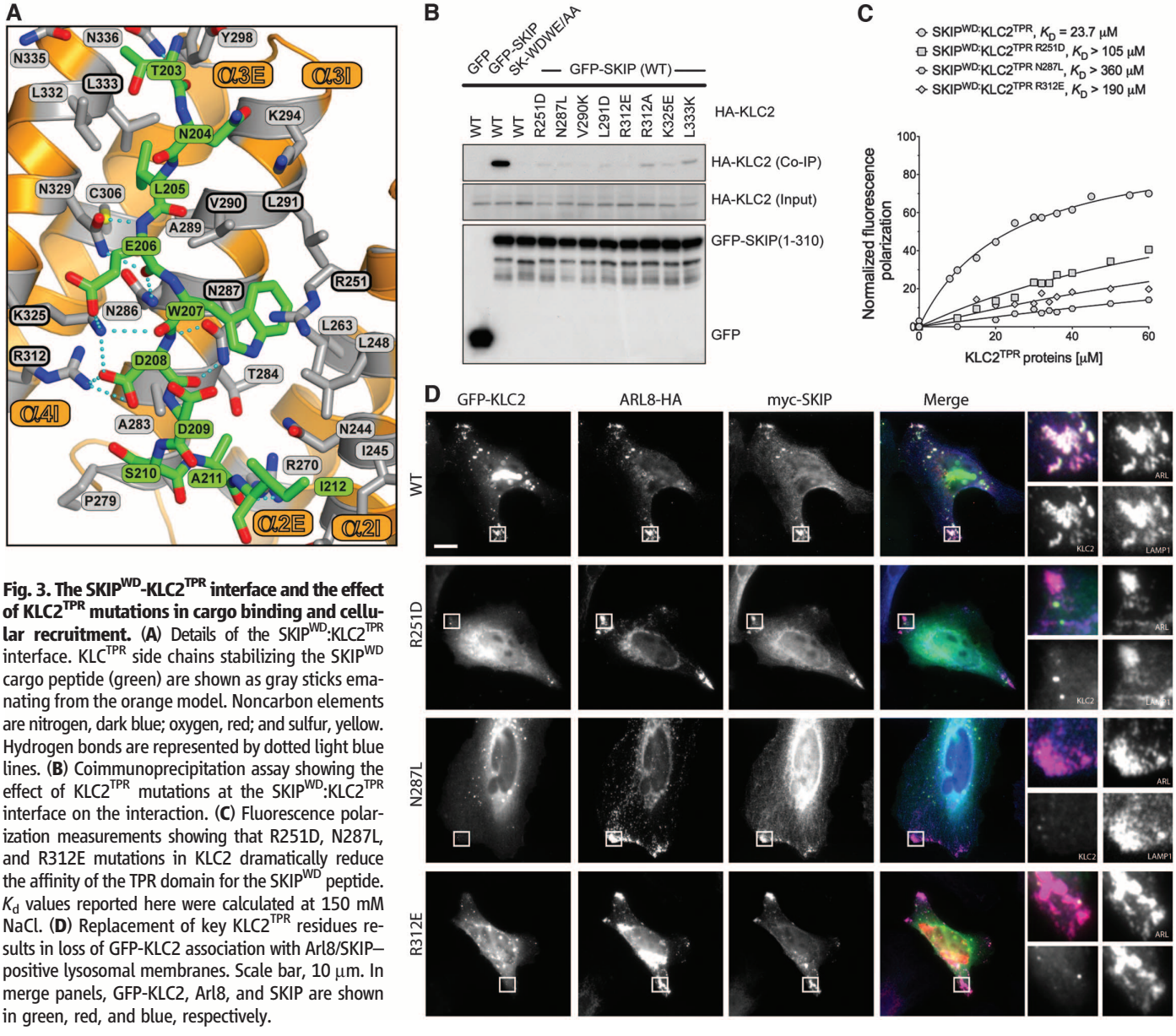

Fig. 3. The SKIP^{WD}-KLC2^{TPR} interface and the effect of KLC2^{TPR} mutations in cargo binding and cellular recruitment. (**A**) Details of the SKIP^{WD}:KLC2^{TPR} interface. KLC^{TPR} side chains stabilizing the SKIP^{WD} cargo peptide (green) are shown as gray sticks emanating from the orange model. Noncarbon elements are nitrogen, dark blue; oxygen, red; and sulfur, yellow. Hydrogen bonds are represented by dotted light blue lines. (**B**) Coimmunoprecipitation assay showing the effect of KLC2^{TPR} mutations at the SKIP^{WD}:KLC2^{TPR} interface on the interaction. (**C**) Fluorescence polarization measurements showing that R251D, N287L, and R312E mutations in KLC2 dramatically reduce the affinity of the TPR domain for the SKIP^{WD} peptide. K_d values reported here were calculated at 150 mM NaCl. (**D**) Replacement of key KLC2^{TPR} residues results in loss of GFP-KLC2 association with Arl8/SKIP–positive lysosomal membranes. Scale bar, 10 μm. In merge panels, GFP-KLC2, Arl8, and SKIP are shown in green, red, and blue, respectively.

relationship to the kinesin-1 tetramer and examine the importance of cargo-induced TPR conformational change in motor activation.

References and Notes

1. N. Hirokawa, Y. Noda, Y. Tanaka, S. Niwa, *Nat. Rev. Mol. Cell Biol.* **10**, 682 (2009).
2. M. P. Dodding, M. Way, *EMBO J.* **30**, 3527 (2011).
3. E. Boucrot, T. Henry, J. P. Borg, J. P. Gorvel, S. Méresse, *Science* **308**, 1174 (2005).
4. J. G. Gindhart, *Brief. Funct. Genomics Proteomics* **5**, 74 (2006).
5. L. D. D'Andrea, L. Regan, *Trends Biochem. Sci.* **28**, 655 (2003).
6. J. W. Hammond, K. Griffin, G. T. Jih, J. Stuckey, K. J. Verhey, *Traffic* **9**, 725 (2008).
7. M. P. Dodding, R. Mitter, A. C. Humphries, M. Way, *EMBO J.* **30**, 4523 (2011).
8. T. Aoyama *et al.*, *J. Cell Sci.* **122**, 4177 (2009).
9. A. Konecna *et al.*, *Mol. Biol. Cell* **17**, 3651 (2006).
10. M. R. Schmidt *et al.*, *Proc. Natl. Acad. Sci. U.S.A.* **106**, 15344 (2009).
11. Y. Araki *et al.*, *EMBO J.* **26**, 1475 (2007).
12. T. Kawano *et al.*, *Traffic* **13**, 834 (2012).
13. C. Rosa-Ferreira, S. Munro, *Dev. Cell* **21**, 1171 (2011).
14. H. Zhu *et al.*, *PLoS ONE* **7**, e33943 (2012).
15. J. R. McGuire, J. Rong, S. H. Li, X. J. Li, *J. Biol. Chem.* **281**, 3552 (2006).
16. L. A. Ligon, M. Tokito, J. M. Finklestein, F. E. Grossman, E. L. Holzbaur, *J. Biol. Chem.* **279**, 19201 (2004).
17. G. W. Morgan *et al.*, *PLoS Pathog.* **6**, e1000785 (2010).
18. L. Pellegrini *et al.*, *Nature* **420**, 287 (2002).
19. E. Krissinel, K. Henrick, *J. Mol. Biol.* **372**, 774 (2007).
20. L. Radnai *et al.*, *J. Biol. Chem.* **285**, 38649 (2010).
21. E. T. Mack *et al.*, *J. Am. Chem. Soc.* **134**, 333 (2012).

Acknowledgments: Scientists of I24 beamline (Diamond Light Source, Didcot, UK) are gratefully acknowledged for their support during data collection. ARL8b-HA and myc-SKIP were a kind gift from S. Munro, (Laboratory of Molecular Biology–Medical Research Council, Cambridge). We thank T. Blundell and R. Nookala (University of Cambridge) for useful discussions. Coordinates and structure factor files for have been deposited in the Protein Data Bank under accession number 3ZFW. The authors declare no competing financial interests. M.P.D and A.L. are supported by a Wellcome Trust Research Career Development Fellowship to M.P.D. and a London Law Trust Medal Fellowship to M.P.D. S.P. is supported by a British Heart Foundation grant awarded to R.A.S.

Supplementary Materials

www.sciencemag.org/cgi/content/full/science.1234264/DC1
Materials and Methods
Supplementary Text
Figs. S1 to S7
Table S1
References (*22*–*33*)

19 December 2012; accepted 7 March 2013
Published online 21 March 2013;
10.1126/science.1234264

Actin-Propelled Invasive Membrane Protrusions Promote Fusogenic Protein Engagement During Cell-Cell Fusion

Khurts Shilagardi, Shuo Li, Fengbao Luo, Faiz Marikar, Rui Duan, Peng Jin, Ji Hoon Kim, Katherine Murnen, Elizabeth H. Chen*

Cell-cell fusion is critical for the conception, development, and physiology of multicellular organisms. Although cellular fusogenic proteins and the actin cytoskeleton are implicated in cell-cell fusion, it remains unclear whether and how they coordinate to promote plasma membrane fusion. We reconstituted a high-efficiency, inducible cell fusion culture system in the normally nonfusing *Drosophila* S2R+ cells. Both fusogenic proteins and actin cytoskeletal rearrangements were necessary for cell fusion, and in combination they were sufficient to impart fusion competence. Localized actin polymerization triggered by specific cell-cell or cell-matrix adhesion molecules propelled invasive cell membrane protrusions, which in turn promoted fusogenic protein engagement and plasma membrane fusion. This de novo cell fusion culture system reveals a general role for actin-propelled invasive membrane protrusions in driving fusogenic protein engagement during cell-cell fusion.

Cell-cell fusion occurs in many biological processes such as fertilization, myogenesis, placenta formation, bone remodeling, and immune response (*1*–*3*). Transmembrane fusogenic proteins are implicated in the fusion of multiple cell types in *Caenorhabditis elegans* (*4*), whereas actin polymerization is implicated in the fusion of muscle cells in *Drosophila*, zebrafish, and mice (*5*–*7*). It remains unknown whether fusogenic proteins and the actin cytoskeleton coordinate during cell-cell fusion, and if so, how this is accomplished. We addressed these questions by reconstituting cell fusion de novo in the otherwise nonfusing S2R+ cells, a hemocyte-like cell line derived from *Drosophila* embryos (*8*).

Transfection of known components of *Drosophila* myoblast fusion, including cell adhesion molecules (*9*, *10*) and actin cytoskeletal regulators (*11*–*14*), failed to induce S2R+ cell fusion, despite causing extensive cell adhesion and F-actin enrichment at cell-cell contact sites (fig. S1, A to C). Expression of the *C. elegans* fusogenic protein Eff-1 (*15*, *16*) induced low-level S2R+ cell fusion (Fig. 1, A and F). Multinucleate syncytia were observed 24 hours after Eff-1 transfection, and by 72 hours after transfection, ~12% (12.1 ± 1.1%) of Eff-1–positive cells were in multinucleate syncytia, with each syncytium containing a median number of eight nuclei (Fig. 1, F and G). These Eff-1–induced multinucleate syncytia resulted from cell fusion (fig. S2, A to B′′′), and Eff-1 was required in both fusion partners (fig. S2C), similar to findings reported for moth Sf9 cells (*16*).

Because close membrane apposition is a prerequisite for membrane fusion, we asked whether Eff-1–induced fusion could be enhanced by coexpressing cell adhesion molecules. Dumbfounded (Duf) and Sticks and stones (Sns) are immunoglobulin (Ig) domain–containing transmembrane proteins that are required for *Drosophila* myoblast fusion (*9*, *10*) but are not normally expressed in S2R+ cells (fig. S1D). Exogenous Duf, but not Sns, promotes homophilic cell adhesion in cultured *Drosophila* cells (*17*–*19*), as does Echinoid (Ed), an Ig domain–containing transmembrane protein not implicated in myoblast fusion (*20*, *21*). Among the three proteins, only Sns enhanced Eff-1–mediated fusion (Fig. 1, B, C, D, and F), which suggests that membrane apposition mediated by cell adhesion per se is not sufficient to promote Eff-1–mediated fusion. Nearly 90% (86.3 ± 2.9%) of the Sns-Eff-1–coexpressing cells were in multinucleate syncytia (Fig. 1C), representing a factor of 7 increase over Eff-1–induced fusion (Fig. 1F). These large syncytia contained up to 220 nuclei, with a median number of 44 nuclei per cell (Fig. 1G). Live imaging confirmed that Sns-Eff-1–induced syncytial formation resulted from cell fusion (fig. S3, A and B, and movies S1 and S2). Besides Sns, overexpression of an α subunit (αPS2) of the cell-matrix adhesion molecule integrin (*22*), which has been implicated in multiple types of cell fusion events (*23*–*26*), enhanced Eff-1–mediated fusion by a factor of 5 (63.9 ± 4.3%) with a median number of 20 nuclei per cell (Fig. 1, E to G). The marked enhancement of Eff-1–mediated cell fusion by Sns and integrin, neither of which facilitated homophilic cell adhesion nor interacted with Eff-1 more strongly than did Duf (fig. S4), prompted us to examine the cellular mechanisms underlying their fusion-enhancing activity.

In *Drosophila*, Sns and Duf trigger distinct actin cytoskeletal changes during myoblast fusion. Sns organizes an F-actin–enriched invasive podosome-like structure (PLS) in the fusion competent myoblast (*27*, *28*), whereas Duf promotes the formation of a thin sheath of actin underlying the apposing founder cell membrane (*27*). Their differential activity in remodeling the actin cytoskeleton was recapitulated in S2R+ cells, as F-actin–enriched foci were observed at cell-cell contact sites marked by the accumulation of Eff-1 and the cell adhesion molecule in Sns-Eff-1–expressing cells (Fig. 1H and fig. S5A) but not in Duf-Eff-1–expressing cells (Fig. 1I and fig. S5B). Live imaging of Sns-Eff-1–expressing cells using green fluorescent protein (GFP) fused to the F-actin–

Department of Molecular Biology and Genetics, Johns Hopkins University School of Medicine, Baltimore, MD 21205, USA.
*Corresponding author. E-mail: echen@jhmi.edu

The light chains of kinesin-1 are autoinhibited

Yan Y. Yip[a,1], Stefano Pernigo[a,1], Anneri Sanger[a], Mengjia Xu[a], Maddy Parsons[a], Roberto A. Steiner[a,2], and Mark P. Dodding[a,2]

[a]Randall Division of Cell and Molecular Biophysics, King's College London, London SE1 1UL, United Kingdom

Edited by Thomas D. Pollard, Yale University, New Haven, CT, and approved January 21, 2016 (received for review October 21, 2015)

The light chains (KLCs) of the microtubule motor kinesin-1 bind cargoes and regulate its activity. Through their tetratricopeptide repeat domain (KLC^{TPR}), they can recognize short linear peptide motifs found in many cargo proteins characterized by a central tryptophan flanked by aspartic/glutamic acid residues (W-acidic). Using a fluorescence resonance energy transfer biosensor in combination with X-ray crystallographic, biochemical, and biophysical approaches, we describe how an intramolecular interaction between the KLC2^{TPR} domain and a conserved peptide motif within an unstructured region of the molecule, partly occludes the W-acidic binding site on the TPR domain. Cargo binding displaces this interaction, effecting a global conformational change in KLCs resulting in a more extended conformation. Thus, like the motor-bearing kinesin heavy chains, KLCs exist in a dynamic conformational state that is regulated by self-interaction and cargo binding. We propose a model by which, via this molecular switch, W-acidic cargo binding regulates the activity of the holoenzyme.

kinesin | KLC | TPR domain | microtubule motor | cytoskeleton

The heterotetrameric microtubule (MT) motor kinesin-1 (also known as conventional kinesin) has diverse roles in protein, ribonuclear protein, vesicular, and organelle transport by virtue of its ability to interact with many different cargoes (1, 2). It is also hijacked by pathogens during infection (3). Accumulating evidence suggests a key role for kinesin-1–dependent MT transport in several neurological disorders including Alzheimer's disease (4). Thus, determining the molecular basis for cargo recognition and regulation of kinesin-1 is important for understanding its role in normal cell function and disease states.

Kinesin-1 is composed of two heavy (KHCs) and two light chains (KLCs) that, in mammalian cells, are encoded by several closely related genes with distinct cell and tissue expression profiles (Kif5A-C and KLC1-4, respectively). The heavy chains have a MT-binding ATPase motor domain at their amino terminus followed by a neck coil and an extended series of coiled coils, separated by a hinge region(s), that results in heavy-chain dimerization (5). The carboxyl-terminal domain of the heavy chains is largely unstructured. The light chains associate with the heavy-chain coiled coils at the carboxyl-terminal portion of the molecule through a series of heptad repeats (6). A highly charged unstructured linker region connects this heavy-chain binding region to a tetratricopeptide repeat domain (KLC^{TPR}) formed of six helix-turn-helix TPR repeats (TPR1-6), followed by a C-terminal region that varies considerably between the different KLCs and splice variants.

In the absence of cargo binding, kinesin-1 exists in a folded, compact state that prevents unnecessary cycles of ATP hydrolysis. This is achieved via an intramolecular interaction in which the C-terminal isoleucine–alanine–lysine (IAK) motif (and flanking amino acids) of a single KHC tail binds at the N-terminal motor dimer interface and participates in a "double-lockdown" mechanism whereby it cross-links the motor domains preventing movement of the neck linker region that is required for ADP release (7–12). In the cargo-bound active state, tail-mediated inhibition is relieved resulting in a more elongated structure that is able to hydrolyze ATP and translocate along MTs (12–16). As well as binding to cargoes, the KLCs are thought to regulate KHC autoinhibition, although the molecular mechanism(s) that couple these two functions are unclear (17). Several studies suggest that KLCs reduce interaction with MTs and help to maintain the autoinhibited state in the absence of cargo (12, 13, 18), whereas in vitro biophysical studies have suggested that the presence of light chains reduces the affinity of the motor domains for the C-terminal autoinhibitory heavy-chain tail through both steric and electrostatic factors (19).

Vesicular cargoes interact via adaptor proteins that can bind to several sites on both KHCs and KLCs, and it is generally thought that these multiple contacts help to stabilize the active state and/or destabilize the inactive state and thus promote cargo-dependent transport (15, 17, 20, 21). It has emerged that diversity of light-chain cargo recognition is accomplished, in part, through TPR domain interaction with short linear peptide motifs (22–25). We have recently described how the TPR domain of KLC2 (KLC2^{TPR}) recognizes one class of these peptides that are characterized by a central tryptophan typically flanked by aspartic or glutamic acid residues (W-acidic). The X-ray structure of KLC2^{TPR} in complex with a W-acidic peptide of the lysosome adaptor SKIP (SKIP^{WD}) shows that these motifs interact with a concave positively charged groove at the KLC^{TPR} N terminus. Both sequence-specific and electrostatic elements contribute to peptide recognition, which is stabilized by residues from TPR2–TPR3 and the internal helix of TPR4 (23). Functional W-acidic motifs have been identified in a growing number of cargo adaptors, including the neuronal protein calsyntenin-1 (CSTN1) that plays a role in the axonal transport of amyloid precursor protein, as well as nesprin-2, gadkin, vaccinia virus A36R, and cayman ataxia protein (BNIP-H), where, in each case, they provide a crucial link between motor and cargo with diverse functions (16, 23, 24, 26–31). It is interesting to

Significance

Despite its importance for a host of cellular processes and contribution to neurological, viral, and bacterial disease, the molecular mechanisms underlying the regulation of the heterotetrameric motor kinesin-1 by its light chains and the binding of its cargo are not well understood. Here, we describe how a previously unnoticed intramolecular interaction between the light chain tetratricopeptide repeat domain (KLC2^{TPR}) and a highly conserved peptide motif within an unstructured region of the molecule occludes a key cargo binding site on the light-chain TPR domain. Cargo binding displaces this intramolecular interaction, effecting a global overall conformational change in KLCs that results in a more extended conformation. We propose a model describing how, via this molecular switch, cargo binding regulates the activity of the holoenzyme.

Author contributions: M.P., R.A.S., and M.P.D. designed research; Y.Y.Y., S.P., A.S., and M.X. performed research; Y.Y.Y., S.P., A.S., M.X., M.P., R.A.S., and M.P.D. analyzed data; and R.A.S. and M.P.D. wrote the paper.

The authors declare no conflict of interest.

This article is a PNAS Direct Submission.

Data deposition: The atomic coordinates and structure factors have been deposited in the Protein Data Bank, www.pdb.org (PDB ID code 5FJY).

[1]Y.Y.Y. and S.P. contributed equally to this work.

[2]To whom correspondence may be addressed. Email: mark.dodding@kcl.ac.uk or roberto.steiner@kcl.ac.uk.

This article contains supporting information online at www.pnas.org/lookup/suppl/doi:10.1073/pnas.1520817113/-/DCSupplemental.

note that W-acidic motifs share sequence similarity with the A (acidic) motif of several actin nucleation-promoting factors (NPFs) including WASP, N-WASP, and WAVE1 (32), and the mechanism of binding to KLC^{TPR} is somewhat similar to the interaction of the fission yeast WASP A motif on the Arp2/3 complex (33). Indeed, in the case of gadkin, there also appears to be functional overlap (32).

Here, we describe an intramolecular interaction between KLC^{TPR} and the unstructured region immediately N-terminal to it. This flexible linker features a highly conserved leucine–phenylalanine–proline motif flanked by acidic residues (LFP-acidic) that interacts with KLC^{TPR} partly occluding its W-acidic motif binding site. This autoinhibitory interaction is displaced by cargo binding, resulting in overall conformational changes within the light chains. Thus, paralleling the behavior of KHCs, kinesin-1 KLCs also exist in a dynamic conformational state that is regulated by self-interaction and cargo binding. We propose a model to explain how this previously unnoticed molecular switch may couple KLC^{TPR}–W-acidic peptide recognition to the regulation of kinesin-1 activity.

Results

The KLC Region N-Terminal to Its TPR Domain Features a Conserved LFP-Acidic Motif and Negatively Regulates W-Acidic Cargo Binding. Amino acid sequence alignment of all four KLCs from human and mouse as well as representative kinesin-1 light chains from several diverse species reveals that the heptad repeat region (that interacts with KHC via a predicted coiled coil; Fig. S1*A*) and the TPR domain (that binds cargoes) are highly conserved, whereas the intervening stretch of highly charged amino acids (F139–P195 in mouse KLC2) is considerably more divergent (Fig. 1 *A* and *B*). Within this region, we noticed, however, that a leucine–phenylalanine–proline (LFP) motif (residues 167–169 in mouse KLC2) is totally conserved (in red in Fig. 1*B*). This short motif that is followed by Asn/Ser and flanked by negatively charged Asp/Glu residues (in blue in Fig. 1*B*) is present in all KLCs. No function has been ascribed to this conserved LFP-acidic feature. Analyses using a panel of intrinsic-disorder prediction packages (PrDOS, Disopred, IUPred, DisEMBL) indicate that this protein region is likely unstructured (Fig. S1*B*).

To examine the role of the LFP-acidic motif in light-chain function, we performed GFP-TRAP immunoprecipitation experiments from HeLa cells with two independent W-acidic cargo proteins using full-length wild-type KLC2 or KLC2 where the LFP triplet was replaced by AAA. This revealed that disruption of this sequence enhances binding to both the N-terminal domain of SKIP (amino acids 1–310) and the cytoplasmic domain of CSTN1 (amino acids 879–971) by 36% and 78%, respectively (Fig. 1*C*). Consistently, the LFP/AAA replacement in KLC1 enhanced binding to CSTN1 by 72% (Fig. S1*B*). However, disruption of this motif did not affect binding to the non–W-acidic cargo JIP1, which mutagenesis data suggest binds to a distinct site on $KLC1^{TPR}$ (Fig. S1*D*) (22, 34). Given that the LFP motif is located N-terminal to the TPR domain, we reflected that this could imply a mechanism of cross talk between this linker region and the W-acidic binding site involving residues from TPR2-3 and the internal helix of TPR4 (23). We considered the possibility that this cross talk could be mediated by an intramolecular interaction.

To directly examine the contribution of this region to TPR domain cargo binding in vitro, we performed pull-down assays using purified GST-SKIP (1–310) or GST-CSTN1 (879–971). We compared binding to $KLC2^{TPR}$, $KLC2^{TPR}$ with a N-terminal extension to include the LFP-acidic motif (KLC2 161–480, $KLC2^{extTPR}$) or $KLC2^{TPR}$ fused N-terminally to a competitor W-acidic peptide from SKIP ($KLC2^{WacTPR}$) (Fig. 2*A*). For both SKIP and CSTN1, amino-terminal extension of the TPR domain up to residue 161, to include the LFP-acidic motif, inhibits binding to the W-acidic motif-containing cargoes in a manner comparable to inclusion of a direct competitor peptide attached by a flexible linker (Fig. 2 *B* and *C*). This strongly supports the

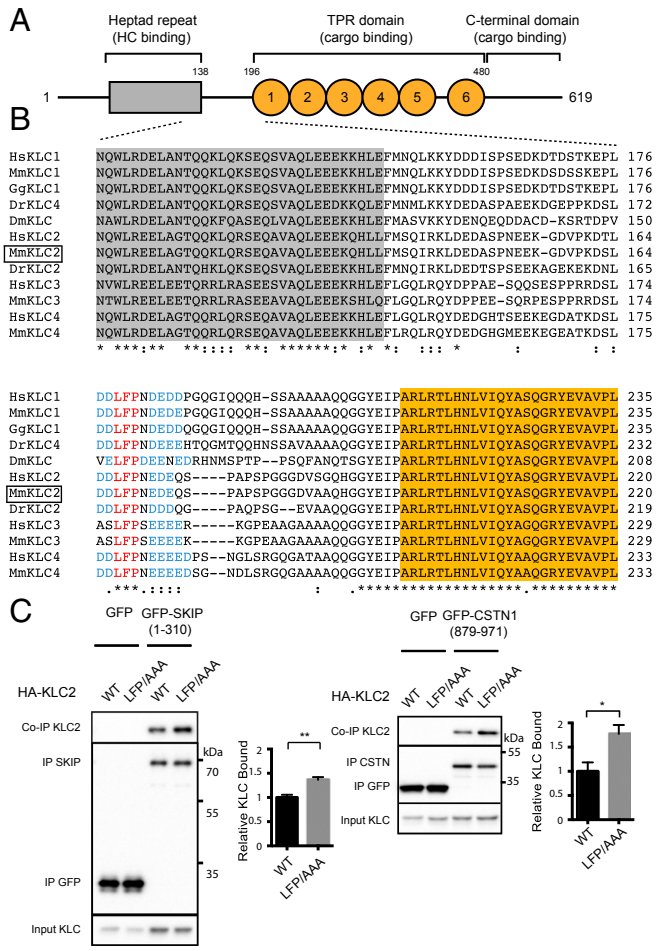

Fig. 1. Mutational disruption of a conserved leucine–phenylalanine–proline (LFP) motif in KLC2 enhances binding to W-acidic cargoes. (*A*) Schematic showing domain organization of KLC2 (numbering refers to mouse protein). The heptad repeat region (HR) that interacts with KHC is shown in gray, and the six TPR repeats comprising the TPR domain are represented by orange circles. (*B*) Multiple sequence alignment using Clustal W showing the region linking the HR and the first TPR repeat in KLCs 1–4 from human and mouse as well as representative fly (Dm), zebrafish (Dr), or chicken (Gg) homologs as annotated in the Homologene database. The highly conserved HR and TPR regions are highlighted in gray and orange, respectively. An asterisk (*) indicates a completely conserved residue, whereas a colon (:) indicates strong conservation of residue properties. A universally conserved LFP motif (red), located within the otherwise-divergent linker region is highlighted in red as well as flanking conserved acidic residues in (blue). (*C*) Western blot analysis of GFP-TRAP immunoprecipitation experiments from transfected HeLa cells showing enhanced binding between GFP-SKIP (1–310) (*Left*) or GFP-CSTN1 (879–971) (*Right*) to HA-KLC2 when the LFP triplet is replaced to AAA. Graphs show quantification of relative binding from three independent experiments. Error bars show SEM. $^{**}P < 0.01$, $^{*}P < 0.05$.

proposition that this linker region can compete with W-acidic cargo for a binding site on the TPR domain through an intramolecular interaction.

The KLC Region N-Terminal to Its TPR Domain Directly Interacts in an LFP Motif-Dependent Manner with the TPR Domain. Next, we used a biophysical assay to test whether the LFP-acidic motif can interact with purified KLC2 proteins. Fluorescence polarization (FP) measurements using a 14-aa N-terminally carboxytetramethylrhodamine (TAMRA)-conjugated peptide comprising the LFP motif and its flanking residues (LFP^{pept}, DSLDDLFPNEDEQS) showed that this sequence binds to $KLC2^{TPR}$ with a dissociation constant (K_D)

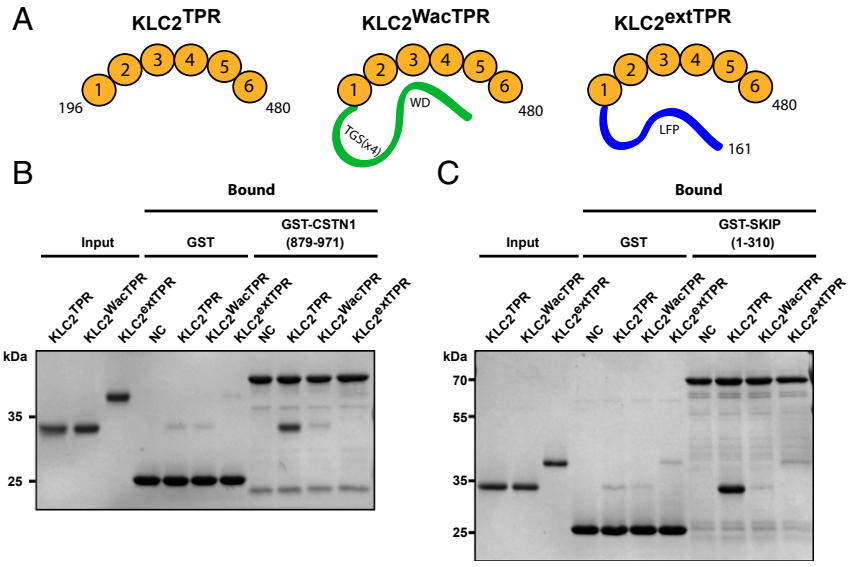

Fig. 2. The LFP-acidic motif-containing HR–TPR linker region inhibits W-acidic cargo binding in vitro. (*A*) Schematic showing KLC2^{TPR}, KLC2^{WacTPR}, and KLC2^{extTPR} proteins used in this work. KLC^{TPR} consists of residues (196–480) of KLC2 comprising its six TPR repeats; KLC^{extTPR} consists of residues (161–480) encompassing the six TPR repeats and an N-terminal extension (ext) to include the conserved LFP-acidic motif. KLC^{WacTPR} comprises residues (196–480) of KLC2 with the first W-acidic motif of SKIP (STNLEWDDSAI, amino acids 202–212) coupled by a flexible $(TGS)_4$ linker. (*B* and *C*) GST–pull-down experiment showing interaction between the above TPR proteins with (*B*) GST-CSTN1 (879–971) or (*C*) GST-SKIP (1–310). The TPR domain alone shows robust binding to both W-acidic cargo proteins, but binding is reduced to background levels by inclusion of the N-terminal region carrying the LFP-acidic motif. Similarly, inclusion of a competitor peptide sequence also inhibits the interaction.

estimated at ∼25 μM (squares in Fig. 3*A*). This interaction requires the LFP sequence because an equivalent peptide, in which this triplet was replaced by AAA (AAA^{pept}, DSLDDAAANEDEQS), did not bind to KLC2^{TPR} (triangles in Fig. 3*A*). Further supporting a self-interaction model, binding between LFP^{pept} and KLC2^{TPR} was also strongly inhibited by the inclusion of the extended endogenous N-terminal sequence (crossed squares in Fig. 3*A*). Similarly, and consistent with our GST–pull-down analysis, the presence of the N-terminal extension also reduced affinity for a TAMRA-conjugated W-acidic cargo peptide from SKIP (SKIP^{WD}, STNLEWDDSAI; K_D increased from 1.05 ± 0.14 to 8.43 ± 0.24 μM) (Fig. 3*B*). Moreover, a competition assay in which increasing amounts of nonlabeled SKIP^{WD} were titrated into a KLC2^{TPR}:TAMRA-LFP^{pept} complex revealed a concentration-dependent decrease in FP (Fig. 3*C*). From this experiment, we estimated a K_I value (35) for the unlabeled SKIP^{WD} peptide of 3.6 μM. This is in good agreement with the K_D value for TAMRA-SKIP^{WD} supporting a model in which W-acidic binding displaces the bound LFP peptide. In a separate experiment, we also validated our immunoprecipitation analysis that indicated that KLC1 LFP/AAA replacement has little effect on JIP1 binding (Fig. S1*D*). Consistent with this, we found that inclusion of an N-terminal extension of KLC1^{TPR} (KLC1^{extTPR}) only marginally reduced its affinity for a TAMRA-conjugated peptide comprising the TPR binding C-terminal 11 aa of JIP1 (YTCPTEDIYLE) (K_D increased from 0.95 ± 0.09 to 2.21 ± 0.06 μM; Fig. S1*E*).

To further define the interaction site on KLC2^{TPR}, we crystallized the extended KLC2^{extTPR} protein. After substantial crystal screening, we were able to obtain a dataset at the 4-Å resolution (data collection and refinement statistics in Table S1). This allowed the modeling of the complete KLC2^{TPR} domain, extending the available structures for this isoform, which lack either the complete TPR1 repeat (3ZFW) or its first α-helix (3CEQ). In the course of crystallographic refinement, difference Fourier maps also revealed the presence of elongated electron density in close proximity of the C-terminal end of the first α-helix of the TPR2 repeat (α2A) (Fig. S2). In all three independent molecules present in the crystallographic asymmetric unit, this residual density was satisfactorily modeled as a short peptide stretch (5 aa in molecules A and B and 2 aa in molecule C) in an extended conformation (Fig. 3 *D* and *E*). Although the limited resolution of the data does not allow for exact amino acid identification, given that our biochemical and biophysical results support an LFP-dependent self-interaction model, the bound peptide (ext in Fig. 3 *D* and *E*) almost certainly originates from the extended flexible region N-terminal to the TPR and involves the LFP-acidic motif. A structural comparison between autoinhibited and cargo-bound KLC2^{TPR} highlights that stabilization of the ext peptide involving the C-terminal portion of α2A does not trigger the conformational change at the N-terminal TPR region observed upon W-acidic cargo binding (23) (Fig. 3*F*). In the latter case, upon W-acidic recognition, an "induced-fit" rigid jaw movement closes TPR2-3 engendering the binding surface and pockets for the SKIP^{WD} peptide. Such movement is not seen in KLC2^{extTPR}. Thus, the interactions involved in ext:KLC2^{TPR} stabilization, appear different from those critical for SKIP^{WD} binding. However, the X-ray structures do reveal a partial overlap between the W-acidic SKIP^{WD} and the ext binding sites on the KLC2^{TPR} domain. In particular, residues immediately C-terminal to the W-acidic motif (SAI in SKIP^{WD}) essentially occupy the same topological location as ext on the KLC2^{TPR} receptor (Fig. 3*F*). Thus, crystallographic analysis fully supports the notion that the autoinhibited (ext-bound) and the W-acidic cargo-bound states are mutually exclusive.

In Vivo Conformational Dynamics of KLC Are Governed by Self-Interaction and Cargo Binding. The above data imply that an intramolecular interaction within KLC2 mediated, at least in part, by amino acids in LFP^{pept}, must be displaced for W-acidic cargo binding to occur. This could have an effect on the overall conformation of the light chain. To test this hypothesis in vivo, we designed a KLC2 fluorescence resonance energy transfer (FRET) conformation biosensor (Fig. 4*A*). A similar approach has been used previously to study conformational change within kinesin-1, but not to assess conformational changes within the light chains themselves (13). To achieve this, we coupled the amino terminus of full-length KLC2 to a donor eGFP and the carboxyl terminus to a HaloTag that allows in-cell conjugation to a tetramethylrhodamine (TMR) FRET acceptor. We then used fluorescence lifetime imaging microscopy (FLIM) to quantify changes in the efficiency of energy transfer from GFP to HaloTag-TMR. These measures subsequently inform on quantitative conformational changes in KLC caused by the modulation of the distance between the N- and C-terminal fluorophores. Western blot analysis of TMR-labeled cell extracts confirmed specific targeting of TMR to the GFP-KLC2-HaloTag biosensor and comparable labeling of wild-type and mutant proteins. Immunoprecipitation showed that the biosensor retained capacity to interact with KHC (Kif5C) (Fig. S3 *A* and *B*). Expression and labeling of the wild-type biosensor in HeLa cells (without addition of exogenous KHC or cargo) gave a robust baseline FRET efficiency of 12.3 ± 0.8% (Fig. 4

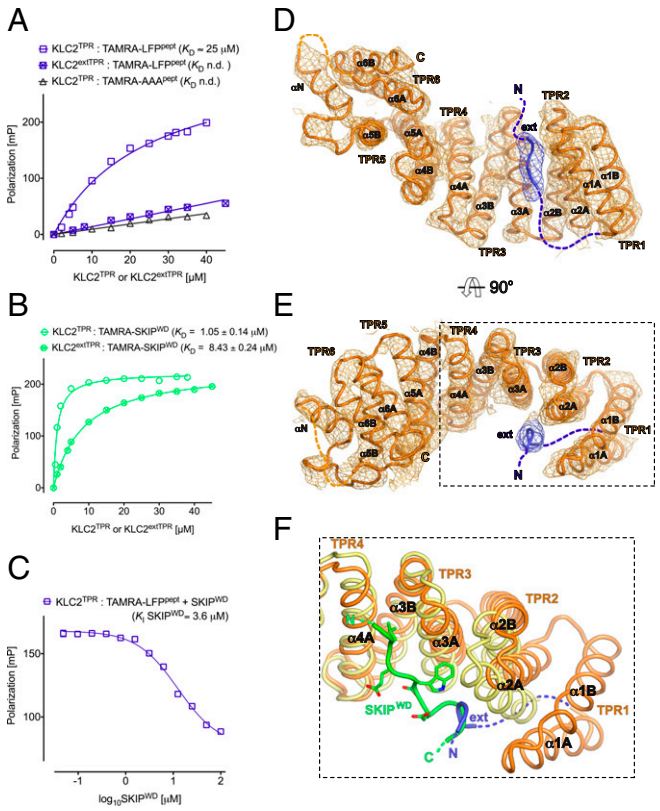

Fig. 3. The HR–TPR linker region interacts in an LFP-dependent manner with $KLC2^{TPR}$ at a binding site partly overlapping with that of cargo W-acidic motifs. (*A*) Fluorescence polarization (FP) measurements showing concentration and LFP-dependent interaction between TAMRA-conjugated LFP^{pept} (DSLDDLFPNEDEQS) and $KLC2^{TPR}$. Mutation of the LFP motif to AAA (DSLDDAAANEDEQS) essentially eliminates binding. Amino-terminal extension of the TPR domain to residue 161 (KLC^{extTPR}) also inhibits interaction with LFP^{pept}. (*B*) FP measurements showing amino-terminal extension of the TPR domain to residue 161 (KLC^{extTPR}) inhibits interaction with $SKIP^{WD}$ compared with $KLC2^{TPR}$ alone. (*C*) FP experiment titrating increasing amounts of nonlabeled $SKIP^{WD}$ in a $KLC2^{TPR}$:LFP^{pept} complex showing that binding of LFP^{pept} and $SKIP^{WD}$ to $KLC2^{TPR}$ are mutually exclusive. (*D* and *E*) Illustrated cartoon representations of the $KLC2^{extTPR}$ X-ray structure in two orthogonal orientations. The peptide originating from the extended N-terminal region (ext in blue) is bound to the $KLC2^{TPR}$ domain (orange). $2mF_o$-DF_c electron density map is shown at the 1.2σ level. Individual TPR repeats composed by helix1-turn-helix2 elements are highlighted. The non-TPR helix between TPR5 and TPR6 is labeled αN. (*F*) Superposition between $KLC2^{extTPR}$ and cargo-bound $SKIP^{WD}$:$KLC2^{TPR}$ (3ZFW) structures in the same orientation as *E*. The $SKIP^{WD}$ W-acidic cargo peptide is shown in green, and the cargo-bound $KLC2^{TPR}$ is shown in yellow. The $KLC2^{extTPR}$ structure is color-coded as in *D* and *E*. The $SKIP^{WD}$ and ext peptides binding sites on $KLC2^{TPR}$ partly overlap.

B and *C*). This was significantly reduced by the replacement of the LFP motif with AAA (3.0 ± 0.3%), demonstrating that the LFP triplet contributes to a relatively compact KLC2 conformation (compare first two columns on graph in Fig. 4*C*). Coexpression of a W-acidic cargo [myc-tagged cytoplasmic domain of CSTN1 (869–971)] reduced wild-type KLC2 FRET efficiency by a similar extent (5.6 ± 0.5%) but did not significantly affect FRET in the LFP/AAA background (3.6 ± 0.5%, compare columns 3 and 4 on graph in Fig. 4*C*). Importantly, introduction of the N287L substitution in KLC2 that disrupts W-acidic cargo binding (23) or mutation of the W-acidic residues in CSTN1 (16, 27, 28), suppressed the cargo-dependent response (Fig. S3 *C* and *D*). In comparison, FRET efficiency for GFP directly coupled to HaloTag-TMR was 31.3 ± 0.76%, whereas expression of the two fluorophores on separate polypeptide chains [N-terminal labeled (GFP-KLC2) and C-terminal labeled (KLC2-Halo)] resulted in low levels of FRET (4.76 ± 1.26%), indicating that the biosensor predominantly reports on intramolecular interaction within KLC2 (Fig. S3 *E* and *F*). To determine whether these cargo/LFP-dependent changes also occur in the context of the kinesin-1 tetramer, equivalent experiments were carried out in the presence of KHC. Inclusion of the heavy chain resulted in an increase in baseline FRET efficiency to 22.5 ± 1.0%, indicating that binding to KHC helps to support a more compact KLC conformation. FRET efficiency was significantly lower in the LFP/AAA replacement biosensor (13.3 ± 0.6%) (columns 5 and 6 on graph in Fig. 4*C*). Cotransfection of cargo reduced FRET efficiency to comparable levels in both backgrounds (6.4 ± 0.5% vs. 7.1 ± 0.5%,

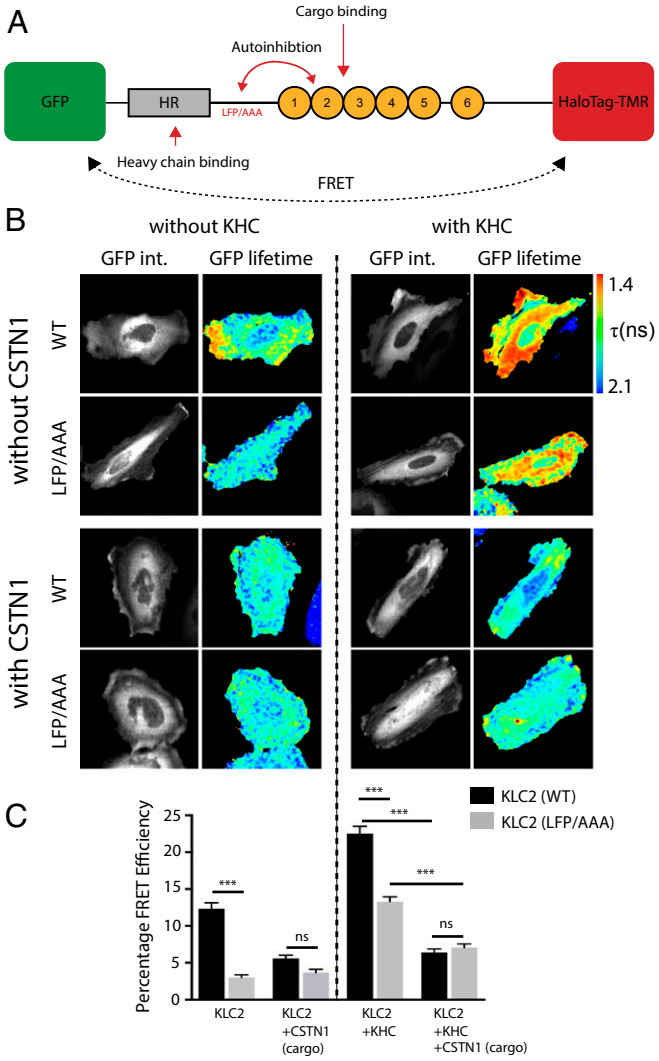

Fig. 4. In vivo conformational dynamics of kinesin light chain are controlled by self-interaction and cargo binding. (*A*) Schematic showing KLC2 FRET biosensor with an N-terminal eGFP and a C-terminal HaloTag that allows covalent coupling of TMR. Red arrows indicate mechanistic questions addressed using the biosensor. (*B*) Multiphoton fluorescent lifetime images of FRET between GFP and TMR-HaloTag. "GFP int." are multiphoton GFP intensity images, whereas lifetime image refers to the fluorescence lifetime of GFP (τ) and is represented by a pseudocolor scale. In these images, a reduction in lifetime (change in color from blue to red) indicates FRET and therefore close association of GFP and TMR-HaloTag. (*C*) Graphs show data from 15 cells expressed as FRET efficiency (*SI Materials and Methods*). (Scale bar: 10 μm.) Error bars are SEM. ***$P < 0.001$. (*Left*) Light-chain biosensor alone [with and without cotransfection of myc-CSTN (879–971) cargo]; (*Right*) equivalent experiments where exogenous KHC is included.

columns 7 and 8 on graph in Fig. 4*C*) showing that KLC undergoes significant cargo-dependent conformational change in the context of the kinesin-1 tetramer. This cargo-dependent change in FRET was again suppressed by the KLC2 N287L variant and W-acidic mutations in CSTN (Fig. S3 *C* and *D*), and separation of the fluorophores on different polypeptides resulted in only minimal levels of FRET (4.09 ± 1.23%), indicating that the measured FRET efficiency remains predominantly intramolecular in the context of the holoenzyme (Fig. S3 *E* and *F*).

To examine the effect of LFP motif-mediated intramolecular interaction in KLC on the MT-dependent ATPase activity associated with KHC, kinesin-1 containing either wild-type or LFP/AAA KLC2 was expressed in, and isolated from, mammalian cells by covalent coupling of GFP-KLC2-Halo to HaloLink resin and subsequent release by TEV protease cleavage of the HaloTag (Fig. S4 *A* and *B*). As assessed by measurement of inorganic phosphate resulting from hydrolysis of ATP, these kinesin-1 preparations had no detectable ATPase activity in the absence of MTs (Fig. S4*C*). However, in the presence of MTs, the ATPase rate of wild-type kinesin-1 was 543.3 ± 7.2 nmol·min^{-1}·mg^{-1} (of KHC). The LFP/AAA substitution resulted in an increase in the ATPase rate to 827.7 ± 21.2 nmol·min^{-1}·mg^{-1}, demonstrating that this intramolecular interaction within the light chain can modulate KHC-associated ATPase activity.

Taken together, these data show that the LFP motif-mediated intramolecular interaction within KLC regulates KLC conformation in the context of the holoenzyme in vivo. This autoinhibitory interaction and conformation are themselves directly governed by W-acidic cargo binding.

Discussion

Despite its importance for a host of cellular processes and contribution to neurological, viral and bacterial disease, the molecular mechanisms underlying the regulation of kinesin-1 by its light chains and the binding of its cargo are not well understood. The data presented here provide conceptual insight into the molecular events that occur both in its regulated state and following W-acidic cargo recognition. We show that, like the kinesin heavy chain, the light chains of kinesin-1 exist in a dynamic conformational state that is regulated by self-interaction and cargo binding. We highlight how recognition of short linear peptide motifs by the TPR domain can be transduced and amplified to result in larger scale modification of the organizational state of the light chain. Thus, we uncover unanticipated mechanistic parallels between the heavy- and light-chain components of the kinesin-1 tetramer.

Such an intramolecular interaction mediated by a TPR domain is reminiscent of the interaction of the N-arm helix of the mitochondrial outer membrane protein Fis1 with its TPR domain (36), although in this case the self-interacting helix forms an important component of the binding interface for other proteins. A closer mechanistic analogy perhaps lies in the regulation of protein phosphatase 5 (Ppp5) activity by its TPR domain where, in its autoinhibited state, the TPR domain engages with the catalytic channel of Ppp5 (37). This conformation is stabilized by the C-terminal αJ helix that contacts a region of the Hsp90 binding groove on the TPR domain. Binding of the C-terminal MEEVD peptide of Hsp90 disrupts this interaction, relieving autoinhibition and activating the phosphatase. The notion that TPR domain function is not restricted to that of a protein–protein interaction module and that peptide binding can be transduced through conformational change to control function is supported by studies of the dimeric bacterial transcription factor and virulence regulator PlcR where TPR binding of the PapR signal peptide is propagated to control the DNA binding properties of helix-turn-helix DNA binding domains (38). We note some functional parallels in another transport/trafficking system with a recent report describing how the interaction of the AP2 β2 hinge (containing a clathrin-binding motif) with the core of the molecule that is disrupted (in an allosteric manner in this case) by phospholipid and cargo binding, promoting clathrin binding activity (39).

In the context of the present study, it is interesting to note that several reports have demonstrated that fusion of W-acidic motifs to otherwise non–kinesin-1 binding proteins is sufficient to promote kinesin-1–dependent transport/dispersion of specific cellular compartments, such as lysosomes (16, 24, 40). The strong implication of these studies is that W-acidic motifs have an intrinsic capacity to promote (at least partial) relief of kinesin-1 autoinhibition. However, given that kinesin-1 ATPase activity is predominantly controlled by an intramolecular interaction between the motor domains and the IAK C-terminal region of a single heavy chain, it was not obvious how a TPR domain–peptide interaction could contribute to this change. Our present data suggest a possible model. Here, we show that mutational disruption of the LFP motif in KLC enhances the inherent MT-stimulated ATPase activity of purified kinesin-1. Rice and colleague (19) demonstrated that the heptad repeat–TPR linker region contributes to light-chain–mediated destabilization of the heavy-chain carboxyl-tail/MT interaction in vitro, implying a mechanism of communication between the linker and heavy-chain tail. Moreover, the same study reported that the TPR domain itself contributes to a light-chain–mediated reduction in the affinity of the KHC head for its C-terminal tail, through a mechanism requiring steric and electrostatic factors. Incorporating that analysis, we propose a model whereby the W-acidic motif-mediated displacement of the highly charged linker from the TPR will result in interactions (predominantly electrostatic) with the heavy-chain tail that combine with steric changes resulting from a large-scale change in conformation of the light chains to promote the cargo-dependent transition of holoenzyme to its active state (Fig. S5).

If so, it would seem likely that this mechanism can be generalized to other W-acidic motif-containing cargo given their shared binding determinants on the KLC^{TPR} (23, 30). The strong sequence conservation of the LFP motif and our similar observation for CSTN1 and KLC1 (Fig. S1*C*) suggests that this will also apply to other light-chain isoforms. However, only a subset of kinesin-1 cargoes contain W-acidic motifs, and it is clear that KLC^{TPR} has the capacity to interact with other peptides, including the C-terminal 11 aa of JIP1 (JIP1^{C11}, sequence YTCPTEDIYLE) (22). Despite this, the LFP/AAA replacement does not affect binding to JIP1 in immunoprecipitation experiments (Fig. S1*D*) and N-terminal extension of the KLC1^{TPR} only has a marginal impact on its affinity for JIP1^{C11}. The JIP1^{C11} peptide is also insufficient to promote activation of transport (16). Indeed, JIP1 requires interactions with the coiled-coil heavy chain and the heavy-chain tail binding protein Fez1 for full activity (15, 17). Although the precise JIP1^{C11} binding site on the KLC^{TPR} still awaits structural definition, mutagenesis experiments highlight a particularly crucial role for residues on TPR4/5 that are distinct from the primary determinants of W-acidic binding on TPR2/3 (22, 23). Thus, it may be that the site of peptide binding on the KLC^{TPR} has different functional outcomes, and that this is in part due to its capacity to displace the LFP motif-containing linker region, resulting in differential requirements for supporting interactions to promote kinesin-1 activity. It is therefore likely that there are multiple pathways to activation of kinesin-1 depending upon site(s) of cargo binding.

The dissociation constant (K_D) of ~25 μM (or the equivalent association constant $K_A = 1/K_D \sim 0.04$ μM^{-1}) measured here by FP between TAMRA-LFP^{pept} and KLC2^{TPR} reflects a bimolecular binding process. However, the proposed mechanism of KLC autoinhibition is unimolecular, as the LFP^{pept} is covalently linked to the TPR domain. The balance between the latched (autoinhibited) and unlatched (available to W-acidic cargoes) states is therefore regulated by the intramolecular association constant K_A^i. This has been shown to be related to K_A by $K_A^i = p(d)K_A$ (Eq. **S1**, *SI Materials and Methods*) where $p(d)$ is known as the

effective concentration, the ligand concentration that would be required to achieve the same fraction of bound state in a bimolecular interaction (41, 42). From the structure of KLC2^{extTPR}, we can estimate the value of $p(d)$ at ~18.2 mM (Eq. **S2**, *SI Materials and Methods*). Thus, using Eq. **S1**, we obtain $K_A^i \sim 728$. The implication of this is that the equilibrium fraction of cargo-available KLC2^{TPR} is only ~0.14%. This suggests that autoinhibition of the light chains tightly regulates cargo binding. A similarly stringent intramolecular regulation has been observed for the myristoylated N-terminal latching to the C-terminal lobe of c-Abl that maintains the kinase in an inactive state (43, 44). The low fraction of cargo-available KLC2^{TPR} raises the obvious question of how significant W-acidic cargo binding is achieved. The X-ray structures of cargo-bound KLC2^{TPR} and autoinhibited KLC2^{extTPR} highlight that only a partial overlap exists between the W-acidic motif and the ext autoinhibitory peptide. In particular, the binding region for the most N-terminal part of the W-acidic motif (N-terminal to the central tryptophan residue) appears accessible even in the ext-bound state (Fig. 3*F*). Thus, one possible mechanism for the relief of KLC autoinhibition is the initial recognition of a portion of the W-acidic cargo motif at this topological location. This could be sufficient to initiate the induced-fit adaptation of the TPR domain, which, in turn, may drive destabilization of ext binding.

Therefore, as well as acting as a component of a pathway to kinesin-1 activation, our findings also suggest that the intramolecular interaction between the linker region and KLC^{TPR} may serve to buffer cargo-binding sensitivity and so provide a point of regulatory access to control the proper loading and unloading of cargo. It is conceivable that binding of other proteins or posttranslational modifications of the light chains could serve to stabilize or destabilize this self-interacting state and thus regulate cargo-binding properties of the TPR domain in a spatial and temporal manner.

Materials and Methods

N-terminal TAMRA-conjugated peptides and nonconjugated peptides used for FP and competition measurements were supplied by Bio-Synthesis. Sequences were as follows: SKIP^{WD}, STNLEWDDSAI; LFP^{pept}, DSLDDLFPNEDEQS; AAA^{pept}, DSLDDAAANEDEQS; and JIP^{C11}, YTCPTEDIYLE. Measurements were performed on a BMG Labtech PolarStar Omega plate reader at 20 °C by incubating 300 nM TAMRA-labeled peptides with the indicated protein at increasing concentrations in 25 mM Hepes, pH 7.5, 150 mM NaCl, and 5 mM β-mercaptoethanol. Estimation of the equilibrium dissociation constant (K_D) for the different peptides was performed assuming a one-site specific-binding model. For competition experiments, a mixture of TAMRA-LFP^{pept} and KLC2^{TPR} at 300 nM and 12 μM, respectively, were incubated with increasing concentrations of unlabeled SKIP^{WD} peptide in buffer supplemented by 5% (vol/vol) DMSO. The concentration-dependent decrease in FP signal was fitted to a sigmoidal equation to derive IC_{50}. Analyses and K_i estimation were performed using the Prism package (GraphPad Software). All data points are the mean of three replicates.

See *SI Materials and Methods* for additional materials and methods.

ACKNOWLEDGMENTS. This work was supported by Biotechnology and Biological Sciences Research Council Project Grant BB/L006774/1 (to M.P.D. and R.A.S.), as well as a Wellcome Trust Research Career Development Fellowship and London Law Trust Medal Fellowship (to M.P.D.).

1. Vale RD (2003) The molecular motor toolbox for intracellular transport. *Cell* 112(4):467–480.
2. Vale RD, Reese TS, Sheetz MP (1985) Identification of a novel force-generating protein, kinesin, involved in microtubule-based motility. *Cell* 42(1):39–50.
3. Dodding MP, Way M (2011) Coupling viruses to dynein and kinesin-1. *EMBO J* 30(17):3527–3539.
4. Morihara T, et al. (2014) Transcriptome analysis of distinct mouse strains reveals kinesin light chain-1 splicing as an amyloid-β accumulation modifier. *Proc Natl Acad Sci USA* 111(7):2638–2643.
5. Hackney DD (2007) Jump-starting kinesin. *J Cell Biol* 176(1):7–9.
6. Diefenbach RJ, Mackay JP, Armati PJ, Cunningham AL (1998) The C-terminal region of the stalk domain of ubiquitous human kinesin heavy chain contains the binding site for kinesin light chain. *Biochemistry* 37(47):16663–16670.
7. Kaan HYK, Hackney DD, Kozielski F (2011) The structure of the kinesin-1 motor-tail complex reveals the mechanism of autoinhibition. *Science* 333(6044):883–885.
8. Dietrich KA, et al. (2008) The kinesin-1 motor protein is regulated by a direct interaction of its head and tail. *Proc Natl Acad Sci USA* 105(26):8938–8943.
9. Hackney DD, Baek N, Snyder AC (2009) Half-site inhibition of dimeric kinesin head domains by monomeric tail domains. *Biochemistry* 48(15):3448–3456.
10. Wong YL, Dietrich KA, Naber N, Cooke R, Rice SE (2009) The Kinesin-1 tail conformationally restricts the nucleotide pocket. *Biophys J* 96(7):2799–2807.
11. Hackney DD, Stock MF (2000) Kinesin's IAK tail domain inhibits initial microtubule-stimulated ADP release. *Nat Cell Biol* 2(5):257–260.
12. Friedman DS, Vale RD (1999) Single-molecule analysis of kinesin motility reveals regulation by the cargo-binding tail domain. *Nat Cell Biol* 1(5):293–297.
13. Cai D, Hoppe AD, Swanson JA, Verhey KJ (2007) Kinesin-1 structural organization and conformational changes revealed by FRET stoichiometry in live cells. *J Cell Biol* 176(1):51–63.
14. Hackney DD, Levitt JD, Suhan J (1992) Kinesin undergoes a 9 S to 6 S conformational transition. *J Biol Chem* 267(12):8696–8701.
15. Blasius TL, Cai D, Jih GT, Toret CP, Verhey KJ (2007) Two binding partners cooperate to activate the molecular motor Kinesin-1. *J Cell Biol* 176(1):11–17.
16. Kawano T, et al. (2012) A small peptide sequence is sufficient for initiating kinesin-1 activation through part of TPR region of KLC1. *Traffic* 13(6):834–848.
17. Fu M-M, Holzbaur ELF (2014) Integrated regulation of motor-driven organelle transport by scaffolding proteins. *Trends Cell Biol* 24(10):564–574.
18. Verhey KJ, et al. (1998) Light chain-dependent regulation of Kinesin's interaction with microtubules. *J Cell Biol* 143(4):1053–1066.
19. Wong YL, Rice SE (2010) Kinesin's light chains inhibit the head- and microtubule-binding activity of its tail. *Proc Natl Acad Sci USA* 107(26):11781–11786.
20. Fu M-M, Holzbaur ELF (2013) JIP1 regulates the directionality of APP axonal transport by coordinating kinesin and dynein motors. *J Cell Biol* 202(3):495–508.
21. Verhey KJ, Hammond JW (2009) Traffic control: Regulation of kinesin motors. *Nat Rev Mol Cell Biol* 10(11):765–777.
22. Zhu H, et al. (2012) Crystal structures of the tetratricopeptide repeat domains of kinesin light chains: Insight into cargo recognition mechanisms. *PLoS One* 7(3):e33943.
23. Pernigo S, Lamprecht A, Steiner RA, Dodding MP (2013) Structural basis for kinesin-1: cargo recognition. *Science* 340(6130):356–359.
24. Dodding MP, Mitter R, Humphries AC, Way M (2011) A kinesin-1 binding motif in vaccinia virus that is widespread throughout the human genome. *EMBO J* 30(22):4523–4538.
25. Verhey KJ, et al. (2001) Cargo of kinesin identified as JIP scaffolding proteins and associated signaling molecules. *J Cell Biol* 152(5):959–970.
26. Aoyama T, et al. (2009) Cayman ataxia protein caytaxin is transported by kinesin along neurites through binding to kinesin light chains. *J Cell Sci* 122(Pt 22):4177–4185.
27. Konecna A, et al. (2006) Calsyntenin-1 docks vesicular cargo to kinesin-1. *Mol Biol Cell* 17(8):3651–3663.
28. Araki Y, et al. (2007) The novel cargo Alcadein induces vesicle association of kinesin-1 motor components and activates axonal transport. *EMBO J* 26(6):1475–1486.
29. Rosa-Ferreira C, Munro S (2011) Arl8 and SKIP act together to link lysosomes to kinesin-1. *Dev Cell* 21(6):1171–1178.
30. Wilson MH, Holzbaur ELF (2015) Nesprins anchor kinesin-1 motors to the nucleus to drive nuclear distribution in muscle cells. *Development* 142(1):218–228.
31. Schmidt MR, et al. (2009) Regulation of endosomal membrane traffic by a Gadkin/AP-1/kinesin KIF5 complex. *Proc Natl Acad Sci USA* 106(36):15344–15349.
32. Maritzen T, et al. (2012) Gadkin negatively regulates cell spreading and motility via sequestration of the actin-nucleating ARP2/3 complex. *Proc Natl Acad Sci USA* 109(26):10382–10387.
33. Ti S-C, Jurgenson CT, Nolen BJ, Pollard TD (2011) Structural and biochemical characterization of two binding sites for nucleation-promoting factor WASp-VCA on Arp2/3 complex. *Proc Natl Acad Sci USA* 108(33):E463–E471.
34. Hammond JW, Griffin K, Jih GT, Stuckey J, Verhey KJ (2008) Co-operative versus independent transport of different cargoes by Kinesin-1. *Traffic* 9(5):725–741.
35. Nikolovska-Coleska Z, et al. (2004) Development and optimization of a binding assay for the XIAP BIR3 domain using fluorescence polarization. *Anal Biochem* 332(2):261–273.
36. Zhang Y, Chan DC (2007) Structural basis for recruitment of mitochondrial fission complexes by Fis1. *Proc Natl Acad Sci USA* 104(47):18526–18530.
37. Yang J, et al. (2005) Molecular basis for TPR domain-mediated regulation of protein phosphatase 5. *EMBO J* 24(1):1–10.
38. Grenha R, et al. (2013) Structural basis for the activation mechanism of the PlcR virulence regulator by the quorum-sensing signal peptide PapR. *Proc Natl Acad Sci USA* 110(3):1047–1052.
39. Kelly BT, et al. (2014) Clathrin adaptors. AP2 controls clathrin polymerization with a membrane-activated switch. *Science* 345(6195):459–463.
40. Pu J, et al. (2015) BORC, a multisubunit complex that regulates lysosome positioning. *Dev Cell* 33(2):176–188.
41. Zhou HX (2001) The affinity-enhancing roles of flexible linkers in two-domain DNA-binding proteins. *Biochemistry* 40(50):15069–15073.
42. Zhou H-X (2006) Quantitative relation between intermolecular and intramolecular binding of pro-rich peptides to SH3 domains. *Biophys J* 91(9):3170–3181.
43. Hantschel O, et al. (2003) A myristoyl/phosphotyrosine switch regulates c-Abl. *Cell* 112(6):845–857.
44. Zhou H-X (2003) How often does the myristoylated N-terminal latch of c-Abl come off? *FEBS Lett* 552(2-3):160–162.
45. Parsons M, Messent AJ, Humphries JD, Deakin NO, Humphries MJ (2008) Quantification of integrin receptor agonism by fluorescence lifetime imaging. *J Cell Sci* 121(Pt 3):265–271.